# SYNTHESIS OF DEGRADABLE THERMORESPONSIVE MICROGELS

# SYNTHESIS AND APPLICATIONS OF DEGRADABLE THERMORESPONSIVE MICROGELS

By DARYL N SIVAKUMARAN, B. Eng., M.ASc.

A Thesis Submitted to the School of Graduate Studies in Partial Fulfillment of the Requirements

for the Degree

Doctor of Philosophy

McMaster University

DOCTOR OF PHILOSOPHY (2015) McMaster University

Department of Chemical Engineering Hamilton, Ontario

| | |
|---|---|
| TITLE: | Synthesis and Applications of Degradable Thermoresponsive Microgels |
| AUTHOR: | Daryl N Sivakumaran, B.Eng. M.ASc. (McMaster University) |
| SUPERVISOR | Professor Todd R. Hoare |
| NUMBER OF PAGES | xx, 253 |

## LAY ABSTRACT

Microgels are solvent-swollen gel particles that have sub-micron diameters and have been widely investigated for a variety of biomedical applications. Temperature-responsive microgels based on poly(N-isopropylacrylamide) (PNIPAM) hold particular promise given that they can swell and deswell in response to changes in temperature, enabling pulsatile or environment-specific release of a drug. However, current thermoresponsive microgels are not degradable and therefore have limited utility in the body. In this thesis, degradable temperature-responsive microgels were developed on two length scales (micron and nano-sized) to enable their ultimate use in the body. Microgels responsive to changes in solution pH or the presence of glucose (both clinically-relevant stimuli) were made using similar techniques. Combinations of these microgels with injectable hydrogels enabled tuning of the rate of drug release by changing physical microgel and/or hydrogel, as investigated both experimentally and theoretically. The research conducted thus has the potential to impact clinical drug delivery vehicle design.

**ABSTRACT**

Microgels are solvent-swollen cross-linked gel particles with sub-micron diameters and have been widely investigated for drug delivery applications. Thermoresponsive microgels based on poly(N-isopropylacrylamide) (PNIPAM) have attracted particular attention given their potential to enable pulsatile or environment-specific drug release. However, current methods to make thermoresponsive microgels yield functionally non-degradable materials, significantly limiting their utility *in vivo*. Herein, hydrazone chemistry was applied to cross-link hydrazide and aldehyde-functionalized precursor polymers together to form degradable PNIPAM microgels on different length scales that enable potential use of thermoresponsive microgels *in vivo* in a way not currently possible.

For micron-scale microgels, microfluidics was employed to create monodisperse microgels between 30-90 μm. For nano-scale microgels, a temperature-driven aggregation/self-assembly technique was developed that resulted in the formation of microgels with sizes between 200-300 nm. In either case, the microgels can be slowly degraded through hydrazone hydrolysis. Functionalized microgels can be made by incorporating pH-responsive 2-dimethylaminoethylmethacrylate (DMAEMA) or glucose-responsive phenylboronic acid in the precursor polymers.

The potential utility of degradable microgels in drug delivery was studied using *in situ* gelling microgel-hydrogel nanocomposites. Changing the microgel cross-link density and whether or not the microgels were physically entrapped or covalently cross-linked to the bulk hydrogel matrix resulted in significant changes in drug release kinetics, with burst release particularly mitigated by increasing the cross-link density of the microgels. Microgels made via microfluidics were then utilized to make fully degradable microgel-hydrogel composites consisting of chemically identical gel chemistries on both the bulk and micro length scales. Carbohydrates (carboxymethyl cellulose and dextran) and PNIPAM gel phases were oriented in different relative geometries to examine how the phase distribution impacted drug release. Results suggest that drug release can be controlled through the selection of polymer type of each phase, with the deswelling phase transitions of PNIPAM playing a particularly large role in slowing release of the drug.

**ACKNOWLEGEMENTS**

The contents of this thesis document are not only the result of the work I've put in, but rather the culmination of many people over many years. I would like to start by thanking my supervisor, Dr. Todd Hoare. Dr. Hoare has been my remarkable academic leader for the past 7 years and without his guidance, innovation, and encouragement, this work would not have been completed. The freedom in which I have been able to conduct my own research is appreciated and his support in sharing my research with others is valued. I am indebted to you and I look forward to having your guidance as I continue my career. I would like to thank my supervisory committee members, Dr. Robert Pelton and Dr. Kim Jones (and Dr. Harold Stover), for their advice and motivation to complete new and exciting research. They are only a small sample of the entire Department of Chemical Engineering faculty and staff that have shaped me and allowed me to call this department my home for over 12 years.

There are several undergraduate students to whom I am forever indebted due to their tireless work; all this despite the challenges they were presented with. Thank you Danielle Maitland, Thomas Oszustowicz, Helen Dorrington, and Eva Mueller for all you have done in making this happen. I owe you everything. The graduate students of the Hoare lab are a select group I have had the privilege of sharing my days with through my graduate studies. Each and every one of you inspire me to do better, to work harder, and to innovate. I cannot replace the friendships we've had over the years and I will miss you all dearly. So many memories, championships, and Phoenix visits. This is especially true of the old guard that have been there from the beginning (Rabia, Scott and Trevor). Special thank you to Madeline for your contributions in completing this thesis (Chapter 5). Please make sure our wonderful lab dynamics remain. It is special and without it, our research will not progress. All the best.

Lastly, I would like to thank those closest to me. To my parents, thank you for supporting me in my life choices, despite the ups and downs. I know I can be a pain, but know that everything I am is because of you. I owe you my life and I will never forget. Thank you to my sister Diane for a certain Solid Edge image and for always being my friend and teammate. Lastly, thank you to my dear fiancé, Michelle. Thank you for your patience and for allowing me to chase my dreams. I love you and cannot wait for the next adventure!

**TABLE OF CONTENTS**

## LIST OF FIGURES

**LIST OF TABLES**

## LIST OF ABBREVIATIONS AND SYMBOLS

| | |
|---|---|
| AA | Acrylic Acid |
| AA-P(NIPAM) | Poly(NIPAM-co-Acrylic Acid) |
| ADH | Adipic acid dihydrazide |
| APS | Ammonium persulfate |
| CMC | Carboxymethylcellulose |
| CMC-Hzd | Hydrazide-functionalized carboxymethylcellulose |
| C2C12 | Mouse muscle myoblast cells |
| Dex-Ald | Aldehyde-functionalized dextran |
| DLS | Dynamic light scattering |
| DMAEMA | 2-dimethylaminoethylmethacrylate |
| DMEM | Dulbecco's Modified Eagle medium-high glucose |
| DMSO | Dimethyl sulfoxide |
| EDC | N'-ethyl-N-(3-dimethylaminopropyl)- carbodiimide |
| FBS | Fetal bovine serum |
| HCl | Hydrochloric acid |
| HS | Horse serum |
| LCST | Lower critical solution temperature |
| log P | Hydrophobic partitioning coefficient |
| MAA | Methacrylic acid |
| MBA | N,N'-methylene bisacrylamide |
| MTT | Thiazolyl blue tetrazolium bromide |

| | |
|---|---|
| NaCl | Sodium chloride |
| NaOH | Sodium hydroxide |
| NHS | N-Hydroxysuccinimide |
| NIPAM | N-Isopropylacrylamide |
| PAA | Poly(acrylic acid) |
| PBA | Phenylboronic acid |
| PBS | Phosphate-buffered saline |
| PCS | Photon correlation spectroscopy |
| PEG | Polyethylene glycol |
| PEO | Poly(ethylene oxide) |
| PGLA | Poly(lactic-co-glycolic acid) |
| P(NIPAM) | Poly(NIPAM) |
| PNIPAM-Hzd | Hydrazide functionalized PNIPAM |
| PNIPAM-Ald | Aldehyde functionalized PNIPAM |
| PS | Penicillin Streptomycin |
| SDS | Sodium dodecyl sulfate |
| TNBS | Trinitrobenzenesulfonic acid |
| VPTT | Volume phase transition temperature |
| 3T3 | *Mus musculus* mouse cells |

## DECLARATION OF ACADEMIC ACHIEVEMENT

The majority of the written work described within the written thesis was conceived, conducted, analyzed, and written by the author of the thesis, in consultation from Dr. Todd Hoare, with the exception to the following:

Chapter 1:

Danielle Maitland and Thomas Oszustowicz was responsible for drug concentration measurements of some samples as well as conducting some of MTT assay work relating to cell viability. Figure 1.6 and 1.7 were completed and included in the Master's degree thesis for the author.

Chapter 2 and 3:

Eva Mueller assisted with the production of microfluidic chips as well as the size measurement of particles using optical microscopy.

Chapter 4 and 5:

Eva Mueller was responsible for the synthesis of some microgel samples as well as the associated DLS measurements. She also assisted in the production of the precursor polymers. Madeline Simpson assisted with synthesis of microgels samples and associated DLS measurements as well as assisting with UV/VIS measurements.

## I. Introduction:

The general increase in quality of life of the global human population is a culmination of several factors, but an increased emphasis on health care has played an important role. The progressive development of different biotechnologies has been vital in helping health care providers treat patients more effectively and with greater efficiency. In particular, the continued focus on biomaterials development (for use in a vast array of different applications) has been key in addressing the needs of patients in applications ranging from biomedical implants to drug delivery. In the context of drug delivery applications, the development of novel biomaterials has played a major role in improving patient quality of life by reducing the frequency of required drug administrations and improving the efficacy of the drugs once administered. Polymeric materials that elicit "smart" properties (i.e. the ability to respond to external stimuli) offer particular future promise in this regard, as they would enable patients or health professionals to dynamically control the delivery and dosage of drug as needed through manipulation of external stimuli such as temperature, magnetic field, pH, or even metabolites such as glucose. This would allow patients to actively control drug intake based on needs of that patient and/or automatically trigger drug release when required based on changes in the local body environment. However, several issues associated primarily with the ability of such smart materials to effectively prolong drug delivery and degrade in a programmed manner still limit the potential translation of these materials. The primary aim of this thesis is thus to develop methods to address these challenges and

thus better enable the application of smart materials for the design of drug delivery vehicles.

## I.1 Hydrogels

Hydrogels are networked three-dimensional water-soluble polymers that can be made from a wide array of different starting monomers into gels with varied compositions. They have the ability to absorb large quantities of water into their network, allowing for the storage and permeability of ions, small molecules, and proteins and thus making them ideal depots for drug delivery applications. Release of drug payloads from hydrogels can be tuned by the pore size of the hydrogels (regulating diffusion-based release) and via tuning of hydrogel-drug interactions through the careful selection of polymer backbone and/or functionalities attached to the polymer backbone that can promote physical or chemical binding of the drug (regulating partition-based release)[1]. Hydrogels also typically elicit low inflammatory responses when used *in vivo* due to their structural similarity to the extracellular matrix of cells[2,3].

The use of hydrogels in drug delivery applications has been widely studied, with varied success. In particular, the highly hydrophilic nature of the hydrogel matrix can provide problems in some drug delivery applications. Although effectively acting as a depot for drug storage, the highly porous and highly hydrated hydrogel network also allows the free release of non-bonded drug (particularly hydrophilic drugs) quite quickly (typically on the order of hours or a few days) through diffusion[4,5]. This hydrophilicity also prevents the effective loading of hydrophobic drugs into the hydrogel matrix, leading

to low loading efficiency for such drugs that constitute a large sub-section of current therapeutics of interest[6]. As such, more research needs to be conducted to make hydrogels a more suitable option for broader-spectrum *in vivo* drug release.

**I.2 Microgels**

Microgels are defined as colloidally-dispersed cross-linked gel particles in the size range of 10 nm to 10 μm that swell in their dispersing solvent[7,8]. Microgels are typically made using the following techniques. The most common method is the polymerization of monomer units in conjunction with particle nucleation. This can occur through the natural precipitation of the polymer out of solution (such as with poly(N-isopropylacrylamide) (PNIPAM) at temperatures above its lower critical solution temperature or LCST[9]) using a precipitation-dispersion based polymerization process in which colloidal stability is facilitated by the ionic initiators typically used (Figure I1); alternately, synthesis may proceed using a pre-formed seed particle from which the microgel can be formed[10]. Microgels can also be created using emulsification in which monomer or polymer units are cross-linked using a water-in-oil (most typically) or oil-in-water dispersion. By using monomers that are only soluble in the droplet phase of the emulsion, gels can form after polymerization cross-links the monomers into a gel whose dimensions are defined by the geometry of the droplets[11]. Lastly, microgels can be created through the complexation of polymers through mechanisms such as polyelectrolye complex formation[12].

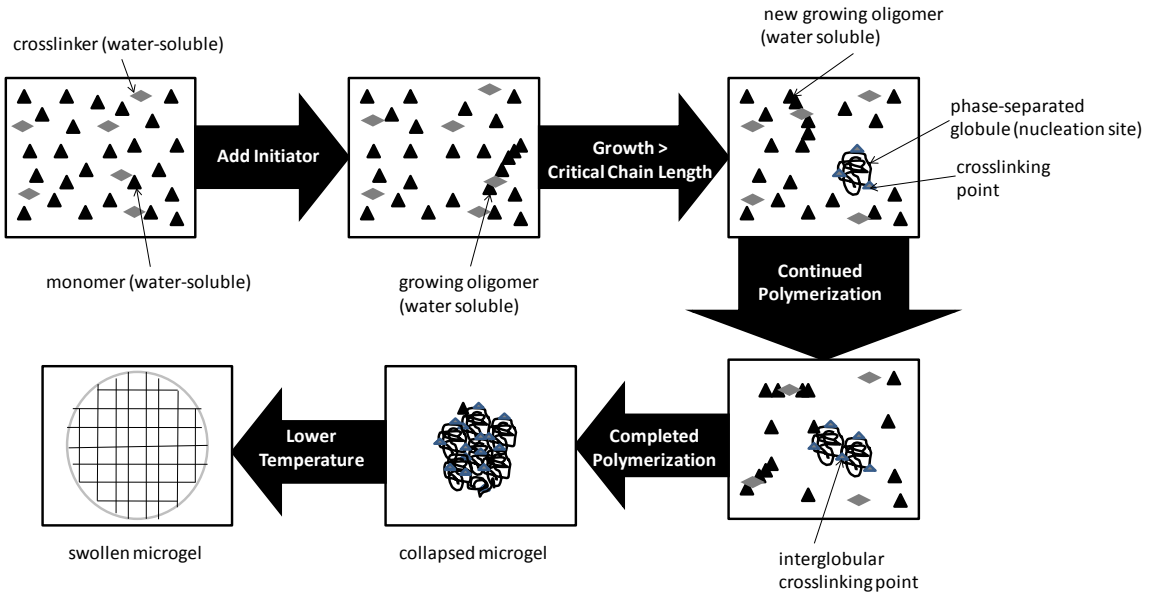


**Figure I1:** Mechanism for the conventional preparation of microgel particles via a precipitation-based polymerization process

The ability to remain colloidally stable is a key characteristic of microgels. Stabilization of these spherical gel particles is typically accomplished by the external structure or surface of the microgel. The surface can be stabilized through the incorporation of electrostatic charge, resulting in electrostatic stabilization[13]. Alternatively, steric stabilization can also be utilized since microgels are typically not smooth at the surface (unlike a metallic or crystalline nanoparticle)[13]. Instead, the soluble polymer chains at the microgel interface can protrude into the solvent in a "hairy" configuration, thus preventing aggregation of the particles due to steric repulsion. These stabilization characteristics in conjunction with internal cross-linking allows microgels to also be dried and resuspended, unlike micelles which will fall apart when taken out of solution.

Colloidally stability in suspension provides many advantages of microgels over typical macro-sized hydrogels. They are free-flowing units, unlike large hydrogels, allowing them to be used in different situations (i.e. injection-based applications) and in different volumes[13,14]. Their small nature allows them to respond to environmental conditions such as temperature, salt concentrations, etc. at much faster time intervals than that of macro-sized hydrogels[7]. In particular applications, their high surface-to-volume ratio can help in solute transport between the microgel environment and the solvent. Additionally, microgels can be assembled into hydrogels, providing bulk characteristics seen at the macro-scale while controlling interactions at the micro- and nano-scale. It is these advantages that afford microgels great potential in a wide variety of applications ranging from oil recovery, environmental rehabilitation[7], wastewater treatment[15,16], catalysis[17], and a myriad of biomedical and drug delivery applications[18-21]..

When considering designing microgels for the use in applications, several factors must be considered. The most important design consideration is the selection of the polymer backbone to be used in microgel production. Backbone selection is critical since it will predominately govern the behavior of the microgel in suspension, including (but not limited to) control of swelling, interactions with environment or metabolites, and the capacity for further functionalization. To add additional properties to the microgel, additional chemistries can be incorporated, either by modifying the existing microgel backbone or by copolymerizing the backbone monomer with another monomer (taking comonomer type, amount, and relative reactivity with the backbone monomer into consideration for each design). For instance, for temperature responsive microgels,

adding a hydrophobic comonomer can lower the LCST of the microgel, whereas adding a hydrophilic comonomer will raise the LCST[22,23]. In addition, selection of comonomers that polymerize faster or slower than PNIPAM will result in different functional distributions ranging from homogenous distribution to a core-shell type design which in turn can change microgel responsiveness[24].

Through the careful selection of comonomers, microgels can be made to be "smart" in that they can respond to external stimuli. PNIPAM microgels are particularly widely studied due to their thermosensitivity. PNIPAM polymers exhibit an LCST of ~32°C, meaning they precipitate out of solution at temperatures above their LCST. This thermosensitivity translates to the microgel which experiences a volume phase transition temperature (VPTT) in that same temperature range (with the temperature tunable based on comonomer selection)[9] over which the microgels will deswell upon heating. pH sensitive microgels in which pH-ionizable functional group are incorporated in the polymer backbone have also been widely prepared[25-27]. In particular for the context of this thesis, PNIPAM has been routinely polymerized with anionic carboxylic acids to form microgels that swell as the pH is increased and the acid groups are deprotonated[26,28,29]. Microgels based on cationic monomers such as 4-vinylpyridine[30] or dimethylaminoethyl methacrylate[31] can similarly promote pH-responsive swelling, in this case deswelling responses as the pH is increased and the cationic groups are deprotonated. Other types of external stimuli that microgels can be made to respond to include glucose[32,33], magnetic fields[34], or light[35].

The interesting properties of microgels provide make them a promising tool for a wide array of applications. However, due to the common polymerization use of free radical polymerization for the formation of smart microgels in particular, microgel backbones are based on C-C bonds, making microgels inherently non-degradable. This property poses a problem for biomedical applications in which clearance from the body is needed. To address this issue, the use of degradable cross-linkers is a possibility. The most popular degradable cross-linkers are based on disulfide linkages that can be cleaved through reduction processes that naturally occur *in vivo*[36,37], usually via glutathione[38] or thiol exchange[39]. For example, inverse miniemulsions have been used to prepare poly(oligo(ethylene oxide) monomethylether methacrylate) microgels cross-linked through copolymerized disulfide-functionalized dimethacrylate cross-linkers[40]. The produced nanogels were stable, able to maintain their shape, and effectively capture doxorubicin for release. Upon exposure to glutathione, the microgels degraded back into soluble polymer fragments. The use of polyvinylalkoxysiloxanes[41], which degrade at basic conditions, or acetal groups[42], which hydrolyze in acidic conditions, are alternatives to disulfides as a method of incorporating degradability into microgels. Lastly, the use of naturally degradable polymeric units as the backbone can provide degradability. For example, thermosensitive dextran-co- N-vinylcaprolactam microgels made by batch emulsion polymerization[43] can undergo enzymatic degradation using dextranase to promote fragmentation of the nanogel structure.

**I.3 Nanoparticles from Self-assembly**

In terms of biomedical applications, the use of conventional precipitation-based free radical polymerization production of microgels offers limitations in terms of degradability. New self-assembly based approaches to make microgels have also been explored to form degradable microgels via dissociating of physical interactions between well-defined polymer precursors, giving degradable products of controlled molecular weight and structure. Note that, depending on the nature of the building blocks and the self-assembly mechanism, some particles may be classified as microgels and others as solid-like coacervates[44,45], depending on the water content of the final nanoparticle formed. Hydrophobic interactions are by far most commonly used in the literature for the formation of physically-cross-linked and assembled microgels. In particular, self-assembly of block copolymers that contain hydrophobic and hydrophilic units can result in nanoparticle formation. For instance, polymers based on cholesteryl group-bearing pullulan will self assemble due to hydrophobic interactions between the polymers; stabilization of these nanoparticles through the free radical copolymerization of 2-methacryloyloxyethyl phosphorylcholine results in nanogels with a diameters of 50-60 nm[46]. It was found that these nanogels can be used to capture and release clinically relevant enzymes[46]. In a similar vein, block copolymers of PNIPAM-PEO have been self-assembled into microgels by utilizing the hydrophobic nature of PNIPAM and hydrophilic units of PEO to assemble the polymers into a particle followed by cross-linking via the addition of methylenebisacrylamide[47]. Particles could also be made by targeting the thermoresponsive block to cause the aggregation of the copolymer. Other

particles have used the thermosensitive blocks of PNIPAM to create nanoparticles; for example, thermal aggregation of PNIPAM-co- N-[4-(1-pyrenyl)butyl]-N-n-octadecylacrylamide] was stabilized by the addition of a cholesterol-bearing pullulan through the association of hydrophobic moieties, leading to particles with diameters around 40 nm[48]. Thermoresponsive blocks made of poly(2-isopropyl-2-oxazoline) have also grafted to side chains of pullulan, resulting in self-association upon increasing the temperature above the LCST into stable particles with hairy shells that had hydrodynamic diameters of ~200 nm[49].

Although these associations predominately use hydrophilic interactions for particle formation, latent functionalities can be used to promote covalent cross-linking for particle stabilization. If the functional group is cleavable, then possible degradability can be easily incorporated into the particle. Again, the most popular strategy for post-assembly cross-linking is based on disulfide chemistry. Chan et al. introduced pendant thiol-sulfide chemistry into the a thermoresponsive block copolymer based on hydrophilic PEG and oligo(ethylene oxide) monomethyl ether methacrylate[50]. Particle formation is driven by thermal collapse of the polymer, with cross-linking then occurring through pendant *in situ* disulfide formation. Particle characteristics can be altered through the manipulation of the pendant hydrophobic–hydrophilic balance with disulfide–thiol–sulfide chemistry. The particles exhibited reduction-driven degradability in the presence of reducing agents such as DL-dithiothreitol. Thiol pendant groups have also been attached to block copolymers made from a hydrophilic poly(ethylene oxide) (PEO) block and a hydrophobic polystyrene (PSt) block[51]. The polymers spontaneously self-assemble

in water to create aggregates whose structure and shape (spheres, rod-like aggregates) could be controlled by modulation of the block groups. Stabilization was maintained through the presence of disulfide linkages created between pendant groups, with degradability achieved through exposure to reducing agents. Other particle systems utilizing disulfide cross-linking as a method of self-assembly stabilization include those based on degradable polyester-block-POEGMA[52], and polysaccharide-grafted PNIPAM[53].

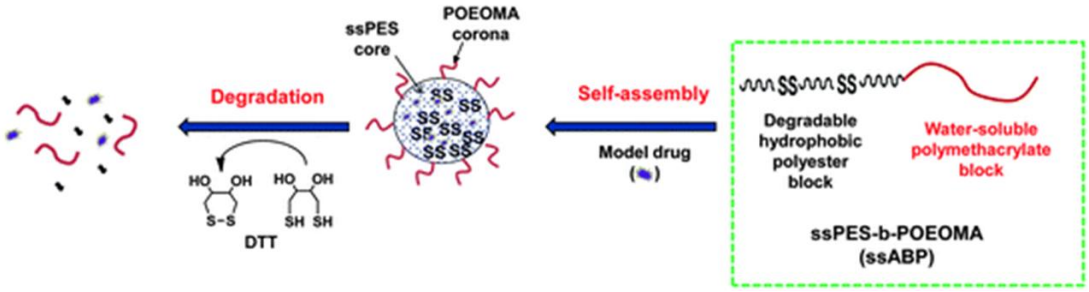


**Figure I2:** Thiol-responsive degradable nanogels based on a disulfide containing ester and oligo(ethylene glycol) methacrylate as controlled nanocarriers made through self-assembly. Degradation and drug payload can be controlled by presence of a reducing agent (DTT) resulting in disulfide degradation[52]. Reprinted with permission. Copyright 2012 Elsevier.

The association between ionic species is another method to assemble well-define block copolymers for particle formation[54]. Typically, to make nanoparticles in this way, the solution pH must be maintained in a region that maintains the presence of charge on both polymers and one of the components needs to be in excess to provide electrostatic stabilization. In one case, colloidal particles were made from polyelectrolyte complexes

formed by mixing dilute solutions of individual homopolymers consisting of poly(vinyl amine) and carboxymethyl cellulose[12]. Particle size could be controlled by changing pH or ionic concentration of the solution. Similarly, nanosized spherical polyelectrolyte complexes have been assembled via the interaction between hyaluronic acid-co-poly(ethylene glycol) block copolymers and poly-L-lysine[55]. The self-assembled nanoparticles had a diameter between 90 to 300 nm with low polydispersities. The nanogels swell in response to the presence of salts, which competes with the electrolyte complexation; consequently, at high salt concentrations, nanogel formation can be reversed to release the constituent polymers back into solution and thus enable potential degradation.

Solvent based coacervation is alternative for the formation of particles. Coacervation results in the formation of precipitated aggregates that can then be cross-linked through bifunctional cross-linking agents. For example, cationic oligoethylenimine precursor polymers were dissolved in a polar organic solvent (DMSO or DMF) and then precipitated via addition of a non-polar organic solvent (diethyl ether), with the nanoprecipitate formed subsequently stabilized by the presence of disulfide-containing tetralysine cross-linker[56]. The resulting nanogels had diameters between 170 to 220 nm, and the cationic nature of the polymer allowed for the nanogels to respond to changes in pH. The presence of the disulfide bonds also allowed for the particles to be degradable through reduction.

## I.4 Microfluidic Polymer Particle Production

The methods for microgel formation described up to this point are typically used for the manufacture of particles on the nanoscale, although some (e.g. inverse emulsion, precipitation) can be extended up to particle sizes in the few microns to a few hundred microns range. However, using either of those approaches in the micron size range typically will result in microgels having very broad size distributions that are less than desirable[57], particularly in the context of biomedical or drug delivery applications.

Alternatively, microfluidics can provide a platform for creating monodisperse hydrogel particles. Microfluidics involves the manipulation of fluid flow at the microscale[58]. One of the major benefits of microfluidics in general is its ability to control fluid flows that enhance mass transfer between different phases and thus facilitate chemical reactions, increasing the overall efficiency of the reaction when compared to typical reactor outputs[59]. However, through the careful manipulation of fluids that are immiscible, well-controlled phase separation (including emulsification) can also occur[57,60]. Both size and shape of the droplets can be controlled depending on fluid flow rates of the dispersed and continuous phase[61]. Since each droplet is exposed to the exact same shear field at the nozzle (in contrast to traditional emulsification processes in which different shears are experienced depending on proximity to the source of the shear and the vessel walls), the produced droplets have a very low size distribution, typically as low as 5% in variation between droplet sizes[57]. The droplets produced are a product of the pressure and shear exerted by the fluids as well as surface tension between the immiscible fluids, with a spherical droplet being the most thermodynamically favourable shape for

the liquid to assume[62,63]. A series of different polymer morphologies can be manufactured including polymer particles[64,65], polymeric Janus particles[66,67], microcapsules[68,69], or nanocrystals[70], depending on the orientation of the emulsification geometry. Although harder to produce, non-spherical shapes can also be produced by altering fluid flow speeds, device configurations, and collection methods, leading to the possibility of orientation-dependent applications[71]. By running these fluid flows continuously, a large quantity of droplets can be formed in quick succession, up to $10^8$ particles per hour per chip (with higher throughputs possible using parallel synthesis techniques)[61].

When the disperse phase (droplet fluid) is loaded with monomer and cross-linkers, polymerizations can occur within the droplet, leading to the formation of polymer particles. Polymerization of the monomer units is usually accomplished through thermal or photo-polymerization downstream from the emulsion production[57]. Initiators can be loaded within the continuous phase (immiscible outer fluid) or within the dispersed phase, depending on the morphology of the droplet desired and the relative solubilities of the precursors[57]. Alternatively, click chemistry can be utilized for the production of particles, utilizing precursor polymers in the disperse phase instead of starting from monomer units[64].

The manipulation of flow for the generation of emulsions (the basis of particle formation) can be accomplished through two different microfluidic device configurations. The first is through the use of capillary tubes[57,72], in which the dispersed phase is delivered into the centerline of the continuous phase flow. This prevents the disperses phase from contacting the side wall (preventing wall-fluid interactions), encouraging the

formation of droplets when the fluids are immiscible[57]. The droplet is then produced from the shearing effects of the continuous phase flowing past the developing dispersed phase droplet. Typical capillary devices utilize cross-flow[73] or co-flow[74] configurations, both of which can result in polydisperse emulsion generation, and are typically made from materials such as PVC, PDMS or (more routinely) glass[57]. When the flow rates of the dispersed phase and continuous phase are controlled, the size of the resulting droplet will be controlled, thus allowing for the manipulation of particle size.

A more advanced capillary tube configuration is the flow-focusing capillary device[75]. The same principles of capillary droplet formation remain; however, the disperse phase is physically focused through an orifice into the continuous phase. Through careful manufacturing techniques, different flow focusing capillary configurations can be made to allow for production of W/O/W double emulsions[76], enabling the production of core-shell microgels, shell-only particles, or microgels encapsulating different materials within a core phase.

An alternative to capillary-base microfluidic configurations is the use of microchannel-based devices. These devices can be made from different materials (glass, silicone, PDMS, etc.) and use micromachining techniques such as photolithography and the use of template masks for their production[57,60]. This provides an advantage over typical capillary-base techniques such that small features with high resolutions (on the scale of tens of micrometers) can be used to help aid in the production of emulsion droplets and ultimately polymeric particles with smaller sizes[57]. There are two common configurations to assemble microchannel-based microfluidic chips: T-junction and flow

focusing designs[60]. In the T-junction design, the dispersed phase is contacted with the continuous phase in a perpendicular geometry, using shear stresses as the phases meet to formulate droplets similar to cross-flow capillary flows. The first T-junction microchannel chips were produced by Nisisako et al. and were able to produce emulsion droplets that contained 1,6-hexanediol diacrylate and a photoinitiator[77]. The stable droplets were recovered in a collection beaker outside the chip and cross-linked after exposure to UV light. By altering fluid flows of either the dispersed or continuous phases, changes in particle size could occur[61]; an increase in the continuous flow rate would result in a decrease in droplet size (and subsequently particle size after polymerization), while an increase in the dispersed flow rate would increase the droplet size[60].

The use channel based flow focusing devices is another method of utilizing microfluidic devices for particle manufacture. Stone et al. first produced emulsions of water and silicone oil using this microfluidic configuration[78]. Kumacheva's group later utilized this approach for the production of polymer particles using a series of acrylate-based monomers[79]. Polymerization of the monomers could be heat or UV initiated downstream similar to other methods.

Similar to capillary-based microfluidics, flow focusing can be used to generate multilayered emulsions which can lead to different particle morphologies[57]. Core-shell[68], shell-only[80], Janus particles[81], and microgel-encapsulated microgels[82] are all accessible morphologies when using flow focusing microfluidic chips. Non-spherical shapes, including discs or plugs, are also possible using similar techniques of reducing channel

dimensions[57]. In addition, also like capillary techniques, flow-focusing can allow for the production of microgel particles using gellable polymeric precursors instead of monomer units, allowing more benign production of particles which can encapsulate drug or protein payloads for biomedical applications[64,83].

The production of homogenous hydrogel particles (microgels) is a promising application of microfluidics. A popular polymer to use involves the gelation between alginate and calcium for the manufacture of homogenous, degradable particles[71,84,85]. Choi et al. use a flow-focusing device combining aqueous streams of alginate and calcium chloride which is emulsified with a continuous phase of hexadecane[84]. Monodispersed microgels with diameters between 60-90 μm can be made by adjusting the flow rate of the continuous phase. Other cross-linking approaches have also been used. Chau et al. produced agarose-gelatin microgels with varying mechanical and compositional properties using a flow focusing device, taking advantage of the gelation between agarose and a phenolic hydroxyl modified gelatin, which is cross-linked through the a enzymatic catalysis process involving horseradish peroxidase and hydrogen peroxide. The produced particles were mainly homogenous containing both polymers, although there were instances of partial segregation of the gelatin component within the particle at times. This natural based microgel is being produced as to provide a platform for cell encapsulation later on.[86].

Core-shell microgels can also be made through the use of microfluidic devices. This allows for the unique design of both phases of the microgel and (ideally) independent responses associated with both the shell and core. Lehmann and Seiffert

produced core-shell microgels consisting of a polyacrylamide core (temperature insensitive) with a PNIPAM shell (temperature sensitive)[68] using a two-step production process. The core consisted of a polyacrylamide microgel made from a microfluidic flow focusing device; the collected microgels were then purified and then fed into a secondary microfluidic device with dimensions that only allowed single particles into a secondary aqueous phase with PNIPAM functionalized with UV cross-linkable groups. The new core-shell droplet was generated through flow focusing and UV polymerized to create the desired morphology. When heated to temperatures above the VPTT, the microgel shell collapsed.

Microgel shell microparticles have also been generated. For example, monodisperse PLGA-alginate core-shell microspheres made through the use of multi-layer capillary microfluidics[87]. Using differently designed microfluidic chips also allowed for the encapsulation of multiple cores within the shell phase, leading to interesting morphologies. Similarly, PLGA particles have been encapsulated by an alginate shell by dropping a suspension of PLGA particles in alginate solution into a calcium solution to cross-link the shell, producing microspheres on the size range of 15 to 50 μm depending on flow rates. The shell could independently control drug release from the PLGA particles.

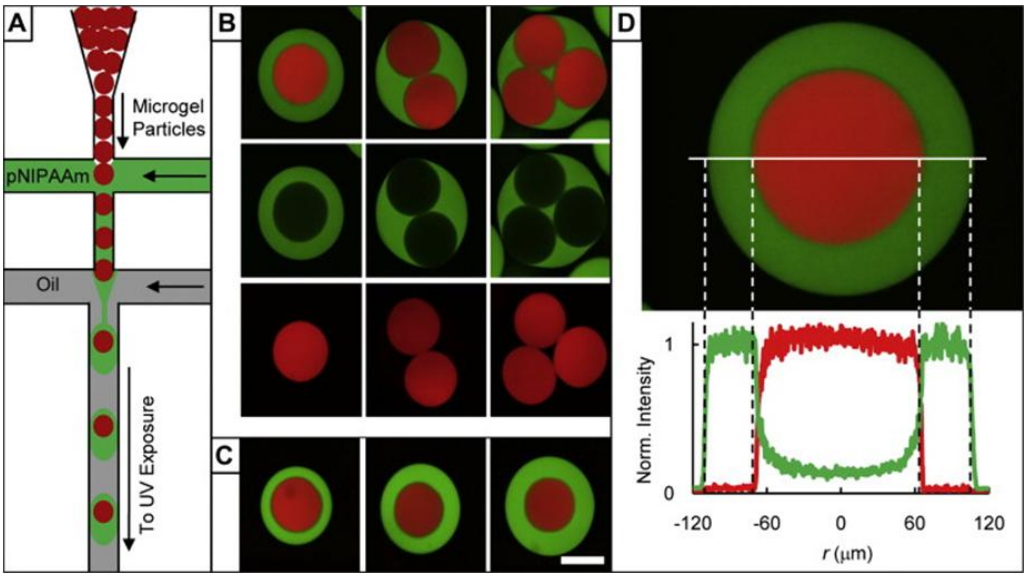


**Figure I3**: Microfluidic fabrication of microgel capsules that consist of two miscible yet distinct layers. (A) Schematic of a microfluidic device forming aqueous pNIPAAm droplets that are loaded with pre-fabricated microgel particles. (B, C) The flow rates of the inner particle phase (red-tagged pNIPAAm), the middle polymer phase (green-tagged pNIPAAm), and the outer oil phase control the number of core particles in each shell (B) as well as the shell-thickness (C). Pictures in the upper row of Panel B show an overlay of the micrographs in the middle and lower row, which depict separate visualizations of the green-tagged pNIPAAm shell and the red-tagged pNIPAAm core. (D) Spatially resolved intensity profiles of the red and green fluorescence in the single-core particle shown in Panel B, showing little interpenetration of its two phases. The scalebar is a length of 100 μm[68]. Reprinted with permission from Seiffert, S.; Thiele, J.; Abate, A. R.; Weitz, D. A. *J. Am. Chem. Soc.* **2010**, *132*, 6606. Copyright 2010 American Chemical Society.

Janus particles represent another potential morphology that is achievable using microfluidics. Janus particles are characterized by their ability to have two distinct surfaces that are contained within the same particle[88]. To produce these particles, adjacent fluid flows are joined at a junction as to prevent mixing prior to droplet formation. Using

flow focusing techniques, Nie et al. produced particles based on methacryloxypropyl dimethylsiloxane and a mixture of pentaerythritol triacrylate, poly(ethylene glycol) diacrylate and acrylic acid[89]. After *in situ* UV polymerization, stable Janus particles were made. Tertiary Janus particles were also produced in the same study, with one polymer phase sandwiched by the other polymer phase using a modified microfluidic chip. Alternatively, polymeric precursors can be used in lieu of monomers to produce Janus particles, affording better control of the polymer phases in the particle. Seiffert et al. produced Janus particles from the combination of three functional precursor polymers based on PNIPAM and cross-linked using dimethylmaleimide (DMMI) under UV irradiation. Phase separation between polymer phases was maintained by not allowing mixing within the droplet by smart chip design and the use of higher molecular weight polymers, which slows internal mixing prior to cross-linking. A specially designed chip was used to manufacture these particles, with the distribution of both precursor polymers controlled through the manipulation of the continuous phase. Full Janus particles or shell-only particles that maintained Janus particle-like separation of polymer phases could be produced depending on the chip geometry.

The shape of the produced particle can also be changed by altering the dimensions of the channels to restrict the formation of spherical microgels and then polymerizing the droplet into particles with shapes such as plugs or pucks[90]. Interesting shapes such as teardrops, mushroom-like, and lamp-like particles based on alginate can be produced by controlling the impact velocity and droplet size when the particle is dropped into a cross-linking barium acetate and glycerol solution[71]. Through the process of photolithography,

precise mask constructs can be made with specifically shaped patterns for particle production. Triangular, hexagonal, and square shaped particles made from poly(ethylene glycol) diacrylate are a few of the possible architectures that are possible using this PDMS fashioned microfluidic chip and UV polymerization of the monomer units as they pass through the mask[62]. T-junctions can also be used to make non-spherical particles. In particular, plug disc-shaped droplets can be produced by the careful manipulation of flows within microchannels with dimensions that don't allow for spherical relaxation after emulsification[90]. This technique has the immense potential for the manufacture of specially designed hydrogels for photonic materials, MEMS, or biomaterials constructs.

Microfluidics-derived microgels have been investigated for drug delivery, although such investigations are still at their relatively early stages. The monodisperse distributions of the particles achievable with microfluidics facilitate highly predictable drug release profiles that are highly desired. Carbohydrate-based microgels made from carboxymethylcellulose and dextran have been shown to encapsulate small molecule drugs like bupivacaine and release them in *vitro*[64]. Seiffert demonstrated the ability of PNIPAM-co-acrylamide core-shell microgels to release FITC-dextran[68], with the release rate higher at lower temperatures when the particle was swollen and reduced above the VPTT of the particle (effectively shutting pores for the drug to escape). The deswelling of the shell did not however change the mobility of the drug within the core phase which ensure the possibility of safe encapsulation of drugs in the future[91]. Similarly, drug encapsulation was completed in a lipid based (Witepsol H15) shell-only particle made using flow focusing capillary techniques[92]. The inner core of the particle was water

loaded with the hydrophilic drug doxorubicin hydrochloride, while the lipid layer was loaded with a hydrophobic drug, paclitaxel. Drug release was facilitated by the degradation of the shell phase, leading to simultaneous release of the drugs that can provide synergistic effects when combating the cancer. This solvent-free platform of particle production shows the potential for producing drug eluting particles and the ability to independently encapsulate multiple components within a single particle[92].

Another potential biomaterial application that may benefit from microfluidic assisted particle production is cell encapsulation. Relative to conventional techniques (e.g. dropping alginate solutions into calcium baths), microfluidics offers the potential to produce smaller encapsulated beads with more controlled numbers of cells per bead, proposed to enhance the long-term viability of the encapsulated cells due to the reduced diffusional pathway for nutrients and oxygen between the cells and the outside of the capsule. Alginate-calcium microgels were made using a capillary microfluidic device and were used to encapsulate yeast cells in particles that had diameters between 60 to 230 μm[93]. After a week of growth, 65% of the yeast cells displayed viability, showing the potential for microfluidics as a tool for cell encapsulation. Microfluidics also enables the use of other mild *in situ* gelling chemistries to encapsulate cells that provide higher microgel stability *in vivo.* For example, PEG-4MAL-based microgels have been made using a flow focusing device utilizing cross-linking between a PEG-4MAL macromer functionalized with the cell adhesive peptide RGD and the small molecule cross-linker dithiothreitol (DTT)[94]. The microgels produced were 300–800 μm in diameter and were

used to encapsulate human mesenchymal stem cells (hMSCs), with the RGD peptide used to support cell adhesion. Cells were cultured within the produced particles and had viability in culture for up to 7 days with loss of viability.

### I.5 Microgel-Hydrogel Composites

The properties of microgels as drug delivery systems offer possible solutions to some of the limitations of hydrogel-based delivery systems. However, the high mobility of microgels *in vivo* away from the target site and high release rates of drugs are limitations that need to be addressed. By combining microgels and hydrogels to form soft nanocomposite hydrogels (also known as "plum pudding" hydrogels), the limitations of both microgel and hydrogels can be mitigated[6,95,96]. The bulk hydrogel can mask any issues the microgel may introduce regarding biocompatibility by hiding the microgel in the bulk gel matrix, while entrapment in the bulk gel will arrest microgel migration away from the target site[6]. By drug loading the microgels, the hydrogel will also mitigate burst effects seen from microgel formulations as well as add an additional diffusive barrier for drug release, resulting in slower and more controlled drug concentrations in patients[97]. Composites can offer the ability to independently engineer both hydrogel and microgel phases to allow for more control in the tailored design of the release profile. For example, by designing microgels with high affinity for the drug (through electrostatics, hydrogen bonding, or hydrophobic/hydrophillic domains) and a hydrogel with a low (or lower) affinity for the drug, partitioning effects may be tuned to significantly reduce the release rate of the drug[98]. The cross-link densities of the bulk gel and microgel phases can be

manipulated to control diffusional release through the composites. Microgels can also add structural stability to the hydrogel matrix, increasing its modulus and improving its capacity to withstand potential daily wear and tear if implanted subcutaneously. For example, Meid et al. studied mechanical properties of polyacrylamide hydrogels embedded with PNIPAM microgels in comparison to the hydrogels alone[99] and found significant enhancement in the mechanical stability of the hydrogels, due to an increase in physical cross-linking points between the hydrogel and microgel phase. In particular, above the VPTT of the microgels, the collapse of the microgels changes their mechanical behavior to mimic that of hard fillers, which in turn allows for an even strong composite gel[99]. The changing size of the inner microgels also reduces the size of the external hydrogel, although the transition is slow and minimal[100].

There are several examples of nanoparticle-hydrogel composites applied to the challenge of drug delivery in the literature. Calcein release from liposomes entrapped within carbopol and hydroxyethylcellulose-based hydrogels can be controlled by manipulating the characteristics of the liposome membrane[101]. Doxorubicin was loaded into biodegradable poly(D,L-lactide-co-glycolide) (PLGA) microspheres and encapsulated within gelatin hydrogels, with bioactive DOX delivery sustained over the period of days when released from the composites as opposed to the microspheres alone[102]. Microgels made of N-isopropylacrylamide-N-tert-butylacrylamide-acrylic acid embedded in dimethylacrylamide hydrogels enabled the controlled release of rhodamine B[103]. Incorporation of poly(lactic-co-glycolic acid) nanoparticles into a poloxamer 407 hydrogel prolonged drug release by 70% compared to the hydrogel or microgel on its

own[97]. Transforming growth factor-β1 (TGF-β1) encapsulated in PLGA microspheres entrapped in poly(ethylene glycol) hydrogels could be released up to 21 days with reduced burst release[104]. Vascular endothelial growth factor (rhVEGF) release from nanocomposites prepared from PLGA particles inside alginate hydrogels could similarly be sustained over the course of 3 weeks, with an observed increase in active blood vessels being developed in mice models that were studied[105]. Similar results were observed when VEGF was release from nanoparticles made from the coacervation of chitosan with dextran sulfate and embedded in a MatriGel™ matrix[106]; after 2 weeks of release, the composite reduced release by 30% when compared to the hydrogel on its own, with significantly reduced burst phase release. The ability to control the release of incorporated drugs and proteins thus makes composites an attractive tool for potential drug delivery systems as well as a promising approach for the tissue regeneration engineering. However, despite these promising results, extending the release over weeks remains a persistent challenge with reported formulations in the literature.

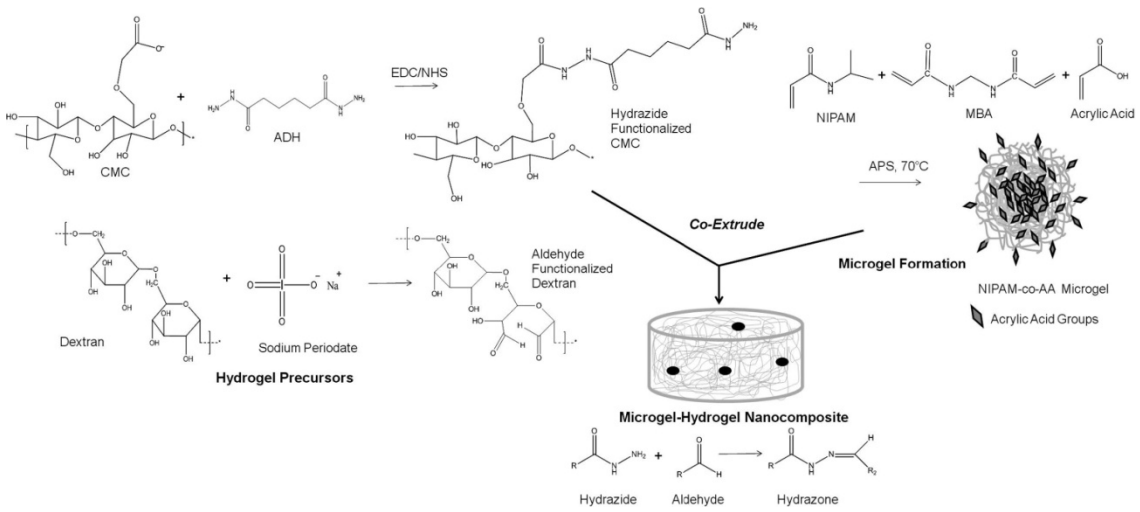


**Figure I4:** The use of hydrogels and microgels with the formation of an *in situ* hydrazone cross-linked microgel-hydrogel nanocomposite using a double-barrel syringe[107]. Reprinted with permission. Copyright 2013 Elsevier

To address the challenge of effectively delivering the bulk hydrogel phase *in vivo* via as non-invasively a mechanism as possible, *in situ*-gelling hydrogels have been investigated. Sivakumaran et al. have immobilized precipitation polymerization prepared PNIPAM-co-acrylic acid (AA-PNIPAM) microgels into hydrogels cross-linked via the reaction of hydrazide and aldehyde-functionalized polymer precursors to form a hydrazone cross-linked network. The hydrogel component of the composite can be based on carbohydrates based on carboxymethylcellulose and dextran[98] or synthetic polymers based on PNIPAM[108] or poly(oligoethylene glycol methacrylate)[109]. The presence of AA-PNIPAM microgels extend drug release profiles well beyond that of hydrogel itself due to the electrostatic interaction between the anionic microgel and the cationic drug, bupivacaine[98], enabling sustained drug release over the course of over one month. Furthermore, when superparamagnetic iron oxide nanoparticles (SPIONs) are added to

the hydrogel, on-demand, pulsatile drug release can be accomplished through the external manipulation of a alternating magnetic field (AMF)[108]. This response is achieved due to changes in temperature elicited by magnetic heating of SPIONS using the AMF, leading to microgel deswelling and the generation of free volume in the hydrogel to promote drug release. These additional pores allows for the quick diffusion of the loaded model drug out of the composite on demand. Release of therapeutics from the hydrogel composites is not limited to small molecule drugs, but also encompasses the release of proteins.

**I.6 Objectives**

Given the clearly promising and unique properties of microgels in the context of particularly biomedical applications but the significant limitations of current microgels and microgel-based devices for use in the body, there exists a significant opportunity to rationally engineer microgel-based technologies to address these limitations. The work conducted in this thesis is focused on the development and production of new "smart" microgels that maintain the environmentally-responsive properties of the conventional microgels but also incorporate properties that will aid in the translation of these materials to the clinic. Formation of microgels was explored on both the microscale and the nanoscale, with a particular focus on creating monodisperse microgels that are degradable into clearable polymer fragments. Our general approach to this problem is to fabricate microgels made from polymeric precursors of known molecular weight and then cross-link those polymers using degradable cross-linking units. The potential utility of these materials specifically in drug delivery applications is subsequently examined.

Chapter 1 focuses on making modifications to the local cross-linking distribution within the microgel phase of microgel-hydrogel composites and how these modifications affect drug release from the nanocomposites. Changing the cross-linking density of the acrylic acid-functionalized PNIPAM microgel or covalently binding the microgel to the carbohydrate hydrogel phase can tune drug release from the composites. Drug release was slowed from the nanocomposites by cross-linking the microgels to hydrogel phase (eliminating the potential for thermal deswelling of the microgel to facilitate convective drug transport) or increasing the cross-link density within the microgel (resulting the mitigation of a burst release and effectively increasing the diffusional path for the drug to leave the system).

Chapter 2 focuses on the preparation of degradable PNIPAM microgels utilizing flow-focusing microfluidic techniques and cross-linking though hydrazone bond formation. Through this technique, degradable monodisperse microgels of controlled size could be made that still exhibited a VPTT akin to microgels made from traditional precipitation methods.

Chapter 3 describes the use of these microfluidics-produced microgels to produce microgel-hydrogel composites in which both the microgel and bulk gel phases are compositionally identical, enabling unambiguous investigation of the effect of the presence of microscale inhomogeneities as well as the relative ordering of different types of phases (specifically, thermoresponsive and non-thermoresponsive) on drug release.

Chapter 4 continues the focus on microgel development utilizing polymeric precursors by describing a new technique (modeled on the conventional precipitaton/aggregation approach of making nanoscale microgels from monomeric precursors) in which microgels can be fabricated via the temperature-induced precipitation of the hydrazide-functionalized PNIPAM oligomer followed by stabilization of the aggregate using an aldehyde-functionalized PNIPAM oligomer. The nano-sized produced microgels are colloidally stable, with their size controllable by changing production parameters such as polymer content, degree of cross-linking, solution temperature, and reaction time. The microgels display thermosensitive characteristics and are fully degradable through the hydrolysis of the hydrazone bonds.

Finally, Chapter 5 expands on the method developed in Chapter 4 to create functionalized thermoresponsive microgels on the nanoscale, providing proof-of-concept demonstrations of using the same precipitation techniques to create pH-responsive and glucose-responsive microgels.

## I.7 References


(1) Mateen, R.; Hoare, T. *Journal of Materials Chemistry B* **2014**, *2*, 5157.

(2) Rami, L.; Malaise, S.; Delmond, S.; Fricain, J.-C.; Siadous, R.; Schlaubitz, S.; Laurichesse, E.; Amédée, J.; Montembault, A.; David, L.; Bordenave, L. *Journal of Biomedical Materials Research Part A* **2014**, *102*, 3666.

(3) Aziz, M. A.; Cabral, J. D.; Brooks, H. J. L.; McConnell, M. A.; Fitzpatrick, C.; Hanton, L. R.; Moratti, S. C. *Journal of Biomedical Materials Research Part B: Applied Biomaterials* **2015**, *103*, 332.

(4) Zhao, C.; Zhuang, X.; He, P.; Xiao, C.; He, C.; Sun, J.; Chen, X.; Jing, X. *Polymer* **2009**, *50*, 4308.

(5) Wu, D.-Q.; Sun, Y.-X.; Xu, X.-D.; Cheng, S.-X.; Zhang, X.-Z.; Zhuo, R.-X. *Biomacromolecules* **2008**, *9*, 1155.

(6) Hoare, T. R.; Kohane, D. S. *Polymer* **2008**, *49*, 1993.

(7) Fernandez-Nieves, A.; Wyss, H.; Mattsson, J.; Weitz, D. A. *Microgel Suspensions: Fundamentals and Applications*; John Wiley & Sons, 2011.

(8) Saunders, B. R.; Laajam, N.; Daly, E.; Teow, S.; Hu, X.; Stepto, R. *Adv. Colloid Interface Sci.* **2009**, *147–148*, 251.

(9) Pelton, R. *Adv. Colloid Interface Sci.* **2000**, *85*, 1.

(10) Wu, X.; Pelton, R. H.; Hamielec, A. E.; Woods, D. R.; McPhee, W. *Colloid. Polym. Sci.* **1994**, *272*, 467.

(11) Landfester, K.; Willert, M.; Antonietti, M. *Macromolecules* **2000**, *33*, 2370.

(12) Feng, X.; Pelton, R.; Leduc, M.; Champ, S. *Langmuir* **2007**, *23*, 2970.

(13) Saunders, B. R.; Vincent, B. *Adv. Colloid Interface Sci.* **1999**, *80*, 1.

(14) Thorne, J.; Vine, G.; Snowden, M. *Colloid. Polym. Sci.* **2011**, *289*, 625.

(15) Morris, G. E.; Vincent, B.; Snowden, M. J. *J. Colloid Interface Sci.* **1997**, *190*, 198.

(16) Parasuraman, D.; Sarker, A.; Serpe, M. *Colloid. Polym. Sci.* **2013**, *291*, 1795.

(17) Gichinga, M. G.; Striegler, S.; Dunaway, N. A.; Barnett, J. D. *Polymer* **2010**, *51*, 606.

(18) Wang, Q.; Libera, M. *Colloids Surf., B* **2014**, *118*, 202.

(19) Hoare, T.; Pelton, R. *Langmuir* **2008**, *24*, 1005.

(20) Zhou, T.; Wu, W.; Zhou, S. *Polymer* **2010**, *51*, 3926.

(21) Zhang, X.; Lu, S.; Gao, C.; Chen, C.; Zhang, X.; Liu, M. *Nanoscale* **2013**, *5*, 6498.

(22) Wang, Q.; Zhao, Y.; Xu, H.; Yang, X.; Yang, Y. *J. Appl. Polym. Sci.* **2009**, *113*, 321.

(23) Saunders, B. R.; Crowther, H. M.; Morris, G. E.; Mears, S. J.; Cosgrove, T.; Vincent, B. *Colloids Surf. Physicochem. Eng. Aspects* **1999**, *149*, 57.

(24) Hoare, T.; Pelton, R. *Langmuir* **2004**, *20*, 2123.

(25) Bai, Y.; Zhang, Z.; Deng, M.; Chen, L.; He, C.; Zhuang, X.; Chen, X. *Polym. Int.* **2012**, *61*, 1151.

(26) Hoare, T.; Pelton, R. *Macromolecules* **2004**, *37*, 2544.

(27) Wei, J.; Ju, X.-J.; Xie, R.; Mou, C.-L.; Lin, X.; Chu, L.-Y. *J. Colloid Interface Sci.* **2011**, *357*, 101.

(28) Kratz, K.; Hellweg, T.; Eimer, W. *Colloids Surf. Physicochem. Eng. Aspects* **2000**, *170*, 137.

(29) Khan, A. *J. Colloid Interface Sci.* **2007**, *313*, 697.

(30) Nur, H.; Pinkrah, V. T.; Mitchell, J. C.; Benée, L. S.; Snowden, M. J. *Adv. Colloid Interface Sci.* **2010**, *158*, 15.

(31) Liu, G.; Li, X.; Xiong, S.; Li, L.; Chu, P.; Yeung, K.; Wu, S.; Xu, Z. *Colloid & Polymer Science* **2012**, *290*, 349.

(32) Bitar, A.; Fessi, H.; Elaissari, A. *J. Biomed. Nanotechnol.* **2012**, *8*, 709.

(33) Hoare, T.; Pelton, R. *Macromolecules* **2007**, *40*, 670.

(34) Chiang, W.-H.; Ho, V. T.; Chen, H.-H.; Huang, W.-C.; Huang, Y.-F.; Lin, S.-C.; Chern, C.-S.; Chiu, H.-C. *Langmuir* **2013**, *29*, 6434.

(35) Li, M.-H.; Keller, P. *Soft Matter* **2009**, *5*, 927.

(36) Wang, Y.; Nie, J.; Chang, B.; Sun, Y.; Yang, W. *Biomacromolecules* **2013**, *14*, 3034.

(37) Ulasan, M.; Yavuz, E.; Bagriacik, E. U.; Cengeloglu, Y.; Yavuz, M. S. *J Biomed Mater Res A* **2014**, DOI: 10.1002/ jbm.a.35146.

(38) Oh, J. K.; Bencherif, S. A.; Matyjaszewski, K. *Polymer* **2009**, *50*, 4407.

(39) Gaulding, J. C.; Smith, M. H.; Hyatt, J. S.; Fernandez-Nieves, A.; Lyon, L. A. *Macromolecules* **2011**, *45*, 39.

(40) Oh, J. K.; Siegwart, D. J.; Lee, H.-i.; Sherwood, G.; Peteanu, L.; Hollinger, J. O.; Kataoka, K.; Matyjaszewski, K. *J. Am. Chem. Soc.* **2007**, *129*, 5939.

(41) Agrawal, G.; Wang, J.; Bruster, B.; Zhu, X.; Moller, M.; Pich, A. *Soft Matter* **2013**, *9*, 5380.

(42) Binauld, S.; Stenzel, M. H. *Chem. Commun.* **2013**, *49*, 2082.

(43) Aguirre, G.; Ramos, J.; Forcada, J. *Soft Matter* **2013**, *9*, 261.

(44) Shewan, H. M.; Stokes, J. R. *J. Food Eng.* **2013**, *119*, 781.

(45) Katona, J. M.; Sovilj, V. J.; Petrović, L. B. *Carbohydr. Polym.* **2010**, *79*, 563.

(46) Morimoto, N.; Endo, T.; Ohtomi, M.; Iwasaki, Y.; Akiyoshi, K. *Macromol. Biosci.* **2005**, *5*, 710.

(47) Zhu, P. W.; Napper, D. H. *Macromolecules* **1999**, *32*, 2068.

(48) Akiyoshi, K.; Kang, E.-C.; Kurumada, S.; Sunamoto, J.; Principi, T.; Winnik, F. M. *Macromolecules* **2000**, *33*, 3244.

(49) Morimoto, N.; Obeid, R.; Yamane, S.; Winnik, F. M.; Akiyoshi, K. *Soft Matter* **2009**, *5*, 1597.

(50) Chan, N.; An, S. Y.; Yee, N.; Oh, J. K. *Macromol. Rapid Commun.* **2014**, *35*, 752.

(51) Zhang, Q.; Re Ko, N.; Kwon Oh, J. *RSC Advances* **2012**, *2*, 8079.

(52) Aleksanian, S.; Khorsand, B.; Schmidt, R.; Oh, J. K. *Polymer Chemistry* **2012**, *3*, 2138.

(53) Morimoto, N.; Qiu, X.-P.; Winnik, F. M.; Akiyoshi, K. *Macromolecules* **2008**, *41*, 5985.

(54) Kang, M. K.; Hong, S. K.; Kim, J.-C. *J. Appl. Polym. Sci.* **2012**, *125*, 1993.

(55) Novoa-Carballal, R.; Pergushov, D. V.; Muller, A. H. E. *Soft Matter* **2013**, *9*, 4297.

(56) Urakami, H.; Hentschel, J.; Seetho, K.; Zeng, H.; Chawla, K.; Guan, Z. *Biomacromolecules* **2013**, *14*, 3682.

(57) Serra, C. A.; Chang, Z. *Chem. Eng. Technol.* **2008**, *31*, 1099.

(58) Whitesides, G. M. *Nature* **2006**, *442*, 368.

(59) Losey, M. W.; Jackman, R. J.; Firebaugh, S. L.; Schmidt, M. A.; Jensen, K. F. *Microelectromechanical Systems, Journal of* **2002**, *11*, 709.

(60) Teh, S.-Y.; Lin, R.; Hung, L.-H.; Lee, A. P. *Lab Chip* **2008**, *8*, 198.

(61) Xu, S.; Nie, Z.; Seo, M.; Lewis, P.; Kumacheva, E.; Stone, H. A.; Garstecki, P.; Weibel, D. B.; Gitlin, I.; Whitesides, G. M. *Angew. Chem. Int. Ed.* **2005**, *44*, 724.

(62) Dendukuri, D.; Pregibon, D. C.; Collins, J.; Hatton, T. A.; Doyle, P. S. *Nat. Mater.* **2006**, *5*, 365.

(63) Garstecki, P.; Fuerstman, M. J.; Stone, H. A.; Whitesides, G. M. *Lab Chip* **2006**, *6*, 437.

(64) Kesselman, L. R. B.; Shinwary, S.; Selvaganapathy, P. R.; Hoare, T. *Small* **2012**, *8*, 1092.

(65) Wang, Y.; Tumarkin, E.; Velasco, D.; Abolhasani, M.; Lau, W.; Kumacheva, E. *Lab Chip* **2013**, *13*, 2547.

(66) Seiffert, S.; Romanowsky, M. B.; Weitz, D. A. *Langmuir* **2010**, *26*, 14842.

(67) Hu, Y.; Wang, S.; Abbaspourrad, A.; Ardekani, A. M. *Langmuir* **2015**, *31*, 1885.

(68) Seiffert, S.; Thiele, J.; Abate, A. R.; Weitz, D. A. *J. Am. Chem. Soc.* **2010**, *132*, 6606.

(69) Kim, J.-W.; Utada, A. S.; Fernández-Nieves, A.; Hu, Z.; Weitz, D. A. *Angew. Chem.* **2007**, *119*, 1851.

(70) Zheng, B.; Tice, J. D.; Roach, L. S.; Ismagilov, R. F. *Angew. Chem. Int. Ed.* **2004**, *43*, 2508.

(71) Hu, Y.; Azadi, G.; Ardekani, A. M. *Carbohydr. Polym.* **2015**, *120*, 38.

(72) Wang, J.-T.; Wang, J.; Han, J.-J. *Small* **2011**, *7*, 1728.

(73) Steinbacher, J. L.; Moy, R. W. Y.; Price, K. E.; Cummings, M. A.; Roychowdhury, C.; Buffy, J. J.; Olbricht, W. L.; Haaf, M.; McQuade, D. T. *J. Am. Chem. Soc.* **2006**, *128*, 9442.

(74) Serra, C.; Berton, N.; Bouquey, M.; Prat, L.; Hadziioannou, G. *Langmuir* **2007**, *23*, 7745.

(75) Takeuchi, S.; Garstecki, P.; Weibel, D. B.; Whitesides, G. M. *Adv. Mater.* **2005**, *17*, 1067.

(76) Utada, A. S.; Lorenceau, E.; Link, D. R.; Kaplan, P. D.; Stone, H. A.; Weitz, D. A. *Science* **2005**, *308*, 537.

(77) Nisisako, T.; Torii, T.; Higuchi, T. *Chem. Eng. J.* **2004**, *101*, 23.

(78) Anna, S. L.; Bontoux, N.; Stone, H. A. *Appl. Phys. Lett.* **2003**, *82*, 364.

(79) Seo, M.; Nie, Z.; Xu, S.; Mok, M.; Lewis, P. C.; Graham, R.; Kumacheva, E. *Langmuir* **2005**, *21*, 11614.

(80) Hu, Y.; Wang, J.; Li, C.; Li, Z.; Liang, R.; Wang, Q.; Wang, H.; Zhu, J.; Yang, Y. *Science of Advanced Materials* **2015**, *7*, 902.

(81) Shepherd, R. F.; Conrad, J. C.; Rhodes, S. K.; Link, D. R.; Marquez, M.; Weitz, D. A.; Lewis, J. A. *Langmuir* **2006**, *22*, 8618.

(82) Duncanson, W. J.; Lin, T.; Abate, A. R.; Seiffert, S.; Shah, R. K.; Weitz, D. A. *Lab Chip* **2012**, *12*, 2135.

(83) Tumarkin, E.; Kumacheva, E. *Chem. Soc. Rev.* **2009**, *38*, 2161.

(84) Choi, C.-H.; Jung, J.-H.; Rhee, Y.; Kim, D.-P.; Shim, S.-E.; Lee, C.-S. *Biomed. Microdevices* **2007**, *9*, 855.

(85) Lian, M.; Collier, C. P.; Doktycz, M. J.; Retterer, S. T. *Biomicrofluidics* **2012**, *6*.

(86) Chau, M.; Abolhasani, M.; Thérien-Aubin, H.; Li, Y.; Wang, Y.; Velasco, D.; Tumarkin, E.; Ramachandran, A.; Kumacheva, E. *Biomacromolecules* **2014**, *15*, 2419.

(87) Wu, J.; Kong, T.; Yeung, K. W. K.; Shum, H. C.; Cheung, K. M. C.; Wang, L.; To, M. K. T. *Acta Biomater.* **2013**, *9*, 7410.

(88) Binks, B. P.; Fletcher, P. D. I. *Langmuir* **2001**, *17*, 4708.

(89) Nie, Z.; Li, W.; Seo, M.; Xu, S.; Kumacheva, E. *J. Am. Chem. Soc.* **2006**, *128*, 9408.

(90) Dendukuri, D.; Tsoi, K.; Hatton, T. A.; Doyle, P. S. *Langmuir* **2005**, *21*, 2113.

(91) Lehmann, S.; Seiffert, S.; Richtering, W. *J. Colloid Interface Sci.* **2014**, *431*, 204.

(92) Windbergs, M.; Zhao, Y.; Heyman, J.; Weitz, D. A. *J. Am. Chem. Soc.* **2013**, *135*, 7933.

(93) Martinez, C. J.; Kim, J. W.; Ye, C.; Ortiz, I.; Rowat, A. C.; Marquez, M.; Weitz, D. *Macromol. Biosci.* **2012**, *12*, 946.

(94) Headen, D. M.; Aubry, G.; Lu, H.; García, A. J. *Adv. Mater.* **2014**, *26*, 3003.

(95) McGillicuddy, F. C.; Lynch, I.; Rochev, Y. A.; Burke, M.; Dawson, K. A.; Gallagher, W. M.; Keenan, A. K. *J. Biomed. Mater. Res. A* **2006**, *79A*, 923.

(96) Soddemann, M.; Richtering, W. In *Mesophases, Polymers, and Particles*; Springer Berlin Heidelberg: 2004; Vol. 129, p 88.

(97) Chen, P.-C.; Kohane, D. S.; Park, Y. J.; Bartlett, R. H.; Langer, R.; Yang, V. C. *J. Biomed. Mater. Res. A* **2004**, *70A*, 459.

(98) Sivakumaran, D.; Maitland, D.; Hoare, T. *Biomacromolecules* **2011**, *12*, 4112.

(99) Meid, J.; Dierkes, F.; Cui, J.; Messing, R.; Crosby, A. J.; Schmidt, A.; Richtering, W. *Soft Matter* **2012**, *8*, 4254.

(100) Song, W.; Guan, Y.; Zhang, Y.; Zhu, X. X. *Soft Matter* **2013**, *9*, 2629.

(101) Mourtas, S.; Fotopoulou, S.; Duraj, S.; Sfika, V.; Tsakiroglou, C.; Antimisiaris, S. G. *Colloids Surf., B* **2007**, *55*, 212.

(102) DeFail, A. J.; Edington, H. D.; Matthews, S.; Lee, W.-C. C.; Marra, K. G. *Journal of Biomedical Materials Research Part A* **2006**, *79A*, 954.

(103) Lynch, I.; de Gregorio, P.; Dawson, K. A. *J. Phys. Chem. B* **2005**, *109*, 6257.

(104) DeFail, A. J.; Chu, C. R.; Izzo, N.; Marra, K. G. *Biomaterials* **2006**, *27*, 1579.

(105) Lee, J.; Bhang, S.; Park, H.; Kim, B.-S.; Lee, K. *Pharm. Res.* **2010**, *27*, 767.

(106) des Rieux, A.; Ucakar, B.; Mupendwa, B. P. K.; Colau, D.; Feron, O.; Carmeliet, P.; Préat, V. *J. Controlled Release* **2011**, *150*, 272.

(107) Sivakumaran, D.; Maitland, D.; Oszustowicz, T.; Hoare, T. *J. Colloid Interface Sci.* **2013**, *392*, 422.

(108) Campbell, S.; Maitland, D.; Hoare, T. *ACS Macro Letters* **2015**, 312.

(109) Smeets, N. M. B.; Bakaic, E.; Patenaude, M.; Hoare, T. *Chem. Commun.* **2014**, *50*, 3306.

# Chapter 1

# TUNING DRUG RELEASE FROM SMART MICROGEL-HYDROGEL COMPOSITES VIA CROSS-LINKING

**Authors:** Daryl Sivakumaran, Danielle Maitland, Thomas Oszustowicz, and Todd Hoare

**Publication:** Journal of Colloid and Interface Science, 392, 422-430

**Publication Date:** February 2013



## 1.1 Abstract

Soft nanocomposite hydrogels consisting of thermoresponsive microgels physically entrapped or covalently cross-linked to a non-thermoresponsive hydrogel are synthesized and tested for their capacity to facilitate long-term drug release of a small molecule drug. Copolymer microgels based on N-isopropylacrylamide and acrylic acid were synthesized that exhibited ionic affinity for binding to bupivacaine, a cationic local anesthetic. These microgels were subsequently physically entrapped within an *in situ*-gelling carbohydrate-based hydrogel network cross-linked via hydrazide-aldehyde chemistry; alternately, hydrazide-functionalized microgels were prepared that covalently cross-linked to the bulk hydrogel phase. Both the overall rate of drug release and the magnitude of the burst release were significantly decreased when microgels were restricted from undergoing a phase transition between the preparation temperature of the nanocomposite (25°C) and the test temperature (37°C), whether deswelling was inhibited by increasing the cross-link

density within the microgel itself or by cross-linking the microgel to the bulk hydrogel network. This result facilitates facile tuning of soft nanocomposite drug delivery systems to achieve targeted drug release kinetics.

**Keywords**

Microgels, *in-situ* gelling, nanocomposite hydrogels, drug delivery

## 1.2 Introduction

Hydrogels have been widely investigated for facilitating the controlled release of a variety of clinically-relevant drugs[1-9]. Hydrogels have found particular utility in the area of controlled release since they can be loaded with high fractions of drugs due to their high internal free volume and can be fabricated to have similar physical, mechanical, and chemical properties to native extracellular matrix, which generally results in high biocompatibility in a variety of biological environments[10-13]. However, traditional hydrogels suffer from two key limitations to their facile use in biological applications: (1) their high elasticity coupled with their macroscopic dimensions make them difficult to administer via injection, instead requiring surgical insertion[1]; (2) the highly hydrated microstructure results in poor uptake of hydrophobic drugs[14] and rapid release of hydrophilic drugs[1,15], limiting both the types and the rates of drug release that are possible from hydrogel-based systems. While a range of physical self-assembly approaches[3,16-18] and several rapid covalent bond forming chemistries compatible with physiological conditions[5,19-21] have been developed to facilitate injectability, the long-term release of hydrophilic drugs remains a challenge, with few formulations reported to achieve release durations for greater than one month.[15]

In order to address this problem, a range of multi-phase, “plum pudding” hydrogels have been developed in which a variety of nano or micron-sized drug carriers (e.g. liposomes[22], polymer nanoparticles[23], polymer microparticles[24], and microgels[25-28]) are physically entrapped inside hydrogels. Relative to single phase bulk hydrogels, multi-

phase hydrogels can introduce affinity sites that facilitate increased loading of a target drug[29] as well as additional diffusive and/or partitioning barriers to tune the release of that drug through the bulk hydrogel phase[30-32]. For example, the burst effect often seen in microgel-based drug release could be mitigated in a composite hydrogel system[32,33]. Relative to the use of the drug carriers alone, the hydrogel can immobilize the nanocarrier at the injection site to facilitate local drug delivery[1,34] and mask any potential immune or inflammatory reactions to the nanocarrier[35].

Microgel-hydrogel (i.e. "soft") nanocomposites have particular advantages for the delivery of water-soluble drugs. Given that both phases of a microgel-hydrogel nanocomposite are hydrogel-based, these materials offer the unique potential to independently engineer both the hydrogel and microgel phase to optimize the drug release profile through the use of differential drug partitioning[36] or cross-linking[37] between the two gel phases. In addition, the degree of swelling of both hydrogel-based phases can be tuned to dynamically create internal stresses or free volume[28,37,38] within the soft nanocomposite system, offering the potential for on-demand control over both drug partitioning and drug diffusion over the course of drug release.

We have previously reported[33] on the formation of soft nanocomposite hydrogels based on entrapping anionically-functionalized microgels (based on thermoresponsive poly(N-isopropylacrylamide))[39] inside a non-thermoresponsive *in situ*-gelling carbohydrate-based hydrogel (formed via hydrazide-aldehyde chemistry)[40]. The anionic microgels exhibited a high local affinity for cationic drugs (using bupivacaine, a local anesthetic, as a drug model), facilitating drug release for up to 60 days depending on the

acid content of the microgel (i.e. the ionic affinity of the embedded microgel phase for the drug). The cross-linking density of bulk hydrogels can also be modified to tune the average pore size and thus the rate of drug diffusion from the hydrogel[41]. However, the impact of the microgel phase transition on the drug release profile (i.e. the partitioning and diffusion of drug through the hydrogel) was not thoroughly investigated. Richtering's group has previously shown that the phase transition behavior of embedded microgels can have a significant impact on the swelling, mechanical, and optical properties of the nanocomposite[28,37]. Given the rapid speed of the hydrazide-aldehyde reaction in our nanocomposite hydrogel system, the hydrogel phase entraps the microgels before the microgels undergo their phase transition; as such, we expect that regulating the phase transition of the microgel may have significant impacts on both drug affinity and drug diffusion over time from the soft nanocomposite system.

To investigate the impact of the microgel phase transition on drug transport through soft nanocomposites, we show in this paper physical constraint of the phase transition of microgels by (a) increasing the cross-link density within individual microgels and (b) covalently attaching the microgel to the hydrogel phase using the same hydrazide-aldehyde chemistry applied to form the bulk hydrogel. Specifically, we investigate whether the duration and/or the uniformity of the drug release from soft nanoparticle systems can be changed by locally constricting the occurrence of a phase transition.

**Experimental**

*Materials:* N-isopropylacylamide (NIPAM, 99%), acrylic acid (AA, 99%), ammonium persulfate (APS, 99%), N,N'-methylenebisacrylamide (MBA, 99%), sodium carboxymethyl cellulose (CMC) [MW 250,000, DS = 0.9], adipic acid dihydrazide (ADH, 98%) N-hydroxysuccinimide (NHS, 97%), N'-ethyl-N-(3-dimethylaminopropyl)-carbodiimide (EDC, commercial grade), dextran from *Leuconstroc spp* [$M_r$ – 500,000], ethylene glycol (99.8%), sodium periodate (>99.8%), and bupivacaine hydrochloride (99%) were all purchased from Sigma Aldrich (Oakville, ON). Sodium dodecyl sulfate (SDS, electrophoresis grade) was obtained from Bioshop Canada (Burlington, ON). Dimethyl sulfoxide (DMSO, reagent grade) was purchased from Caledon Laboratory Chemicals (Georgetown, ON). 3T3 *Mus musculus* mouse cells, C2C12 mouse muscle myoblast cells and RAW 264.7 macrophage mouse cells were acquired from ATCC: Cederlane Laboratories Ltd. (Burlington, ON). Media contents included Dulbecco's Modified Eagle Medium-high glucose (DMEM), fetal bovine serum (FBS), horse serum (HS), and penicillin streptomycin (PS), all of which were obtained from Invitrogen Canada (Burlington, ON). Recovery cell culture freezing and trypsin-EDTA were purchased from Invitrogen Canada (Burlington, ON). Thiazolyl blue tetrazolium bromide (MTT) was purchased from Sigma Aldrich (Oakville, ON).

*Microgel Synthesis:* Acrylic acid-functionalized poly(NIPAM)-based microgels (AA-NIPAM) were synthesized via a mixed precipitation-emulsion polymerization according to the formulations given in Table 1.1. Microgels were synthesized based on methods

described by Hoare and Pelton[39]. Microgel polymerization was conducted using a three-necked flask with attached condenser and mixing through the use of a magnetic stirrer at a rate of 200rpm. Polymerization formulations contained specified amounts of NIPAM monomer, acrylic acid, MBA cross-linker, and SDS were dissolved in 150mL of Milli-Q water. The contents were allowed mix at 70˚C with a nitrogen purge for 30 minutes prior to the addition of APS (dissolved in 10mL of Milli-Q water) for the initiation of polymerization. Polymerization was allowed to occur for 12 hours and was followed by purification though dialysis against Milli-Q water in membrane tubing from Spectrum Labs with a molecular weight cut-off of 12,000 – 14,000 Da. A minimum of 6 dialysis cycles were conducted prior to the solutions being lyophilized and stored dry for future use.

**Table 1.1:** Recipes for acrylic acid-functionalized microgels

| **Microgel Code** | **NIPAM (g)** | **Acrylic Acid (g)** | **MBA (g)** | **SDS (g)** | **APS (g)** | **mol % AA in microgel (theoretical)** | **mol % AA in microgel (actual)** |
|---|---|---|---|---|---|---|---|
| AA6% - MBA -l% | 1.4 | 0.058 | 0.02 | 0.2 | 0.1 | 6.1 | 6.8 ± 1.0 |
| AA6% - MBA -5% | 1.4 | 0.058 | 0.1 | 0.2 | 0.1 | 6.1 | 7.9 ± 1.2 |
| AA6% - MBA -9% | 1.4 | 0.058 | 0.18 | 0.2 | 0.1 | 6.1 | 7.2 ± 1.0 |
| AA20%- MBA -1% | 1.4 | 0.232 | 0.02 | 0.2 | 0.1 | 20.6 | 15.7 ± 2.1 |
| AA20%- MBA -5% | 1.4 | 0.232 | 0.1 | 0.2 | 0.1 | 20.6 | 20.3 ± 1.2 |
| AA20%- MBA -9% | 1.4 | 0.232 | 0.18 | 0.2 | 0.1 | 20.6 | 18.7 ± 2.7 |
| AA33% - MBA – 5% | 1.4 | 0.464 | 0.1 | 0.2 | 0.1 | 33 | 28.2 ± 1.2 |

The percentage of acrylic acid incorporated into the microgel was measured via conductometric titration, performed using a Burivar-I2 automatic buret (ManTech associates). 50 mg CMC-A was dissolved in 50 mL of $10^{-3}$M NaCl. The pH was adjusted to ~3 using 0.1M HCl, after which base-into-acid titration was performed using 0.1 M NaOH Acculute standards at a rate of 10 min/unit pH.

*Hydrazide Functionalized Carboxymethyl Cellulose and AA-NIPAM Modification:* Hydrazide functionalization of CMC and AA-NIPAM was conducted using NHS/EDC chemistry[42] according to the recipes given in 1.2. The "Hzd-xx" indication in the material code refers to the percentage of –COOH groups that were converted to hydrazide groups as a result of the EDC coupling chemistry performed.

**Table 1.2:** Recipes for hydrazide-functionalized carboxymethyl cellulose polymer and AA-NIPAM microgels

| **Code** | **AA-NIPAM (g)** | **CMC (g)** | **ADH (g)** | **NHS (g)** | **EDC (g)** | **$H_20$ (mL)** | **% -available COOH Groups Reacted** | **hydrazide groups per polymer chain/microgel** |
|---|---|---|---|---|---|---|---|---|
| CMC-Hdz-44 | 0 | 1 | 3 | 0.07 | 0.3 | 200 | 44% ± 5 | ~ 550 |
| AA-6%-Hdz-44 | 1 | 0 | 3 | 0.07 | 0.3 | 200 | 33% ± 2 | ~ 5.3 x $10^5$ |
| AA-33%-Hzd-44 | 1 | 0 | 3 | 0.07 | 0.3 | 200 | 42% ± 6 | ~ 6.9 x $10^7$ |

Carboxymethyl cellulose (250kDa) or AA-NIPAM microgel was dissolved in 200mL Milli-Q water at 200rpm using magnetic stirring within a 250mL round bottom flask. Appropriate amounts of adipic acid dihydrazide (ADH) were added to the polymer solution, which resulted in a solution pH of ~ 7. N-hydroxysuccinimide (NHS) was dissolved in 4 mL DMSO:$H_20$ (1:1) and N'-ethyl-N-(3- dimethylaminopropyl)-carbodiimide (EDC) was dissolved in 1 mL of 1:1 DMSO:$H_20$. The NHS solution was then added drop-wise to the polymer:ADH mixture followed by the drop-wise addition of the EDC solution. For modification to occur, the pH of the solution was continuously maintained at 6.8 using 0.1M NaOH during a 1 hour reaction period. The resulting polymer was dialyzed with membrane tubing (Spectrum Labs, molecular weight cut-off 3,500 Da) for a minimum of 6 dialysis cycles prior the polymers solutions being lyophilized and stored. Hydrazide functionalization was determined by measuring the moles of –COOH in unmodified CMC or AA-NIPAM microgels and comparing it to that of the hydrazide-modified polymers, assuming that the functionalization of a single hydrazide group on to the polymer/microgel consumes one carboxylic acid group, using potentiometric and conductometric titration as described previously (see Supplementary Data, Figure S1.1).

*Aldehyde Functionalized Dextran (B Polymer):* Aldehyde functionalization of dextran was achieved through sodium periodate-mediated oxidation. Dextran (1.5 g) was dissolved in 150 mL Mill-Q water under magnetic stirring at 200rpm. Sodium periodate (0.8 g) was dissolved in 10 mL water and added dropwise to the dextran solution, and

allowed to stir for 2 hours for oxidation to occur. The reaction was stopped with the addition of ethylene glycol (0.4 mL), which was injected into the solution and allowed to react for 1 hour. The aldehyde functionalized dextran was then dialyzed using membrane tubing (Spectrum Labs, molecular weight cut-off 3,500 Da) for a minimum of 6 wash cycles with Milli-Q water. The purified polymer was lyophilized and stored dry. The resultant aldehyde content 37% ± 6% hydroxyl conversation of the dextran was measured using the TNBS assay on the final product[43].

*Hydrogel-Microgel Composite:* Hydrogel-microgel composites were created through the use of hydrazide-functionalized CMC (CMC-Hdz) and aldehyde functionalized dextran (Dex-B) as injectable precursors. The composites were formed with the use of a double-barrelled syringe (Medmix Systems, Switzerland), in which each reactive component (in solution or suspension) is placed into separate 2mL barrels. The individual polymers are dissolved in 0.15M saline to give a precursor concentration of 2w/v%. One barrel contains the CMC-Hdz polymer where as the other barrel contains the Dex-B polymer, AA-NIPAM microgels (80mg, 4w/v%), and bupivacaine (20mg, 5mg/mL). When hydrazide functionalized AA-NIPAM was used, the microgels were placed in the barrel containing the CMC-Hdz instead of the Dex-B barrel to prevent premature gelation in the syringe. A 20-gauge needle was affixed to the mixer end of the double barrel syringe to facilitate extrusion of the hydrogel precursors into cylindrical silicone rubber moulds (diameter 0.95 cm and height 0.32 cm) for testing drug release kinetics; all gels were

removed from the moulds prior to testing immediately after gelation was complete such that there was no significant drug loss in the moulds.

*Rheology:* Mechanical measurements on the hydrogel composite and hydrogel-microgel composite were performed by following procedures set by Motlagh[44]. Complex viscosity ($\eta^*$) and storage (G') and loss moduli (G") were measured with an ARES rheometer (TA Instruments) using parallel-plate geometry. The parallel plate geometry had a diameter of 7 mm and a gap (gel thickness) of 1 mm. A stress sweep was first performed to identify the linear viscoelastic range of each hydrogel composite, followed by a frequency sweep over the range of 0.1-100 rad/s to determine the shear-dependent complex viscosity, G', and G" of the composite. All rheological measurements were conducted at 21°C.

*Dynamic Light Scattering:* Particle sizing of the microgels was conducted with dynamic light scattering using a 90° detection angle and a 632.8 nm laser (Brookhaven Instruments). Dried microgels were suspended in 10 mM phosphate-buffered saline (PBS, pH 7.4, overall ionic strength 0.15 M) at a concentration of 4 mg/mL, producing an intensity count between 100-250 kilocounts per second. At least five replicates were conducted for each sample; the experimental uncertainties represent the standard deviation of the replicate measurements.

*Electrophoretic Mobility:* Electrophoretic mobility was measured using a ZetaPlus zeta potential analyser operating in PALS (phase analysis light scattering) mode (Brookhaven

Instruments). Samples were prepared in 10mM PBS (pH 7.4, overall ionic strength 0.15 M) and measured in triplicate, with each run consisting of 15 cycles; the experimental uncertainties represent the standard error of the replicate measurements.

*Microgel Drug Release Studies:* Drug release studies of bupivacaine from AA-NIPAM microgels were conducted with 1mL Float-a-Lyzer cellulose membranes (Spectrum Laboratories) with a molecular weight cut-off of 100 kDa. A mixture of 4 mg/mL AA-NIPAM and 5mg/mL bupivacaine was made, with 0.67mL of the mixture transferred into separate Float-a-Lyzer membranes ($n$ = 6). 10mM PBS (6mL, pH 7.4, ionic strength 0.15 M) was used as an elution medium. This form of PBS was used as it is isotonic with the body and thus a reasonable mimic of *in vivo* conditions, at least from an ionic perspective (crucial given the importance of electrostatics/ion exchange in regulating drug release in this system). Sampling occurred every 30 minutes for the first 3 hours to detect any burst release; samples continued to be collected until drug was no longer detected in the eluent using a DU 800 UV/visible spectrophotometer (Beckman Coulter) operating at a wavelength of 262 nm.

*Hydrogel and Microgel-Hydrogel Composite Drug Release Studies:* Drug release from the hydrogels and composites were completed within a 12-well cell culture plates with the gels contained within cell culture inserts (2.5 cm diameter, 8 μm pore size). The cell inserts were punctured with 20 gauge needle a total of 20 times to ensure flow of elution media into and around the hydrogel. A total of 2mL of 10 mM PBS was used in each cell culture well as an elution media for bupivacaine release; while the buffer was added

inside the well, the punctures placed in the membrane allowed free flow of PBS between the insert and the outside well, with the 2mL volume added ensuring the gel remained fully submerged in buffer at all times. A total of 6 hydrogels or composites were used for each formulation to determine their drug release profile. During the drug release phase, hydrogels and composites were incubated in an orbital shaker at 37°C at an oscillation rate of 100 rpm. Elution media was changed every 30 minutes for the first 2 hours to capture burst release effects and every hour for the next 5 hours and daily of the course of the gel lifetime. Note that all drug concentrations assayed represent <10% of the solubility of the drug in the 10 mM PBS release solution such that infinite sink conditions were satisfied in all cases. At each time point, the inserts were removed from the multiwell plate, placed into a new plate with fresh (temperature equilibrated) buffer, and returned to the incubating shaker; the previous plate with the release media from the previous time point was then sealed with parafilm for no more than one day prior to testing. Note that these procedures were consistent for all drug release kinetics experiments on bulk hydrogels reported in this thesis. Drug concentrations were measured using a DU 800 UV/visible spectrophotometer (Beckman Coulter) at a wavelength of 262 nm.

*Gel Swelling:* Swelling of the microgel-hydrogel composites was determined by measuring gel mass immediately after gelation and comparing this initial mass to the mass of the gel after it has been submersed in 10 mM PBS at 37°C at various times. The percentage mass changes were calculated according to the following equation:

$$\%Mass\,Change = \frac{Mass_{37^oC} - Mass_{20^oC}}{Mass_{20^oC}} \quad (1)$$

The mass of the gels was measured at each time point of the release study which allowed for tracking of the gel mass and the subsequent degradation/swelling through the duration of the entire study. At least six replicates were conducted for each sample; the experimental uncertainties represent the standard deviation of the replicate measurements.

## 1.4 Results

*Hydrogel Precursor and Microgel Characterization:* The reactions performed to functionalize the carbohydrates successfully generated hydrazide and aldehyde-reactive carbohydrates that offer the possibility of preparing *in situ*-gelling hydrogels with varying cross-linking densities. Acrylic acid was incorporated nearly quantitatively into all microgels (Table 1.1), consistent with previous literature observations[45]; however, low cross-link densities led to significantly lower acrylic acid incorporations relative to theory. Since crosslinker is typically consumed early in the microgel synthesis[45], this result is likely attributable to the lack of cross-linker available later in the synthesis to covalently connect AA-rich polymer chains to the growing microgel particles. Table 1.3 shows the microgel particle size and electrophoretic mobility (related to surface charge density[46]) at both the preparation temperature for the nanocomposite hydrogels (25°C) and at physiological temperature (37 °C).

**Table 1.3:** Hydrodynamic diameter and electrophoretic mobility of AA-NIPAM microgels with varying cross-linker contents in 10 mM PBS (pH 7.4, ionic strength 0.15 M)

| **Microgel** | **Particle Size (nm)** | | **% deswelling** | **Electrophoretic Mobility ($x10^{-8}$ $m^2/Vs$)** | |
|---|---|---|---|---|---|
| | **25°C** | **37°C** | | **25°C** | **37°C** |
| AA6% - MBA -l% | 168 ± 5 | 107 ± 3 | -36% ± 2% | -0.59 ± 0.33 | -0.98 ± 0.29 |
| AA6% - MBA -5% | 133 ± 8 | 89 ± 1 | -33% ± 2% | -0.67 ± 0.13 | -1.10 ± 0.34 |
| AA6% - MBA -9% | 115 ± 4 | 79.0 ± 2 | -31% ± 2% | -0.73 ± 0.24 | -1.63 ± 0.60 |
| AA20%- MBA -1% | 460 ± 10 | 325 ± 13 | -29% ± 2% | -0.99 ± 0.13 | -1.42 ± 0.19 |
| AA20%- MBA -5% | 271 ± 19 | 206 ± 5 | -24% ± 2% | -1.00 ± 0.21 | -1.83 ± 0.25 |
| AA20%- MBA -9% | 145 ± 1 | 143 ± 3 | -1% ± 1% | -1.31 ± 0.19 | -1.99 ± 0.52 |

Overall, microgels with increased cross-linker contents had smaller particle sizes and smaller mobilities at both 25°C and 37°C, consistent with previous studies[47,48] and thermodynamic gel swelling theory assuming all other attributes of the microgel remain constant[49]. Decreases in particle size are observed as the microgel passes through the phase-transition temperature, again consistent with previous literature[39]. This result suggests that the tested microgels will deswell relative to their entrapped size within the soft nanocomposite hydrogel as they are heated to physiological temperature. However, as the degree of cross-linking is increased (at both acrylic acid loadings tested), the

magnitude of the deswelling transition is decreased due to the increased elastic driving force opposing hydrogel swelling; for example, high cross-link density AA-20%- MBA-9% microgels effectively do not deswell while low cross-link density AA-20%-MBA-l% microgels undergo a ~3-fold decrease in volume over the same temperature range. Thus, by modifying the cross-link density of the microgels, the deswelling transition can be tuned and, in some cases, even turned off without changing the overall acid content (i.e. number of affinity groups for cationic drug targets) in the microgel.

Microgels with the same overall AA content but lower cross-link densities exhibit lower absolute electrophoretic mobilities than microgels with higher cross-link densities, consistent with the higher capacity for swelling in microgels with lower cross-link densities (i.e. lower elastic resistances to swelling). In addition, the absolute electrophoretic mobility of each microgel increases as the temperature is increased, attributable to the decrease in swelling (and thus increase in effective charge density) that occurs upon a phase transition. Interestingly, this increase in absolute mobility occurs even when the bulk size of the microgel does not significantly change (e.g. AA-20%-MBA-9%), suggesting that internal structural rearrangements occur within the microgels as they are heated.

Table 1.4 shows the size and electrophoretic mobility properties of microgels functionalized with reactive hydrazide groups. The microgel code “Hzd-xx” refers to the percentage of acrylic acid groups converted to hydrazide groups in the hydrazide-functionalized microgel (as measured by conductometric titration).

**Table 1.4:** Hydrodynamic diameter and electrophoretic mobility of AA-NIPAM microgels functionalized with adipic dihydrazide

| **Microgel** | **Particle Size (nm)** | | **% deswelling** | **Electrophoretic Mobility ($x10^{-8}$ $m^2/Vs$)** | |
|---|---|---|---|---|---|
| | **25°C** | **37°C** | | **25°C** | **37°C** |
| AA-6%-MBA –5% | 133 ± 8 | 89 ± 1 | -33% ± 2% | -0.67 ± 0.13 | -1.10 ± 0.34 |
| AA-6%--MBA-5%-Hzd-44 | 121 ± 7.6 | 77 ± 5.2 | -36% ± 5% | -0.54 ± 0.34 | -0.97 ± 0.24 |
| AA-33% -MBA–5% | 324.5 ± 8.5 | 282.2 ± 7.2 | -13% ± 1% | -1.28 ± 0.18 | -2.45 ± 0.22 |
| AA-33% -MBA–5%- Hzd-44 | 280.2 ± 4.1 | 222.1 ± 9.9 | -21% ± 1% | -1.00 ± 0.19 | -1.96 ± 0.25 |

Hydrazide functionalization of microgels results in a decrease in the particle size, a lower absolute electrophoretic mobility, and a higher magnitude of microgel deswelling upon heating relative to the unmodified microgels, all due to the consumption of ionic acrylic groups during the hydrazide attachment process. However, all microgels remained colloidally stable and thermoresponsive following hydrazide functionalization prior to cross-linking into the hydrogel.

*Mechanical Characterization:* Gelling times for hydrogel formation following injection through the double barrelled syringes varied between 5-15 seconds. The hydrogels produced were mechanically robust and easily handled over multiple cycles without

inducing any mechanical degradation. Rheological tests were performed to determine the impact of microgel stiffness and microgel conjugation to the bulk hydrogel network on the mechanical properties of the hydrogels. The effect of physically embedding microgels with different internal cross-link densities on the gel mechanical properties is shown in Figure 1.1.

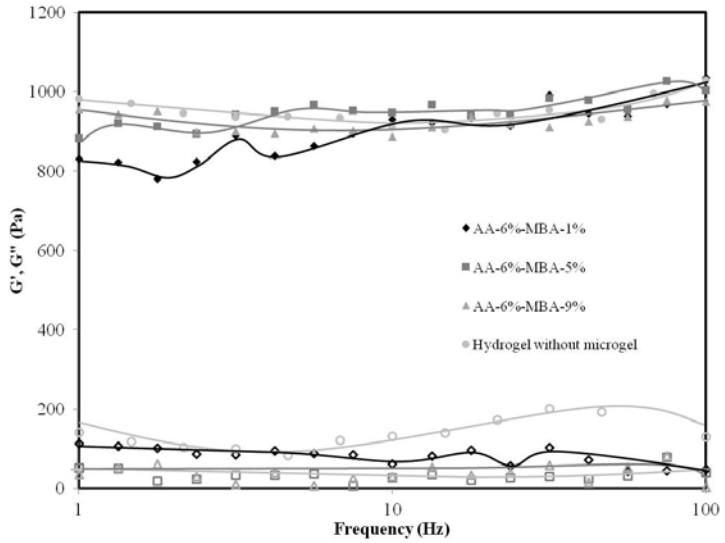


**Figure 1.1:** G' and G" values for CMC-Hdz/Dextran-B hydrogels containing physically-entrapped AA-6% NIPAM microgels prepared with various amounts of MBA (G' – filled, G"-unfilled)

The incorporation of microgels with varying amounts of cross-linker has no significant impact on the mechanical properties of the composite, with both G' and G" of the soft nanocomposite remaining unchanged regardless of the cross-link density of the embedded microgel; this effect was confirmed with the AA-20% microgels (Supplementary Data, Figure S1.2). The presence of the microgels similarly has no significant impact on the

hydrogel mechanical properties. Thus, the mechanical properties of the soft nanocomposite are independent of the mechanical properties of the physically entrapped microgel phase, at least within the range of microgel:hydrogel mass ratios and microgel elasticities considered in our work.

When the microgels are functionalized with hydrazide groups such that they can also participate in the gelation chemistry, Figure 1.2 shows that the elastic modulus of the hydrogels significantly increases as a function of the degree of hydrazide functionalization of the AA-NIPAM microgels.

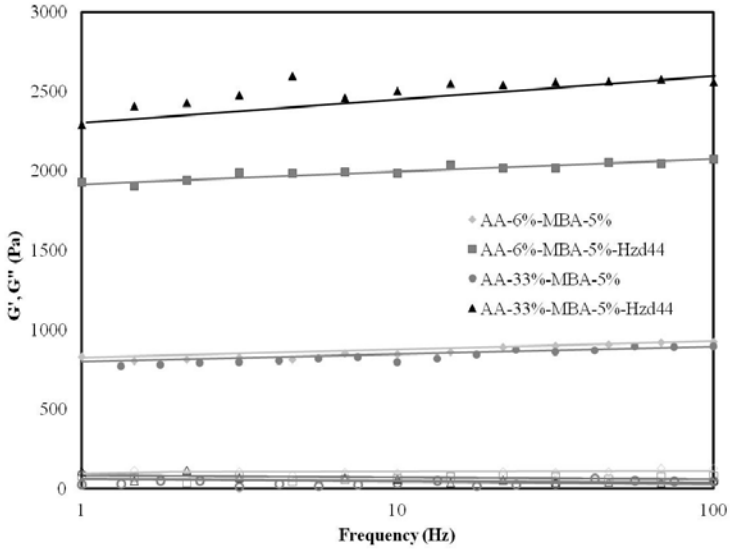


**Figure 1.2:** G' and G" values for CMC-Hdz/Dextran-B hydrogels containing hydrazide-functionalized microgels (G'- filled, G"-unfilled)

Microgel AA-6% -MBA-5%-Hzd-44, modified such that ~3 mol% of all monomer residues contain hydrazide groups, exhibited a ~140% increase in elastic modulus

relative to a physically entrapped soft nanocomposite hydrogel containing the same fraction of AA-6%-MBA-5% microgels without hydrazide groups. Increasing the total number of hydrazide groups in the microgel further increases the elastic modulus of the hydrogel, as indicated by the ~20% increase in G' comparing AA-6% -MBA-5%-Hzd-44 (~ $5.3 \times 10^5$ hydrazide groups per microgel) and AA-33% -MBA-5%-Hzd-44 (~ $6.9 \times 10^7$ hydrazide groups per microgel, Table 1.3). These results suggest that hydrazide-functionalized microgels are participating in the cross-linking reaction forming the bulk gel and thereby effectively increase the local cross-link density within the soft nanocomposite.

*Drug Release Kinetics – Physically Entrapped Microgels:* Bupivacaine release was assayed from a range of hydrogel-microgel composites, using 10 mM PBS as the release medium. Figure 1.3 and Supplementary Data, Figure S1.3 show the effect of increasing the amount of cross-linker in AA-6% (Fig. 1.3) and AA-20% (Fig. S1.3) microgels on the drug release kinetics of hydrogel-entrapped microgel soft nanocomposites.

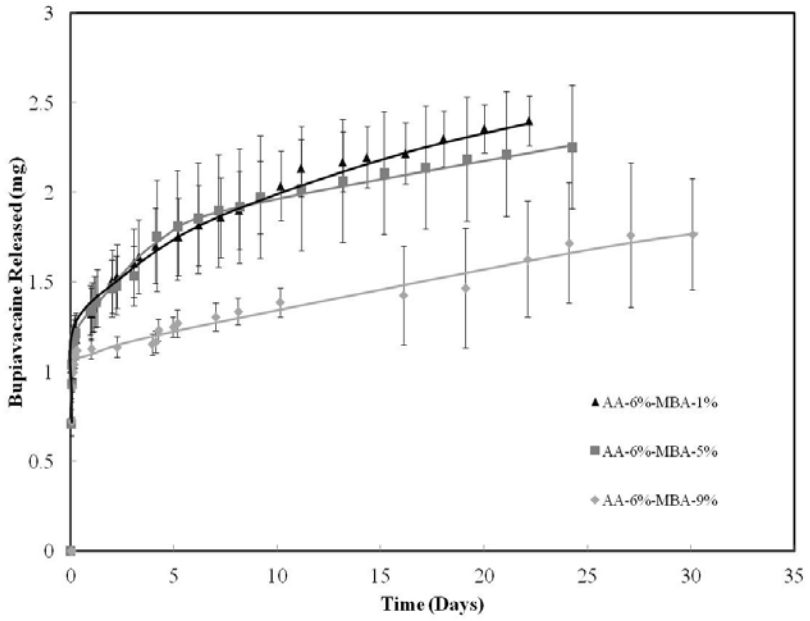


**Figure 1.3:** Bupivacaine release from nanocomposite hydrogels consisting of a 50:50 (wt%) mixture of AA-6% microgels with various MBA contents embedded inside a CMC-Hzd/Dex-B hydrogel

As the mole percentage of N,N'-methylenebisacrylamide cross-linker in the microgel is increased, both the amount of drug released and the rate of drug release decreased throughout the entire duration of drug delivery for both AA-6% and AA-20% microgels. Furthermore, the burst release of drug observed at short times was reduced as the degree of cross-linking was increased. This trend is echoed by microgel-only drug release experiments, in which microgels with higher cross-link densities released drug with a lower burst over a longer period of time compared to less cross-linked microgels that could undergo larger phase transitions with the same degree of AA functionalization

(Supplementary Data, Figure S1.4). However, drug release from microgels alone was completed after ~2 days for AA-6% microgels and ~4 days for AA-20% microgels (Fig. S1.4, with the difference attributable to the higher electrostatic interactions between the microgels and the cationic drug), significantly shorter durations of release than were achieved with the microgel-hydrogel composites (Figs. 1.3 and 1.S3). Thus, while the relative release kinetics are correlated with the microgel behavior, the absolute release kinetics are strongly influenced presence of the bulk hydrogel. It is important to note that the differences in cross-link density of the microgels do not affect the overall swelling characteristics of the composite (Figure 1.4), further indicating the independence of the microgel and hydrogel phases in physically-entrapped nanocomposite hydrogels.

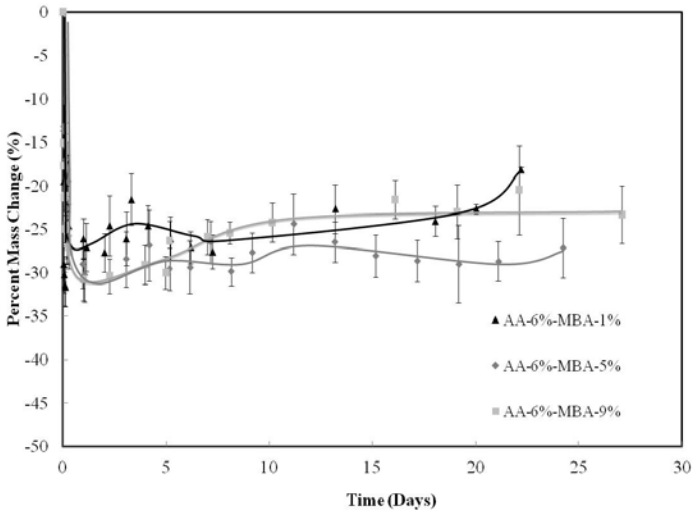


**Figure 1.4:** Deswelling response from CMC-Hzd/Dextran-B nanocomposite hydrogels containing physically-entrapped AA-20% microgels prepared with varying contents of MBA cross-linker

Our previous observation that increasing the acrylic acid content of the microgel (i.e. increasing the number of anionic binding sites for cationic bupivacaine) decreases both the amount and rate of drug released over the full duration of a release experiment[33] still applies as the amount of cross-linker used to prepare the embedded microgel phase is decreased, as shown in Figure 1.5.

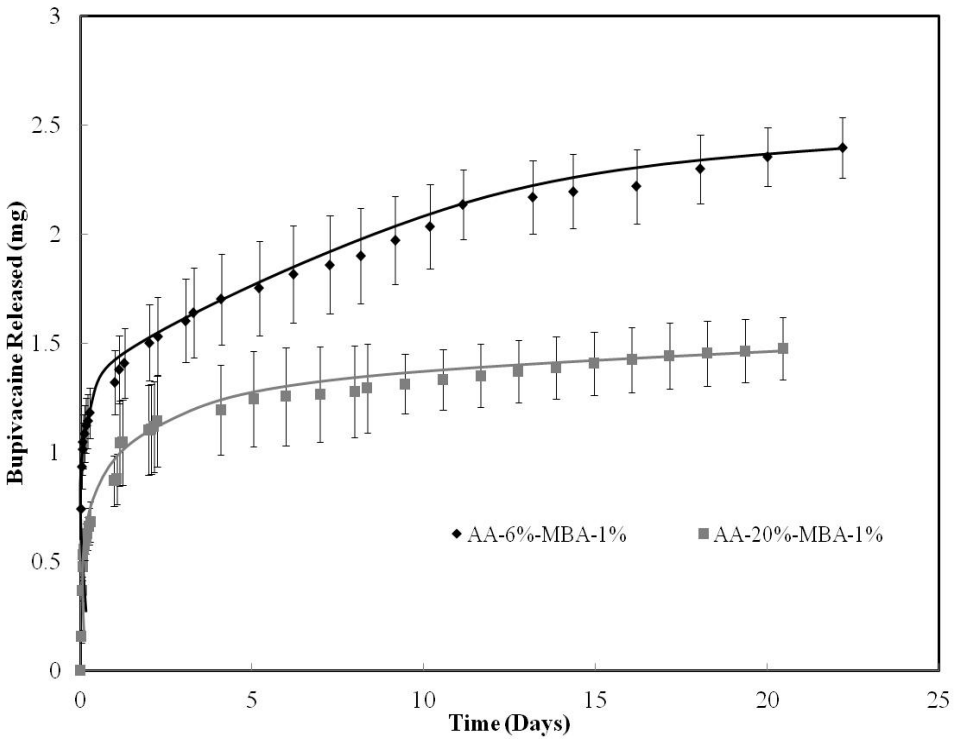


**Figure 1.5:** Bupivacaine release from nanocomposite hydrogels consisting of a 50:50 (wt%) mixture of AA-NIPAM-MBA-1% microgels prepared with 6mol% and 20mol% acrylic acid embedded inside a CMC-Hzd/Dextran-B hydrogel

An identical trend was observed for the highly-cross-linked MBA-9% microgels (see Supplementary Data, Figure S1.5), showing that this effect is independent of the cross-

link density. Based on this result, the observed differences in drug release kinetics cannot be attributed to differences in bupivacaine affinity to the microgels as a function of cross-linker content. Coupling all these observations with the observed size changes in the microgels as they are heated from the gel preparation temperature to physiological temperature (Table 1.3), the swelling/deswelling responses of embedded microgels within the bulk hydrogel phase appear to be the primary driver for controlling drug release kinetics from soft nanocomposite hydrogels.

*Drug Release Kinetics – Hydrazide-Cross-linkable Microgels:* To further test this hypothesis, drug release studies were conducted on soft nanocomposite hydrogels prepared with hydrazide-functionalized microgels. Hydrazide-modified microgels were mixed with CMC-Hzd in the double barrel syringe and co-extruded with Dextran-B to generate composite hydrogels in which the microgel phase is covalently cross-linked to the bulk hydrogel. By cross-linking the microgel directly to the non-thermoresponsive gel network, we anticipate being able to "frustrate" the thermal phase transition within the microgel as the soft nanocomposite is heated, as previously demonstrated with other microgel-hydrogel systems[37]. Drug release kinetics for composite hydrogels prepared with cross-linkable (hydrazide-functionalized) microgels and non-cross-linkable (acid-functionalized) microgels of the same base composition are shown in Figure 1.6.

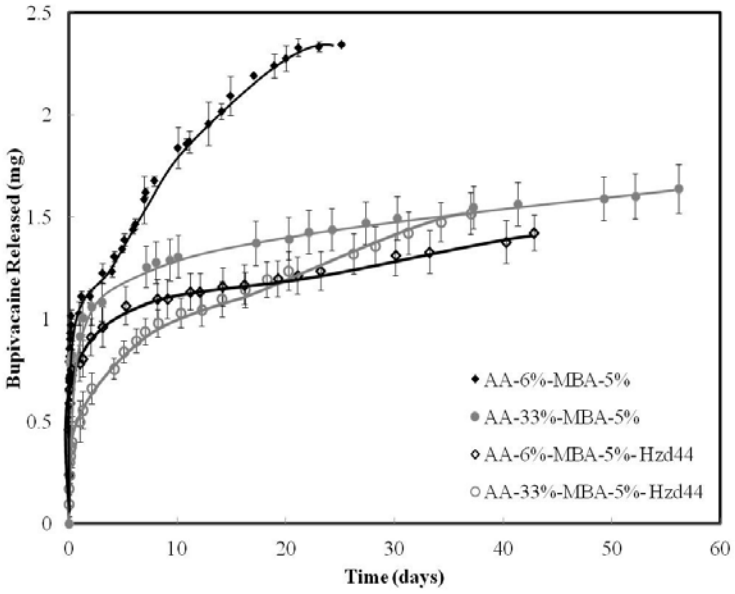


**Figure 1.6:** Bupivacaine release from nanocomposite hydrogels consisting of a 50:50 (wt%) mixture of AA-NIPAM - MBA–5% microgels prepared with 6mol% and 33mol% acrylic acid physically entrapped (filled points) or covalently cross-linked via hydrazide functionalization (unfilled points) inside a CMC-Hzd/Dextran-B hydrogel

For both degrees of functionalization tested, cross-linking microgels to the bulk hydrogel matrix significantly slows the drug release rate relative to hydrogels in which the microgels are only physically entrapped. This observation is consistent with hydrazide-mediated microgel cross-linking physically restricting the deswelling of the microgels. By restricting deswelling, no convective drug transport occurs out of the microgel phase as the microgel deswells and expels water (as has been previously demonstrated for poly(NIPAM)-based drug delivery devices); furthermore, the formation of a macroporous

hydrogel, in which deswelling of the entrapped microgel within the swelling bulk hydrogel phase creates large free volumes for facile drug diffusion around the embedded microgel phase, is avoided.

An alternative hypothesis accounting for this result is that hydrazide-mediated microgel cross-linking may increase the overall cross-link density within the network, reducing the average pore size and thus the overall diffusion coefficient of drug through the polymer network. The rheological results in Figure 1.2 indicate a significantly increased elastic modulus in nanocomposite hydrogels prepared with hydrazide-functionalized microgels, suggesting a higher overall cross-link density in these systems. To assess the validity of this alternative hypothesis, the swelling responses of nanocomposite hydrogels containing both hydrazide-cross-linked and physically entrapped microgels were measured, the results of which are shown in Figure 1.7. Figure 1.7 indicates that cross-linking the microgel to the bulk hydrogel network has no significant impact on the overall swelling/deswelling responses of the soft nanocomposite as a function of time (i.e. neither the deswelling response nor the degradation response observed at $t > 20$ days for AA-6% microgels and $t > 30$ days for AA-33% microgels are changed by microgel cross-linking). This result suggests that the overall cross-link density of the nanocomposite is not significantly changed by cross-linking the microgel to the bulk hydrogel network.

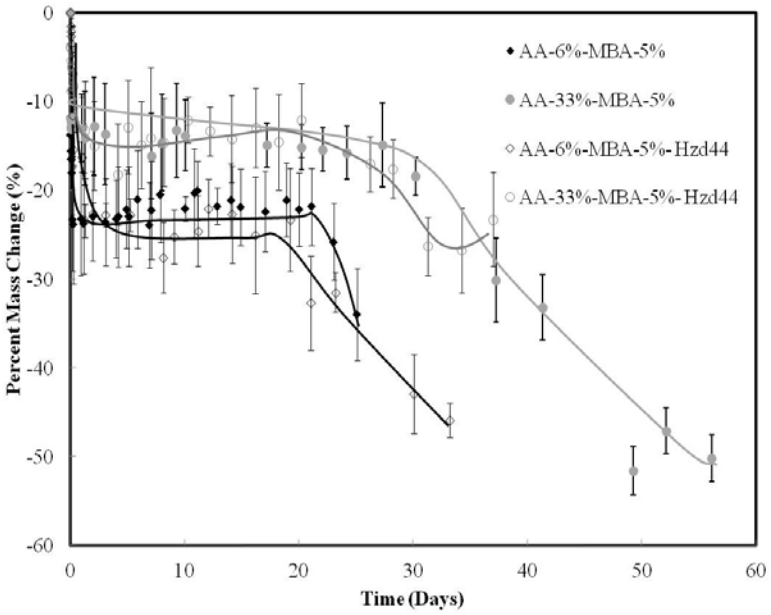


**Figure 1.7**: Deswelling responses from CMC-Hzd/Dextran-B nanocomposite hydrogels containing physically-entrapped and covalently-cross-linked AA-6%-MBA-5% and AA-33%-MBA-5% microgels

Another possible reason for the trend shown in Fig. 1.6 is that hydrazide functionalization increases the affinity (and thus partitioning) of drug to the microgel phase. However, the rate of bupivacaine release from hydrazide-functionalized microgels slightly increases relative to that observed for the same microgels before hydrazide functionalization (Supplementary Data, Figure S1.6). This result is consistent with the reduction in the total number of $–COO^-$ groups in the microgel due to hydrazide functionalization but is opposite to the release trend observed with the nanocomposite

hydrogels (Fig. 1.6). This result again suggests that the interphase cross-linking plays the critical role in controlling drug release from nanocomposite hydrogels.

**1.5 Discussion**

The results presented herein indicate that drug release from soft nanocomposite hydrogels containing a thermoresponsive entrapped phase and a non-thermoresponsive bulk phase can be tuned effectively by the degree by which the thermal phase transition is restricted or promoted by the nanocomposite microstructure. These results are consistent with findings from previous work on these soft nanocomposite hydrogels[33], in which drug release from soft nanocomposite hydrogels was found to be regulated by both diffusion effects and electrostatic binding (partitioning affinity) between drug and anionic functional groups. Electrostatic binding between cationic bupivacaine and the anionic acrylic acid groups on AA-NIPAM microgels promotes the higher proportional uptake of the drug into the microgel phase. Additionally, increasing the density of functional groups within the microgel or hydrogel phase significantly slows release of bupivacaine from the nanocomposite systems, consistent with ion exchange primarily driving the slow release behaviour.

Microgels that are simply physically entrapped inside hydrogels are free to shrink according to changes in their environment, largely unconstrained by the surrounding hydrogel phase (as has been illustrated in previous work on similar systems)[37]. In this sense, microgel swelling and the swelling responses of the nanocomposite hydrogel are largely decoupled, facilitating the creation of local free volume in the network upon

microgel collapse and/or active “squeezing” of drug from the microgel phase as it collapses. Conversely, microgels that are covalently cross-linked to the bulk hydrogel network are mechanically restricted from undergoing decoupled swelling responses from the bulk hydrogel phase. As a result, neither convection nor free volume creation can occur to increase the rate of drug transport from the microgel phase, reducing the overall rate of drug release observed (Figure 1.6). Similarly, if microgels with high internal cross-link densities are physically entrapped inside a bulk gel network, the microgel phase transition is also restricted as the microgels are heated, in this case due to the inherent elasticity of the particles themselves instead covalent bonds between the microgels and the bulk network. In this case, the magnitude of drug release is governed by the magnitude of the microgel deswelling response (Figures 1.3 and S1.3 and Table 1.3); lower degrees of deswelling result in slower overall drug release and lower burst releases. In either case, the drug release kinetics are predominantly governed by the magnitude of the thermal phase transition permitted by the microstructures in these soft nanocomposite hydrogel systems.

Based on these results and our previous work, drug release in soft nanocomposite hydrogels can be precisely tuned by three factors: (1) the cross-linking density of the bulk or embedded gel phase (controlling drug diffusion through each phase); (2) the magnitude of relative swelling/deswelling responses between the two phases (controlling drug convection from of each phase); and (3) the affinity of drug for each phase (controlling drug partitioning within each phase). For small molecule drugs, the overall cross-link density of the network appears to be significantly less important than the other two

factors; this is illustrated directly in Figure 1.7 in this work, in which cross-linking microgels to the hydrogel phase had no significant impact on the swelling responses of the hydrogel that would govern diffusion-based drug release. However, it is important to note that the effect of microgel cross-linking cannot be fully decoupled from the effect of drug partitioning due to the fact that anionic $–COO^-$ groups are consumed via adipic acid dihydrazide functionalization to create cross-linkable microgels, thereby reducing the number of available ionic binding sites for bupivacaine. This effect is illustrated in Figure 1.6 when comparing the differential drug release responses of the 6 mol% and 33 mol%-functionalized microgels upon microgel cross-linking. For the 6 mol% functionalized microgel, hydrazide functionalization consumes only 33% of the available carboxylic acid groups present in the microgel (reducing the free –COOH content to 4 mol%); this represents a relatively small change in the total number of available $–COO^-$ groups for bupivacaine complexation and thus the microgel affinity for bupivacaine binding (Table 1.2). Correspondingly, a large decrease in drug release rate is observed when the microgel is cross-linked to the hydrogel matrix due to frustration of the microgel phase transition. In comparison, adipic acid dihydrazide functionalization of the 33 mol% functionalized microgels results in the consumption of 42% of available –COOH groups, reducing the –COOH content of the microgel from 33 mol% to ~20 mol% (Table 1.2). In this case, a large number of $–COO^-$ groups are consumed by the cross-linking reaction, reducing the microgel affinity for bupivacaine and thus increasing the rate of drug diffusion from network. As a result, the observed difference in release

kinetics between the entrapped and cross-linked microgels is significantly lower for the 33 mol% AA microgel relative to the 6 mol% AA microgel.

The capacity to independently tune the bulk and embedded or cross-linked microgel phases in soft nanocomposite systems provides exceptional control over both the mechanical properties and the kinetics of drug release from these networks. While bupivacaine was used as a model drug in this study due to its cationic charge (providing an affinity interaction with the anionic microgels), the principles described herein should apply to any microgel-hydrogel-drug combination provided that the microgel is engineered to have a higher affinity for the target drug than the bulk hydrogel phase. Together with their facile injectability (provided by the *in situ*-gelling hydrazide-aldehyde chemistry used to fabricate the bulk hydrogel phase) and their generally low cytotoxicity (Supplementary Data, Figure S1.7), these materials (or degradable analogues thereof) have significant potential for facilitating long-term local drug delivery.

## 1.6 Conclusions

Drug release from soft nanocomposite hydrogels containing a thermoresponsive microgel phase within a non-thermoresponsive carbohydrate phase can be tuned by changing the magnitude of the thermal phase transition in the microgel. Reduced overall rates of drug release as well as reduced burst release profiles are observed when microgels have higher internal cross-link densities and/or are covalently cross-linked to the bulk hydrogel phase; in either case, the thermal phase transition is frustrated by the elasticity of the microgel and/or hydrogel network, resulting in reduced convective

transport of drug from the microgel and reduced free volume generation within the soft nanocomposite upon microgel deswelling. This result may be applied to tune drug release profiles for different drugs using injectable soft nanocomposite hydrogel systems.

**1.7 Acknowledgments:** Funding from the Natural Sciences and Engineering Research Council of Canada (NSERC) and the Ontario Ministry of Research and Innovation (Early Researcher Award program) is gratefully acknowledged.

## 1.8 References


(1) Hoare, T. R.; Kohane, D. S. *Polymer* **2008**, *49*, 1993-2007.

(2) Andrade-Vivero, P.; Fernandez-Gabriel, E.; Alvarez-Lorenzo, C.; Concheiro, A. *J. Pharm. Sci.* **2007**, *96*, 802-813.

(3) Bos, G. W.; Jacobs, J. J. L.; Koten, J. W.; Van Tomme, S.; Veldhuis, T.; van Nostrum, C. F.; Den Otter, W.; Hennink, W. E. *Eur. J. Pharm. Sci.* **2004**, *21*, 561-567.

(4) Bouhadir, K. H.; Kruger, G. M.; Lee, K. Y.; Mooney, D. J. *J. Pharm. Sci.* **2000**, *89*, 910-919.

(5) Cai, S.; Liu, Y.; Zheng Shu, X.; Prestwich, G. D. *Biomaterials* **2005**, *26*, 6054-6067.

(6) Cho, K. Y.; Chung, T. W.; Kim, B. C.; Kim, M. K.; Lee, J. H.; Wee, W. R.; Cho, C. S. *Int. J. Pharm.* **2003**, *260*, 83-91.

(7) Galeska, I.; Kim, T.-K.; Patil, S.; Bhardwaj, U.; Chatttopadhyay, D.; Papadimitrakopoulos, F.; Burgess, D. *AAPS J.* **2005**, *7*, E231-E240.

(8) Liu, J.; Lin, S.; Li, L.; Liu, E. *Int. J. Pharm.* **2005**, *298*, 117-125.

(9) Nishi, K. K.; Jayakrishnan, A. *Biomacromolecules* **2006**, *8*, 84-90.

(10) Fujimoto, K. L.; Ma, Z.; Nelson, D. M.; Hashizume, R.; Guan, J.; Tobita, K.; Wagner, W. R. *Biomaterials* **2009**, *30*, 4357-4368.

(11) Chen, C.-H.; Chang, C.-H.; Wang, K.-C.; Su, C.-I.; Liu, H.-T.; Yu, C.-M.; Wong, C.-B.; Wang, I. C.; Whu, S.; Liu, H.-W. *Knee Surgery, Sports Traumatology, Arthroscopy* **2011**, *19*, 1597-1607.

(12) Park, H.; Park, K. *Pharm. Res.* **1996**, *13*, 1770-1776.

(13) Gao, J.; Liu, R.; Wu, J.; Liu, Z.; Li, J.; Zhou, J.; Hao, T.; Wang, Y.; Du, Z.; Duan, C.; Wang, C. *Biomaterials* **2012**, *33*, 3673-3681.

(14) Chen, M.-C.; Tsai, H.-W.; Liu, C.-T.; Peng, S.-F.; Lai, W.-Y.; Chen, S.-J.; Chang, Y.; Sung, H.-W. *Biomaterials* **2009**, *30*, 2102-2111.

(15) Kang, G. D.; Cheon, S. H.; Song, S.-C. *Int. J. Pharm.* **2006**, *319*, 29-36.

(16) Qiao, M.; Chen, D.; Ma, X.; Liu, Y. *Int. J. Pharm.* **2005**, *294*, 103-112.

(17) Lim, D. W.; Nettles, D. L.; Setton, L. A.; Chilkoti, A. *Biomacromolecules* **2007**, *8*, 1463-1470.

(18) Chen, P. *Colloids Surf. Physicochem. Eng. Aspects* **2005**, *261*, 3-24.

(19) Ito, T.; Yeo, Y.; Highley, C. B.; Bellas, E.; Benitez, C. A.; Kohane, D. S. *Biomaterials* **2007**, *28*, 975-983.

(20) Luo, Y.; Kobler, J. B.; Heaton, J. T.; Jia, X.; Zeitels, S. M.; Langer, R. *Journal of Biomedical Materials Research Part B: Applied Biomaterials* **2010**, *93B*, 386-393.

(21) Elbert, D. L.; Pratt, A. B.; Lutolf, M. P.; Halstenberg, S.; Hubbell, J. A. *J. Controlled Release* **2001**, *76*, 11-25.

(22) Popescu, M.-T.; Mourtas, S.; Pampalakis, G.; Antimisiaris, S. G.; Tsitsilianis, C. *Biomacromolecules* **2011**, *12*, 3023-3030.

(23) Baumann, M. D.; Kang, C. E.; Tator, C. H.; Shoichet, M. S. *Biomaterials* **2010**, *31*, 7631-7639.

(24) Baumann, M. D.; Kang, C. E.; Stanwick, J. C.; Wang, Y.; Kim, H.; Lapitsky, Y.; Shoichet, M. S. *J. Controlled Release* **2009**, *138*, 205-213.

(25) Bernardo, M. V.; Blanco, M. D.; Olmo, R.; Teijón, J. M. *J. Appl. Polym. Sci.* **2002**, *86*, 327-334.

(26) Gordijo, C. R.; Koulajian, K.; Shuhendler, A. J.; Bonifacio, L. D.; Huang, H. Y.; Chiang, S.; Ozin, G. A.; Giacca, A.; Wu, X. Y. *Adv. Funct. Mater.* **2011**, *21*, 73-82.

(27) Hirakura, T.; Yasugi, K.; Nemoto, T.; Sato, M.; Shimoboji, T.; Aso, Y.; Morimoto, N.; Akiyoshi, K. *J. Controlled Release* **2010**, *142*, 483-489.

(28) Musch, J.; Schneider, S.; Lindner, P.; Richtering, W. *J. Phys. Chem. B* **2008**, *112*, 6309-6314.

(29) Hoare, T.; Sivakumaran, D.; Stefanescu, C. F.; Lawlor, M. W.; Kohane, D. S. *Acta Biomater.* **2012**, *8*, 1450-1458.

(30) Chen, P.-C.; Kohane, D. S.; Park, Y. J.; Bartlett, R. H.; Langer, R.; Yang, V. C. *J. Biomed. Mater. Res. A* **2004**, *70A*, 459-466.

(31) McGillicuddy, F. C.; Lynch, I.; Rochev, Y. A.; Burke, M.; Dawson, K. A.; Gallagher, W. M.; Keenan, A. K. *J. Biomed. Mater. Res. A* **2006**, *79A*, 923-933.

(32) Lynch, I.; de Gregorio, P.; Dawson, K. A. *J. Phys. Chem. B* **2005**, *109*, 6257-6261.

(33) Sivakumaran, D.; Maitland, D.; Hoare, T. *Biomacromolecules* **2011**, *12*, 4112-4120.

(34) Yeo, Y., Ito, T., Bellas, E., Highley, C. B., Marini, R., & Kohane, D. S. *Ann. Surg.* **2007**, *245*, 819–824.

(35) Panayiotou, M.; Pöhner, C.; Vandevyver, C.; Wandrey, C.; Hilbrig, F.; Freitag, R. *React. Funct. Polym.* **2007**, *67*, 807-819.

(36) Lynch, I.; Dawson, K. A. *J. Phys. Chem. B* **2004**, *108*, 10893-10898.

(37) Meid, J.; Friedrich, T.; Tieke, B.; Lindner, P.; Richtering, W. *PCCP* **2011**, *13*, 3039-3047.

(38) Lynch, I.; Dawson, K. A. *The Journal of Physical Chemistry B* **2003**, *107*, 9629-9637.

(39) Hoare, T.; Pelton, R. *Macromolecules* **2004**, *37*, 2544-2550.

(40) Martínez-Sanz, E.; Ossipov, D. A.; Hilborn, J.; Larsson, S.; Jonsson, K. B.; Varghese, O. P. *J. Controlled Release* **2011**, *152*, 232-240.

(41) Kim, S. W.; Bae, Y. H.; Okano, T. *Pharm. Res.* **1992**, *9*, 283-290.

(42) Hudson, S. P.; Langer, R.; Fink, G. R.; Kohane, D. S. *Biomaterials* **2010**, *31*, 1444-1452.

(43) Bouhadir, K. H.; Hausman, D. S.; Mooney, D. J. *Polymer* **1999**, *40*, 3575-3584.

(44) Motlagh, G. H.; Hrymak, A. N.; Thompson, M. R. *J. Polym. Sci., Part B: Polym. Phys.* **2007**, *45*, 1808-1820.

(45) Hoare, T.; McLean, D. *J. Phys. Chem. B* **2006**, *110*, 20327-20336.

(46) Hoare, T.; Pelton, R. *Langmuir* **2004**, *20*, 2123-2133.
(47) Woodward, N. C.; Chowdhry, B. Z.; Snowden, M. J.; Leharne, S. A.; Griffiths, P. C.; Winnington, A. L. *Langmuir* **2003**, *19*, 3202-3211.
(48) Senff, H.; Richtering, W. *Colloid & Polymer Science* **2000**, *278*, 830-840.
(49) Lowman, A. M.; Dziubla, T. D.; Bures, P.; Peppas, N. A. *Advances in Chemical Engineering* **2004**, *29*, 75-130.

## S1: Chapter 1 – Supplementary Information

## TUNING DRUG RELEASE FROM SMART MICROGEL-HYDROGEL COMPOSITES VIA CROSS-LINKING

**Authors:** Daryl Sivakumaran, Danielle Maitland, Thomas Oszustowicz, and Todd Hoare

**Publication:** Journal of Colloid and Interface Science, 392, 422-430

**Publication Date:** February 2013

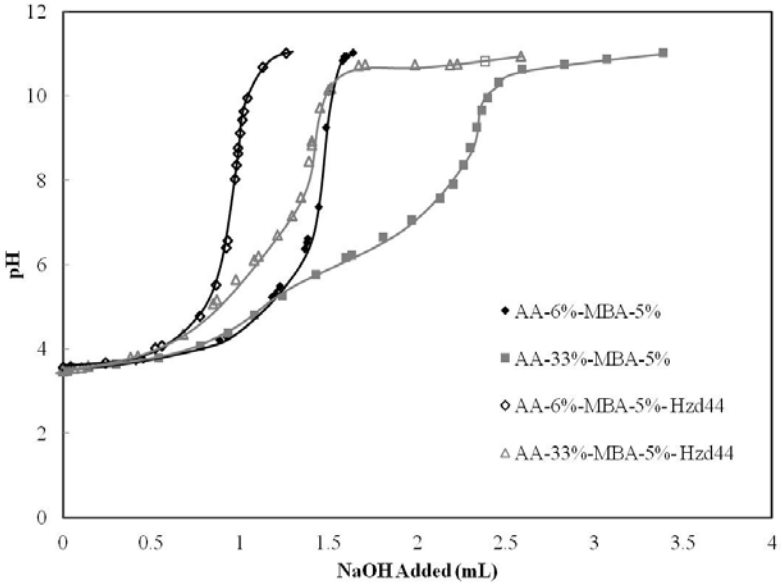


**Figure S1.1**: Titration of hydrazide-functionalized AA-NIPAM microgels

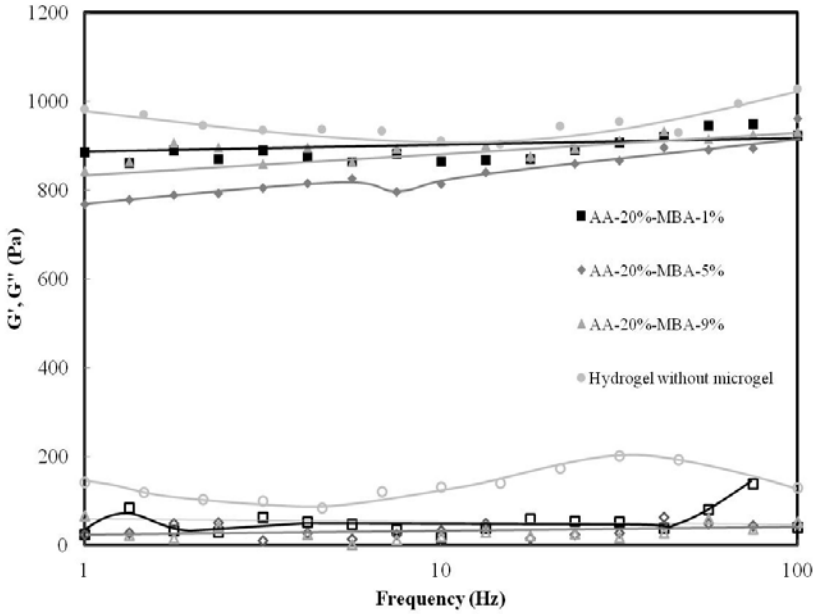


**Figure S1.2:** G' and G" values for CMC-dextran hydrogels with physically embedded AA-20% NIPAM microgels containing various amounts of MBA (G'-filled, G"-unfilled)

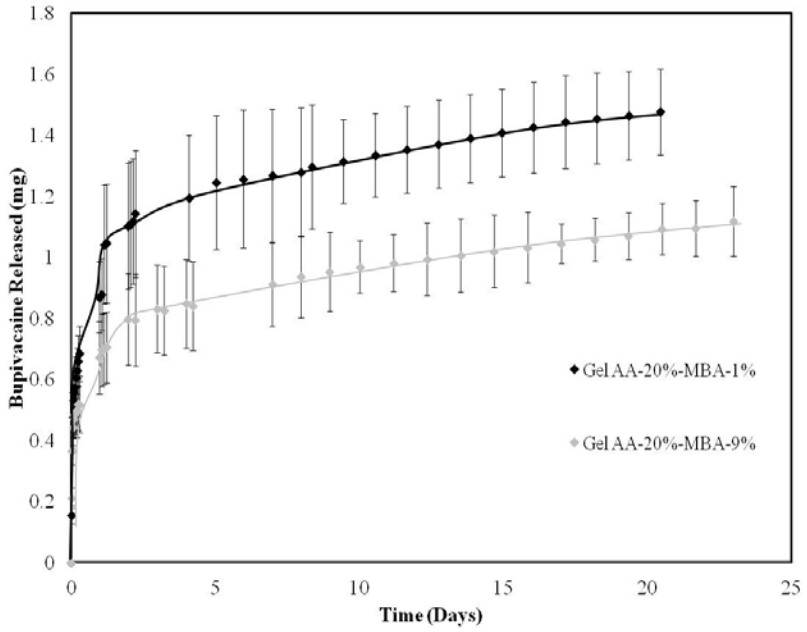


**Figure S1.3:** Bupivacaine release from nanocomposite hydrogels consisting of a 50:50 (wt%) mixture of AA-20% microgels with various MBA contents embedded inside a CMC-Hzd/Dex-B hydrogel

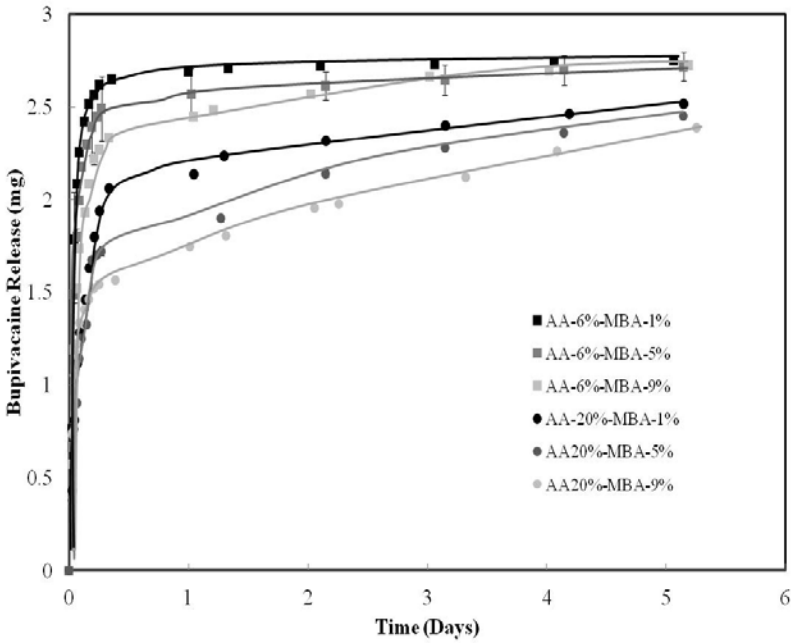


**Figure S1.4:** Bupivacaine release from AA-NIPAM microgels with varying MBA content

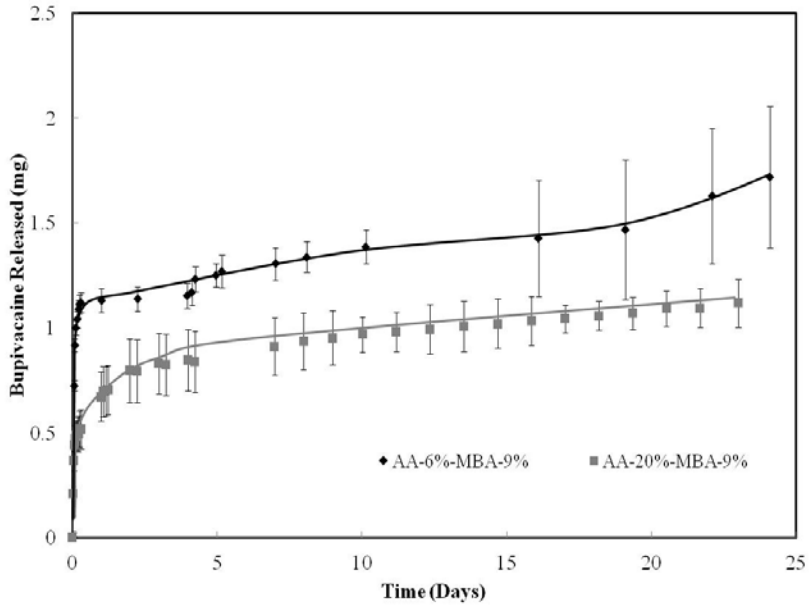


**Figure S1.5**: Bupivacaine release from nanocomposite hydrogels consisting of a 50:50 (wt%) mixture of AA-NIPAM-MBA-9% microgels prepared with 6mol% and 20mol% acrylic acid embedded inside a CMC-A/Dextran-B hydrogel

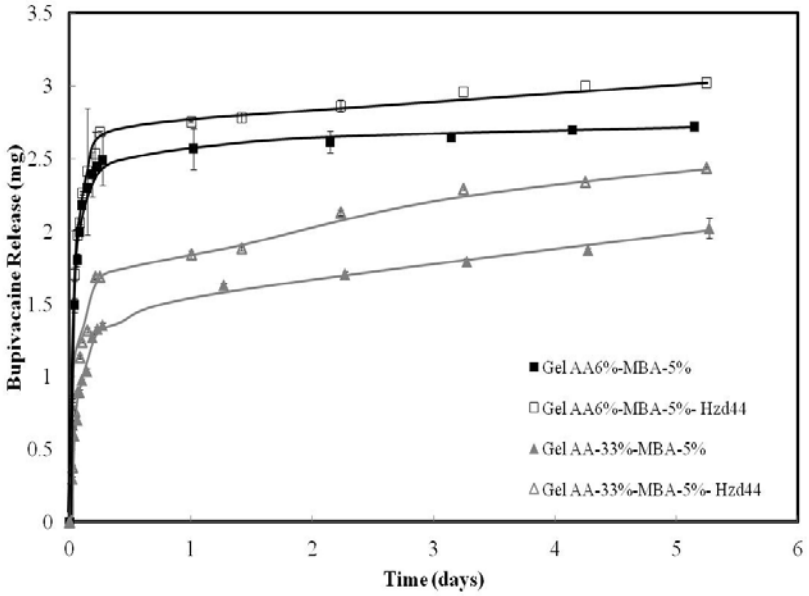


**Figure S1.6:** Bupivacaine release from hydrazide-functionalized AA- NIPAM microgels compared to release observed from the same microgels without hydrazide groups

**S1.1 Cell Viability Testing*:*** Cell viability was assayed with respect to 3T3 *Mus musculus* mouse cells C2C12 mouse muscle myoblast cells, and RAW 264.7 macrophage cells, characteristic cells present in the intermuscular or subcutaneous environments. Cell proliferation media contained 50 mL FBS and 5 mL PS for every 500mL of DMEM. Differentiation media for C2C12 cells (to facilitate differentiation of myoblasts to myotubes) used 10 mL HS instead of FBS with exposure for 24 hours. Tests were conducted in polystyrene 24 well plates containing either 10,000 3T3 cells and 1mL FBS containing media or with 50,000 C2C12 cells and 1 mL HS containing media.
Cells were exposed to solutions of CMC-hdz44, Dex-B, and AA-NIPAM microgels with concentrations between 0.1 mg/mL to 1 mg/mL for a period of 24 hours. Cell viability was assessed via the thiazolyl blue tetrazolium bromide (MTT) assay, modified from manufacturer's protocols as described by Pawlikowska[1]. Resolubilized formazan (in DMSO) precipitation was read in a microplate reader (Biorad, Model 550) at 540 nm, with absorbance of the plate and medium used as a control. Viability was measured as a function of formazan absorption at 540 nm relative to a blank well in which no polymer was exposed to cells. Each sample was tested 4 times each to ensure consistent behaviour among the cell response, with the error bars representing the standard deviation of the measurements.

To assess whether the polymers, microgels, and nanocomposite hydrogels described herein may be useful for drug delivery applications *in vivo*, an *in vitro* thiazolyl blue tetrazolium bromide (MTT) assay was used. Three cell types were screened, characteristic of cells present at intermuscular or subcutaneous injection sites: 3T3 *Mus*

*musculus* mouse cells, C2C12 mouse muscle myoblast cells, and RAW 264.7 macrophage cells. Figure S6 shows the cell viability (measured as a percentage of the MTT signal observed in the presence of the materials relative to a cell-only control) for the composite hydrogel precursors on C2C12 cells.

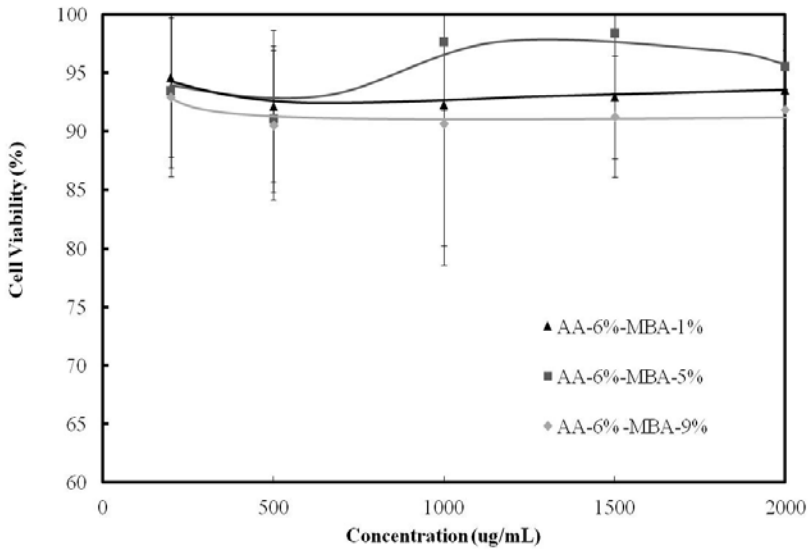


**Figure S1.7:** C2C12 cell viability (using the MTT assay, relative to cell-only controls) via exposure to AA-6% microgels with varying cross-linker content.

No significant cytotoxicity is noted for any of the AA-6% microgels at concentrations up to 1 mg/mL, typically considered a threshold for cytotoxicity assessment[2]. Similar results were obtained for 3T3 cells and RAW 247.6 macrophages. These results are consistent with prior studies involving PNIPAM-based microgels[3] and hydrazide-aldehyde cross-linked hydrogels[4].

**S1.2 10mM Phosphate Buffered Saline Recipe (0.15M ionic strength)**

8 g NaCl

1 g KCl

13.4 g $Na_2HPO_4$

1.2 g $KH_2PO_4$

1 L $dH_20$

**S1.3 References**

(1) Pawlikowska, P.; Gajkowska, B.; Orzechowski, A. *Cell Tissue Res.* **2007**, *327*, 571-581.

(2) Deneer, J. W.; Seinen, W.; Hermens, J. L. M. *Aquat. Toxicol.* **1988**, *12*, 185-192.

(3) Chen, P.-C.; Kohane, D. S.; Park, Y. J.; Bartlett, R. H.; Langer, R.; Yang, V. C. *J. Biomed. Mater. Res. A* **2004**, *70A*, 459-466.

(4) Ito, T.; Yeo, Y.; Highley, C. B.; Bellas, E.; Benitez, C. A.; Kohane, D. S. *Biomaterials* **2007**, *28*, 975-983.

# Chapter 2

# MICROFLUIDIC PRODUCTION OF DEGRADABLE THERMORESPONSIVE POLY(N-ISOPROPYLACRYLAMIDE)-BASED MICROGELS

**Authors:** Daryl Sivakumaran, Eva Mueller, and Todd Hoare

**Publication:** To be submitted in 2015

## 1.1 Abstract

Highly monodisperse and hydrolytically degradable thermoresponsive microgels on the tens-to-hundred micron size scale have been fabricated based on simultaneous on-chip mixing and emulsification of aldehyde and hydrazide-functionalized poly(N-isopropylacrylamide) precursor polymers. The microfluidic chip can run for extended periods without upstream gelation and can produce monodisperse (< 10 % particle size variability) microgels on the size range of ~30-90 μm, with size tunable according to the flow rate of the oil continuous phase. Fluorescence analysis indicates a uniform distribution of each reactive pre-polymer inside the microgels. The microgels retain the reversible volume phase transition behavior of conventional microgels but can be hydrolytically degraded back into their oligomeric precursor polymer fragments, offering potential for microgel clearance following use *in vivo*. Such materials offer potential as injectable, localized smart drug delivery vehicles and/or cell encapsulation matrices.

**Keywords** poly(N-isopropylacrylamide), microgel, microfluidics, hydrazone chemistry

## 2.2 Introduction

Microgel particles with sizes on the micron scale have significant potential as drug delivery vehicles[1], cell encapsulation matrices[2], microreactors for chemical reactions[3], and biosensing platforms[4]. The high internal void fraction of microgels is critical to their success in each of these applications, as it enables efficient encapsulation of drugs or therapeutics as well as facile transport of nutrients to (and wastes from) entrapped cells or analytes to entrapped biosensing receptors. In addition, from the perspective of drug delivery, microgels on the tens or hundreds of microns size scale, while still injectable, can evade phagocytosis and/or uptake by the reticuloendothelial system based on their size[5], enabling them to stay where they are injected (in contrast to nanoparticulate gel particles) and thus facilitate longer-term local drug delivery. Alginate microparticles, formed via ionic cross-linking with calcium ions, are by far the most commonly reported particles on this scale[6], although several types of microgels based on polyethylene glycol[2,7,8] have also been reported. More recent interest has been focused on microgels based on "smart" materials that can swell and deswell in response to changes in their environment. Temperature-responsive microgels, mainly based on poly(N-isopropylacrylamide)[9] or related N-alkylacrylamide polymers, have attracted particular attention due to their capacity for reversible, triggered deswelling upon heating, enabling on-demand drug delivery[10-12], controlled diffusion-based access to entrapped cells[13], or on-off biosensing of environmental analytes[14,15], among other potential applications.

Traditional methods for making microgels in the tens-to-hundreds of microns length scale include spray drying[16], inverse emulsion techniques[17], or shearing bulk hydrogels[18]. However, the major drawback of all these techniques is the relatively broad polydispersities that result from these processes that can lead to varied results in biomedical applications in particular given the strong observed dependence of tissue response on particle size[19-21]. In addition, these methods require drying, direct cell contact with solvents, and/or the application of locally high shear rates, all of which can be highly detrimental to cell viability and/or protein stability.

Microfluidics offers an alternative to traditional particle-forming techniques to produce microgels on the tens-to-hundreds of microns scale. While the chemistry used in microfluidics-based processes mirrors in most cases that traditionally used for inverse emulsion approaches, the highly controlled geometry at the point of emulsification results in highly uniform shear being applied to each formed particle[22], leading to the creation of droplets and, following gelation, microgels with low polydispersities. This concept has been utilized to make a wide array of polymeric microgels within the droplets, typically inducing gelation on-chip following droplet formation via free radical copolymerization of monomers with divinyl or diacrylate cross-linkers using photoinitiators[23] or redox reactions[24,25] to drive the polymerization. Cross-linking of reactive pre-polymer(s) inside the droplets has also been demonstrated, offering the significant advantage of more direct control over the degree or cross-linking and degradability based on the degree of functionalization of the prepolymer(s), the molecular weight of the prepolymer(s), and/or the amount of cross-linker added. Covalent gelation via UV exposure of pendant

polymerizable groups (e.g. dimethylmaleimide groups[26,27]), enzymatic gelation (e.g. agarose-gelatin)[28], ionic gelation[29] (e.g. alginate-calcium[30] or chitosan-tripolyphosphate[31]), or thermogelation (e.g. lowering the temperature of gelatin-based droplets[32]) have all been reported. Alternatively, click chemistries including thiol-ene chemistry[2], strain-promoted azide–alkyne cycloaddition[33], or vinylsulfone-thiol reactions[34] can be utilized for cross-linking pre-polymers inside the droplet; however, the relatively slower nature of these reactions (while helpful to allow for particle formation without the need to perform simultaneous mixing and emulsification) can lead to significant particle agglomeration in the collection flask prior to gelation.

The fabrication of monodisperse "smart", environmentally-responsive polymer-based microgels on this length scale offers particular potential for applications. Poly(N-isopropylacrylamide) (PNIPAM) microgels that exhibit a volume phase transition temperature upon heating may particularly benefit from a microfluidics-based fabrication technique, allowing for the production of monodispersed particles that are harder to obtain using traditional polymerization techniques[35]. In addition, from a drug or cell delivery context, microfluidics offers the potential for comparatively low-shear encapsulation of non-reactive components within the particle matrix by simply adding that component to the reaction mixture prior to microgel formation (as demonstrated using FITC-dextran[36]). Reported microfluidic techniques for synthesizing PNIPAM microgels include the use of capillary microfluidic devices[24] or PDMS-based soft lithographic devices using flow focusing[35,37], with NIPAM monomer and cross-linker (typically N,N-methylenebisacrylamide) polymerized directly on-chip following droplet

formation using either a thermal initiator[24] or photoinitiator[37] to induce polymerization. By changing flow rates and chip design, the morphology of the microgels can be altered between a uniform microgel[24], a core-shell configuration[11] or a hollow shell[37]. Porous PNIPAM-based microgels have been prepared by adding varying amounts of short-chained PEG (acting as a porogen) into the monomer solution[38], while multi-responsive microgels have also been designed by copolymerization of NIPAM with other functional monomers (e.g. a phenylboronic acid (PBA)-containing comonomer to create a microgel that is both temperature and glucose responsive[14]). However, all these existing methodologies rely on polymerization of NIPAM via standard free radical (co)polymerization inside the microfluidics-templated droplets, resulting in a network of carbon-carbon backbone polymers that is not functionally degradable. Such a network is problematic in many biomedical applications, as it cannot readily be cleared from the body following use.

In this paper, we report the production of highly monodisperse and degradable PNIPAM microgels using a microfluidic chip that can simultaneously mix and emulsify two reactive pre-polymers functionalized with hydrazide (PNIPAM-Hzd) and aldehyde (PNIPAM-Ald) groups. Gelation of PNIPAM-Hzd and PNIPAM-Ald occurs within seconds on the bulk scale; thus, the mixing microfluidic chip developed previously in our group is ideal for this application, as mixing and droplet formation occur nearly simultaneously in the flow focusing geometry used. The formed microparticles display thermosensitivity akin to other PNIPAM particles, with the absolute size of the particles controllable by changing the oil flow rate during microfluidic production. In addition, the

microgels can be degraded back into the oligomeric pre-polymer products via hydrazone cross-link hydrolysis, offering a unique potential relative to previous PNIPAM microparticles on this scale in the context of biomedical applications.

## 2.3 Experimental

*Materials:* N-isopropylacrylamide (NIPAM, 99%), acrylic acid (AA, 99%), thioglycolic acid (98%), aminoacetaldehyde dimethyl acetal (99%), 2,2,6,6-tetramethyl-1-piperidinyloxy (TEMPO, 98%), fluoroscein isocyanate isomer 1 (>90%), rhodamine 123 (85%), sodium cyanoborohyride (95%), and methacryloyl chloride (purum) were all purchased from Sigma Aldrich (Oakville, Canada) and used as received except for NIPAM which was purified further with by washing with a 60:40 toluene: hexane mixture and recrystallization. Adipic acid dihydrazyde (ADH, Alfa Aesar, 98%), *N*'-ethyl-*N*-(3-dimethylaminopropyl)-carbodiimide (EDC, Carbosynth, Compton CA, commercial grade), and 2,2-azobisisobutryic acid dimethyl ester (AIBMe, Wako Chemicals, 98.5%) were all used as received. Milli-Q grade distilled deionized water (DIW) was used for all experiments. Hydrochloric acid (1 M) was received from LabChem Inc. (Pittsburgh, PA). Ethanol was purchased from Commercial Alcohols (Brampton, ON). Cell culture media contents included Dulbecco's Modified Eagle Medium-high glucose (DMEM), fetal bovine serum (FBS), and Penicillin Streptomycin (PS), all obtained from Invitrogen Canada (Burlington, ON).

*Fabrication of Microfluidic Chip:* A master mould of the microfluidic chip was patterned on a 3 inch silicon wafer utilizing photolithography using a SU-8 2075 photoresist (MicroChem, MA, USA). Soft lithography using polydimethylsiloxane (Sylgard 184, Dow Chemicals) was then performed using the master mould as a template. The fluid inlets were made from Masterflex silicone tubing (Cole Palmer, Ontario, Canada) and were placed on the master mould prior to PDMS addition. The chip was then cured for 1.5 h at 70 °C, after which it was bonded to a glass microscope slide by exposure to 40 W oxygen plasma for 30 s at 0.3 mTorr and left to bond overnight.

*Prepolymer Synthesis:* Functional PNIPAM prepolymers were made following protocols developed by Patenaude and Hoare[39]. Briefly, hydrazide polymers (PNIPAM-Hzd) were synthesized by via free radical copolymerization of NIPAM (4.5g) and acrylic acid (0.5 g - 15 mol% total monomer) in 20 mL of ethanol using thioglycolic acid (TGA, 80 μL) as the chain transfer agent and 2,2-azobisisobutyric acid dimethyl ester (AIBME, 0.056 g) as the initiator (reaction temperature = 56°C). The resulting polymer had a molecular weight of 21.6 kDa (as measured using gel permeation chromatography with a Waters 590 HPLC pump, three Waters Styragel columns (HR2, HR3, HR4; 30 cm x 7.8 mm (ID); 5 μm particles) at 40°C, a Waters 410 refractive index detector operating at 35 °C, and DMF as the solvent) and ~15 mol% of acrylic acid (i.e. stoichiometric incorporation, as measured using base-into-acid conductometric titration). Acid groups were then converted to hydrazide groups by grafting a 5-fold excess of adipic acid dihydrazide to free –COOH groups using carbodiimide chemistry, resulting in an overall conversion of

95% of acrylic acid residues to hydrazide functionalities (resulting in ~14 mol% of the total monomer residues being functionalized with a hydrazide group). Aldehyde polymers (PNIPAM-Ald) were prepared by copolymerizing NIPAM (4 g) with N-(2,2-dimethoxyethyl)methacrylamide[40] (DMEMAm, 0.95 g, 13.4 mol% total monomer) using the same polymerization conditions used for the hydrazide polymer, resulting in a polymer with a molecular weight of ~15.1 kDa. Conversion of the pendant acetal groups in DMEMAm into aldehyde groups was completed by exposing the polymer to 1M HCl for 24 hours, resulting in 12 mol% of total monomer residues in the polymer bearing aldehyde functionalized groups. All polymers were dialyzed against Milli-Q water for 6 cycles of at least 6 hours and lyophilized for storage.

*Microgel Fabrication:* Microgels were made using the two-stage microfluidic chip previously published in our group using the geometry and process illustrated in Figure 2.1[9].

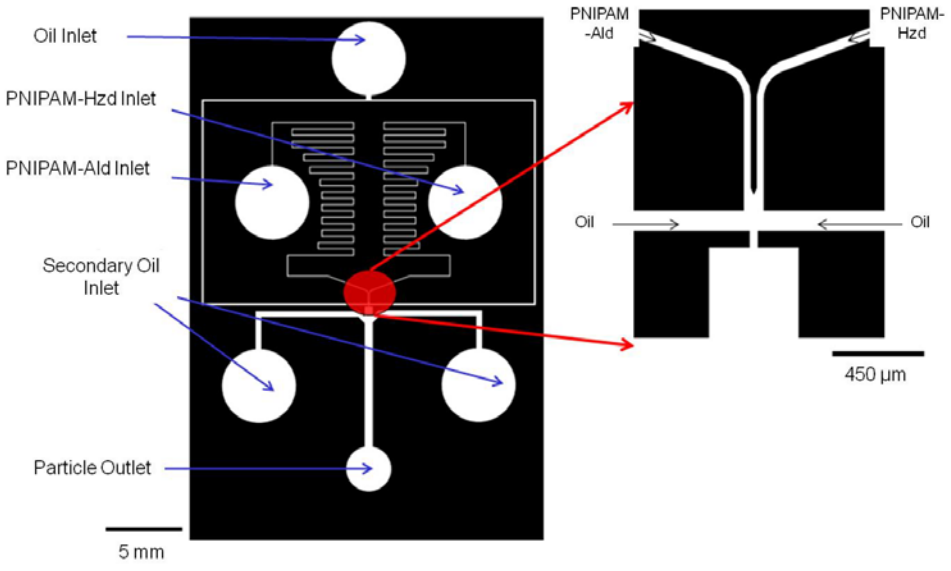


**Figure 2.1:** Microfluidic chip design

Briefly, the chip includes two inlets (used here for PNIPAM-Hzd and PNIPAM-Ald) that are separated from a short pre-mixing channel by zig-zag channels; these zig-zag channels are used to establish a pressure gradient to resist back-flow of each prepolymer into the other prepolymer reservoir (a process that would lead to undesired gelation prior to droplet formation). The two functional polymers are then co-streamed through a short mixing channel primarily useful to stabilize the flow, followed by droplet generation using a flow-focusing geometry and paraffin oil as the continuous phase. PNIPAM-Hzd and PNIPAM-Ald were dissolved at 6 wt% in deionized water and loaded into separate 5 mL syringes connected to the two inlet reservoirs, while heavy paraffin oil containing 1 wt% Span 80 was loaded into a 60 mL syringe and attached to the continuous phase inlet. An aqueous phase flow rate of 0.03 mL/h was delivered using a KDS Legato 200 infusion syringe pump, with a variety of continuous flow rates ranging from 1.1 mL/h to 5.5 mL/h (also delivered via a KDS Legato 200 syringe pump) investigated to control the particle size and particle monodispersity. Note that the oil flow rate was chosen as the variable flow parameter based on previous results that suggested changing the aqueous flow rate either resulted in extremely small particle production rates or particle populations with significantly higher size variability[9]. No controlled viscosity matching occurred between the aqueous and continuous phases, as particle formation was readily completed. The microfluidic device was initially primed by filling the connecting tubes with the appropriate fluid, connecting them to the chip, starting the oil flow to ensure the device was operational and defect-free, and then starting the polymer solution flow to produce particles. Particles were not collected until 1 hour into production to ensure flow

stabilization in the chip, with the device then run continuously until all the oil was consumed (12-55 hours depending on the oil flow rate). The products were collected in test tubes under magnetic agitation to help prevent aggregation of the particles.

*Microgel Purification:* Fabricated microgels were allowed to settle by gravity for 60 minutes, after which the majority of the paraffin oil phase was removed from the top of the test tubes. The microgels were then washed with pentane at least five times using a volume ratio of 10 mL pentane for every 0.5 mL of microgel solution to ensure complete removal of oil and surfactant. Residual pentane following the final extraction step was allowed to evaporate in the fumehood, after which the purified microgels were resuspended in water or PBS (10 mm buffer concentration, pH 7.4, 0.15 M overall ionic strength) for testing.

*Scanning Electron Microscopy:* Particles were air dried and mounted onto conductive tape attached to scanning electron microscopy stubs. The particles were sputter coated with a 30 nm layer of gold and imaged using Tescan Vega II LSU scanning electron microscope (Tescan USA, PA) operating at 10 kV.

*Fluorescence Tagging:* Fluorescent probes were attached to both hydrazide and aldehyde functionalized PNIPAM to track the distribution of each prepolymer within the microgel particles. PNIPAM-Hzd was tagged with fluorescein (PNIPAM-Hzd-FITC) by reacting

fluorescein isocyanate (~30 mg, 1 mol% total monomer units) overnight with 500 mg of PNIPAM-Hzd in 250 mL of pH 9.4 carbonate buffer (0.1M ionic strength). PNIPAM-Ald was tagged with rhodamine 123 (PNIPAM-Ald-Rho) by reacting rhodamine (~30 mg, 1.5 mol% total monomer units) overnight with 500 mg of PNIPAM-Ald and 15 mg sodium cyanoborohydride in 250 mL of pH 5 acetate buffer (0.1 M ionic strength). Both tagged polymers were dialyzed over the course of 3 days (minimum 6x6 hour cycles) and lyophilized for storage.

*Microscope Analysis of Microgels:* Microgel solutions (~10 µL) were placed on glass slides and imaged using an Olympus BX51 optical microscope. Particles were heated using a Linkam THMS600 T-controlled stage, with a temperature ramping rate of 1°C/min. Cooling of the heated stage was not controlled, such that cooling did not occur at a fixed temperature rate between samples; however, the actual temperature of the stage at each image collected was measured precisely at each sampling point to relate particle size to temperature during cooling. Thermal cycling occurred in the same manner, with a 30 minute wait time enforced following cooling prior to the next heating cycle to ensure microgel equilibration. Images of microgel populations were analyzed in bright field mode for measuring particle size as a function of temperature using Q Capture (V.2.98.0) and Image Pro Plus (V.7.0.1.658), with a total of 100 microgels per sample measured; all reported microgel sizes are based on the mean size of these 100 microgels, with errors given as the standard deviation of that mean. Fluorescent measurements were made using

the same microscope using an excitation wavelength of 475 nm for samples labeled with FITC, 525 nm for samples labeled with rhodamine 123, and sequential exposure of the microgel to each wavelength to acquire composite polymer distribution images.

*Degradation:* To track the degradation of the microgels, 1 M HCl was used to expedite the hydrolysis process such that microgel dissolution could be observed in real time on the microscope stage. A 10 µL suspension of microgels was placed on a microscope slide followed immediately by the application of 40 µL of 1 M HCl (time point t=0). Subsequent images were taken at one-minute intervals over the first 15 minutes and then at 15-minute intervals for up to 2 hours or until no defined microgel particles were observable under the microscope. Degradation products were analyzed via GPC to determine if the microgels degraded back to precursor polymers. The microgels were exposed to 1M HCl and left to degrade over 24 hours before GPC analysis. The degradation products were then analyzed using the same GPC conditions described in the polymer synthesis steps following reaction of the degradation product with 10 mg of sodium cyanoborohydride for every 15 mg of polymer (~10X molar excess) to reduce existing aldehyde groups to alcohols and ensure that no gelation occurred within the GPC column.

*Microgel Cytotoxicity:* Cell viability was assessed after exposure to precursor polymers and microgels using 3T3 *Mus musculus* fibroblasts in cell media consisting of 500 mL DMEM, 50 mL FBS, and 5 mL PS. A total of 10,000 cells were seeded within each well

of a polystyrene 24-well plate and then exposed to polymer and microgel concentrations of 0.1 mg/mL to 1 mg/mL for 24 hours. Viability was measured using a thiazolyl blue tetrazolium bromide (MTT) assay using protocols described by Pawlikowska[41]. The formation of formazan by healthy cells was determined through the use of a microplate reader (Biorad, Model 550) at wavelength of 540 nm. Cell viability was calculated by dividing the measured absorbance of the exposed cells to those of cells that had no polymer exposure. Four replicates were conducted for each sample tested, with error bars representing the standard deviation of those experiments.

**Results and Discussion**

*On-Chip Mixing:* The microfluidic chip design incorporates a short pre-nozzle flow stabilization channel; however, previous analysis has demonstrated that no significant mixing occurs in this channel such that the nozzle and flow focusing geometry together are primarily responsible for facilitating sufficient mixing in the aqueous phase to enable uniform microgel formation[9]. To ensure complete mixing of each reactive polymer within the microgel during microfluidic production, Figure 2.2 shows the distribution of NIPAM-Hzd-FITC and NIPAM-Ald-Rho in microgels produced using the microfluidic chip. The fluorescence intensity is uniform across the diameter of the microgel, suggesting that both PNIPAM-Ald and PNIPAM-Hzd are uniformly distributed throughout the microgel volume. Thus, the combination of mixing due to shear-induced flows at the nozzle and polymer self-diffusion inside the droplet prior to gelation together facilitate the formation of uniform microgel particles.

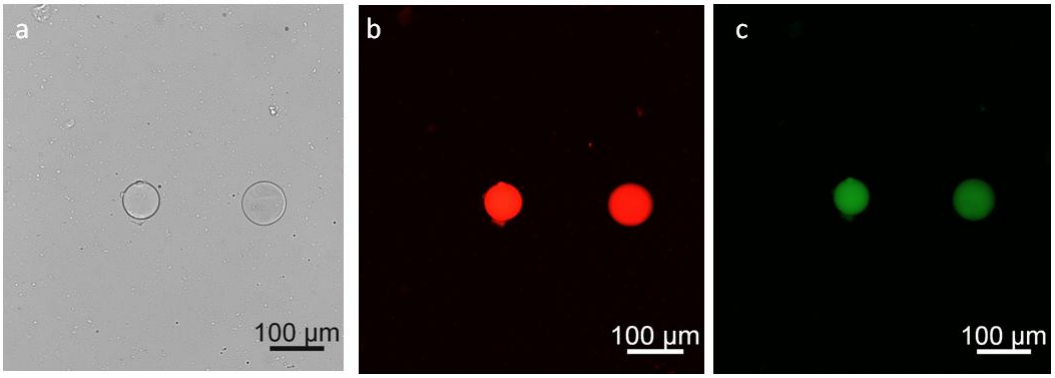


**Figure 2.2:** Brightfield (a), rhodamine channel (b), and fluorescein channel (c) images of microgels prepared via on-chip cross-linking of PNIPAM-Hzd-FITC and PNIPAM-Ald-Rho produced via microfluidics

*Controlling Microgel Particle Size:* Microgels could successfully be produced by varying the oil flow rate from 1.1 mL/h to 5.5 mL/h; higher flow rates were attempted but tended to lead to failure of the microfluidic chip at the glass-PDMS bonded interface. Oil was removed fully from the system through the use of multiple washes with pentane, after which any residual pentane was removed via evaporation. Effective oil removal was verified both visually (via the lack of visible oil droplets under the microscope) as well as physically (by the maintenance of the characteristic thermosensitivity displayed by the microgels, suggesting a hydrophilic:hydrophobic balance consistent with that of an all-aqueous environment). Microgels produced at various oil flow rates (following resuspension in Milli-Q water after separation from the paraffin oil and washing with pentane) are shown in Figure 2.3, with the average size and standard deviation of microgels produced at each flow rate ($n$ = 100 particles per particle, image analysis) included below each image. The microgel size can be varied systematically with the oil

flow rate, with higher oil flow rates resulting in smaller particle sizes. This result is consistent with the higher local shear at the junction point between the oil and aqueous phases at higher oil flow rates. However, at the lowest oil flow rate tested, the polydispersity of the particles also increased to a significant degree (± 20% standard deviation relative to < 10% at the lower flow rates), likely attributable to the somewhat poorer oil flow stability afforded by the syringe pump at this slower flow rate. However, even at the lower flow rate, these polydispersities are still significantly lower than could achieve with traditional inverse emulsion approaches.

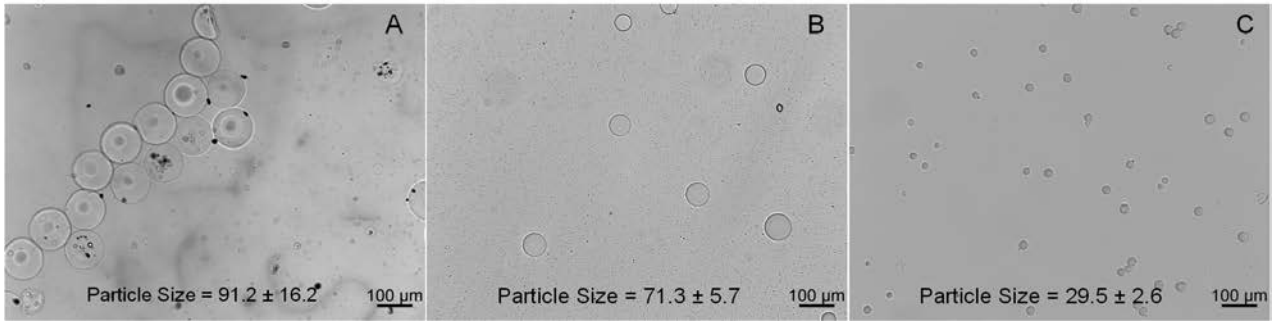


**Figure 2.3:** Optical microscopy images and mean sizes and standard deviations ($n$ = 100 particles counted, image analysis) of microgels produced at oil flow rates (a) 1.1 mL/h, (b) 3.3 mL/h, and (c) 5.5 mL/h

*Microgel Morphology:* The microgels produced were further analyzed using scanning electron microscopy to assess the morphology of the particles. Consistent with the light microscopy images, the particles were uniform in size, with the slight degree of aggregation observed likely attributable to drying artifacts. The individual particles have a

smooth surface with no pitting or phase separation between polymer components, indicating that the precursor polymers are uniformly mixed within the microfluidic chip.

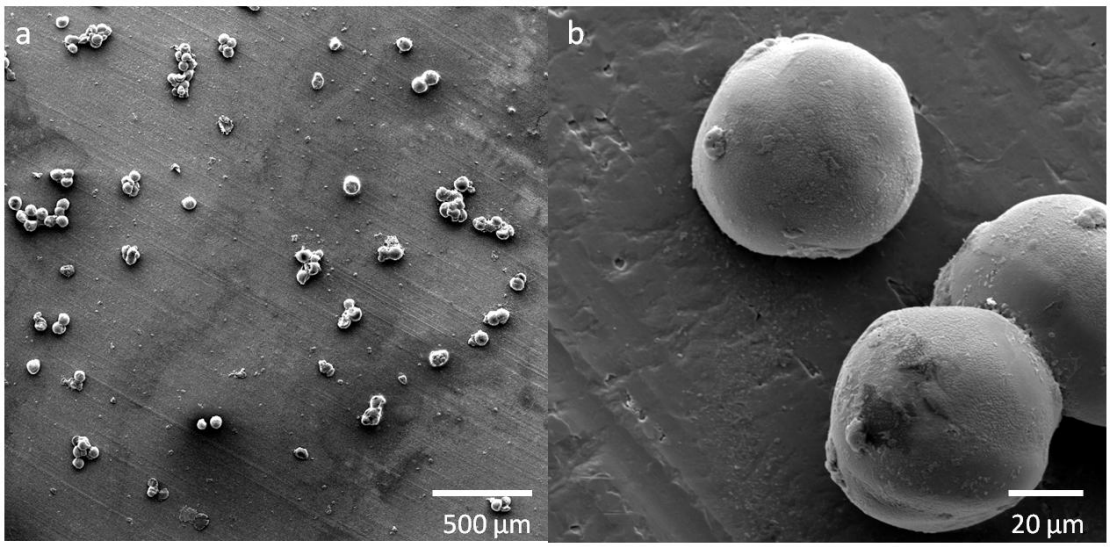


**Figure 2.4:** SEM of microgels produced at an oil flow rate of 3.3 mL/hr at 80x zoom (a) and 1460x zoom (b)

*Thermosensitivity:* PNIPAM homopolymers typically exhibit a lower critical solution temperature (LCST) of ~32ºC. Given the presence of hydrophilic hydrazide and aldehyde functional groups on the pre-polymers, PNIPAM-Hzd and PNIPAM-Ald have higher LCST values of ~58ºC and ~48ºC respectively[40]; however, following consumption of these groups to form hydrazone linkages, the volume phase transition temperature of the cross-linked bulk hydrogel was similar to conventional PNIPAM hydrogels (~33-34ºC)[39]. A heated microscope stage was used to image the microgels as a function of temperature and determine the VPTT of the microgels as a function of particle size. Figure 2.5 shows the optical images of representative microgels following a single heating-cooling cycle,

Table 2.1 shows the mean microgel sizes ($n$ = 100) measured over a single heating-cooling cycle, and Figure 2.6 shows the swelling ratio of microgels prepared at different oil flow rates as a function of temperature.

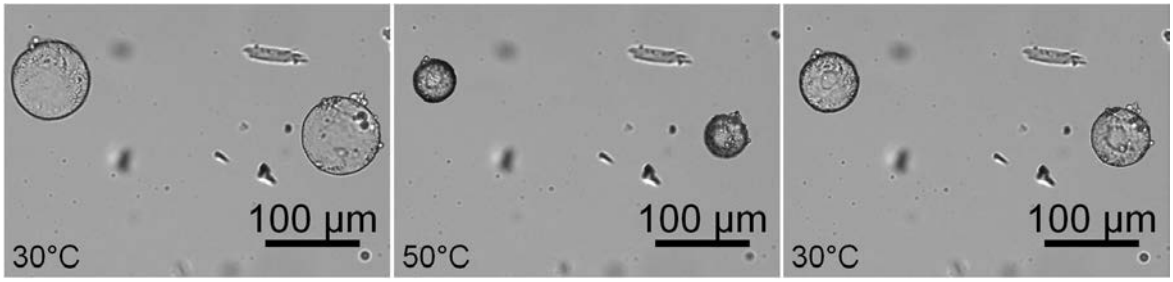


**Figure 2.5:** Optical hot stage microscope images of microgels in 10 mM PBS (a) at 30 ºC prior to heating, (b) at 50 ºC following one heating cycle and, (c) at 30 ºC following one heating-cooling cycle; oil flow rate = 3.3 mL/h

**Table 2.1:** Particle sizes before heating, after heating, and after one heating/cooling cycle for microgels prepared using different oil flow rates ($n$ = 100 particles counted)

| Oil Speed (mL/hr) | Before Heating (30ºC) (µm) | Heating (50ºC) (µm) | Cooling (30ºC) (µm) |
|---|---|---|---|
| 1.1 | 101 ± 15 | 46 ± 7 | 82 ± 7 |
| 3.3 | 81 ± 5 | 43 ± 2 | 66 ± 5 |
| 5.5 | 25 ± 1 | 14 ± 1 | 22 ± 1 |

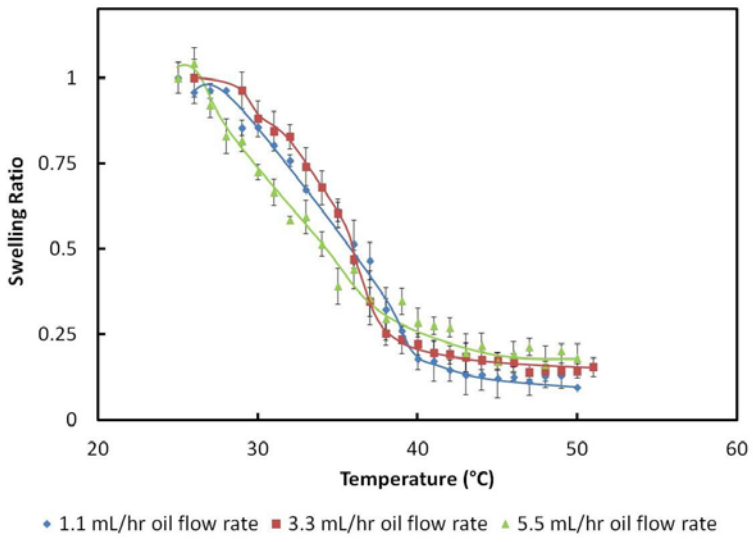


**Figure 2.6.** Swelling ratio as a function of temperature for microgels prepared using different oil flow rates ($n$ = 100 particles counted)

Figure 2.6 suggests that the microgels exhibit very similar behavior to conventional, free radical-cross-linked PNIPAM microgels, with a volume phase transition occurring over the temperature range of ~30-40ºC and the midpoint VPTT (i.e. the point at which the 50% of the volume reduction has occurred) lying at ~34ºC for each microgel teste, independent of particle size. Similarly, the magnitude of deswelling is (within error) the same for each of the microgels tested, with ~50% diameter reductions (corresponding to ~90% volume reductions) observed upon deswelling. This result suggests that the cross-link density of the microgels is relatively independent of particle size, suggesting that the mixing of PNIPAM-Ald and PNIPAM-Hzd is consistent and uniform at all oil flow rates tested.

Upon cooling the microgels back to room temperature, the microgels reswell; however, consistent with bulk PNIPAM hydrogels[42,43] (including hydrazone-cross-linked bulk hydrogels made from the same oligomeric precursors as reported in our earlier work[39,40]), some degree of hysteresis is observed following a single heating-cooling cycle, with only ~80% volume recovery observed (see Figure 2.5, Table 2.1, and the particle size versus temperature data collected over the first heating/cooling cycle provided in Supplementary Information, Figure S2.1). When microgels were exposed to additional heat cycling, no additional hysteresis was observed, with swollen and collapsed particle sizes reproducible within error over at least three additional heat-cool cycles (Table 2.2).

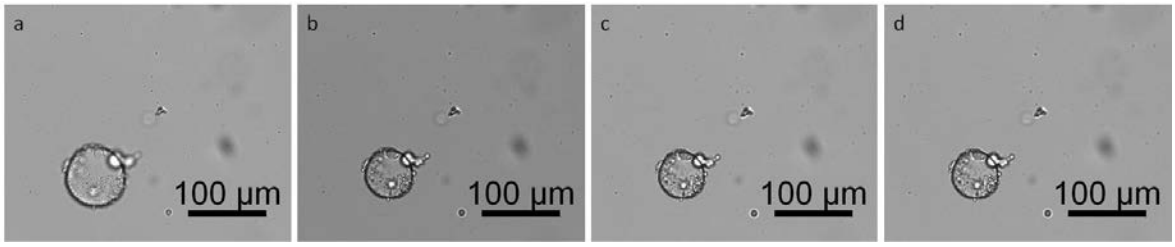


**Figure 2.7:** Optical hot stage microscope images of microgels undergoing heat cycling (images at 25°C after being heat and cooled to 50°C) (a) before heating (b) after 1 thermal cycle (c) after 2 thermal cycles (d) after 3 thermal cycles; oil flow rate = 3.3 mL/h

**Table 2.2:** Microgel sizes during thermal cycling of microgels produced at an oil flow rate of 3.3 mL/hr

| **Cycle** | **Size at 25ºC (µm)** | **Size at 50ºC (µm)** |
|---|---|---|
| 0 (starting) | 79 ± 6 | 44 ± 3 |
| 1 | 69 ± 5 | 39 ± 3 |
| 2 | 64 ± 2 | 41 ± 1 |
| 3 | 63 ± 3 | --- |

*Degradation:* Unique to the PNIPAM microgels produced herein, the microgels can degrade back into oligomeric precursor polymers via hydrolytic cleavage of the acid-labile hydrazone bond to promote clearance of the microgel following its use *in vivo*. To confirm the ability of the microgels to degrade and track the evolution of this degradation process on a measurable timescale, microgels were exposed to 1 M HCl on a microscope slide, with microgel size and shape assessed as a function of time. Figure 2.8 shows the optical microscopy images of this degradation process for microgels made using an oil flow rate of 3.3 mL/h, while Figure 2.9 shows a graph of particle diameter versus time for the same microgel. Upon exposure to 1 M HCl, visual changes in microgel size and shape become noticeable almost immediately; within minutes, the microgels swell by almost 33%, while after 2 hours the microgels become roughly double their original size, with increased polydispersity (Figs. 2.8 and 2.9). These results together suggest that hydrazone bond hydrolysis is occurring, resulting in a reduction in the net cross-link density within the microgel. Upon prolonged exposure (> 2 hours), the microgels completely lose contrast with the surrounding water (Fig. 2.8, 120 min.), suggesting a loss of particle integrity indicative of degradation. Gel permeation chromatography following 24 hours of exposure to 1 M HCl shows that the microgel degradation products have the same molecular weight as the PNIPAM-Hzd and PNIPAM-Ald precursor polymers (Fig. 2.10), indicating that the microgel does break down into its component prepolymer building blocks.

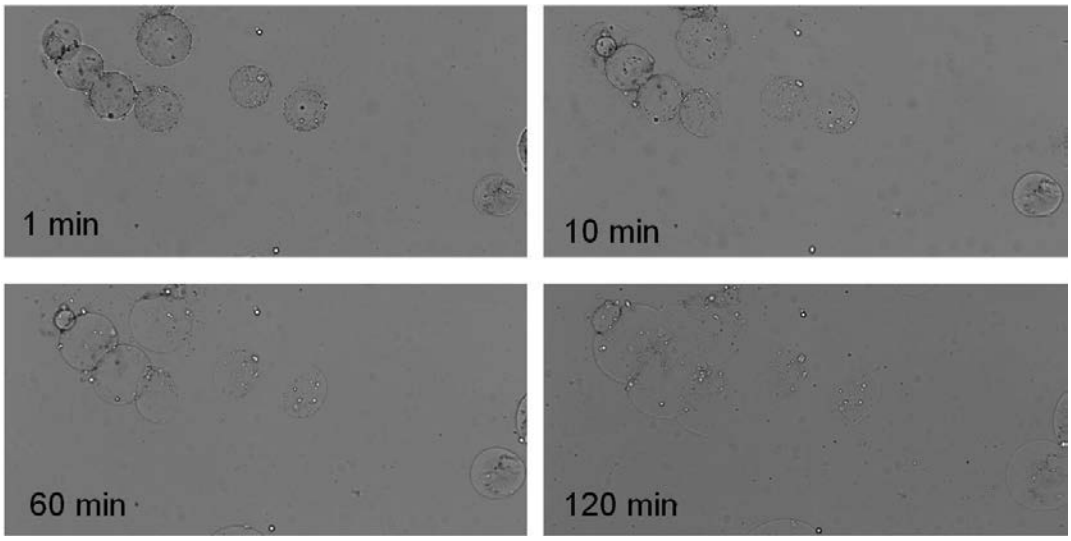


**Figure 2.8:** Optical microscopy images tracking microgel degradation over time in 1 M HCl (oil flow rate = 3.3 mL/h)

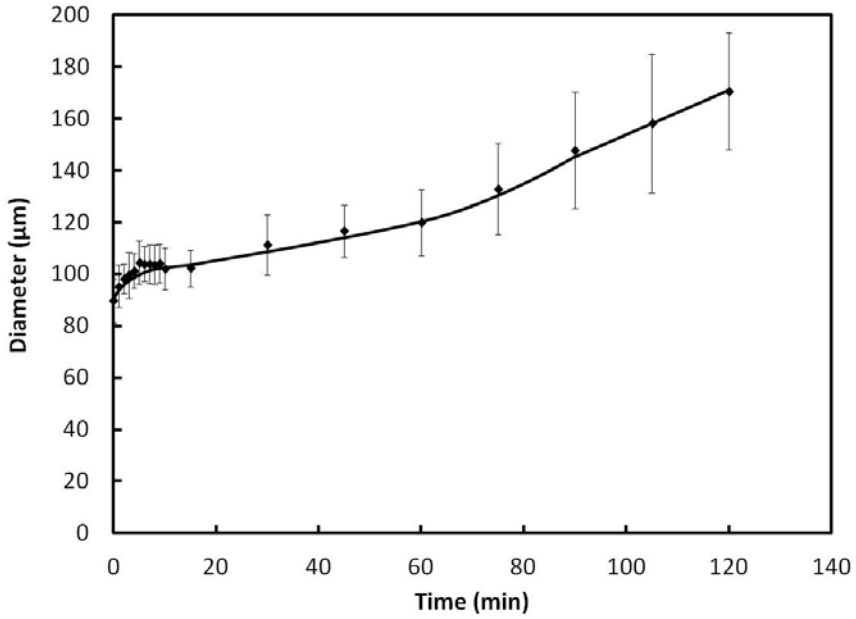


**Figure 2.9:** Measured change in diameter over time after exposure of microgels fabricated with an oil flow rate of 3.3 mL/h to 1 M HCl ($n$ = 100 particles counted)

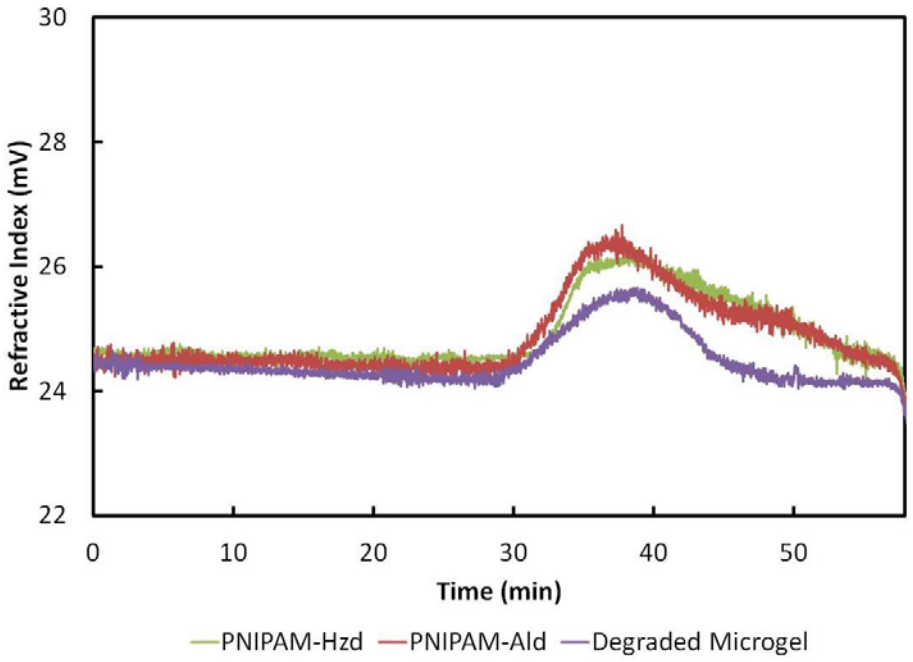


**Figure 2.10:** GPC analysis of microgels degradation products versus precursor polymers. This capacity for degradation into well-defined polymer segments lies in sharp contrast to microgels prepared with conventional precipitation techniques, in which minimal or no control over the molecular weight of the C-C backbone polymers between cross-links can be exercised.

*Cell Viability:* The toxicity of the precursor polymers and microgels produced were assessed using a MTT assay with 3T3 *Mus musculus* fibroblasts. Figure 2.11 displays the cell viabilities of the components with respect to cell-only controls.

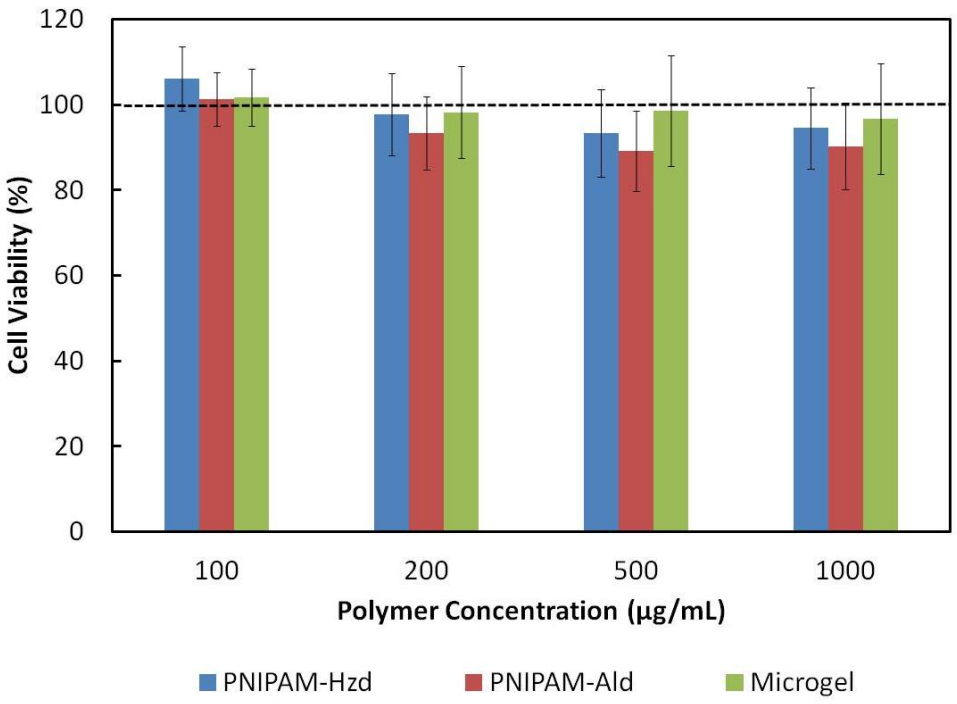


**Figure 2.11:** MTT results of 3T3 fibroblast cytotoxicity to PNIPAM-Ald and PNIPAM-Hzd precursor polymers and microgels relative to a cell-only control

No significant cell cytotoxicity was observed by the cells when exposed to the precursor polymers or the produced microgels at concentrations between 0.1 mg/mL and 1 mg/mL. This is consistent with previous studies involving PNIPAM functionalized with hydrazide or aldehyde groups as well as PNIPAM microgels prepared via conventional routes[40,44].

Taken together, the results demonstrate that the microfluidics approach proposed herein is capable of producing cytocompatible, low polydispersity and uniformly cross-linked populations of PNIPAM-based microgels with thermoresponsivities similar to microgels produced via traditional free radical gelation methods while also facilitating degradation of the hydrogel back into oligomeric precursor polymers. Such materials

may have significant applications as “on-demand” or externally addressable drug delivery vehicles, cell encapsulation matrices, or *in situ* biosensing probes, applications that could not be served by conventional free radical cross-linked microgels.

## 2.5 Conclusions

A microfluidic chip that can simultaneously mix and emulsify two reactive precursor polymers (here, hydrazide and aldehyde-functionalized-PNIPAM) is used to fabricate monodisperse degradable PNIPAM microgels on the size range of 30-90 μm, with size tunable based on the flow rate of the continuous oil phase used to prepare the particles in inverse emulsion. The microgels are fully degradable into their oligomeric prepolymer components via acid-catalyzed hydrolysis and exhibit analogous thermoswelling responses to conventional PNIPAM microgels, with a volume phase transition temperature of ~34ºC, a volumetric deswelling ratio of ~90%, and reversible swelling/deswelling capabilities (albeit with slight hysteresis on the first heating-cooling cycle again consistent with conventional PNIPAM microgels on this size scale). These particles avoid both the *in vivo* stability problems that plague ionically-cross-linked microgel beads (e.g. alginate-calcium) as well as the non-degradability and non-clearance issues associated with conventional free radical polymerized PNIPAM microgels, making them of potential interest for biomedical applications.

**2.6 Acknowledgements:** Funding from the Natural Sciences and Engineering Research Council of Canada (NSERC, Discovery Grant Program) and the Ontario Early Researcher Awards (Ontario Ministry of Research and Innovation) is gratefully acknowledged.

## 2.7 References

(1) Bysell, H.; Månsson, R.; Hansson, P.; Malmsten, M. *Adv. Drug Del. Rev.* **2011**, *63*, 1172.

(2) Rossow, T.; Heyman, J. A.; Ehrlicher, A. J.; Langhoff, A.; Weitz, D. A.; Haag, R.; Seiffert, S. *J. Am. Chem. Soc.* **2012**, *134*, 4983.

(3) Hou, C.; Zhang, Q.; Wang, H.; Li, Y. *J. Mater. Chem.* **2011**, *21*, 10512.

(4) Islam, M. R.; Serpe, M. J. *Biosens. Bioelectron.* **2013**, *49*, 133.

(5) Best, J. P.; Yan, Y.; Caruso, F. *Advanced Healthcare Materials* **2012**, *1*, 35.

(6) Lian, M.; Collier, C. P.; Doktycz, M. J.; Retterer, S. T. *Biomicrofluidics* **2012**, *6*.

(7) Headen, D. M.; Aubry, G.; Lu, H.; García, A. J. *Adv. Mater.* **2014**, *26*, 3003.

(8) Wu, Y.; Wang, L.; Guo, B.; X Ma, P. *Journal of Materials Chemistry B* **2014**, *2*, 3674.

(9) Kesselman, L. R. B.; Shinwary, S.; Selvaganapathy, P. R.; Hoare, T. *Small* **2012**, *8*, 1092.

(10) Huang, S.; Zeng, S.; He, Z.; Lin, B. *Lab Chip* **2011**, *11*, 3407.

(11) Seiffert, S.; Thiele, J.; Abate, A. R.; Weitz, D. A. *J. Am. Chem. Soc.* **2010**, *132*, 6606.

(12) Liu, Y.-M.; Wu, W.; Ju, X.-J.; Wang, W.; Xie, R.; Mou, C.-L.; Zheng, W.-C.; Liu, Z.; Chu, L.-Y. *RSC Advances* **2014**, *4*, 46568.

(13) Trongsatitkul, T.; Budhlall, B. M. *Langmuir* **2011**, *27*, 13468.

(14) Zhang, M.-J.; Wang, W.; Xie, R.; Ju, X.-J.; Liu, L.; Gu, Y.-Y.; Chu, L.-Y. *Soft Matter* **2013**, *9*, 4150.

(15) Mou, C.-L.; He, X.-H.; Ju, X.-J.; Xie, R.; Liu, Z.; Liu, L.; Zhang, Z.; Chu, L.-Y. *Chem. Eng. J.* **2012**, *210*, 212.

(16) Kang, M. K.; Kim, J. C. *Polym. Test.* **2010**, *29*, 784.

(17) Wu, Q.; Su, T.; Mao, Y.; Wang, Q. *Chem. Commun.* **2013**, *49*, 11299.

(18) Oh, J. K.; Drumright, R.; Siegwart, D. J.; Matyjaszewski, K. *Prog. Polym. Sci.* **2008**, *33*, 448.

(19) Katare, Y. K.; Muthukumaran, T.; Panda, A. K. *Int. J. Pharm.* **2005**, *301*, 149.

(20) Joshi, V.; Geary, S.; Salem, A. *AAPS J* **2013**, *15*, 85.

(21) Wang, Q.; Libera, M. *Colloids Surf., B* **2014**, *118*, 202.

(22) Tan, Y.-C.; Cristini, V.; Lee, A. P. *Sensors Actuators B: Chem.* **2006**, *114*, 350.

(23) Park, J. I.; Saffari, A.; Kumar, S.; Günther, A.; Kumacheva, E. *Annu. Rev. Mater. Res.* **2010**, *40*, 415.

(24) Kim, J.-W.; Utada, A. S.; Fernández-Nieves, A.; Hu, Z.; Weitz, D. A. *Angew. Chem.* **2007**, *119*, 1851.

(25) Luo, R.-C.; Ranjan, S.; Zhang, Y.; Chen, C.-H. *Chem. Commun.* **2013**, *49*, 7887.

(26) Seiffert, S.; Weitz, D. A. *Soft Matter* **2010**, *6*, 3184.

(27) Seiffert, S.; Romanowsky, M. B.; Weitz, D. A. *Langmuir* **2010**, *26*, 14842.

(28) Chau, M.; Abolhasani, M.; Thérien-Aubin, H.; Li, Y.; Wang, Y.; Velasco, D.; Tumarkin, E.; Ramachandran, A.; Kumacheva, E. *Biomacromolecules* **2014**, *15*, 2419.

(29) Marquis, M.; Davy, J.; Fang, A.; Renard, D. *Biomacromolecules* **2014**, *15*, 1568.

(30) Choi, C.-H.; Jung, J.-H.; Rhee, Y.; Kim, D.-P.; Shim, S.-E.; Lee, C.-S. *Biomed. Microdevices* **2007**, *9*, 855.

(31) Yang, C.-H.; Lin, Y.-S.; Huang, K.-S.; Huang, Y.-C.; Wang, E.-C.; Jhong, J.-Y.; Kuo, C.-Y. *Lab Chip* **2009**, *9*, 145.

(32) Sakai, S.; Ito, S.; Inagaki, H.; Hirose, K.; Matsuyama, T.; Taya, M.; Kawakami, K. *Biomicrofluidics* **2011**, *5*, 013402.

(33) Steinhilber, D.; Rossow, T.; Wedepohl, S.; Paulus, F.; Seiffert, S.; Haag, R. *Angew. Chem. Int. Ed.* **2013**, *52*, 13538.

(34) Allazetta, S.; Hausherr, T. C.; Lutolf, M. P. *Biomacromolecules* **2013**, *14*, 1122.

(35) Shah, R. K.; Kim, J.-W.; Agresti, J. J.; Weitz, D. A.; Chu, L.-Y. *Soft Matter* **2008**, *4*, 2303.

(36) Duncanson, W. J.; Lin, T.; Abate, A. R.; Seiffert, S.; Shah, R. K.; Weitz, D. A. *Lab Chip* **2012**, *12*, 2135.

(37) Choi, C.-H.; Jung, J.-H.; Kim, D.-W.; Chung, Y.-M.; Lee, C.-S. *Lab Chip* **2008**, *8*, 1544.

(38) Huang, S.; Lin, B.; Qin, J. *Electrophoresis* **2011**, *32*, 3364.

(39) Patenaude, M.; Hoare, T. *ACS Macro Letters* **2012**, *1*, 409.

(40) Patenaude, M.; Campbell, S.; Kinio, D.; Hoare, T. *Biomacromolecules* **2014**, *15*, 781.

(41) Pawlikowska, P.; Gajkowska, B.; Orzechowski, A. *Cell Tissue Res.* **2007**, *327*, 571.

(42) Burmistrova, A.; Richter, M.; Uzum, C.; Klitzing, R. *Colloid. Polym. Sci.* **2011**, *289*, 613.

(43) Cao, Z.; Du, B.; Chen, T.; Li, H.; Xu, J.; Fan, Z. *Langmuir* **2008**, *24*, 5543.

(44) Sivakumaran, D.; Maitland, D.; Hoare, T. *Biomacromolecules* **2011**, *12*, 4112.

**S2: Chapter 2 - Supplmentary Information**

**MICROFLUIDIC PRODUCTION OF DEGRADABLE THERMORESPONSIVE POLY(N-ISOPROPYLACRYLAMIDE)-BASED MICROGELS**

**Authors:** Daryl Sivakumaran, Eva Mueller, and Todd Hoare

**Publication:** To be submitted in 2015

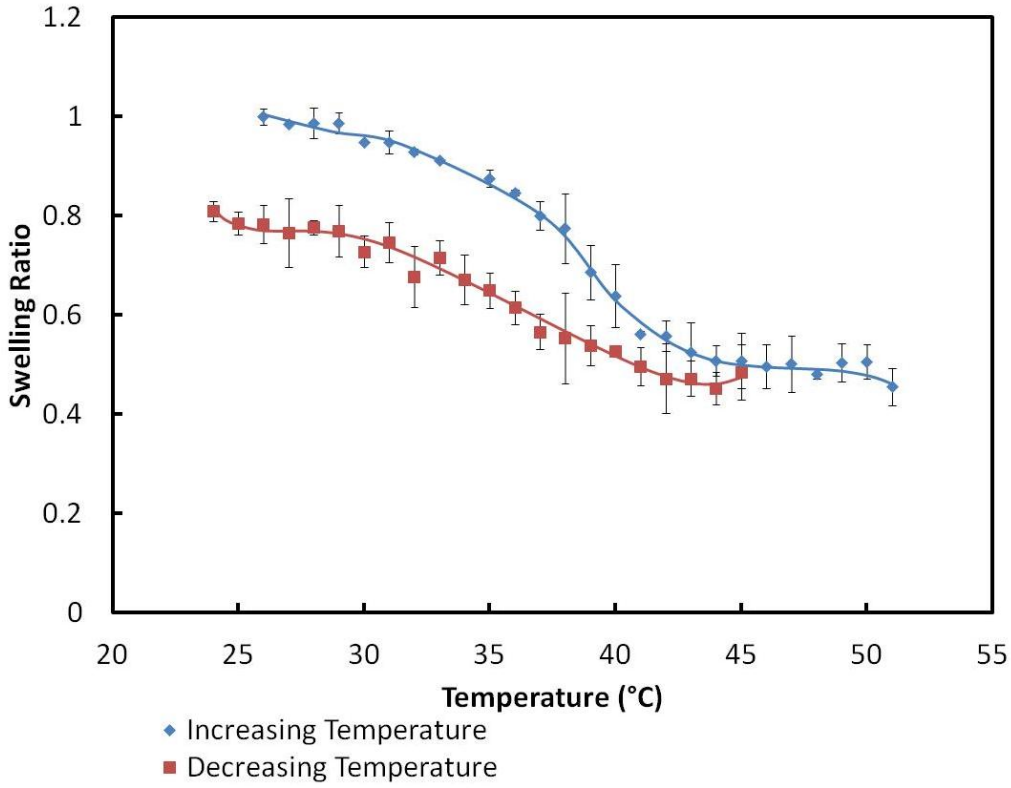


**Figure S2.1:** Swelling ratio hysteresis associated with the first heating/cooling for PNIPAM microgels made with an oil flow rate of 1.1 mL/h

# Chapter 3

# PREPARATION AND DRUG RELEASE KINETICS MANIPULATION OF FULLY DEGRADABLE MICROGEL-HYDROGEL COMPOSITES PREPARED USING IN SITU GELLING CHEMISTRY AND MICROFLUIDICS

**Authors:** Daryl Sivakumaran and Todd Hoare

**Publication:** To be submitted in 2015

## 3.1 Abstract

Fully degradable microgel-hydrogel composites were created utilizing hydrazone cross-linking to form gels on both the bulk and micro length scales. Carbohydrates (carboxymethyl cellulose and dextran) and thermoresponsive poly(N-isopropylacrylamide) (PNIPAM) were used as the two base hydrogel backbones, with each functionalized with hydrazide and aldehyde groups to facilitate hydrazone bond formation and thus covalent gelation upon mixing. Microgels were fabricated using flow-focusing microfluidics to create monodisperse microgel particles cross-linked via the exact same chemistry used to prepare the bulk hydrogel, ensuring a uniform cross-linking density through the entire network that (unique to other studies in this area) allows for explicit investigation of the effect of embedded microgel phases on the release kinetics independent of the cross-link density or microgel morphology. Results suggest that release of bupivacaine hydrochloride can be controlled through the manipulation of polymer type and polymer selection for each phase (microgel versus hydrogel),

particularly in the burst phase. Specifically, the deswelling phase transitions observed for PNIPAM-based microgels and hydrogels above their volume phase transition temperature were observed to significantly reduce release of bupivacaine when PNIPAM was the continuous phase but not when PNIPAM was the dispersed phase; furthermore, the incorporation of microphases even of the exact same composition into a bulk hydrogel effectively reduced the burst release from the hydrogel.

**Keywords:** Microgels, microfluidics, composite hydrogels, drug delivery

## 3.2 Introduction

Hydrogels have been extensively studied as potential drug delivery vehicles[1-3] since they have many desirable properties in that context. Hydrogels can be designed to exhibit similar physical, mechanical, and chemical properties to the natural extracellular matrix, making them more likely than many other biomaterials to exhibit biocompatible responses in different biologically relevant environments[4,5]. In addition, hydrogels can be loaded with high drug fractions due to their high water content and thus high internal free volumes[5-7]. However, this high water content can also prove to be a barrier to the use of hydrogels as effective release vehicles, as this hydrated microstructure makes the loading of hydrophobic drugs difficult[8] and the release of hydrophilic drugs faster than desired[5]. Additionally, the macroscopic dimensions of traditional hydrogels make them hard to administer through minimally non-invasive methods such as injection, requiring the use of surgical methods that reduce patient comfort and can result in lower patient compliance with the therapy[5].

The challenge of injectability has been addressed via the development of many different rapid covalent bond forming chemistries that can be applied to network polymers together either upon mixing (e.g. through a double barrel syringe) or upon exposure to the physiological environment (typically using heat or pH as a gelation trigger). “Click” chemistry allows for the bonding of reactive functional groups at physiological conditions[9] and has been widely utilized to make hydrogels[10-12]. Diels-Alder reactions utilize a cycloaddition between diene and dienophile groups to create cross-links[13,14]. The reaction is reversible but typically only at temperatures well above

physiological temperature[15,16]; coupled with the slow gelation kinetics (10-160 min), the use of this chemistry in the body is challenging[14]. Thiol-Michael addition can be utilized to take advantage of thiol reactions to form thioethers using such as functionalities as maleimides[15,16] or vinyl sulfones[17-19] but again typically result in non-degradable cross-links. Hydrazide-aldehyde reactions to form hydrazone bonds can form a hydrolytically degradable linkage and can facilitate rapid gelation (on the order of seconds to minutes) depending on cross-linker concentration, making the potential utility of hydrazone chemistry as a hydrogel cross-linking method highly promising[20,21]. Hydrogels based on natural polymers (e.g. cellulose[22], dextran[23], or hyaluronic acid[24]) or synthetic polymers (e.g. poly(ethylene glycol) (PEG)[25], poly(N-isopropylacrylamide (PNIPAM)[26], or poly(oligoethylene glycol methacrylate) (POEGMA)[21]) have been prepared effectively using hydrazone chemistries for a variety of biomedical applications.

Facilitating hydrophilic drug loading and slow release from hydrogels has proven to be somewhat challenging, particularly for extended release (i.e. weeks or months) applications. One such method involves the creation of multi-phase hydrogels that contain micron or nano-sized drug carriers within the hydrogel[27]. These drug carriers can be made from liposomes[28], nanoparticles[29], or polymeric microgels[30], depending on the physical properties of the drug to be delivered. In particular, the presence of microgels within a bulk hydrogel phase can present key characteristics to help facilitate longer drug release times for more hydrophilic drugs. Firstly, microgels can easily be functionalized with affinity sites that can bind drugs through hydrophobic/hydrophilic interactions, hydrogen bonding, or electrostatics[31]. By functionalizing only the microgel (i.e. the dispersed

phase) with drug affinity sites, a partitioning gradient of drug is established between the microgel and bulk gel phases that at least partially counteracts the high concentration gradient of drug between the inside and outside of the hydrogel phase, resulting in slower drug release. Microgels can also introduce diffusive or partitioning barriers into the matrix that could assist in controlling the release of drug[32], including the mitigation of the burst release effect seen in traditional hydrogels[27]. In this sense, the ability to independently design the chemistry and cross-link density of both the hydrogels and microgels separately provides the opportunity to individually tune both phases to achieve the desired release profile depending on the characteristics of each phase.

Previously, we have reported the formation of a microgel-hydrogel composite utilizing acrylic acid functionalized PNIPAM-based microgels as the dispersed phase and a hydrazone cross-linked carbohydrate hydrogel based on carboxymethyl cellulose and dextran as the continuous phase[27,33]. The presence of acrylic acid within the backbone makes the microgels anionic, enhancing the affinity of the microgel phase for the cationic drug payload (bupivacaine hydrochloride). Tuning of drug release from these composites can be achieved through the independent manipulation of the cross-linking density and/or composition of the hydrogel and microgel phases. While changing the degree of cross-linking within the bulk hydrogel phase was observed to influence release kinetics by altering the diffusion through the composite, manipulation of the microgel phase demonstrated the potential for far greater control of drug release kinetics from the composite. Altering the affinity of the cationic drug for the anionic microgels by increasing the acrylic acid content significantly slowed drug release to the point that

sustained release of the small molecule drug bupivacaine could be achieved over at least 40 days, an exceptionally long-term release relative to previous reports of small molecule release from hydrogels[5,34]. Increasing the cross-linking content of the charged microgel, which subsequently reduces the degree of deswelling across the phase transition temperature from the preparation temperature (25°C) to the release temperature (37°C), can also be used to reduce the magnitude of burst release observed from the composites.

However, despite the advantages of microgels in this context, conventional PNIPAM-based microgels such as those described above also suffer from key limitations in terms of their use in such an application. Due to their smaller (typically < 1 micron) diameters, microgels are more likely to elicit inflammatory responses thus are often cleared from the injection site and deposited within the liver or spleen[35]. This effect is typically suppressed in microgel-hydrogel composites in which the microgels are immobilized within the hydrogel, but may still result in mild chronic inflammation as the composites degrade. Conventional PNIPAM microgels also suffer from an inherent lack of degradability[36] (limiting their potential *in vivo* use) as well as a non-homogeneous microstructure, in which cross-linker and (in some cases) functional affinity comonomer are not uniformly distributed within the microgel but are rather localized in the core (cross-linker) or the shell[37,38]. In this sense, unambiguous differentiation between the effect of the presence of the dispersed phase and the composition/microstructure of the dispersed versus continuous phases on drug release is not directly possible.

In this work, we aim to directly address these challenges by preparing degradable microgels on the order of tens of microns using droplet-based microfluidics to cross-link

hydrazide and aldehyde-functionalized carbohydrates (CMC/dextran) or PNIPAM in a templated inverse emulsion. In this sense, the cross-link densities and mass fractions of polymer within the microgel phase should be identical to that of the bulk hydrogel, eliminating all uncertainty in terms of interpreting the effect of microgel cross-link density, water content, and functional group distributions on the observed release behaviors. It is thus the intent of this study to determine if the presence of a microgel phase (even if that phase has an identical composition to the bulk phase) plays a role in governing drug release from the composites.

### 3.3 Experimental

*Materials:* N-isopropylacrylamide (NIPAM, 99%), acrylic acid (AA, 99%), thioglycolic acid (98%), aminoacetaldehyde dimethyl acetal (99%), 2,2,6,6-tetramethyl-1-piperidinyloxy (TEMPO, 98%), N-hydroxysuccinimide (NHS, 97%), sodium cyanoborohyride (95%), methacryloyl chloride (purum), sodium carboxymethyl cellulose (CMC, $M_W$ 250 000, DS=0.9), dextran from *Leuconstroc spp*. (Dex, $M_W$ 500 000), ethylene glycol (99.8%), sodium periodate (>99.8%) , and bupivacaine hydrochloride (99%) were all purchased from Sigma Aldrich (Oakville, Canada). Adipic acid dihydrazyde (ADH, Alfa Aesar, 98%), *N*'-ethyl-*N*-(3-dimethylaminopropyl)-carbodiimide (EDC, Carbosynth, Compton CA, commercial grade), and 2,2-azobisisobutryic acid dimethyl ester (AIBMe, Wako Chemicals, 98.5%) were all used as received. Dimethyl sulfoxide (DMSO, reagent grade) and acetonitrile (HPLC grade) was purchased from Caledon Laboratory Chemicals (Georgetown, ON). Milli-Q grade

distilled deionized water (DIW) was used for all experiments. Hydrochloric acid (1M) was received from LabChem Inc. (Pittsburgh, PA). Ethanol was purchased from Commercial Alcohols (Brampton, ON).

*Fabrication of Microfluidic Chip:* A mould template outlining the microfluidic chip was patterned on a 3-inch silicon wafer using photolithography with a SU-8 2075 photoresist (MicroChem, MA, USA). The microfluidic chip was generated using the mould template via soft lithography with polydimethylsiloxane (Sylgard 184, Dow Chemicals). The inlets for the microfluidic chip were made from Masterflex silicone tubing (Cole Palmer, Ontario, Canada) and were placed onto the mould prior to PDMS addition. The chip was cured at 70 °C for 1.5 h prior to being bonded to a glass microscope slide through oxygen plasma exposure at 40 W for 30 s at 0.3 mTorr, with the bond allowed to form overnight.

*Synthesis of Hydrazide-Functionalized PNIPAM (PNIPAM-Hzd):* Functional PNIPAM precursor polymers were made following protocols developed by Patenaude and Hoare[20]. Hydrazide functionalized polymers were made via EDC-mediated conjugation of a large excess of adipic acid dihydrazide (ADH) to a PNIPAM-co-acrylic acid polymer. The starting copolymer was synthesized via free radical polymerization of NIPAM (4.5g) and acrylic acid (0.5 g - 15 mol% total monomer) in 20 mL of ethanol with thioglycolic acid as a chain transfer agent (80 µL), and 2,2-azobisisobutyric acid dimethyl ester (AIBME, 0.056 g) as the initiator (reaction temperature = 56°C). The resulting polymer had a final molecular weight of 21.6 kDa and an acrylic acid functionalization of 15 mol% (base-

into-acid conductometric titration, ManTech). Hydrazide attachment to the residual –COOH groups was completed using carbodiimide chemistry to conjugate a 5-fold molar excess of ADH using a 3-fold molar excess of EDC. Conductometric titration indicated that 95% of the acrylic acid groups were converted to hydrazide functionalities.

*Synthesis of Aldehyde-Functionalized PNIPAM (PNIPAM-Ald):* Aldehyde-functionalized PNIPAM was prepared via copolymerization of NIPAM (4 g) and N-(2,2-dimethoxyethyl)methacrylamide (DMEMAm, 0.95 g, 13.4 mol% of total monomer) followed by hydrolysis of the acetal groups in DMEMAm to yield aldehyde groups. Molecular weight was controlled using thioglycolic acid chain transfer agent (80 μL) with polymerization occurring in absolute ethanol and initiated by AIBME initiator (0.056 g). The resulting polymer (MW 20 kDa, 12 mol% aldehyde on a total monomer basis by $^{1}H$ NMR analysis) was subjected to 24 hours of hydrolysis in 1M HCl to convert the acetal groups to aldehydes.

*Synthesis of Hydrazide-Functionalized Carboxymethyl Cellulose (CMC-Hzd):* CMC (250 kDa, 1 g) was dissolved in 200 mL Milli-Q water under magnetic stirring in a round bottom flask. ADH (3 g) was added to the polymer solution and allowed to dissolve fully. N-hydroxysuccinimide (NHS, 0.07 g) was dissolved in a 4 mL DMSO:$H_2O$ (1:1) solution and added dropwise to the CMC/ADH mixture. Subsequently, EDC (0.3 g) was dissolved in 1 mL of 1:1 DMSO:$H_2O$ and also added dropwise to the reaction solution, with the solution pH maintained at 6.8 using 0.1 M NaOH for a period of 1 hour. The modified

polymer was dialyzed against Milli-Q water for six cycles (each lasting a minimum of 6 hours) using membrane tubing (Spectrum Labs, molecular weight cut-off 3,500 Da) and subsequently lyophilized and stored. Conductometric titration resulted in the conversion of 44% of the -COOH groups on the CMC backbone to hydrazides (based on the difference in measured –COOH contents before and after ADH conjugation).

*Synthesis of Aldehyde-Functionalized Dextran (Dex-Ald):* Dextran (1.5 g) was dissolved in Milli-Q water (150 mL) under magnetic stirring. Sodium periodate (0.8 g) was dissolved in 10 mL of Milli-Q water and added dropwise to the dextran solution. Oxidation was allowed to occur over the course of 2 hours, after which the reaction was stopped through the addition of ethylene glycol (0.4 mL). The polymer was then dialyzed (Spectrum Labs, molecular weight cut-off 3,500 Da) over 6 x 6 hour wash cycles, lyophilized, and stored dry[39].

*Microgel Formation via Microfluidics*: Microgels were created using a two-stage microfluidic chip previously reported by our lab (Figure 3.1)[40]. The microfluidic chip contains two polymer inlets (one for hydrazide-functionalized precursor polymers and the other for aldehyde-functionalized precursor polymers) protected by a short zig-zag channel to create a pressure gradient preventing back-flow of each polymer into the complementary polymer reservoir (which, if it occurred, would lead to undesired gelation within the chip). 6 wt% solutions of PNIPAM-Hzd and PNIPAM-Ald and 1 wt% solutions of CMC-Hzd and Dex-Ald (both in water) were used to match the

concentrations used for bulk gel preparation[20,26]. These concentrations result in quick-gelling (under a minute) and stable hydrogel structures. The polymers are then co-streamed through a pre-mixing channel to stabilize the flow prior to contacting the continuous phase (paraffin oil, 1 wt% Span 80) using flow-focusing geometry to create polymer droplets. The aqueous polymer phase was run at a flow rate of 0.03 mL/h while the continuous oil phase was run at 3.3 mL/hr (both using KDS Legato 200 infusion syringe pumps). Prior to particle production, the microfluidic chip was primed by flowing oil through the chip to ensure that no apparent defects were presented. The polymer solution flows were then started to begin the production of polymeric particles, although particle collection for analysis was not started until 1 hour into production to ensure polymer flow stabilization. Particles were collected into centrifuge tubes under gentle magnetic agitation which were pre-filled with an additional 5 mL of paraffin oil to help prevent aggregation. Collection of particles lasted until the oil phase was consumed (approximately 15-18 hours).

*Microgel Purification:* After collection, microgel particles were allowed to settle under gravity, followed by removal of the majority of (top phase) paraffin oil. Subsequent washing steps (5-8 per sample) were conducted by adding pentane at a ratio of 10 mL of pentane for every 0.5 mL of microgel solution to ensure removal of excess paraffin oil and residual surfactant. The solution was shaken vigorously, and the particles were allowed to resettle prior to the next washing step. Any residual pentane that remained after the last washing step was evaporated under a gentle nitrogen purge overnight, after

which the purified microgels were resuspended in 10 mM PBS (pH 7.4, 0.15 M overall ionic strength).

*Microgel-Hydrogel Composite Formation:* To form injectable composite hydrogels, microfluidics-derived microgels were co-injected with hydrazide and aldehyde-functionalized linear polymers through a double-barreled syringe (Medmix Systems, Switzerland). One barrel contained the hydrazide-functionalized polymer (either CMC-Hzd (20 mg, 2% w/v) or NIPAM-Hzd (60 mg, 6% w/v)) dissolved in 1 mL of 0.15 M saline; the other barrel contained the aldehyde-functionalized polymer (either Dex-Ald (20 mg, 2% w/v) or NIPAM-Ald (60 mg, 6% w/v) dissolved in 1 mL of 0.15 M saline. Where relevant, microgels were added to both solutions (~1 330 000 particles per mL of solution) to comprise a total of 20 vol% of the total volume of each solution. Bupivacaine hydrochloride (the model drug) was dissolved at a concentration of 5 mg/mL in both solutions. The resultant hydrogel-microgel mixture was ejected through a 20G needle into cylindrical moulds (diameter 0.64 cm and height 0.32 cm) prepared from silicone rubber obtained from McMaster Carr (Elmhurst, IL). The resultant liquid was allowed to cure into hydrogel (~2-3 minutes), allowing for all drug in the original solutions to be trapped effectively within the hydrogel-microgel matrix. Given that no gel dewatering was observed during or after the gelation process, all bupivacaine in the original solution becomes directly entrapped inside the resulting gel; based on the dimensions of the samples used for testing, this corresponds to a loading of 0.51 mg bupivacaine per test sample.

*Hydrogel and Microgel-Hydrogel Composite Drug Release Studies:* Drug release studies were conducted in 12-well cell culture plates using cell culture inserts (2.5 cm diameter, 8 μm pore size, perforated 20 times with a 20-gauge needle to ensure free flow of 10 mM PBS (pH 7.4, 0.15 M overall ionic strength) and drug into and out of the insert) to contain the hydrogel samples. A total of 2 mL of 10 mM PBS was used as release media, with n=6 hydrogel-microgel composites sampled per test configuration. The hydrogel samples were incubated at 37 °C in an orbital shaker at an oscillation rate of 100 rpm. Drug release samples were collected every 30 minutes for the first 6 hours, every hour for the next 3 hours, and intermittently over the course of the gel lifetime, with the release buffer fully replaced at each sampling step to ensure maintenance of infinite sink conditions. Quantification of drug release was completed with high-performance liquid chromatography (HPLC) using a 2707 Autosampler, 2489 UV/Visible Detector and 1525 Binary HPLC Pump (all from Waters Corporation), a reversed-phase Atlantis C18 column (100 mm x 4.6 mm, Waters Corporation), and a mobile phase consisting of phosphate buffer (pH=6.8, 35% by volume) and acetonitrile (65%) (flow rate 2 mL/min). An absorbance of 263 nm was used to measure bupivacaine content of the elution samples, with errors expressed as the standard deviation of the replicates. Drug elution samples pre-filtered through a 0.45 μm syringe filter (Pall Corp) to remove any possible aggregates prior to analysis.

The same drug release studies were completed with the hydrogels and microgels individually, using the same method described above (omitting the microgels) for the hydrogel-only studies. For microgel release studies, ~137 000 microgels (to match the

average concentration of microgel present in each microgel-hydrogel composite) were suspended in a 5 mg/mL bupivacaine solution in 10 mM PBS and allowed to incubate for 24 hours to facilitate drug loading. The solution was then placed in 1 mL Float-a-Lyzer membranes (molecular weight cut-off 100 kDa, $n = 4$) to track release kinetics, using 6 mL of fresh 10 mM PBS as the elution medium. Microgels were sampled every 30 minutes for the first 6 hours followed by intermittent drug release measurements thereafter, with full replacement of the elution medium at each step to ensure maintenance of infinite sink conditions. Quantification of drug elution was completed using high-performance liquid chromatography (HPLC) as described above.

*Gel Swelling:* Swelling of the microgel-hydrogel composite was determined by comparing the mass of the gel at a particular time point following incubation in 10 mM PBS (pH 7.4, 0.15 M overall ionic strength) at physiological temperature to the mass of the gel immediately following formation. The mass of the cell insert and the gel were measured during drug release studies at each time point of drug release sampling (n=6 per sample). Percentage mass changes were calculated according to Equation (1):

$$\%Volume\ Change = \frac{Volume_{37^oC} - Volume_{20^oC}}{Volume_{20^oC}} \quad (1)$$

*Partition Studies:* Hydrogels were made as described above but with no drug dissolved in the prepolymer solutions. This hydrogel was submerged in a 2 mL of a 5 mg/mL solution of bupivacaine in 10 mM PBS (pH 7.4, 0.15 M overall ionic strength) for 24 hours at

room temperature (20°C) and at physiological temperature (37°C). After 24 hours, the hydrogel was removed and the amount of drug remaining in the solution was analyzed via HPLC (using the conditions described above). For measuring drug partitioning into microgels, a similar test was conducted by suspending 120 000 microgels in 10 mM PBS (pH 7.4, 0.15 M overall ionic strength) inside a 1 mL Float-a-Lyzer membrane (molecular weight cut-off 100 kDa) and then submerging the entire membrane inside 6 mL of a 5 mg/mL bupivacaine solution in 10 mM PBS (pH 7.4, 0.15 M overall ionic strength).

### 3.4 Model Fitting of Drug Release Kinetics

Assuming that the two phases are functioning independently of each other (as is supported by previous research[32]), and assuming the microgels are uniformly distributed through the hydrogel matrix with little or no self-interactions, modelling of the drug release of the composite can be approximated as a function of combined resistances to drug diffusion through both the bulk and embedded phases. The release profiles from the hydrogels and microgels alone will first fit, following by the composite hydrogel systems, to assess the validity of these assumptions. Focus will be on the initial stages of the release, since the potential for burst release is a significant issue when designing drug release devices; furthermore, the non-100% plateau release values observed with PNIPAM-based hydrogels are difficult to model using diffusion kinetics-based techniques[41], although the model to follows attempts to also compensate for convective-based release upon PNIPAM gel phase deswelling.

Diffusion-based release kinetics from hydrogels, microgels, and composites can be modelled based on Fick's 2nd Law of Diffusion[42], which relates the change in concentration over time as a function of the diffusion coefficient of the solute (*D*), the concentration of the drug ($C_A$), the position within the gel (*x* and *r*, where *x* and r are defined as 0 at the half-height and central axis of the cylinder respectively) and the time elapsed (*t*) (Equation 2):

$$\frac{1}{r}\frac{\partial}{\partial r}\left(rD\frac{\partial C_A}{\partial r}\right) + D\frac{\partial^2 C_A}{\partial x^2} = \frac{\partial C_A}{\partial t} \qquad (2)$$

For a non-infinite cylinder (accounting for both radial and axial flux, as required based on the 0.64cm diameter x 0.32cm height dimensions of the test samples used), the following boundary and initial conditions will apply (assuming a well-mixed interface):

1. Initial condition: $C=C_o$ at t=0 and for $-H < x < H$ and $0 < r < r_o$ (i.e. uniform drug concentration throughout the sample at t=0 of the release process)
2. Boundary condition 1: $C = C_{inf} = 0$ at $t > 0$ and x=-H, H
3. Boundary condition 2: $dc/dx = 0$ at $t > 0$ and $x = 0$
4. Boundary condition 3: $C = C_{inf} = 0$ at $t > 0$ at $r = r_o$
5. Boundary condition 4: $dc/dr = 0$ at $t > 0$ and $r = 0$

Here, $C_o$ is the initial concentration, $C_{inf}$ is the concentration of drug in the bulk solution, H is the half height of the cylinder, and $r_o$ is the outer radius of the cylinder. Using these

boundary conditions the amount of drug released from a cylindrical hydrogel disk at any given time can be calculated (Equation 3)[43]:

$$\frac{M_t}{M_\infty} = 1 - \frac{32}{\pi^2}\sum_{n=1}^{\infty}\frac{1}{q_n^2}\exp\left(-\frac{q_n^2}{r^2}Dt\right) x \sum_{p=0}^{\infty}\frac{1}{(2p+1)^2}\exp\left[\frac{-(2p+1)^2\pi^2 Dt}{H^2}\right] \quad (3)$$

Here, $M_t/M_\infty$ is the fraction of drug released, $D$ is the diffusion coefficient of the solute through the hydrogel, $q_n$ are the roots of the Bessel function of the first kind of zero order [$J_0(q_n)=0$], $r$ is the radius of the cylinder, and $H$ is the height of the cylinder. This equation can be used to determine release profiles for a small molecule drug such as bupivacaine[43].

To account for convection effects of a shrinking hydrogel, Eq. 3 cannot be used. Instead, convection effects can be accounted for based on Equation 4[44]:

$$\frac{\partial C}{\partial T} = D\,\frac{\partial^2 C}{\partial x^2} - v\frac{\partial C}{\partial x} \quad (4)$$

Here, the relevant boundary conditions are:

(c,0) = 1 for 0 < x < ) X(0)

X(0) = L

∂c/∂x (0,t) = 0 for t > 0

c (X(t), t) = 0 for t > 0

To facilitate analytical solutions to this equation, the convection term can be removed using the Landau transformation, with the drug release rate instead expressed as a function of the moving boundary front X(t), the rate of the movement of the boundary front ($\dot{X}$) and the Laudau function ζ (Equation 5) [44]. Note that t=τ for the transformation.

$$\frac{\partial c}{\partial \tau} = \frac{D}{X^2}\frac{\partial^2}{\partial \zeta^2} - \frac{\dot{X}}{X} \quad \text{in } 0 < \zeta < 1, \tau > 0 \quad (5)$$

For the transformed equation, the relevant boundary conditions are:

$$c(\zeta, 0) = 1 \qquad 0 < \zeta < 1$$

$$\partial c/\partial x\ (0,\tau) = 0 \qquad \text{for } \tau > 0$$

$$c\ (X(t), \tau) = 0 \qquad \text{for } \tau > 0$$

This transformed expression allows us to express the convective portion of the drug release in the context of a particulartype of boundary front movement. In the case of these nanocomposite hydrogels, which swell or deswell over the time period of the release to reach an equilibrium swelling ratio, a logistic boundary front movement function is most appropriate, enabling Equation 6 to be used to model drug release:

$$\frac{M_t}{M_\infty} = 1 - \sum_{n=0}^{\infty} \frac{8e^{-\frac{D}{2r}(\frac{(2n+1)\pi}{2mL})^2[(m-1)^2+4(m-1)]}}{(2n+1)^2\pi^2}\, e^{-D(\frac{(2n+1)\pi}{2mL})^2 t} \quad (6)$$

Here, D is the diffusion coefficient, r is shrinking factor (i.e. the rate at which the gel shrinks, which can be estimated from the gravimetric swelling data), m is the ratio of final to initial length of the gel, and L is the initial length of the gel. The moving boundary

function X(t) can be expressed as a function of the shrinking factor, which is displayed in the above equation. This model can be used to estimate the diffusion of a drug from the hydrogel, as the hydrogel shrinks during early time points of release. This expression for fraction of drug release assumes logistic growth/shrinking in which the gel size eventually reaches an asymptotic condition and no longer grows/shrinks. Also, perfect sink conditions are assumed, with all drug contained within the hydrogel at initial conditions and the drug concentration assumed to be equal to zero at the growing/shrinking boundary. Additionally, this model assumes 1D release geometry, which given the dimensions of the release sample is not a fully satisified assumption in this case (i.e. L/r = 1 as opposed to >10 as typically required for the semi-infinite assumption to be satisfied). However, any 2D model for this case would require the use of finite element modeling which is beyond the scope of this thesis, allowing this approach to at least give insight into the importance of convection in the release process. In addition, comparing the 1D simple diffusion model to the 2D simple diffusion model used resulted in a relatively small error (<10%) in the calculated diffusion coefficients; as such, while the limitations of using a 1D model for this case are recognized, such an approach can still lend some physical insight into the drug delivery kinetics of these systems.

For the microgels, the drug (solute) will be modelled as diffusing though a sphere. It is again assumed that the drug concentration is initially uniform across the entire cross-section of the sphere (initial condition 1) and that the following boundary and initial conditions that apply:

1. $C = C_o$ at t=0 and for $0 < r < r_o$

2. $C = C_{inf} = 0$ at $t > 0$ and $r = r_o$
3. $dc/dr = 0$ at $t > 0$ and $r = 0$

Here, $C_o$ is the initial concentration, $C_{inf}$ is the concentration of drug in the bulk solution, and *r* is the distance from the center of the microgel to the surface. The fraction of drug release from the particle can thus be modelled by Equation 7:[45]

$$\frac{M_t}{M_\infty} = 1 - \frac{6}{\pi^2}\sum_{n=1}^{\infty}\frac{1}{n^2} * \exp\left[\frac{-Dn^2\pi^2 t}{r^2}\right] \quad (7)$$

where *D* is the diffusion coefficient of the drug through the microgel network and *r* is the radius of the particle. To avoid the use of infinite series in the subsequent expressions derived, approximate solutions can be used for the early time and late time parts of the drug release process. For early release ($M_t/M_\infty < 0.6$) from a sphere, Equation 8 applies[46]:

$$\frac{M_t}{M_\infty} = 6\sqrt{\frac{Dt}{r^2\pi}} - \frac{3Dt}{r^2} \quad (8)$$

where r is the radius of the sphere. The differential of the above equation is:

$$\frac{dM_t/M_\infty}{dt} = 3\sqrt{\frac{D}{r^2\pi t}} - \frac{3D}{r^2} \quad (9)$$

For late time periods ($0.4 < M_t/M_\infty < 1$), the fraction of drug release from the spherical microgel can be defined by Equation 10[46]:

$$\frac{M_t}{M_\infty} = 1 - \frac{6}{\pi^2}\exp\left(\frac{-\pi^2 Dt}{r^2}\right) \quad (10)$$

where r is again the radius of the sphere. The differential of the above equation is:

$$\frac{dM_t/M_\infty}{dt} = \frac{6D}{r^2}\exp\left(\frac{-\pi^2 Dt}{r^2}\right) \quad (11)$$

For release kinetics measurements, microgels were placed inside a Float-a-Lyzer dialysis tube, and drug release was measured outside of the tube at defined intervals. In this geometry, although a high molecular weight cut-off membrane (100 kDa) was used to minimize any membrane effects, the diffusion of drug through the membrane also contributes a kinetic contribution to the measured release in the receiving media. To find the true diffusion coefficient of the microgels, the following mass balance was considered for free drug within the dialysis tubing[47]:

$$\frac{dM_D}{dt} = M_\infty \frac{dM_t/M_\infty}{dt} - K_m M_D(t) \quad (12)$$

Here, $M_D$ is the mass of free drug inside the dialysis membrane and $K_m$ is the rate constant associated with drug diffusion through the membrane. In this equation, the first term represents the release rate of drug out of the spherical microgels (*in* to the solution inside the dialysis tube) while the second term represents the diffusion of drug through the membrane (*out* of the solution inside the dialysis tube). The (measured) concentration of drug outside the dialysis membrane ($M(t)$) can then be related to the concentration of free drug in the solution inside the dialysis membrane ($M_D$) again by a mass balance[47]:

$$\frac{dM(t)}{dt} = K_m M_D(t) \quad (13)$$

Here, the drug *in* to the receiving buffer is diffused through the membrane; there is no mechanism for drug to move *out* of the receiving buffer in the closed receiving system used. By using the drug-only control data (tracking release of a known drug concentration without microgels from inside the membrane) to identify $K_m$, fitting the (measured) *M(t)* values to find $M_D(t)$ for the microgel release, and substituting the $d(M_t/M_\infty)/dt$ terms for both early and late time approximations into Eq. 11, the diffusion coefficient of drug release from the microgels themselves can be calculated. Fully derived models for both the short and long time approximations can be accessed in S4: Supplementary Information.

The diffusion coefficient of drug through each hydrogel and the microgel phase considered was first determined by fitting the drug release data measured for each hydrogel and microgel alone, with Equations 3 and 6 used to fit drug release for the hydrogels and Equations 12 used to fit drug release from the microgels. A diffusion coefficient was calculated by minimizing the sum of square differences between the experimental data and calculated model data for the first 3 hours of release, corresponding to the burst release time that is the particular target of this model (note that the early time approximations apply primarily to this section of the release curves).

To estimate the theoretical diffusion coefficient of the composite, the calculated empirical diffusion coefficients of the hydrogel and microgel components were combined through a weighted sum, with weightings determined based on the relative volume

fraction of each phase in the composite hydrogel. This approach effectively models the diffusional resistances of the multiple phases in series, as per Equation 14:

$$D_C = \varphi_H D_H + \varphi_M D_M \quad (14)$$

Here $D$ is the diffusion coefficient of the composite ($D_C$), hydrogel component ($D_H$) and microgel component ($D_M$). Predicted composite diffusion coefficients were also calculated assuming the diffusional resistances between the microgel and bulk gel phases were in parallel, but poorer fits were achieved. We hypothesize this is a direct result of there being no independent pathway for drug release through the microgel phase alone at the volume fraction of microgels used (~20 vol%); as such, no true parallel option for diffusion exists in this system. Composites were empirically modelled using a slab configuration, with the data compared to the predicted diffusion coefficient calculated by the series approximation in Equation 14.

### 3.5 Results

*Microgel Production:* Microgels were produced utilizing a microfluidic device to simultaneously mix and emulsify monodisperse aqueous droplets of hydrazide and aldehyde-functionalized polymer precursors, which subsequently gel confined inside the droplets to form monodisperse microgel populations on the order of tens of microns in diameter. Figure 3.1 shows that largely monodisperse microgel populations based on both CMC-Hzd/Dextran-Ald cross-linking (Fig. 3.1a) and PNIPAM-Hzd/PNIPAM-Ald cross-linking (Fig. 3.1b) can be prepared (3.3 mL/hr oil flow and 0.03 mL/hr aqueous stream flow). CMC-Hzd/Dextran-Ald microgels exhibited diameters of 67.6 ± 6.2 μm

whereas PNIPAM-Hzd/PNIPAM-Ald microgels exhibited diameters of 65 ± 5.3 μm (n=100 particles measured for each microgel). Of note, this equivalent size persisted independent of the significantly higher viscosity of the CMC-Hzd/Dextran-Ald precursor polymers relative to PNIPAM-Hzd/PNIPAM-Ald, confirming that the interfacial shear applied at the emulsification step is the key driving force for regulating microgel size.

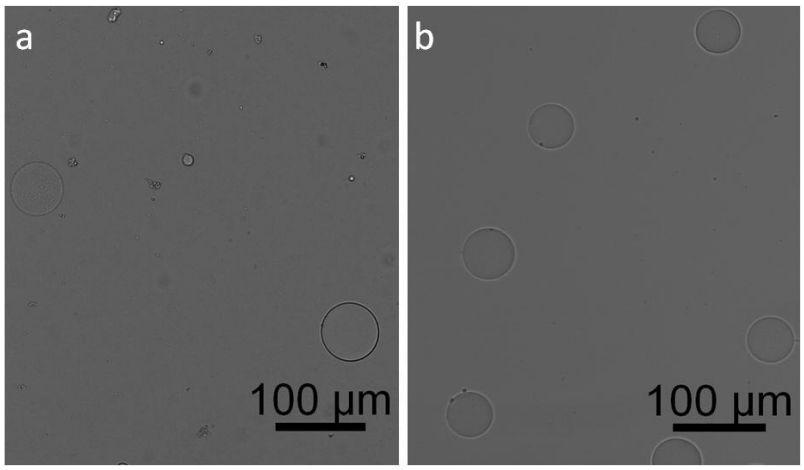


**Figure 3.1:** Microgels produced based on a) carbohydrates (CMC and dextran) and b) PNIPAM

*Composite Production:* Microgel-hydrogel composites were made by suspending microfluidic-produced microgels in solutions containing each of the precursor polymers. The hydrogel precursor polymers dissolved readily in the presence of the microgels. Gelation of the composite required between 30-60 seconds, with the CMC-Hzd/Dextran-Ald (~30 sec) hydrogel gelling somewhat faster than the PNIPAM-Hzd/PNIPAM-Ald hydrogel (~60 sec). This difference in gelation kinetics is likely due to the higher

molecular weight of the carbohydrate pre-polymers, resulting in less required bond formation to effectively create a cross-linked hydrogel network.

*Drug Release from Microgels and Hydrogels:* Drug release from the microgels and hydrogels individually (prior to composite formation) is shown in Figure 3.2.

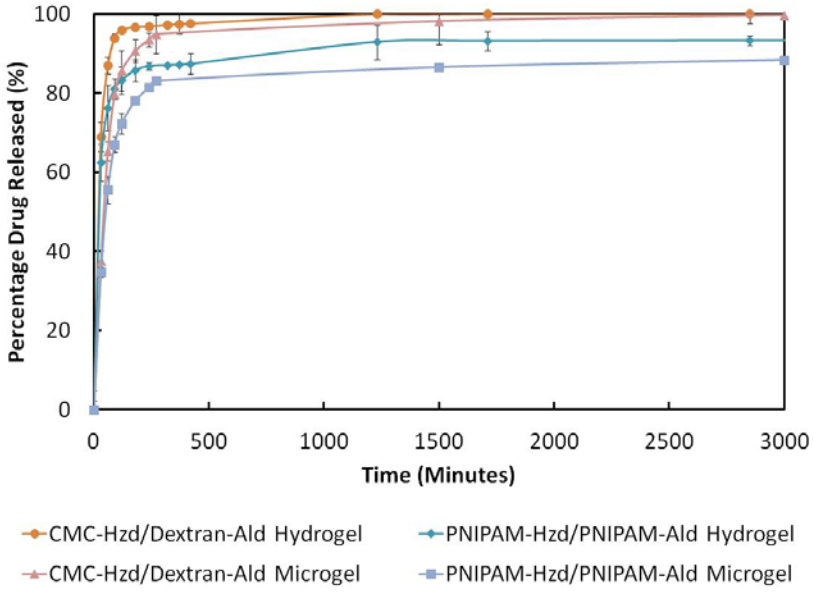


**Figure 3.2:** Bupivacaine release kinetics from microfluidic produced microgels and *in situ*-gelling hydrogels made from carbohydrates (CMC-Hzd/Dextran-Ald) and PNIPAM (PNIPAM-Hzd/PNIPAM-Ald).

Microgels and hydrogels based on both polymer pairs exhibited rapid, burst-like release of bupivacaine from their networks. This is particularly evident for CMC-Hzd/Dextran-Ald hydrogels or microgels, in which nearly 100% drug release is achieved over the course of only 1-2 hours. Only somewhat slower release was observed from PNIPAM-based hydrogels, which we attribute to the deswelling of the thermoresponsive hydrogel

when placed at physiological temperature (above the volume phase transition temperature of the hydrogel (Figure 3.3) and microgel). Although the deswelling typically results in convectively-enhanced burst release from the hydrogel, it can also effectively trap drug inside a network of significantly lower effective pore size, resulting in the lower equilibrium plateau drug release observed for PNIPAM-based samples. In contrast, the CMC-Hzd/Dextran-Ald hydrogels exhibit nearly zero net swelling change over the full incubation period (Figure 3.3), resulting in the maintenance of a more hydrated network throughout the release period and nearly 100% drug release at the plateau value.

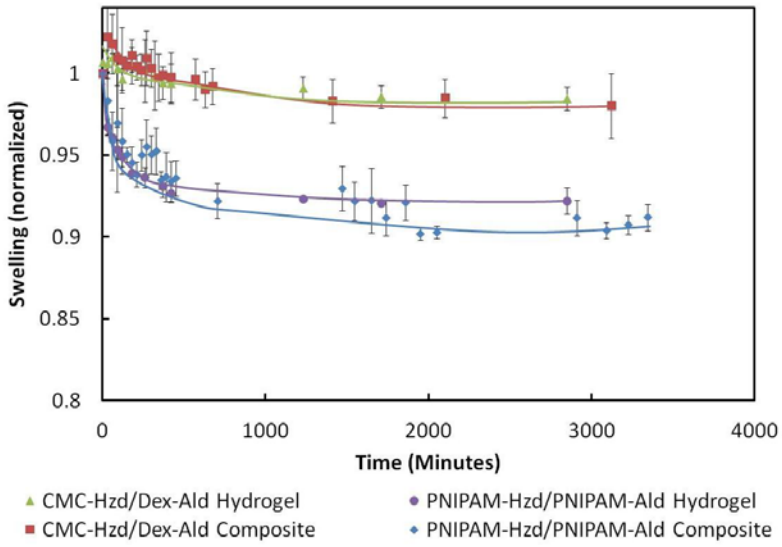


**Figure 3.3:** Deswelling kinetics of bulk hydrogels made from carbohydrates (CMC-Hzd/Dextran-Ald) and PNIPAM (PNIPAM-Hzd/PNIPAM-Ald) relative to composites prepared containing 20 wt% microgels of the same chemistry

Of note, contrary to expectations, microgels of both CMC-Hzd/Dextran-Ald and PNIPAM-Hzd/PNIPAM-Ald released drug slightly slower than their corresponding bulk hydrogels; typically, one would expect that the smaller size of the microgel would result in a lower average diffusional path for drug release and thus faster overall drug release. We attribute this difference to the different methods used to load drug into the bulk hydrogel and microgel phases. Microgels were loaded following gelation via equilibration with a bupivacaine drug solution; hydrogels were loaded by simply mixing the drug in the precursor solutions, resulting in entrapment of the full mass of drug added as the gel forms. Indeed, partitioning studies performed by loading both the microgel and the hydrogel via the same diffusion-based technique from the same total volume indicates that a significantly high amount of drug will partition into the hydrogel phase than the microgel phase of the same composition (Table 3.1); this result suggests that if the bulk and microgel samples were loaded with the same diffusion-based technique, slower drug release would be expected from a bulk gel even excluding the geometric considerations. As such, while the partitioning result suggests that the hydrogels should contain somewhat more bound drug than the microgel, the entrapment-based loading technique used also results in the hydrogel containing significantly more free drug, as there is no opportunity for free drug to partition outside the hydrogel phase prior to the release experiment. This results in faster release of more drug from the hydrogel relative to the microgels in this particular case.

**Table 3.1:** Drug partitioning of bupivacaine into microgels and hydrogels as measured at room temperature (gel preparation condition) and 37°C (test condition).

| | **Drug Loaded (mg of drug/cm$^3$ of gel)** | **Partition Coefficient of Drug in Gel Phase** |
|---|---|---|
| PNIPAM-Hzd/PNIPAM-Ald Microgel | 0.66 ± 0.02 | 0.23 ± 0.01 |
| CMC-Hzd/Dextran-Ald Microgel | 0.32 ± 0.10 | 0.11 ± 0.01 |
| PNIPAM-Hzd/PNIPAM-Ald Hydrogel (20°C) | 2.11 ± 0.18 | 0.89 ± 0.07 |
| CMC-Hzd/Dextran-Ald Hydrogel (20°C) | 2.37 ± 0.05 | 0.96 ± 0.04 |
| PNIPAM-Hzd/PNIPAM-Ald Hydrogel (37C) | 3.06 ± 0.15 | 1.23 ± 0.12 |
| CMC-Hzd/Dextran-Ald Hydrogel (37°C) | 3.85 ± 0.20 | 1.55 ± 0.16 |

*Drug Release from Composite:* Microgel-hydrogel composites were prepared based on the following combinations: i) CMC-Hzd/Dextran-Ald microgel in a CMC-Hzd/Dextran-Ald hydrogel matrix ii) PNIPAM-Hzd/PNIPAM-Ald microgel in a CMC-Hzd/Dextran-Ald hydrogel matrix iii) CMC-Hzd/Dextran-Ald microgel in a PNIPAM-Hzd/PNIPAM-Ald hydrogel matrix iv) PNIPAM-Hzd/PNIPAM-Ald microgel in a PNIPAM-Hzd/PNIPAM-Ald hydrogel matrix. Collectively, this series of composites permits explicit investigation of the effect of the presence of internal phases independent of chemistry (composites containing like gel phases) and the orientation of those phases as either the bulk or continuous phase relative to the other (composites containing one gel phase with each chemistry). Figure 3.4 shows the resulting drug release kinetics from each type of composite tested.

Focusing first on the composites made with CMC-Hzd/Dextran-Ald as the continuous hydrogel phase, drug release is rapid with a very large burst over short time frames, with ~80% of drug released after 2 hours independent of the identity or presence of the internal microgel phase. This result is expected since the CMC-Hzd/Dextran-Ald hydrogel matrix is extremely hydrophilic, has minimal specific affinity for the cationic drug (partition coefficient of 0.96, Table 3.1), and does not deswell over time to restrict the porosity of the gel network. However, CMC-Hzd/Dextran-Ald bulk gel composites with PNIPAM-Hzd/PNIPAM-Ald microgels experienced a significantly higher amount of drug release during the initial burst phase ($p = 0.024$ comparing the two kinetic profiles between 0-180 minutes) relative to composites with CMC-Hzd/Dextran-Ald microgels (Fig. 3.4b). This result is most likely attributable to the thermal deswelling of the microgels that can convectively enhance release any diffusion-based release of drug partitioned into the microgel phase. However, after just 90 minutes, this convective effect ceases to affect drug release (as the microgels reach approximately their equilibrium swelling values at 37°C) and the release profiles become independent of the identity of the microgel phase. It should also be noted that the plateau % release observed at the end of the burst period occurs at a significantly lower level (~80% total drug release) relative to that observed for the single-phase CMC-Hzd/Dextran-Ald hydrogel or microgel (~100% total drug release). For the composite containing PNIPAM-based microgels, this differential plateau may be attributed to drug entrapment within the microgel phase upon deswelling; however, the origin of the effect in the composite prepared with the same CMC-Hzd/Dextran-Ald chemistry is less clear and seems to suggest that the presence of a

phase boundary has a significant effect on the release profile even if the chemistry of the continuous and dispersed phases are the same.

More significant effects of phase orientation are observed when PNIPAM-Hzd/PNIPAM-Ald is used as the continuous (bulk) phase of the composite. In comparison to the carbohydrate bulk hydrogels, drug release from composites prepared with a PNIPAM-Hzd/PNIPAM-Ald bulk phase is significantly slower. This result can again be explained by the deswelling of the PNIPAM hydrogels, which results in smaller pore sizes and subsequently reduced diffusion of drug through the composite.

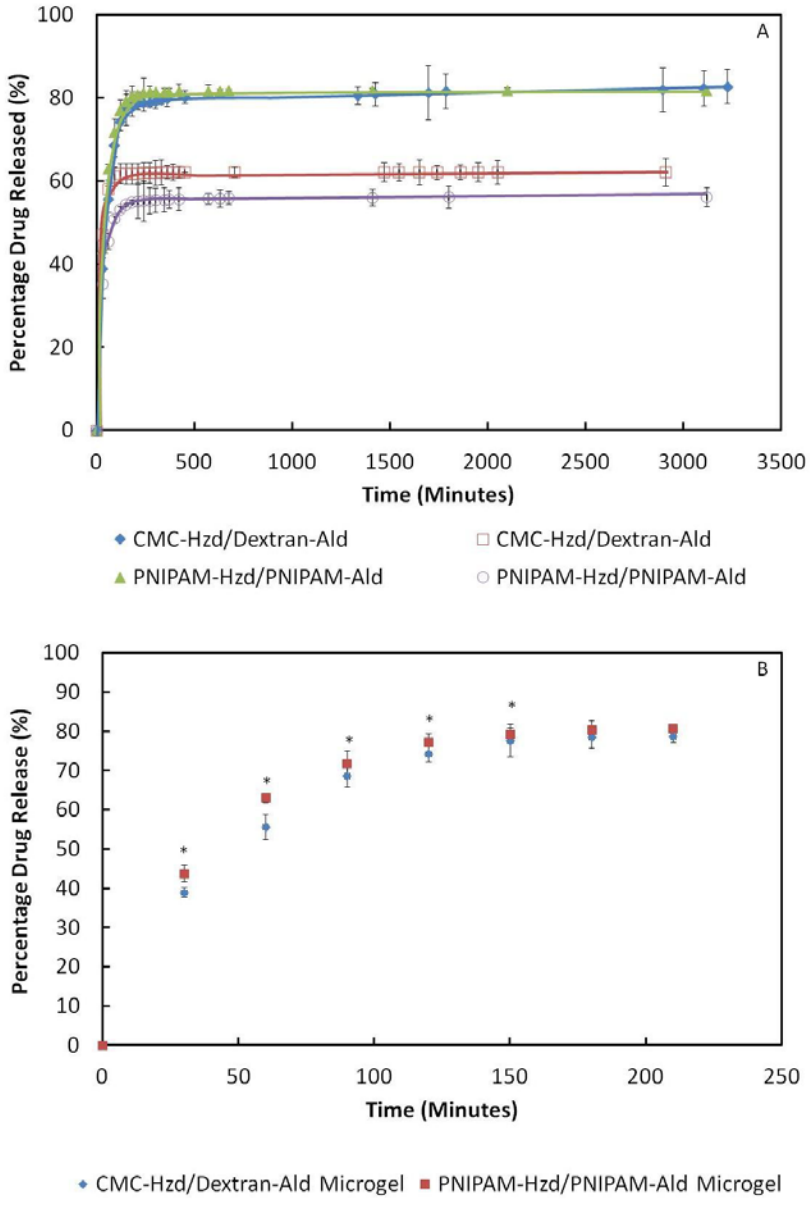


**Figure 3.4**: a) Drug release kinetics from microgel-hydrogel composites. The legend refers to the type of microgel used to form the composite; samples with solid markers were prepared with a CMC-Hzd/Dextran-Ald bulk gel while samples with unfilled markers were prepared with a NIPAM-Hzd/NIPAM-Ald bulk gel. b) Early stage (burst) release from composites based on a CMC-Hzd/Dextran-Ald bulk hydrogel containing different microgels (* represents significant difference between data points ($p < 0.05$))

However, the identity of the microgel phase in this case results in a significant difference in bupivacaine release, with a CMC-Hzd/Dextran-Ald microgel phase promoting higher drug release from the composite relative to PNIPAM-Hzd/PNIPAM-Ald microgels. This again can be explained by the volume phase transition of PNIPAM. Deswelling of the PNIPAM microgel results in trapping of more drug with microgel phase upon microgel collapse; in addition, collapse of the internal microgel phase would eliminate an elastic barrier to deswelling in the bulk PNIPAM gel and lead to bulk gel deswelling and a concurrent decrease in bulk gel porosity. This effect has been previously demonstrated in the literature with conventional PNIPAM microgels on the hundreds of nanometer length scale[48-50], and based on the presented data (drug release coupled with the small but significant enhanced thermal deswelling observed for the PNIPAM/PNIPAM nanocomposite at equilibrium compared to a PNIPAM bulk gel in Figure 3.3 ($p = 0.02$) is still operative on this larger length scale. In contrast, composites containing CMC-Hzd/Dextran-Ald microgels (which do not deswell as a function of temperature) would neither experience drug entrapment due to microgel collapse nor facilitate additional bulk gel collapse via the generation of free volume within the composite, leading to higher maintained porosity and thus enhanced release relative to the PNIPAM/PNIPAM composite. Expressed in a different way, the initial deswelling of the PNIPAM bulk gel is the only factor suppressing release in CMC-Hzd/Dex-Ald microgel composites but is one of multiple contributing factors in the PNIPAM-Hzd/PNIPAM-Ald microgel composites. Collectively, these results suggest that drug release profiles from microgel-hydrogel composites can be controlled through independent manipulation of the microgel

or hydrogel phase even when neither phase has particular affinity for the drug. Of note, the plateau release observed following the burst phase is again significantly lower for composites prepared even with the same chemistry relative to either phase tested individually; for example, PNIPAM-Hzd/PNIPAM-Ald microgels or hydrogels alone exhibited plateau releases in the 80-90% total release range following the burst regime (Fig. 3.2) while a PNIPAM-Hzd/PNIPAM-Ald hydrogel-PNIPAM-Hzd/PNIPAM-Ald microgel nanocomposite shows a plateau release at only ~50% total drug loading (Fig. 3.4). While the slightly higher overall mass fraction of polymer in the composites relative to the hydrogels alone may account in part for this difference (for example, 6.2 total mass % in composite, 6 total mass % in hydrogel alone for PNIPAM-Hzd/PNIPAM-Ald nanocomposite gels), this result may also be attributable to the differential deswelling kinetics of the bulk and microgel PNIPAM phases. Drug convectively transported out of the microgel phase (which deswells somewhat faster than the bulk hydrogel phase) may be trapped more effectively by the more slowly deswelling bulk hydrogel phase than if the drug is contained within a single phase hydrogel which is deswelling at the same rate throughout.

### 3.6 Discussion

The creation of physically entrapped microgel-hydrogel composites based hydrazone bond creation (using macro-gelation of hydrogels and microfluidic gelation of microgels) presents the opportunity for tunable drug release profiles, particularly in the burst regime. Specifically, release of drug from composite hydrogels (particularly during

the burst phase) can be adjusted based on the temporal manipulation of the pore sizes within both the hydrogel and microgel phases. Composites based on CMC-Hzd/Dextran-Ald bulk gels are very highly hydrated, leading to reduced diffusional resistance for release of drug and thus faster drug release relative to composites based on PNIPAM-Hzd/PNIPAM-Ald bulk gels. The release profiles from these carbohydrate-based composites also indicated very little partitioning of the slightly hydrophobic drug (partition coefficient = 0.89 and logP = 0.18[51]) into the hydrophobic chains of the PNIPAM microgel, as release profiles of composite hydrogels prepared with PNIPAM or carbohydrate-based microgels quickly equalized between the after an initial burst of drug from the PNIPAM microgels caused by thermal microgel deswelling. The presence of the microgel phase results in a slightly slower release profile, which may be attributed to the higher mass fraction within the composite (due to the presence of the microgels) relative to the hydrogel on its own.

Lower burst releases resulted from the use of PNIPAM-Hzd/PNIPAM-Ald hydrogels as the bulk gel phase, a result of the thermal deswelling of the hydrogel reducing the diffusibility of drug inside the gel matrix. Introduction of a PNIPAM-based microgel phase that could also deswell resulted in even lower burst release profiles and high drug entrapment within the matrix, while a CMC-Hzd/Dextran-Ald microgel phase both itself remained swollen and elastically restricted further bulk gel deswelling to result in higher burst drug release and less efficient drug entrapment. This ability to control drug release profiles based on the swelling responses of both the microgel and hydrogel in response to changes in temperature demonstrates the potential of smart composites for

fabricating controlled release vehicles. However, it should be noted that an improved understanding over the fate of the nanocomposites over longer periods of time (i.e. to clearly identify how or if the drug remaining in the composite after the plateau phase is reached) must be acquired to fully understand how such systems could be applied in real controlled release applications.

Model fitting of the drug delivery kinetics of these composite systems yields further insight into their fundamental properties. Empirical model fits of the early time drug release results for hydrogels and microgels based on CMC-Hzd/Dextran-Ald and PNIPAM-Hzd/PNIPAM-Ald (modelled using Equations 3, 12 (CMC hydrogels), and 5 (PNIPAM hydrogels)) are shown in Figure 5.

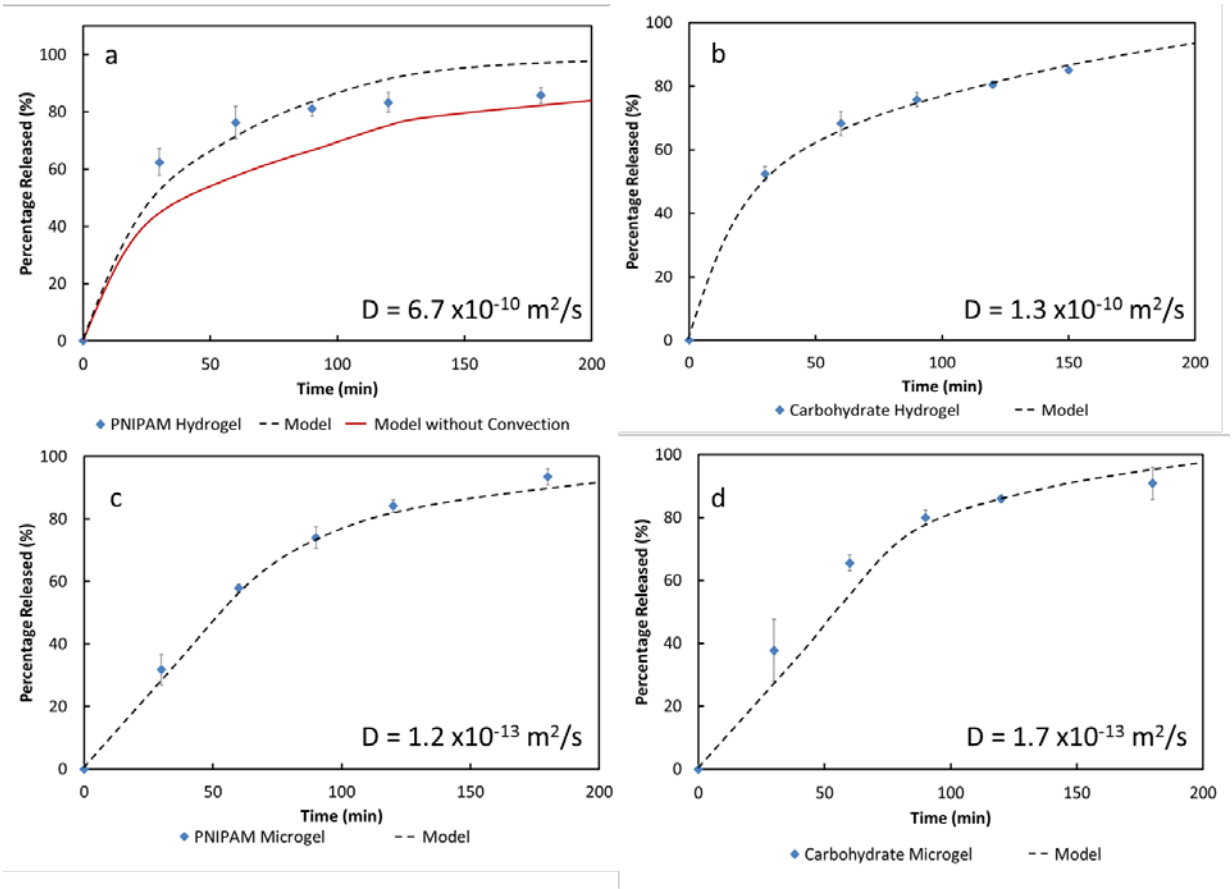


**Figure 3.5:** Experimental release data (points) and model best fit (dashed line) from PNIPAM-Hzd/PNIPAM-Ald hydrogels (a), CMC-Hzd/Dextran-Ald hydrogels (b), PNIPAM-Hzd/PNIPAM-Ald microgels (c), and CMC-Hzd/Dextran-Ald microgels (d) is represented by the data points. The best-fit diffusion coefficients are shown embedded in the graph. The red line indicates the model without accounting for convection using only the 2-D diffusion model (Equation 3).

The slab and spherical release models provided reasonable fits to the experimental data without requiring any adjustable parameters ($R^2 > 0.86$) except the NIPAM hydrogel ($R^2 = 0.49$), as the model cannot absolutely capture the thermally-driven burst release followed by the thermally-retarded diffusion at longer times facilitated by the gel collapse even when convection is considered. However, incorporating a convective contribution

in the model does significantly improve the fit to the experimental data in this case ($R^2$ = 0.49 with convection and 0.11 without convection). Of interest, even without considering convection, the fit of the PNIPAM microgel release data is good ($R^2$ = 0.97), suggesting that the smaller dimensions of the microgel can help to avoid potential issues such as skin effects and differential heating between the surface and inside of the gel that complicate modeling release in bulk thermoresponsive hydrogels[52-54]. The higher diffusion coefficients identified for the NIPAM hydrogel is consistent with the burst effect that is observed in these gels. Interestingly, even when membrane effects are considered, the measured diffusion coefficients for drug release from the microgels are significantly lower than those from the bulk hydrogels with similar compositions. This result may indicate that (1) the possible Schiff base formation between the amine on bupivacaine and excess aldehydes and/or (2) the degree of cross-linking proceed to a greater extent within the microgel assembly geometry than the bulk gel assembly geometry, which differ (necessarily) significantly in terms of contact time between the reactive pre-polymers, the nature and rate of mixing between the pre-polymers, and the dimensions of the gelation process despite being chemically identical in terms of the polymer chemistries, concentrations, solution viscosities, and drug loadings. This result is of potential interest in terms of using microfluidic-based gelation strategies to alter the release kinetics of drugs versus what would be achieved using more conventional gelation approaches and warrants future investigation moving forward.

Each individual phase diffusion coefficient measured was then substituted into Equation 14 to estimate the average diffusion coefficient inside the composite hydrogels (assuming that there is no significant change in swelling of either phase when they are in equilibrium with each other rather than just water) without including any adjustable fitting parameters. Good fits were obtained for the carbohydrate-carbohydrate composite and also to some degree the carbohydrate bulk gel – PNIPAM microgel composite (Figures 6a and 6b, $R^2 > 0.74$) utilizing the weighted diffusion coefficient and the slab model with no adjustable fitting parameters, indicative of the essentially pure diffusion control over drug release in microgel-in-hydrogel composites in which the bulk phase (the carbohydrate) does not undergo a phase transition (i.e. no convective contributions are observed in drug release). In comparison, fits for systems in which PNIPAM is the bulk gel were reasonable at shorter time points but diverged significantly at longer time points (Figures 6c and 6d), with consideration of convection improving the fit but still falling short of completely capturing the trend in the data. In particular, the poorer plateau fit achieved for the PNIPAM/PNIPAM composite (Fig 6c and 6d) is likely related to the fact that both the microgel and hydrogel phases are deswelling upon heating from room temperature to physiological temperature; the relative rates of this deswelling would govern whether drug is released via convection or entrapped via gel collapse. Furthermore, at later times, after both the bulk and microgel phases have fully collapsed, the diffusion coefficient of drug would also become significantly lower than would be approximated during the burst period modeled, resulting in somewhat of a plateau in the later times experimentally that is not accurately captured by the model that applies a single average diffusion coefficient

during the collapse phase. These relative kinetics are not straight-forward to track using the bulk gravimetry experiments applied here to relate swelling to drug release, but will be tracked in future work using confocal microscopy approaches to attempt to improve our understanding of the relative rates of phase collapse in the PNIPAM-in-PNIPAM composite gel system.

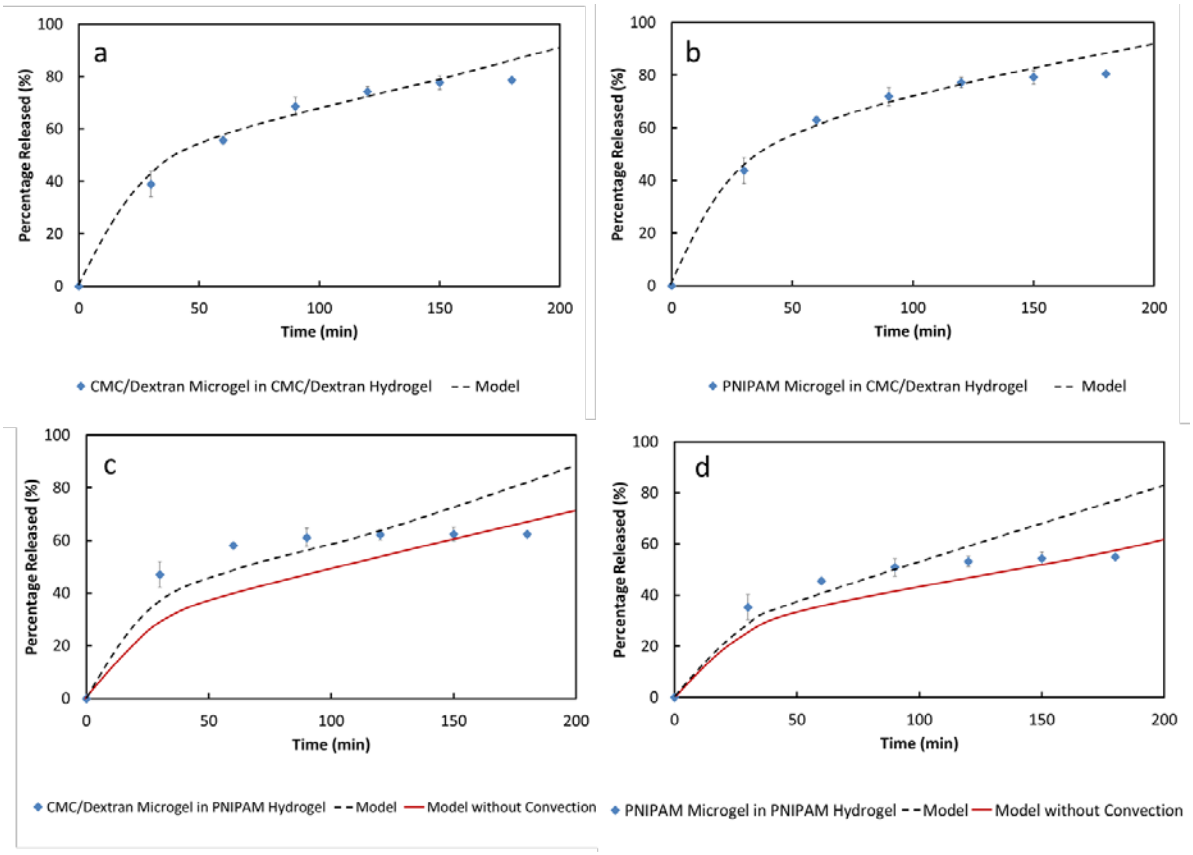


**Figure 3.6:** Release of bupivacaine from a) CMC-Hzd/Dextran-Ald microgels in CMC-Hzd/Dextran-Ald hydrogel, b) PNIPAM-Hzd/PNIPAM-Ald microgels in CMC-Hzd/Dextran-Ald hydrogel, c) CMC-Hzd/Dextran-Ald microgels in PNIPAM-Hzd/PNIPAM-Ald hydrogel, d) PNIPAM-Hzd/PNIPAM-Ald microgels in PNIPAM-Hzd/PNIPAM-Ald hydrogel composites Data points represent experimental data and the dashed line represents the calculated model based on the use of a calculated *D* as a weighted sum of the phase volume fractions (Equation 13). The red line indicates the model without accounting for convection using a simple 2-D model (Equation 3).

### 3.7 Conclusions

Fully degradable microgel-hydrogel composites prepared with the same composition and cross-link density and distribution in both the bulk and dispersed gel phases demonstrate differential drug release kinetics as a function of both the chemistry and the relative orientation of the two gel phases. Hydrogels or composite gels prepared entirely with carbohydrates (CMC-Hzd/Dex-Ald) do not deswell as a function of time or temperature and thus exhibit rapid burst release of drug no matter the orientation of the phases, although the incorporation of a microgel phase even of the same hydrophilic carbohydrate composition reduces the burst from ~100% to ~80%. In contrast, hydrogels or composite gels prepared with poly(N-isopropylacrylamide) exhibit thermal deswelling when heated from their preparation condition (at room temperature) to their test condition (at physiological temperature), resulting in the reduction in burst release and an improved entrapment of drug as a function of time. Diffusion coefficients of bupivacaine through microgel-hydrogel composites can be well-predicted based on the geometric volume-weighted sum of the diffusion coefficients of individual components used to make the composite for composite hydrogels where CMC-Hzd/Dextran-Ald is the continuous phase; however, when PNIPAM-Hzd/PNIPAM-Ald is the continuous phase, predictive fits are only achieved when the model is adjusted to account for the collapse of the hydrogel network, which both convectively transports drug out of the gel at short times and then traps drug at longer times. In particular, combining a thermosensitive microgel phase within a thermosensitive bulk gel phase results in increased entrapment relative to the use of a non-deswelling carbohydrate microgel phase, which both itself remains

swollen and prevents further deswelling of the bulk thermoresponsive hydrogel. These results demonstrate the potential of using composite gel approaches to regulate drug diffusion from hydrogels.

**3.8 Acknowledgements:** The Natural Sciences and Engineering Research Council of Canada (NSERC) is acknowledged for funding this work. Thank you to Eva Mueller for her help preparing HPLC samples and counting and sizing microgel particles.

**3.9 References:**

(1) Bernardo, M. V.; Blanco, M. D.; Olmo, R.; Teijón, J. M. *J. Appl. Polym. Sci.* **2002**, *86*, 327.

(2) Cho, K. Y.; Chung, T. W.; Kim, B. C.; Kim, M. K.; Lee, J. H.; Wee, W. R.; Cho, C. S. *Int. J. Pharm.* **2003**, *260*, 83.

(3) Overstreet, D. J.; Huynh, R.; Jarbo, K.; McLemore, R. Y.; Vernon, B. L. *Journal of Biomedical Materials Research Part A* **2013**, *101A*, 1437.

(4) Owen, S. C.; Fisher, S. A.; Tam, R. Y.; Nimmo, C. M.; Shoichet, M. S. *Langmuir* **2013**, *29*, 7393.

(5) Hoare, T. R.; Kohane, D. S. *Polymer* **2008**, *49*, 1993.

(6) Qiu, Y.; Park, K. *Adv. Drug Del. Rev.* **2012**, *64, Supplement*, 49.

(7) Gupta, P.; Vermani, K.; Garg, S. *Drug Discovery Today* **2002**, *7*, 569.

(8) Gou, M.; Li, X.; Dai, M.; Gong, C.; Wang, X.; Xie, Y.; Deng, H.; Chen, L.; Zhao, X.; Qian, Z.; Wei, Y. *Int. J. Pharm.* **2008**, *359*, 228.

(9) Jiang, Y.; Chen, J.; Deng, C.; Suuronen, E. J.; Zhong, Z. *Biomaterials* **2014**, *35*, 4969.

(10) Hermann, C. D.; Wilson, D. S.; Lawrence, K. A.; Ning, X.; Olivares-Navarrete, R.; Williams, J. K.; Guldberg, R. E.; Murthy, N.; Schwartz, Z.; Boyan, B. D. *Biomaterials* **2014**, *35*, 9698.

(11) Hu, X.; Li, D.; Zhou, F.; Gao, C. *Acta Biomater.* **2011**, *7*, 1618.

(12) Truong, V. X.; Ablett, M. P.; Gilbert, H. T. J.; Bowen, J.; Richardson, S. M.; Hoyland, J. A.; Dove, A. P. *Biomaterials Science* **2014**, *2*, 167.

(13) Nimmo, C. M.; Owen, S. C.; Shoichet, M. S. *Biomacromolecules* **2011**, *12*, 824.

(14) Wei, H.-L.; Yang, Z.; Zheng, L.-M.; Shen, Y.-M. *Polymer* **2009**, *50*, 2836.

(15) Baldwin, A. D.; Kiick, K. L. *Polymer Chemistry* **2013**, *4*, 133.

(16) Pounder, R. J.; Stanford, M. J.; Brooks, P.; Richards, S. P.; Dove, A. P. *Chem. Commun.* **2008**, 5158.

(17) Zustiak, S. P.; Leach, J. B. *Biomacromolecules* **2010**, *11*, 1348.

(18) Qiu, B.; Stefanos, S.; Ma, J.; Lalloo, A.; Perry, B. A.; Leibowitz, M. J.; Sinko, P. J.; Stein, S. *Biomaterials* **2003**, *24*, 11.

(19) Zustiak, S. P.; Leach, J. B. *Biotechnol. Bioeng.* **2011**, *108*, 197.

(20) Patenaude, M.; Hoare, T. *ACS Macro Letters* **2012**, *1*, 409.

(21) Smeets, N. M. B.; Bakaic, E.; Patenaude, M.; Hoare, T. *Chem. Commun.* **2014**, *50*, 3306.

(22) Wang, G.-F.; Chu, H.-J.; Wei, H.-L.; Liu, X.-Q.; Zhao, Z.-X.; Zhu, J. *Chem. Pap.* **2014**, *68*, 1390.

(23) Liu, Z. Q.; Wei, Z.; Zhu, X. L.; Huang, G. Y.; Xu, F.; Yang, J. H.; Osada, Y.; Zrínyi, M.; Li, J. H.; Chen, Y. M. *Colloids Surf., B* **2015**, *128*, 140.

(24) Yu, F.; Cao, X.; Li, Y.; Zeng, L.; Yuan, B.; Chen, X. *Polymer Chemistry* **2014**, *5*, 1082.

(25) Lin, C.-C.; Raza, A.; Shih, H. *Biomaterials* **2011**, *32*, 9685.

(26) Patenaude, M.; Campbell, S.; Kinio, D.; Hoare, T. *Biomacromolecules* **2014**, *15*, 781.

(27) Sivakumaran, D.; Maitland, D.; Hoare, T. *Biomacromolecules* **2011**, *12*, 4112.

(28) Popescu, M.-T.; Mourtas, S.; Pampalakis, G.; Antimisiaris, S. G.; Tsitsilianis, C. *Biomacromolecules* **2011**, *12*, 3023.

(29) Campbell, S. B.; Patenaude, M.; Hoare, T. *Biomacromolecules* **2013**, *14*, 644.

(30) Supasuteekul, C.; Milani, A. H.; Saunders, J. M.; Lally, S.; Freemont, T.; Saunders, B. R. *Soft Matter* **2012**, *8*, 7234.

(31) Hoare, T.; Young, S.; Lawlor, M. W.; Kohane, D. S. *Acta Biomater* **2012**, *8*, 3596.

(32) Lehmann, S.; Seiffert, S.; Richtering, W. *J. Am. Chem. Soc.* **2012**, *134*, 15963.

(33) Sivakumaran, D.; Maitland, D.; Oszustowicz, T.; Hoare, T. *J. Colloid Interface Sci.* **2013**, *392*, 422.

(34) Smeets, N. M. B.; Hoare, T. *J. Polym. Sci., Part A: Polym. Chem.* **2013**, *51*, 3027.

(35) Hoare, T.; Sivakumaran, D.; Stefanescu, C. F.; Lawlor, M. W.; Kohane, D. S. *Acta Biomater.* **2012**, *8*, 1450.

(36) Guan, Y.; Zhang, Y. *Soft Matter* **2011**, *7*, 6375.

(37) Hoare, T.; Pelton, R. *Langmuir* **2004**, *20*, 2123.

(38) Hoare, T.; Pelton, R. *Curr. Opin. Colloid Interface Sci.* **2008**, *13*, 413.

(39) Patenaude, M.; Hoare, T. *Biomacromolecules* **2012**, *13*, 369.

(40) Kesselman, L. R. B.; Shinwary, S.; Selvaganapathy, P. R.; Hoare, T. *Small* **2012**, *8*, 1092.

(41) Xu, X.-D.; Wei, H.; Zhang, X.-Z.; Cheng, S.-X.; Zhuo, R.-X. *J. Biomed. Mater. Res. A* **2007**, *81A*, 418.

(42) Lin, C.-C.; Metters, A. T. *Adv. Drug Del. Rev.* **2006**, *58*, 1379.

(43) Siepmann, J.; Siepmann, F. *Int. J. Pharm.* **2008**, *364*, 328.

(44) Bierbrauer, F. *Hydrogel Drug Delivery: Diffusion Models* **2005** bierbrauerf.weebly.com/uploads/2/8/3/9/2839114/res-grant-report.pdf

(45) Zarzycki, R. M., Z. ; Nawrotek, K. *Ecological Chemistry and Engineering. S* **2010**, *17*, 117.

(46) Siepmann, J.; Siegel, R.; Siepmann, F. In *Fundamentals and Applications of Controlled Release Drug Delivery*; Siepmann, J., Siegel, R. A., Rathbone, M. J., Eds.; Springer US: 2012, p 127.

(47) Fugit, K. D.; Anderson, B. D. *Mol. Pharm.* **2014**, *11*, 1314.

(48) Musch, J.; Schneider, S.; Lindner, P.; Richtering, W. *J. Phys. Chem. B* **2008**, *112*, 6309.

(49) Meid, J.; Friedrich, T.; Tieke, B.; Lindner, P.; Richtering, W. *PCCP* **2011**, *13*, 3039.

(50) Meid, J.; Dierkes, F.; Cui, J.; Messing, R.; Crosby, A. J.; Schmidt, A.; Richtering, W. *Soft Matter* **2012**, *8*, 4254.

(51) Sudoh, Y.; Cahoon, E. E.; De Girolami, U.; Wang, G. K. *Anesth. Analg.* **2004**, *98*, 672.

(52) Yoon, J. A.; Gayathri, C.; Gil, R. R.; Kowalewski, T.; Matyjaszewski, K. *Macromolecules* **2010**, *43*, 4791.

(53) Richter, A.; Howitz, S.; Kuckling, D.; Arndt, K.-F. *Sensors Actuators B: Chem.* **2004**, *99*, 451.

(54) Lou, X.; Vijayasekaran, S.; Sugiharti, R.; Robertson, T. *Biomaterials* **2005**, *26*, 5808.

**S3: Chapter 3 – Supplementary Information:**

**Preparation and Drug Release Kinetics Manipulation of Fully Degradable Microgel-Hydrogel Composites Prepared Using In situ Gelling Chemistry and Microfluidics**

Solutions for Microgel Diffusion Coefficient

**SOLUTION FOR EARLY TIME [$0 < M_t/M_{inf} < 0.6$]**

---

units: D = $m^2/s$; r = m, t= s; $K_m$ = 1/s;
$C_o$ (the concentration of free drug in solution inside the dialysis tube) is a function of time (t) based on a mass balance of drug entering the dialysis tube solution (i.e. diffusing out of a spherical microgel) and leaving the dialysis tube solution (i.e. diffusing through the release membrane):

$$\frac{dC_o(t)}{dt} = C_{\inf}\left[3\sqrt{\frac{D}{r^2\Pi.t}} - \frac{3D}{r^2}\right] - K_m.C_o(t) \quad \text{[S1a]}$$

Converting concentrations to masses to relate the inside ($C_o$) and outside ($C_{inf}$) release kinetic expressions between the microgel and solution inside the dialysis tube:
$C_{inf} = M_{inf}/V_{inf}$, $Co = M_o/V_o$

Relating the volume ratio of microgels to bulk solution inside the dialysis tube:
$V_{inf} = 0.2\ V_{total}$, $V_o = 0.8V_{total}$

Let us introduce two constants a1= $3\sqrt{(D/r^2\Pi)}$ and a2 = $3D/r^2$

$$\frac{dM_o(t)}{dt} + K_m.M_o(t) = 4M_{\inf}\left[\frac{a1}{\sqrt{t}} - a2\right] \quad \text{[S1b]}$$

The solution to this differential equation is thus:

$$M_o(t) = 4M_{\inf}\left[\frac{a1}{\sqrt{K_m}} * \sqrt{\pi} * erfi(\sqrt{K_m\, t}) * e^{-K_m t}\right] - 4M_{\inf}\left[\frac{a2}{K_m}\right] + B.e^{-K_m t} \quad \text{[S2]}$$

where erfi is the imaginary error function.

BOUNDARY CONDITION: $M_0$ (0) (at t=0) = 0, so B = $4M_{inf}$. $a2/K_m$ [Note erfi (0) = 0]

The drug concentration inside the dialysis tube can be related to the drug concentration outside the dialysis tube based on a mass balance, in which no drug leaves the outside solution but drug can enter the outside solution via diffusion through the membrane from inside the dialysis bag.

Thus $$\frac{dC(t)}{dt} = K_m.C_o(t)$$ ---------- [S3a]

Again, to make the system self-consistent given the different volumes of the inside and outside dialysis phases,
$C = M/V$ (outside), $C_o = M_o/V_o$ (inside)

Relating the relative volumes of the fluid inside and outside the dialysis tube:
$1/6\ V = V_o$

Thus, converting Eq. S3a to a mass basis instead of concentration yields:

$$\frac{dM(t)}{dt} = \frac{1}{6}K_m.M_o(t)$$ ---------- [S3a]

Substituting the solution for $M_o(t)$ from Eq. S2 relates the drug release kinetics from the microgel to the measured drug concentration outside the dialysis tube:

$$\frac{dM(t)}{dt} = \frac{4}{6}K_m.M_{\inf}\left\{\left[\frac{a1}{\sqrt{K_m}} * \sqrt{\pi} * erfi(\sqrt{K_m t}) * e^{-K_m t}\right] - \left[\frac{a2}{K_m}\right] + \left[\frac{a2}{K_m}\right].e^{-K_m t}\right\}$$ [S3b]

Integration yields:

$$\frac{M(t)}{M_{\inf}} = \frac{4}{6} * 2a1\sqrt{t} - \frac{a1}{\sqrt{K_m}} * \sqrt{\pi} * erfi(\sqrt{K_m t}) * e^{-K_m t} - a2.t - \left[\frac{a2}{K_m}\right].e^{-K_m t} + Q$$ [S4]

BOUNDARY CONDITION: M (0) (At t=0) = 0, thus $Q = a2/K_m$ [Note that erfi (0) = 0]

---

**The complete solution is thus:**

$$\frac{M(t)}{M_{\inf}} = \frac{4}{6} * 2a1\sqrt{t} - \frac{a1}{\sqrt{K_m}} * \sqrt{\pi} * erfi(\sqrt{K_m t}) * e^{-K_m t} - a2.t - (a2/K_m).e^{-K_m t} + (a2/K_m)$$ ----[S5]

Note that a1 and a2 are in terms of D and r, as shown above.

**SOLUTION FOR LATE TIME [0.4 < $M_t/M_{inf}$ <1.0] - Using Single term series**

Applying the logic used to derive Eq. S1a but instead using the late time approximation for representing differential drug release kinetics from the microgel:

$$\frac{dM_o(t)}{dt} = M_{\inf}\left[6\frac{D}{r^2}e^{(-\frac{\pi^2 Dt}{r^2})}\right] - K_m.M_o(t) \quad \text{[S6a]}$$

For simplification let us introduce one constant a3 = $\pi^2 D/r^2$

$$\frac{dM_o(t)}{dt} + K_m.M_o(t) = 4M_{\inf}.\frac{6a3}{\pi^2}.e^{-a3t} \quad \text{[S6b]}$$

The solution is:

$$M_o(t) = -4M_{\inf}.\frac{6a3}{\pi^2.(a3-K_m)}.e^{-(a3)t} + B.e^{-K_m t} \quad \text{[S7a]}$$

BOUNDARY CONDITION: $M_0$ (0) (at t=0) = 0, B= $4M_{inf}$*6a3 /$\pi^2$(a3-Km), thus $M_0$(t) can be written as;

$$M_o(t) = 4M_{\inf}.\frac{6a3}{\pi^2}.\frac{(e^{-K_m t} - e^{-[a3t]})}{(a3-K_m)} \quad \text{[S7b]}$$

Using equation $\frac{dC(t)}{dt} = K_m.C_o(t)$ [S8a]

Substituting the solution for $M_o$(t) from Eq. 7:

$$\frac{dM(t)}{dt} = \frac{4}{6}K_m.M_{\inf}.\frac{6a3}{\pi^2}.\frac{(e^{-K_m t} - e^{-[a3t]})}{(a3-K_m)} \quad \text{[S8b]}$$

Integrating:

$$M(t) = -\frac{4}{6}K_m.\{M_{\inf}.\frac{6a3}{\pi^2}.\frac{(\frac{e^{-K_m t}}{K_m} - \frac{e^{-[a3t]}}{a3})}{(a3-K_m)}\} + Q \quad \text{[S9]}$$

BOUNDARY CONDITION: M (∞) (At t=∞) = $M_{inf}$, thus Q = $M_{inf}$

Thus, the complete solution is:

$$\frac{M(t)}{M_{\inf}} = \frac{4}{6}\left(1 - K_m.\left\{\frac{6a3}{\pi^2}.\frac{\left(\frac{e^{-K_m t}}{K_m} - \frac{e^{-[a3t]}}{a3}\right)}{(a3 - K_m)}\right\}\right) \qquad \text{[S10]}$$

Note that a is expressed in terms of D and r, as shown above.

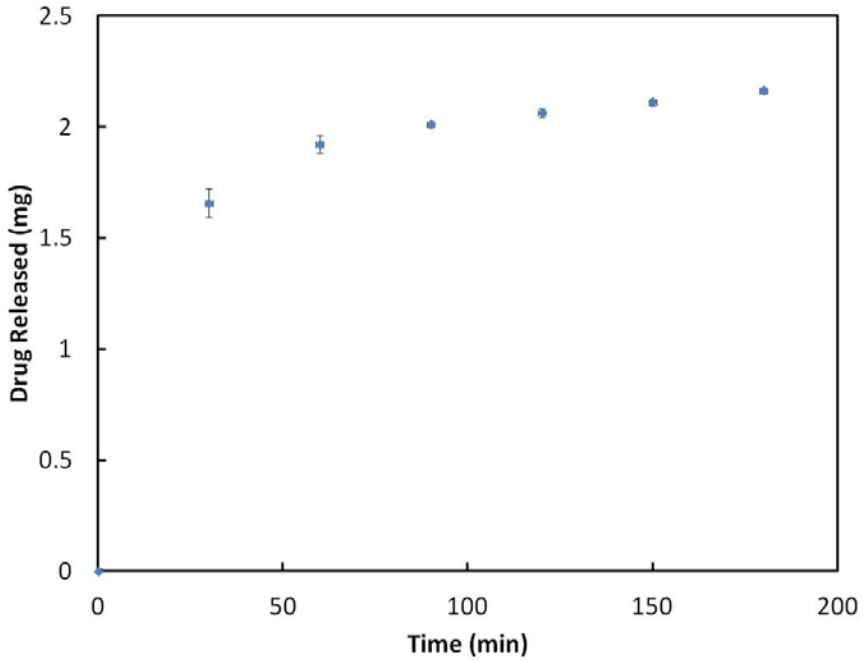


**Figure S3.1:** Bupivacaine release from Float-a-lyzer (100 kDa molecular weight cut-off) without microgels; this data was used to estimate $K_m$ for the membrane mass transfer resistance in the model for microgel release accounting for membrane effects

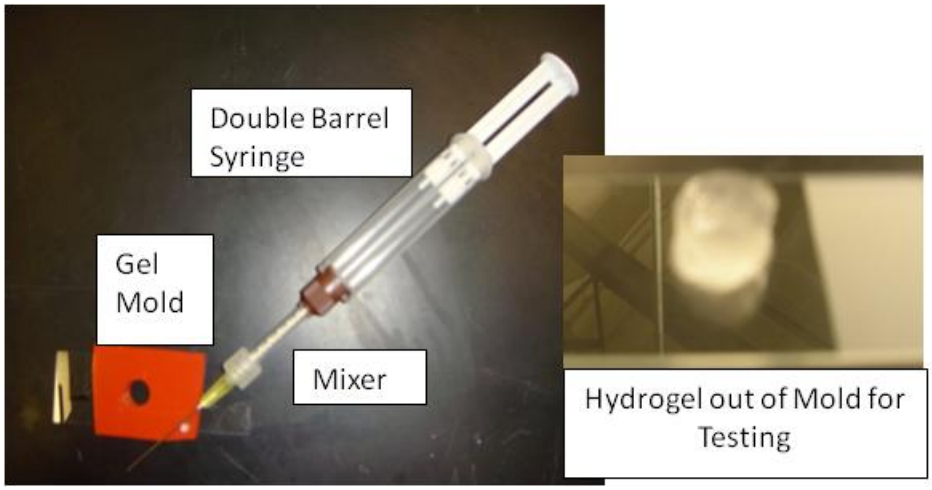


**Figure S3.2:** Double barrel syringe and mould set up, including a picture of the hydrogel removed from the mould and ready for testing

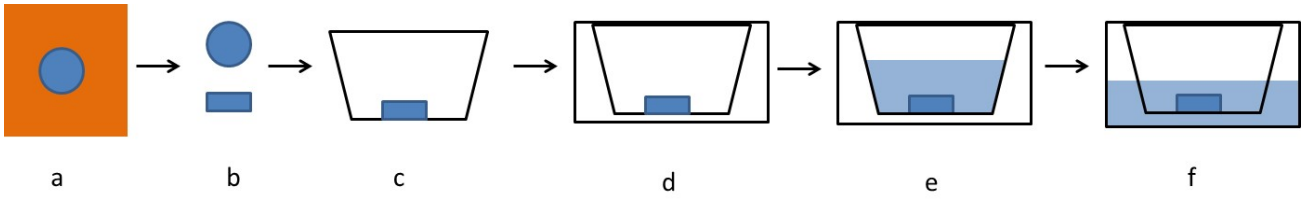


**Figure S3.3:** Steps for testing: (a) gel is formed within silicone mould; (b) gel is removed from mould (top and side views); (c) gel is placed into cell insert; (d) the insert is then placed into a multiwell plate. (e) gel is submerged with 10 mM PBS. (f) fluid within the insert is free to flow into the multiwall plate. Steps C to F are repeated between time points

# Chapter 4

# TEMPERATURE-INDUCED ASSEMBLY OF MONODISPERSE, COVALENTLY CROSS-LINKED, and DEGRADABLE POLY(N-ISOPROPYLACRYLAMIDE) MICROGELS BASED ON OLIGOMERIC PRECURSORS

**Authors:** Daryl Sivakumaran, Eva Mueller, and Todd Hoare

**Publication:** Langmuir, 31(21), 5767-5778

**Publication Date:** June 2015



## 4.1 Abstract

A simple, rapid, solvent-free, and scalable thermally-driven self-assembly approach is described to produce monodisperse, covalently cross-linked, and degradable poly(N-isopropylacrylamide) (PNIPAM) microgels based on mixing hydrazide (PNIPAM-Hzd) and aldehyde (PNIPAM-Ald) functionalized PNIPAM precursors. Pre-heating of a seed PNIPAM-Hzd solution above its phase transition temperature produces nanoaggregates that are subsequently stabilized and cross-linked by the addition of PNIPAM-Ald. The ratio of PNIPAM-Hzd:PNIPAM-Ald used to prepare the microgels, the time between PNIPAM-Ald addition and cooling, the temperature to which the PNIPAM-Hzd polymer solution is pre-heated, and the concentration of PNIPAM-Hzd in the initial seed solution can all be used to control the size of the resulting microgels. The microgels exhibit similar thermal phase transition behavior to conventional precipitation-based microgels

but are fully degradable into oligomeric precursor polymers. The microgels can also be lyophilized and redispersed without any change in colloidal stability or particle size and exhibit no significant cytotoxicity *in vitro*. We anticipate that microgels fabricated using this approach may facilitate translation of the attractive properties of such microgels *in vivo* without the concerns regarding microgel clearance that exist with other PNIPAM-based microgels.

**Keywords:** poly(N-isopropylacrylamide), self-assembly, microgels, degradability, colloidal stability

## 4.2 Introduction

Microgels, solvent-swollen cross-linked gel particles with sub-micron diameters, have been widely investigated as potential materials of interest for wastewater treatment[1, 2], catalysis[3], and a myriad of biomedical and drug delivery applications[4, 5, 6, 7]. Temperature-responsive microgels based on N-vinylcaprolactam (PVCL)[8, 9, 10], N-isopropylacrylamide (NIPAM)[11, 12], or poly(oligo(ethylene glycol) methacrylate) (POEGMA)[13, 14, 15] have attracted particular attention as "smart", switchable materials with the potential to dynamically change pore size, water content, and/or hydrophilicity upon heating above their volume phase transition temperature (VPTT). However, in the context of biomedical applications, the conventional precipitation-based free radical polymerization method used to make microgels offers challenges in terms of degradability and thus the ultimate clearance of the microgels from the body, given that free radical polymerization results in non-degradable carbon-carbon backbones with molecular weights that are typically indeterminate. Given that renal clearance is typically possible only with molecular weight fragments no larger than 60,000 g/mol[16], such materials are likely to accumulate within the liver and spleen, leading to potential chronic toxicity issues and a strong unlikelihood of any ultimate approval of such materials for clinical use.

One approach to address this challenge is to use a cross-linker which contains a degradable linkage between the cross-linking groups to prepare the microgel. The most popular degradable cross-linkers are based on disulfide linkages that can be cleaved *in vivo* by reduction[9, 14] (often facilitated by glutathione[17]) and/or thiol exchange reactions[18].

Diacrylate cross-linkers containing disulfide linkages have been used to prepare degradable microgels based on PVCL[9] and POEGMA[14, 19]. Analogous strategies using polyvinylalkoxysiloxanes[20], which degrade at basic conditions, or acetal groups[21], which hydrolyze in acidic conditions, have also been used to prepare thermoresponsive microgels that are degradable. Alternately, degradability can be introduced by including degradable polymeric units directly into the microgel structure; for example, dextran-co-NIPAM microgels have been reported which can be degraded over time via oxidation and/or enzymatic degradation of the dextran component[22, 23]. However, if the goal is to ensure the ultimate clearance of the degradation products, the use of degradable cross-linkers is inherently limited in that the molecular weight of the C-C backbone is not directly controllable using such an approach. While inclusion of chain transfer agents[24] and/or controlled polymerization approaches (particularly reversible addition-fragmentation chain transfer polymerization, RAFT[25, 26, 27, 28]) can limit the molecular weight of the backbone, such approaches introduce additional complexity to the synthesis and, in the case of RAFT, may also limit the type of microgel functionalization that is possible directly in the context of the polymerization process.

To counter these potential problems, microgels can instead be formed from well-defined polymeric precursors of controlled molecular weight and structure, with the microgel pre-polymers directly representing the degradation products. Several physically cross-linked microgels have been reported using this approach, primarily formed via self-assembly of block copolymers that contain one or more hydrophilic blocks[29] (to facilitate

stabilization of the nanoparticle following self-assembly) and thermoresponsive blocks (to drive self-assembly as the copolymer is heated)[30]. If a latent functionality is included in the thermoresponsive block, covalent cross-linking can occur following self-assembly to stabilize the microgel even following cooling; use of a cleavable functional group for this purpose can introduce degradability. Again, disulfide groups have been most widely reported in this context, with microgels based on poly(ethylene oxide)–block-(oligo(ethylene oxide) monomethyl ether methacrylate)[31], polyethylene oxide-block-polystyrene[32], degradable polyester-block-POEGMA[33], and polysaccharide-grafted PNIPAM[34] formed using such an approach. Ionic interactions can also be used to assemble well-defined diblock copolymers in the same manner. For example, hyaluronic acid-co-poly(ethylene glycol) (HA-co-PEG) polymers can be self-assembled into microgels via addition of poly-L-lysine in which complexation between HA and poly-L-lysine leads to the formation of spherical polyelectrolyte complex gels[35]. Alternately, solvent-based coacervation can be used to drive the formation of aggregates that can subsequently be cross-linked via bifunctional cross-linking agents[36], although this approach requires the use of solvents such as DMSO or DMF that can be difficult to fully remove and may induce downstream problems with *in vivo* use. Emulsions can be used to confine bulk gelation processes into a nanoparticulate form[37, 38], although issues with organic solvent use, the generally polydisperse nature of the products, as well as the ultimate stability of the microgels produced can limit the utility of this approach. As such, to our knowledge, there is no previous report of a degradable, monodisperse, covalently

cross-linked, thermoresponsive microgel being prepared from a well-defined precursor polymer (ensuring clearance) using a solvent-free method that does not require the use of ionic or hydrophobic self-assembly units. Such a microgel would offer particular potential for translation from the lab to the clinic.

Recently, we have reported the use of hydrazone chemistry to form degradable thermoresponsive hydrogels based on well-defined hydrazide (PNIPAM-Hzd) and aldehyde (PNIPAM-Ald)-functionalized PNIPAM oligomers[39]. These hydrogels exhibit controlled thermosensitivity akin to conventional PNIPAM hydrogels but are hydrolytically degradable (via hydrazone bond hydrolysis) over the course of weeks to months. Furthermore, the hydrogels and precursor polymers show no significant cytotoxicity at clinically relevant concentrations. Herein, we describe the use of these PNIPAM-Hzd and PNIPAM-Ald precursor polymers in the context of an all aqueous, thermally-driven self-assembly strategy to spontaneously fabricate covalently-cross-linked, thermoresponsive, and monodisperse degradable microgels. The microgels exhibit temperature-responsive deswelling transitions analogous to those observed for conventional PNIPAM microgels but can be completely degraded into oligomeric degradation products. Cross-link density and swelling behavior can be tuned as a function of the pre-polymer concentrations to achieve microgels with targeted swelling properties. Furthermore, the microgels can be lyophilized and resuspended (as with conventional microgels) with no significant change in particle size.

### 4.3 Experimental

*Materials:* N-isopropylacrylamide (NIPAM, 99%), acrylic acid (AA, 99%), thioglycolic acid (98%), aminoacetaldehyde dimethyl acetal (99%), 2,2,6,6-tetramethyl-1-piperidinyloxy (TEMPO, 98%), and methacryloyl chloride (purum) were all purchased from Sigma Aldrich (Oakville, Canada). Adipic acid dihydrazyde (ADH, Alfa Aesar, 98%), *N*'-ethyl-*N*-(3-dimethylaminopropyl)-carbodiimide (EDC, Carbosynth, Compton CA, commercial grade), and 2,2-azobisisobutryic acid dimethyl ester (AIBMe, Wako Chemicals, 98.5%) were all used as received. For all experiments, Milli-Q grade distilled deionized water (DIW) was used. Hydrochloric acid (1M) was received from LabChem Inc. (Pittsburgh, PA) while ethanol was purchased from Commercial Alcohols (Brampton, ON). 3T3 *Mus musculus* mouse cells were acquired from ATCC: Cedarlane Laboratories Ltd. (Burlington, ON). Cell culture supplies included Dulbecco's Modified Eagle Medium-high glucose (DMEM), fetal bovine serum (FBS), penicillin streptomycin (PS), recovery cell culture freezing and trypsin-EDTA which were purchased from Invitrogen Canada (Burlington, ON). Thiazolyl blue tetrazolium bromide (MTT) was purchased from Sigma Aldrich (Oakville, ON).

*Synthesis of N-(2,2-dimethoxyethyl)methacrylamide (DMEMAm) monomer:* The acetal-containing comonomer *N*-(2,2-dimethoxyethyl) methacrylamide (DMEMAm) was synthesized using protocols developed by Smeets et al[40]. Briefly, 50 mL of aminoacetaldehyde dimethylacetal and 100 mg of TEMPO were dissolved in 100 mL of a 5M sodium hydroxide solution at 10 °C. A total of 47 mL of methacryloyl chloride was

then added drop-wise over a period of 2 hours, and the resulting mixture was left to react for 24 hours at room temperature under a nitrogen purge. This mixture was then extracted with 150 mL of petroleum ether to remove impurities. The aqueous phase was saturated with sodium chloride and extracted three times with 75mL aliquots of tert-butyl methyl ether. The organic phase was dried with magnesium sulfate, filtered, and concentrated under reduced pressure.

*Synthesis of hydrazide-functionalized PNIPAM (PNIPAM-Hzd):* Hydrazide-functionalized PNIPAM was produced through single site attachment of a large (five-fold) molar excess of adipic acid dihydrazide to acrylic acid functionalized PNIPAM via carbodiimide coupling chemistry (for structure, see Supplementary Information, Figure S4.1). Briefly, acrylic acid-functionalized PNIPAM was prepared by polymerizing 4.5 g NIPAM and 0.5 g acrylic acid (15 mol% total monomer) using 0.056 g of 2,2-azobisisobutyric acid dimethyl ester (AIBME) as the initiator and 80 μL of thioglycolic acid as the chain transfer agent in 20 mL of absolute ethanol overnight at 56 °C under nitrogen. The solvent was then removed by evaporation, and the polymer was dissolved in 100 mL of Milli-Q water and dialysed against Milli-Q water over six, six-hour cycles. The PNIPAM-co-AA oligomer was then modified with hydrazide groups by dissolving 1 g of PNIPAM-co-AA, 20 g of adipic acid dihydrazide, and 11 g of EDC in 200 mL of Milli-Q water. The pH was adjusted to 4.75 and maintained throughout the reaction via addition of 0.1 M HCl as required to facilitate conjugation of ADH to acrylic acid groups. The resulting solution was dialysed against Milli-Q water over six, six-hour cycles (12-14

kDa MWCO) and lyophilized. Conductometric titration (ManTech Inc.) indicated that 95 mol% of acrylic acid monomer units in the polymer were hydrazide functionalized. $^{1}$H-NMR was performed using Bruker AV700 (32 scans) in deuterated DMSO to ensure functionalization of the PNIPAM backbone (Supplementary Information, Figure S4.2). Gel permeation chromatography was completed using a Waters 590 HPLC pump, three Waters Styragel columns (HR2, HR3, HR4; 30 cm x 7.8 mm (ID); 5 μm particles) at 40°C, a Waters 410 refractive index detector operating at 35 °C, and DMF as the solvent was used to measure the molecular weight of the precursor polymers indicated a number average molecular weight of 23000 kDa and a polydispersity of 1.61.

*Synthesis of aldehyde-functionalized PNIPAM (PNIPAM-Ald):* Aldehyde-functionalized PNIPAM was prepared via copolymerization of NIPAM and DMEMAm followed by hydrolysis of the acetal groups in DMEMAm (for structure, see Supplementary Information, Figure S4.1). Briefly, 4 g of NIPAM, 0.95 g of DMEMAm (13.4 mol% total monomer), 0.056 g AIBME initiator, and 80 μL of thioglycolic acid chain transfer agent were dissolved in 20 mL of absolute ethanol and heated to 56 °C under a nitrogen purge. After polymerization, solvent was removed by evaporation and the resulting polymer redissolved in 1M HCl and allowed to react for 24 hours to convert the acetal groups in DMEMAm into aldehyde groups. The resulting polymer was purified via six, six-hour dialysis cycles (12-14 kDa MWCO) and lyophilized. Silver ion titration[41] indicated that 12 mol% of the total monomers in the polymer were functionalized with an aldehyde group. $^{1}$H-NMR was performed using Bruker AV700 (32 scans) in deuterated DMSO to

ensure functionalization of the PNIPAM backbone (Supplementary Information, Figure S4.2). Gel permeation chromatography was completed using a Waters 590 HPLC pump, three Waters Styragel columns (HR2, HR3, HR4; 30 cm x 7.8 mm (ID); 5 μm particles) at 40°C, a Waters 410 refractive index detector operating at 35 °C, and DMF as the solvent was used to measure the molecular weight of the precursor polymers indicated a number average molecular weight of 20000 kDa and a polydispersity of 1.57.

*Polymer Lower Critical Solution Temperature Measurements:* The lower critical solution temperature (LCST) of the precursor polymers was measured using UV-visible spectrophotometry (Variant Cary Bio 100 UV–vis spectrophotometer) by performing transmittance measurements over a temperature range of 25 to 60°C (1°C intervals) and identifying the temperature at which the transmittance of the sample was 95% (onset LCST). Differential scanning calorimetry (DSC) measurements were also conducted to determine LCST of the precursor polymers using a MicroCal VP-DSC differential scanning calorimeter (MicroCal, USA). Reference and sample solutions were degassed prior to scanning at a temperature increase rate of 1°C per minute from 20°C to 90°C. The heat capacity of the sample was obtained by subtraction of a reference scan versus that of the sample scan, with the transition temperature of the polymer reported at the maximum of the heat capacity curve. Calculations were completed by integrating peak areas using Origin 8.0 (OriginLab Corporation, USA).

*Microgel Self-Assembly:* For the base recipe, microgels were made by first preparing stock solutions of PNIPAM-Hzd (1w/v%) and PNIPAM-Ald (1 w/v%) in separate deionized water solutions. A volume of 5 mL of the PNIPAM-Hzd stock solution was heated to 70˚C for ~5 minutes under magnetic stirring (350 RPM) until the polymer solution became opaque (i.e. above the lower critical solution temperature of PNIPAM-Hzd). A 0.25 mL aliquot of PNIPAM-Ald (5-20 wt% of the mass of PNIPAM-Hzd present in the seed solution) was then added drop-wise into the solution over a period of 5-10 seconds and allowed to stir for an 15 minutes. Microgel solutions were then removed from the temperature-controlled oil bath and allowed to cool at room temperature overnight. Additional experiments were performed by adjusting (one at a time) the temperature (50˚C, 60˚C, 70˚C), the stir rate (200-650 RPM), the time of mixing prior to cooling (1-60 minutes), the concentration of PNIPAM-Hzd in the seed solution (0.2w/v%, 0.5 w/v% and 2 w/v%) and the mass ratio of PNIPAM-Hzd: PNIPAM-Ald (prepared by increasing the concentration of the PNIPAM-Ald stock solution to 2 w/v% (10 wt% of PNIPAM-Hzd), 3 w/v% (15 wt% of PNIPAM-Hzd), and 4 w/v% (20 wt% of PNIPAM-Hzd)) while maintaining the total volumes of each solution added. The Ald:Hzd ratios reported are the mass ratios of aldehyde:hydrazide polymers (12 mol% functionalization for PNIPAM-Ald and 14 mol% functionalization for PNIPAM-Hzd) used to prepare the microgel using this addition procedure.

Larger batch sizes of up to 50 mL were also produced by keeping the stock solution concentrations and the relative volumes of the solutions added the same but scaling up the total volumes used by the factors indicated (2x, 4x, and 10x). Acrolein

(100 µL, 450x molar excess) was added to select solutions to quench unreacted hydrazide groups. Selected samples were also dialyzed over six, six-hour cycles (3500 kDa MWCO), lyophilized, and then resuspended at the same 1 w/v% concentration in Millipore water to assess microgel redispersibility.

*Transmission Electron Microscopy:* Morphology characterization of microgels was performed using transmission electron microscopy (TEM, JEOL 1200EX TEMSCAN). A 3.5 µl aliquot of microgels was deposited onto a Cu/Rh coated Maxtaform$^{TM}$ grid and was stained with uranyl acetate. The stain was left to react for one minute before being removed by repeated rinsing. An accelerating voltage of 100kV was used for imaging.

*Microgel Particle Size Measurements:* Microgel particle sizes were assessed using two different techniques. Dynamic light scattering measurements were performed using a Brookhaven 90Plus Particle Analyser running Particle Solutions Software (Version 2.6, Brookhaven Instruments Corporation). Detection of scattering was completed using a 659 nm laser at a 90° angle configuration. Microgel concentrations were adjusted until an intensity of approximately between 200 to 500 kilocounts per second was achieved. Each measurement was conducted over 2 minutes and was repeated at least 4 times, with intensity-weighted particle sizes and particle size distributions reported as averages plus or minus standard deviations of these replicates. The temperature dependence of microgel size was assessed using the same method by ramping the temperature at 2°C intervals over the temperature range of 25°C to 70°C, using a stabilization period of 5 minutes for

equilibration at each temperature. Alternately, single nanoparticle tracking analysis (NTA) assessments of particle size were conducted using a NanoSight instrument (NanoSight NTA 2.3). Samples were diluted 400-fold from the microgel stock solution in MilliQ water prior to measurement. Measurements were conducted at 25°C for a duration of 60 seconds, with number-weighted microgel sizes and distributions reported.

*Electrophoretic Mobility:* Electrophoretic mobility measurements were conducted using a ZetaPlus zeta potential analyzer (Brookhaven Instruments Corporation) operating in PALS (phase analysis light scattering) mode (V.2.5). Samples were prepared at concentrations of ~2.5 mg/mL in 10mM KCl, with 5 replicates consisting of 30 cycles per replicate (150 total runs) used per sample tested; the experimental uncertainties represent the standard error of the replicate measurements.

*Microgel Degradation:* Microgel solutions were exposed to hydrochloric acid solutions to assess the potential degradability of the microgels as well as characterize the ultimate degradation products. A volume of 5 mL of 1 M hydrochloric acid was added to 1mL of a 10 mg/mL microgel suspension. Size measurements were made at various times using single nanoparticle tracking analysis to determine changes in particle size and particle count as a function of time, reflective of microgel degradation. Gel permeation chromatography using a Waters 590 HPLC pump, three Waters Styragel columns (HR2, HR3, HR4; 30 cm x 7.8 mm (ID); 5 μm particles) at 40°C, a Waters 410 refractive index detector operating at 35 °C, and DMF as the solvent was used to measure the molecular

weight of the precursor polymers as well as the degradation products following 24 hours of treatment with 1M HCl to ensure break-down of the microgels into its precursor polymer components. Degradation products were further analyzed chemically using $^{1}H$ NMR (using DMSO as a solvent), and Fourier transform infrared spectroscopy (FTIR, completed by mixing dried degradation products, precursor polymers, or microgels in KBr and measuring spectra using a Thermo Nicolet 6700 IF spectrometer operating at 2 $cm^{-1}$ resolution), comparing those results to the precursor polymers.

*Microgel Cytotoxicity:* The viability of cells in response to precursor polymer and microgel exposure was completed using 3T3 *Mus musculus* fibroblasts. Cell viability was assayed in proliferation media consisting of 500 mL DMEM, 50 mL FBS, and 5 mL PS. Test were conducted in polystyrene 24 well plates (10,000 cells/well) by exposing cells to microgel concentrations ranging from 0.1 mg/mL to 1 mg/mL for a period of 24 hours. Viability was assessed using the thiazolyl blue tetrazolium bromide (MTT) assay. The concentration of the solubilized formazan product was measured at 540 nm using a microplate reader (Biorad, Model 550) relative to a control well containing the cells but not exposed to the microgels. Cell viability was calculated by dividing the measured absorbance from the test sample by the absorbance value of the cell-only control. Each sample was tested 4 times, with the error bars representing the standard deviation of the measurements.

### 4.4 Results and Discussion

*Microgel Fabrication*: Microgels were formed using polymeric precursors functionalized with hydrazide and aldehyde functional groups as the building blocks and the thermal phase transition in water as the mechanism to drive nanoparticle formation. In the optimal recipe, the PNIPAM-Hzd solution was initially heated up above its lower critical solution temperature (LCST) to form a thermally-collapsed nanoaggregate; the PNIPAM-Ald polymer was subsequently used as a cross-linker to stabilize the aggregates post-formation to create microgel particles. Support for this mechanism of particle formation can be obtained by dynamic light scattering data on the PNIPAM-Hzd nanoaggregates prior to PNIPAM-Ald addition, which indicates that the size of the PNIPAM-Hzd nanoaggregates (266 $\pm$ 1.5 nm at 1 mg/mL concentration, Supplementary Information Figure S4.3) directly templates the size of the resulting microgels at the same temperature (Figure 4.1 and Table 4.1). The mechanism also somewhat mirrors the conventional precipitation-based mechanism of forming conventional PNIPAM microgels in which pre-polymers grow in solution, undergo a phase transition, and then sequentially precipitate on a seed particle to form a microgel[42]; in our case, the polymerization step is already completed but the particle assembly method is the same, (although compressed over a much shorter time scale). Cooling of the nanoaggregate suspension without adding cross-linker results in complete re-dissolution of the polymer (i.e. no signal is observed using dynamic light scattering); in contrast, after the aldehyde-PNIPAM was added, colloidally stable nanoparticles were maintained. For the base microgel (1 wt% PNIPAM-Hzd, Ald:Hzd = 0.10, 70°C fabrication temperature, 350 RPM mixing, 15

minute mixing time), TEM images indicate that the microgels were spherical (Figure 4.1a), and nanoparticle tracking analysis conducted at room temperature confirmed the uniformity of the resulting microgel suspension (Figure 4.1b).

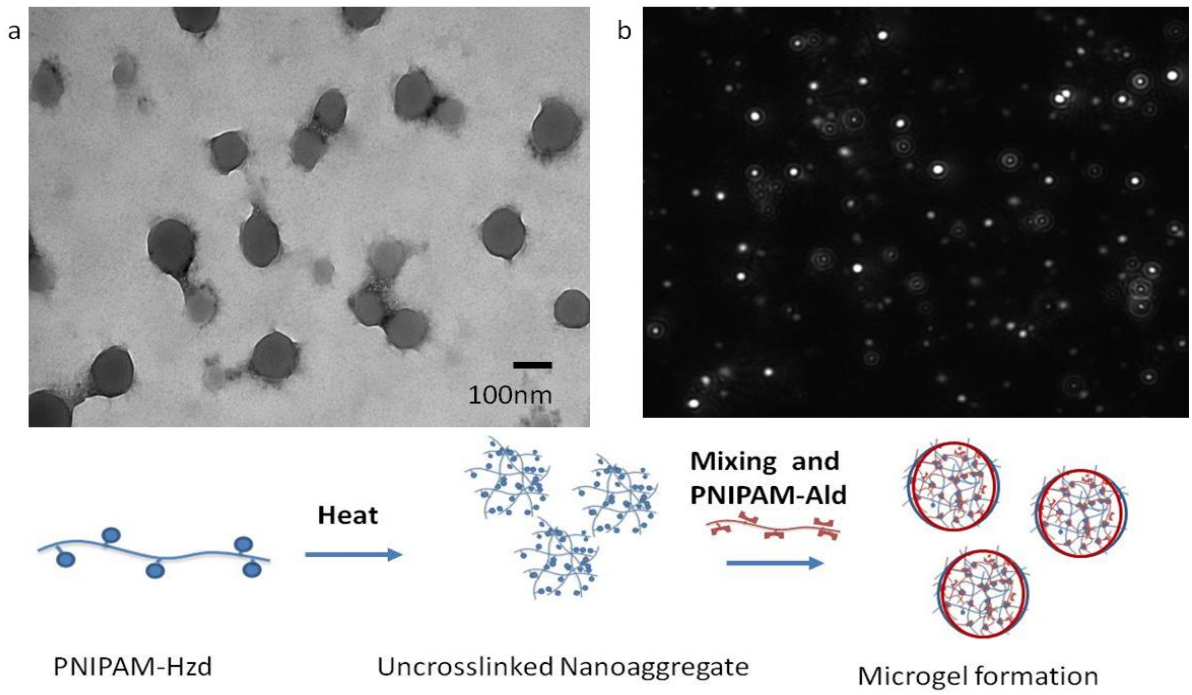


**Figure 4.1:** Images of self-assembled microgels following PNIPAM-Ald cross-linking and cooling: (a) transmission electron microscopy image (100,000x magnification); (b) screenshot of nanoparticle tracking image. The proposed mechanism of microgel production is shown schematically below the images.

The polydispersity of the microgels produced is low, particularly relative to particle populations typically produced using inverse emulsion techniques which represent the alternative method of making microgels of similar sizes without requiring

the use of self-assembling block copolymers. Figure 4.2 shows the full particle size distributions of microgels produced using various Ald:Hzd polymer ratios as measured using dynamic light scattering (intensity-based distribution, Fig. 4.2a) and nanoparticle tracking analysis (single particle number-based distribution, Fig. 4.2b), while Table 4.1 shows the mean particle sizes and polydispersity values measured using each technique.

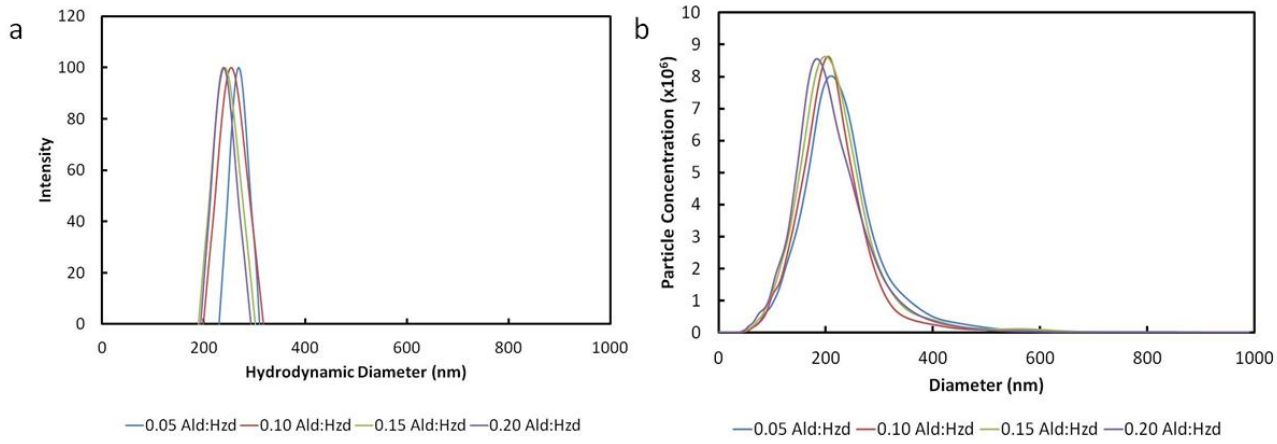


**Figure 4.2:** Particle size distributions measured by (a) dynamic light scattering (intensity distribution, normalized to maximum intensity) and (b) nanoparticle tracking analysis (number distribution) as a function of aldehyde polymer concentration

**Table 4.1:** Size and polydispersity of microgels produced at different Ald:Hzd ratios as measured via dynamic light scattering (DLS) and nanoparticle tracking analysis (NTA)

| Microgel | DLS Size (nm) | NTA Size (nm) | DLS Polydispersity[a] | NTA Polydispersity[b] |
|---|---|---|---|---|
| 0.05 Ald:Hzd | 252± 3 | 207±5 | 0.09± 0.02 | 1.13 ± 0.02 |
| 0.10 Ald:Hzd | 249± 3 | 203±2 | 0.10± 0.01 | 1.11 ± 0.02 |
| 0.15 Ald:Hzd | 228± 1 | 200± 3 | 0.08± 0.03 | 1.12 ± 0.01 |
| 0.20 Ald:Hzd | 219 ± 5 | 196 ±7 | 0.09 ± 0.02 | 1.10 ± 0.10 |

[a] Measured using Brookhaven polydispersity algorithm on intensity-weighted raw data;
[b] Calculated as $D_w/D_n$ based on the number-weighted size distribution measured by NTA

The polydispersity of the microgels is quite narrow independent of the polymer concentration used to prepare the microgels, with a highly reproducible, single size intensity peak appearing in both DLS measurements and nanoparticle tracking measurements. Measured polydispersity values from DLS results were all $\leq 0.1$, generally considered as the critical value to indicate a monodisperse particle population[43]; for the NTA measurements, the value of $D_w/D_n$ (i.e. the weight average:number average particle size) is close to 1, again indicating the microgels are largely monodisperse. Given the importance of maintaining monodisperse particle populations to maximize the predictability of nanoparticle behavior *in vivo*[44], the highly monodisperse particle sizes achieved (coupled with the complete absence of macroaggregate formation over the full range of concentrations tested) suggests the potential of this method to fabricate biomedically-relevant microgel particles. The very rapid nature of this fabrication process (only 5 minutes after the PNIPAM-Hzd polymer is pre-heated) and the fact that the process uses water as the sole solvent (removing the need for extensive purification steps) offer additional advantages in terms of minimizing processing times and particle throughput, particularly relative to other polymerization or emulsion-based techniques.

Increasing the concentration of PNIPAM-Ald in the cross-linking solution results in a small but statistically significant reduction in particle size ($p = 0.015$), as confirmed by both DLS and NTA measurements (Table 4.1). We attribute this decreased size to the increased efficacy of cross-linking when more PNIPAM-Ald is added, condensing the microgel to a greater degree. Note that while the particle sizes measured with DLS and NTA are close in overall size due to the high monodispersity of the particle populations,

the average (number-weighted) diameters of the particles with NTA are consistently lower than the average (intensity-weighted) diameters measured by DLS, as would be expected due to the higher weighting of larger particles in DLS. Interestingly, DLS also indicates a significant decrease in polydispersity as the PNIPAM-Ald concentration is increased while NTA does not. We believe this difference is a result of the differences between the intensity-based and number-based weightings of the DLS and NTA distributions respectively. For DLS, a reduction in the (much more heavily weighted) large particle fraction as the average microgel size is decreased results in a very large decrease in the scattering intensity detected as a result of larger particles; meanwhile, the increased fraction of smaller particles is as not well-detected by DLS on an intensity-weighted basis. Combined together, these effects result in an effective narrowing of the measured particle size distribution. In contrast, NTA analysis is purely number weighted, such that a reduction in higher size particles is directly offset by an increase in lower size particles to maintain a similar polydispersity.

Of note, the electrophoretic mobility lies in the range of $0.55 – 0.73 \times 10^{-8}$ $m^2/Vs$ for all microgels tested, corresponding to a low zeta potential well below that required for purely electrostatic stabilization of nanoparticle dispersions (|zeta potential| > 30 mV)[45, 46]. This result is consistent with the charge neutrality of the polymer building blocks, aside from a small (<2 mol% total monomer) fraction of unfunctionalized acrylic acid residues in PNIPAM-Hzd. This result suggests that colloidal stability of these microgels is due primarily to sterics rather than an electrostatics, making even subtle changes in the

polymer hydrophilicity potentially important in terms of determining the microgel colloidal stability.

*Effect of Self-Assembly Conditions on Microgel Size:* The temperature, mixing time, and stir rate of the self-assembly/cross-linking fabrication procedure were all investigated to identify which factors significantly affect the particle size of the resulting microgel and, by extension, the range over which the microgel size can be tuned by process changes. Temperature is an obvious variable of interest in this respect, as the temperature chosen will control the hydrophobicity of each polymer and thus nature of the first aggregation step and/or the penetration of the cross-linking PNIPAM-Ald polymer into the initial nanoaggregate. Figure 4.3a shows the lower critical solution temperature behaviors of PNIPAM-Hzd and PNIPAM-Ald, while the changes in microgel particle size achieved by lowering the self-assembly temperature from 70°C (base case) to 60°C or 50°C are shown in Fig. 4.3b.

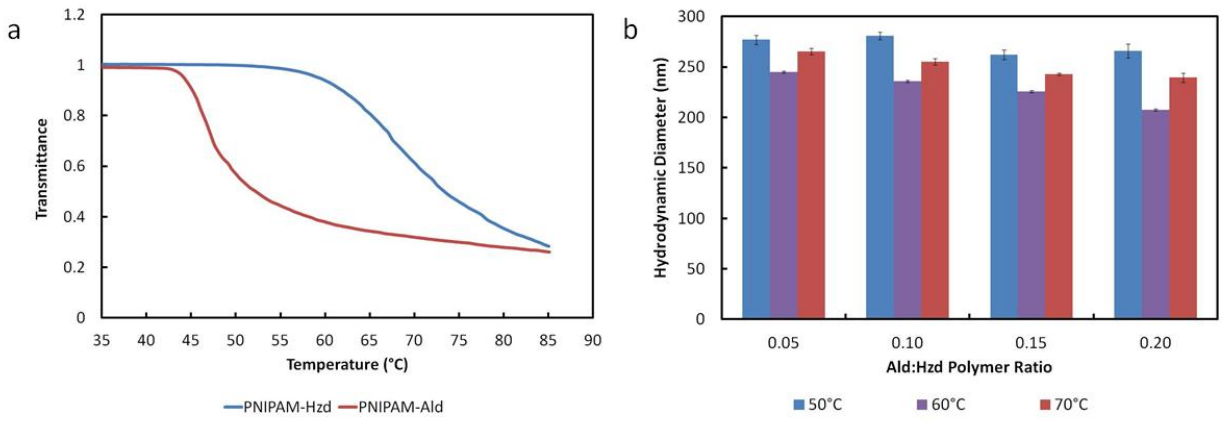


**Figure 4.3:** Effect of temperature on microgel self-assembly process: (a) Lower critical solution temperature behavior of PNIPAM-Hzd and PNIPAM-Ald precursor polymers (both in 1w/v% solutions in distilled water, mimicking microgel production conditions); (b) Hydrodynamic diameter (as measured via DLS) of microgels as a function of Ald:Hzd polymer mass ratio prepared at different temperatures.

The LCST of PNIPAM-Hzd at the concentration used for microgel self-assembly was measured to be ~58°C via both UV/vis spectrophotometry (Fig. 4.3a) and DSC analysis (Supplementary Information, Figure S4.4); as such, at 50°C, the polymer coils are not fully collapsed into precursor particles and the resulting microgel size is larger than observed at 60°C (at which the PNIPAM-Hzd polymer has begun to collapse according to the LCST result). Interestingly, further increasing the temperature to 70°C results in an increase in particle size relative to that observed at 60°C. We attribute this result to two possible factors: (1) the increased hydrophobicity of the chains at 70°C (transmittance ~0.6) relative to 60°C (transmittance ~0.9, Fig. 4.3a), leading to additional hydrophobic interaction-based nanoaggregation and (2) the increased diffusion coefficient at 70°C and thus the increased collision frequency between polymer chains in solutions. Increased

collision frequency between less hydrophilic chains would lead to more polymer on average being incorporated in each nanoaggregate before chain conformation changes can facilitate steric stabilization of the growing microgels. Overall, the results suggest that particle assembly depends on both the magnitude of chain deswelling (and thus the inter-chain polymer affinity) at the fabrication temperature (thermodynamics) and the rate of collision of those polymers (kinetics), with the smallest microgels formed just above the LCST (at which point the polymers are moderately attractive but diffusion is the slowest among any possible attractive condition).

To assess the balance of the thermodynamics and kinetic contributions to controlling particle size, microgels were produced using different stirring speeds during the PNIPAM-Ald addition process; varying the stir rate effectively changes the kinetics of the collisions but not the thermodynamics of inter-chain interactions. Interestingly, stirring speed did not significantly affect particle size over the 200-650 RPM range studied (see Supplementary Information, Figure S4.5). This result suggests the thermodynamics of the volume phase transition (and its impact in inter-polymer interactions and/or polymer-solvent interactions) rather than the kinetics of changing collision frequencies primarily determines particle size.

If the opposite sequence (i.e. using PNIPAM-Ald to form the nanoaggregates and then cross-linking with PNIPAM-Hzd) is used to prepare microgels, nanoparticle formation also occurs. However, a stable suspension of particles was produced only at dilute concentrations of PNIPAM-Ald base polymer (<1 mg/mL) (see Supplementary Information, Figure S4.6). This result suggests that the aldehyde-PNIPAM polymers

have a lower capacity for sterically stabilizing the precursor nanoaggregates than hydrazide-PNIPAM polymers. This is consistent with the significantly lower LCST observed for PNIPAM-Ald relative to PNIPAM-Hzd (Fig. 4.3a); that is, PNIPAM-Ald is more highly condensed and more likely to aggregate to form larger (and more unstable) aggregates than PNIPAM-Hzd at the same temperature. Based on this result, all further optimization and investigation of this system was pursued using PNIPAM-Hzd as the seed polymer and PNIPAM-Ald as the cross-linking polymer.

Changing the mixing time between when PNIPAM-Ald was added and when the sample was removed from heating also impacts the particle size. Figure 4.4 shows the hydrodynamic diameters (measured via DLS) of microgels prepared at different Ald:Hzd polymer ratios and left for different periods of time prior to removal of the microgel from the 70°C heat source.

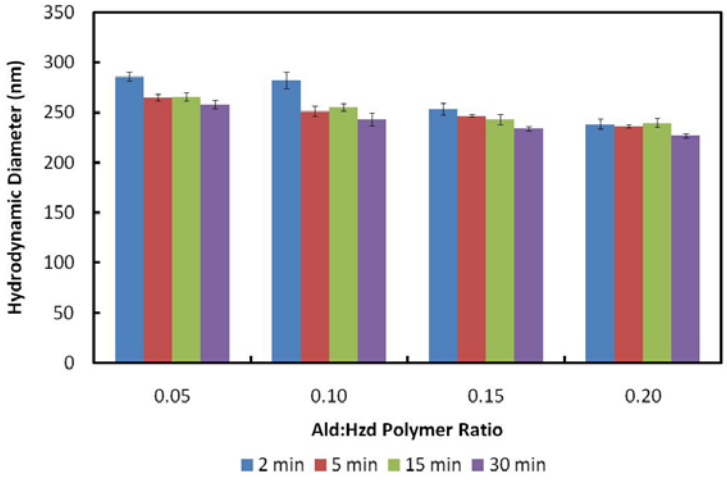


**Figure 4.4** Hydrodynamic diameter (from DLS) of microgels produced using different mixing times of PNIPAM-Ald at 70°C as a function of the Ald:Hzd polymer ratio

As the mixing time was increased, smaller microgels were produced across all Ald:Hzd polymer ratios tested. This is congruent with earlier observations in that less cross-linking (in this case, giving the PNIPAM-Ald polymer less time to do cross-linking) results in less condensation of the initial nanoaggregates and thus larger microgels. Furthermore, as the Ald:Hzd polymer ratio is increased, mixing time has less effect on the particle size. We hypothesize this observation is related to the rate of cross-linking in each mixture; as the amount of (cross-linking) PNIPAM-Ald polymer added increases, more cross-linking occurs at shorter times, reducing the time required to achieve a plateau value of microgel size (i.e. the time at which cross-linking reaches a maximum due to either or both of steric or stoichiometric limitations). If the reaction is allowed to proceed to longer times (t>45min), aggregation between particles begins to occur and large precipitates are formed that are not easily redispersed even upon cooling. We hypothesize this result is related to consumption of the (hydrophilic) hydrazide groups at the microgel interface as the cross-linking reaction proceeds, which may reduce the potential for steric stabilization; we have previously shown that the hydrazone bond is significantly more hydrophobic than either hydrazide or aldehyde groups and thus lowers the LCST of the near-surface polymer chains that are essential to impart steric stability to the microgels[40].

*Effect of Polymer Concentrations on Microgel Size:* Chemical control over the particle size was also investigated by changing the concentration of PNIPAM-Hzd in the initial

seed solution. Figure 4.5 shows the hydrodynamic diameter of microgels prepared at different PNIPAM-Hzd initial concentrations. The Ald:Hzd polymer ratio on the x-axis represents the ratio of hydrazide:aldehyde functionalized polymer added to form the microgels, with the actual concentration of PNIPAM-Ald added to maintain constant Ald:Hzd ratios changed independent of the PNIPAM-Hzd concentration.

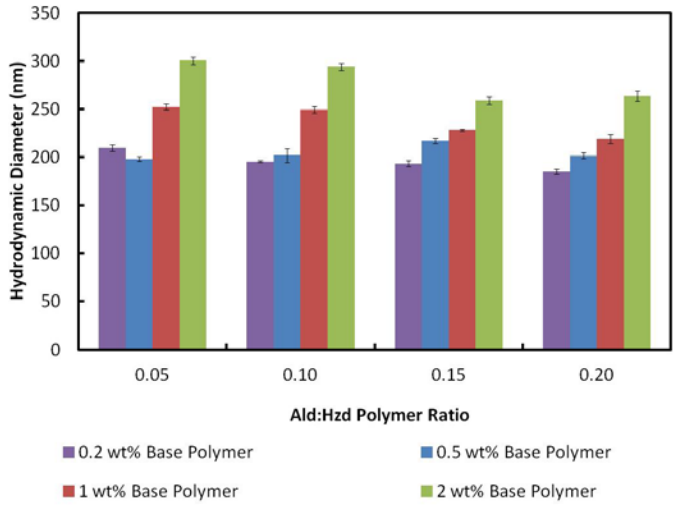


**Figure 4.5:** Hydrodynamic diameter (via DLS) of self-assembled microgels prepared with varying concentrations of PNIPAM-Hzd and PNIPAM-Ald

Of all factors studied, the initial PNIPAM-Hzd concentration has the strongest effect on the microgel particle size, with particle sizes from 200-300 nm achievable depending on the PNIPAM-Ald concentration used for cross-linking. Reducing the concentration of PNIPAM-Hzd in the seed solution significantly decreases the resulting microgel size following PNIPAM-Ald addition. This result is consistent with aggregation kinetics, as polymer solutions with higher concentrations would have an increased probability of collisions between collapsing polymers and existing nuclei and thus result in larger

aggregates that would then be cross-linked into larger microgels. Interestingly, while increasing the Ald:Hzd polymer ratio (i.e. the PNIPAM-Ald concentration) significantly reduces the particle size when 1 w/v% and 2 w/v% PNIPAM-Hzd seed solutions are used ($p$ = 0.003 comparing Ald:Hzd = 0.05 to Ald:Hzd = 0.20), the effect of the Ald:Hzd ratio on particle size was lower as a function of Ald:Hzd polymer ratio for the 0.2-0.5 w/v% PNIPAM-Hzd seed solutions over the full Ald:Hzd ratio tested (albeit still significant, $p$ = 0.015). This result suggests that less cross-linker is required (at least with respect to the inherent steric limitations presented) to fully cross-link the microgels when the seed aggregates are smaller, potentially owing to lower mass transfer limitations to cross-linker diffusion into the seed particles as the diameter of those particles is reduced.

*Scale-up of Self-Assembly Process:* All results discussed to this point were collected using small (5 mL) volume samples that yield relatively low quantities of microgel. For larger-scale testing or production, scale-up of the self-assembly process to larger volumes is required. Figure 4.6 shows the particle size distributions of the base recipe microgels scaled up in total volume by a factor of 2, 4, or 10. No significant increase in hydrodynamic diameter or broadening of the particle size distribution occurs as a function of scaling up the reaction up by a factor of four. Such a result may be expected if the assembly process is primarily thermodynamically-driven, as factors like local shear during mixing would not significantly impact the final particle properties (indeed, this is consistent with our earlier finding that stir speed does not significantly affect the resulting microgel particle size). However, at 10 times scale up, there is a small but significant

change in particle size. Note that between the 4x and 10x scale-up trials, the reaction vessels used had to be changed from a 20 mL vial to a 100 mL round-bottom flask; as such, different effects may play a role in governing microgel size (i.e. heat distribution and mixing in the larger volume) that did not significantly influence microgel size in the smaller volume. However, given that stable microgels were still produced with highly monodisperse particle populations even at this higher scale factor, this result suggests the self-assembly method can be directly and successfully scaled to create larger batches.

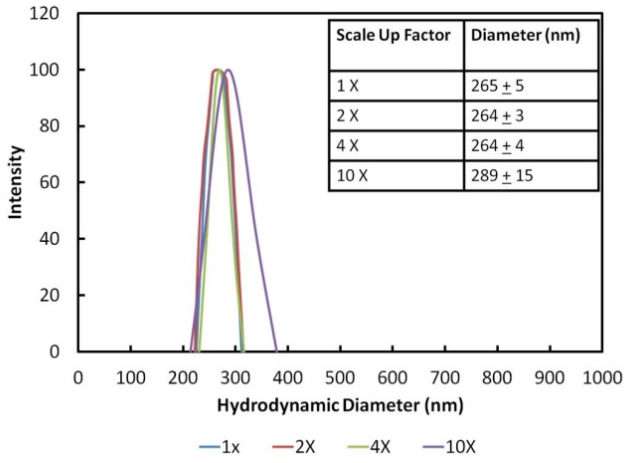


**Figure 4.6:** Particle size distributions (measured via DLS) as a function of the reaction scale; factors in the legend indicate the magnitude by which the total volume of the reaction was increased in each case (all other parameters remained constant). The embedded table shows the average particle sizes produced under each condition.

*Microgel Colloidal Stability:* The microgel particles generated by this self-assembly procedure are very stable over time; indeed, over a period of at least 5 months, the particles remain in suspension with no visible aggregate present (Figure 4.7a). However, there is a net increase in particle size observed over time (in the base case microgel, from

287 ± 1 nm after preparation to 317 ± 5 nm after 5 months of incubation); given the lack of precipitate or phase separation observed at this time, we attribute this result to the slow hydrolysis of the hydrazone cross-links that reduces the elastic resistance to microgel swelling and thus increases the hydrodynamic diameter. Interestingly, microgels that were lyophilized following cooling could easily be resuspended in solution (Figure 4.7b), with no significant change in particle size observed before (247 ± 3 nm) and after (251 ± 6 nm) lyophilization ($p$ = 0.40). This result indicates that these microgels can be dried and stored without affecting their size or colloidal stability, a significant advantage of this approach relative to other methods for self-assembled microgel production which typically produce particles that are harder to resuspend or are less size-stable (i.e. due to changes in the driving forces for self-assembly) following a drying step[47].

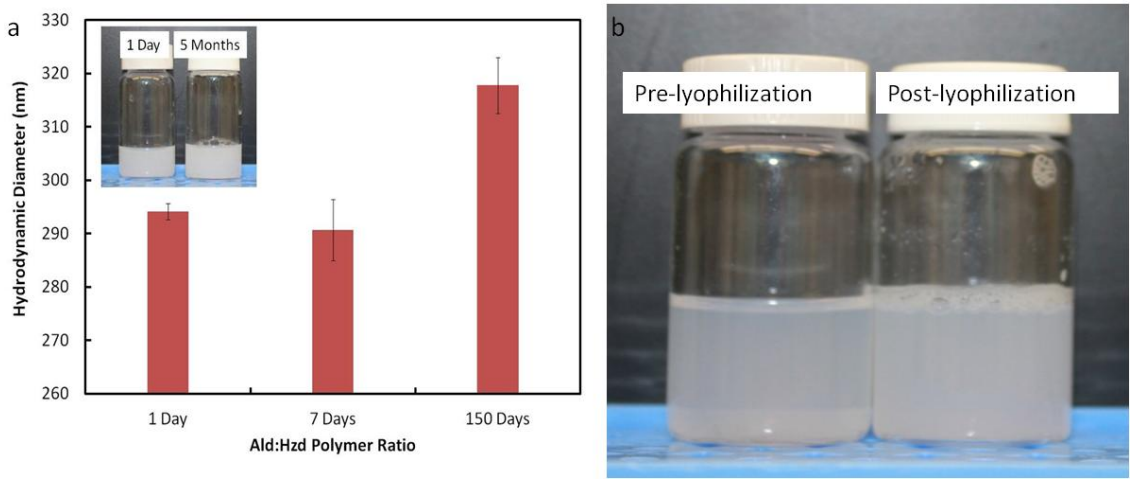


**Figure 4.7:** Colloidal stability of self-assembled microgels: (a) Microgel size over the course of time (inset: pictures of microgels immediately after preparation and following 5 months of storage at room temperature); (b) Pictures of microgels at equivalent concentrations (1 w/v %) before and after lyophilization

*Microgel Degradation:* In addition to the speed and simplicity of the assembly approach used herein, the other major advantage of this approach is that cross-linking occurs via hydrazone bond formation, an equilibrium chemistry that is hydrolytically labile (particularly in slightly to strongly acidic environments, such as the stomach or cell endosomes). To assess the capacity of these microgels to degrade back into the oligomeric building blocks, microgels were exposed to 1M HCl to perform accelerated degradation assays and the degradation products were characterized (Figure 4.8). Note that this experiment was not intended to simulate physiological conditions but rather to confirm on a reasonable timescale that the original pre-polymers could be regenerated following the degradation process.

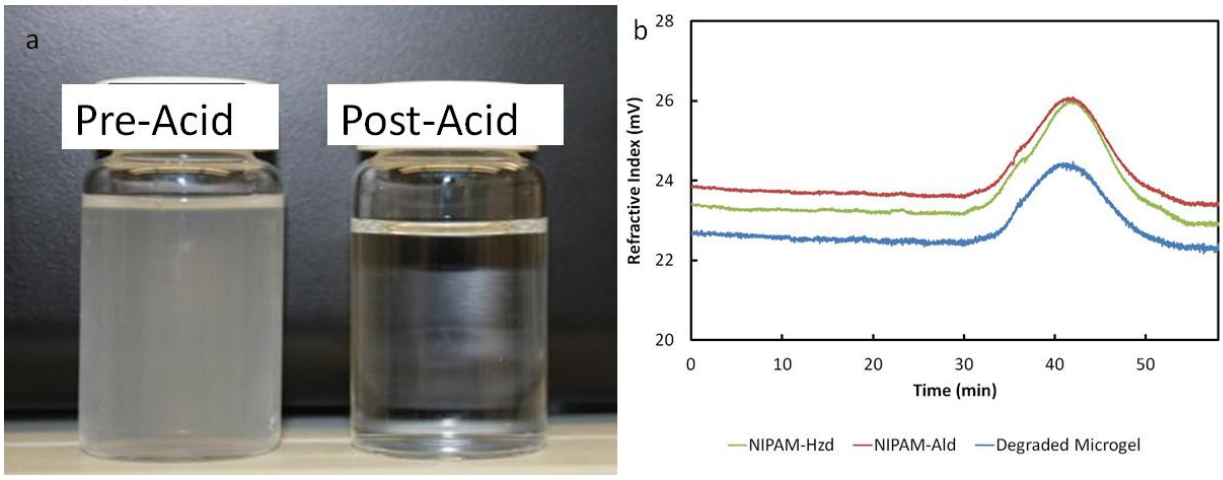


**Figure 4.8:** Degradation of self-assembled, hydrazone cross-linked microgels: (a) Picture of microgel suspension before and after acid treatment (1M HCl, 2 hours); (b) Gel permeation chromatography traces of degradation products from microgel hydrolysis (1M HCl, 24 hours exposure time)

After two hours of exposure, the visual appearance of the microgels solution changed from slightly opaque (indicating microgel presence) to transparent (Fig. 4.8a), with the count rate observed via DLS reducing 100-fold over this period to a point that no detectable particle size can be measured. Similarly, when the degradation products were analyzed using NTA, no discrete scattering units were imaged at the end of the degradation period. Gel permeation chromatography on the degraded microgel product indicates that the microgels were fully cleaved back into the starting PNIPAM-Ald and PNIPAM-Hzd oligomeric building blocks, with elution times of approximately 40 minutes observed for each precursor polymer (corresponding to molecular weights of ~20 kDa, significantly lower than the kidney clearance limit) and the degradation products (Fig. 4.8b). Furthermore, both $^{1}$H NMR and FTIR indicate no significant chemical changes between the pre-polymers and the degradation products, as would be anticipated if hydrazone bond cleavage drove the degradation process. The capacity for such well-defined degradation based on the assembly of well-defined polymer precursors lies in sharp contrast to microgels prepared with conventional precipitation techniques, in which minimal or no control over the molecular weight of the C-C backbone polymers between cross-links can be exercised[7, 14, 18, 48]. Note that a degradation assay conducted in pH 4.5 (lysosomal pH) indicated an increase in the hydrodynamic diameter of the microgels of ~20-25 nm over the course of one month and an additional ~20-25 nm over the course of two months, significantly more swelling than observed at pH 7.4 over five months (Fig. 4.7a). In addition, the least cross-linked microgels (0.05 Ald:Hzd polymer ratio) became colloidally unstable after two months at lysosomal pH, with multiple peaks observed in

the DLS distribution (Figure S4.7); both these observations are indicative of ongoing degradation. These results support the assertion that degradation does occur via an acid-catalyzed mechanism while also emphasizing that degradation is slow under any physiological condition. Such slow degradation is likely desirable in most biomedical applications to, for example, facilitate longer-term controlled release.

*Microgel Phase Transition:* To confirm that the self-assembled microgels exhibit the same thermal phase transition behavior as conventional free radical precipitation-based microgels, particle size was measured as a function of temperature using dynamic light scattering. Figure 4.9a shows the thermal phase transitions of microgels prepared at different PNIPAM-Hzd seed solution concentrations with Ald:Hzd = 0.10, while Figure 4.9b shows thermal phase transitions of microgels prepared at a fixed PNIPAM-Hzd seed solution concentration of 1 w/v% but with varying Ald:Hzd polymer ratios. The VPTT of most of the microgels tested is slightly higher than observed for conventional precipitation-based microgels, with the temperature at which 50% of the overall diameter change was observed being ~38°C on average based on the DLS measurements. This slightly increased VPTT is attributable to the presence of residual hydrazide groups in the microgel; given that PNIPAM-Hzd has an LCST of ~58°C prior to cross-linking (Fig. 4.3a), a higher microgel VPTT would be expected if even a relatively small fraction of the Hzd groups remain unreacted. However, the fact that the thermal collapse of these microgels occurs just slightly above normal physiological temperature makes these materials ideal for many biomedical applications, potentially facilitating (for example)

triggered drug release upon encountering of infection sites[49] or upon external heating of a composite microgel containing magnetic nanoparticles (oscillating magnetic field)[50] or gold nanoshells (near-infrared radiation)[51]. PNIPAM-like behavior with VPTT ~33°C can also be achieved if desired when smaller Ald:Hzd ratios are used (Fig. 4.9b). In addition, the breadth of the transition is relatively narrow and highly comparable to conventional microgels, with the onset (5% collapse) and offset (95% collapse) VPTT values lying within no more than a ~10°C range for all samples tested (Figs. 4.9a and 4.9b).

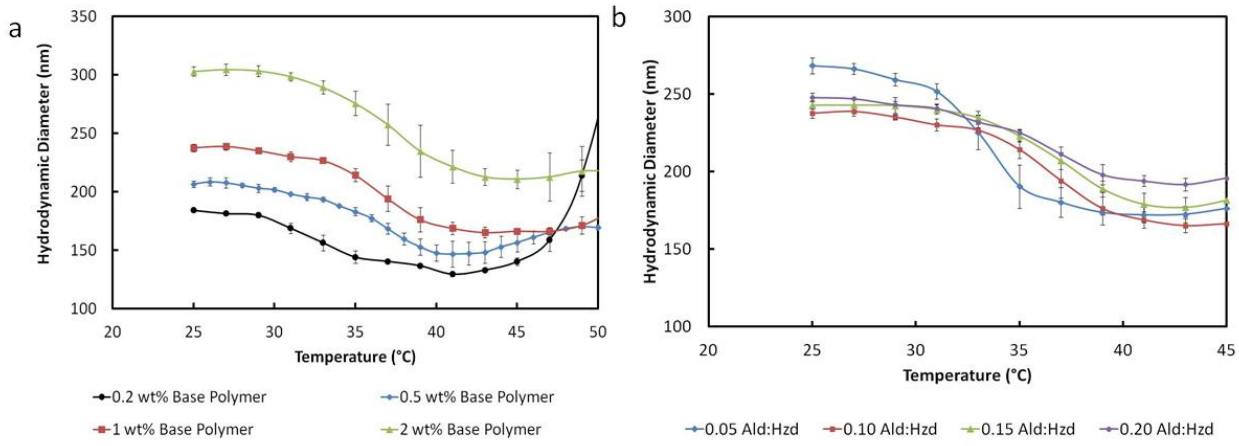


**Figure 4.9:** Hydrodynamic diameter versus temperature profiles (based on DLS) for microgels prepared with (a) different PNIPAM-Hzd seed solution concentrations at a fixed Ald:Hzd polymer ratio of 0.10; (b) a fixed PNIPAM-Hzd seed solution concentration of 1 w/v% but varying Ald:Hzd polymer ratios

Significant changes in the magnitude of the phase transition as well as the stability of the collapsed microgels can be observed as a function of the chemistry of each microgel. For microgels with a fixed Ald:Hzd ratio but varying initial concentrations of

PNIPAM-Hzd (Fig. 4.9a), microgels prepared with lower PNIPAM-Hzd concentrations exhibit both lower magnitudes of deswelling and lower colloidal stabilities upon heating (although no sample tested exhibits significant aggregation below ~45°C, making even these materials relevant as reversible thermoresponsive microgels). We hypothesize this result can be attributed to the smaller size and thus higher specific surface area of microgels prepared at lower PNIPAM-Hzd concentrations, enabling more effective cross-linking with PNIPAM-Ald (i.e. both higher access to the surface and easier penetration into the nanoaggregate) and lower inherent colloidal stability due to the higher interfacial energy of smaller microgel suspensions at a fixed overall mass content. For microgels with a fixed PNIPAM-Hzd concentrations but varying Ald:Hzd ratios (Fig. 4.9b), microgels prepared with lower amounts of PNIPAM-Ald swelled more at low temperature and collapsed more at higher temperature, consistent with the lower total cross-link density that would be expected as the PNIPAM-Ald concentration was decreased.

Thermal cycling experiments indicate a typical hysteresis between the first heating and cooling steps[49,50], with the microgels never completely reswelling to their initial (pre-heating) size in subsequent cycles (Supplementary Information, Figure S4.8). In subsequent heating-cooling cycles, microgels prepared with higher Ald:Hzd ratios undergo highly reversible shrink-swell responses while microgels prepared with lower Ald:Hzd ratios continue to show some degree of hysteresis (although the thermal response is fully maintained, Fig. S4.4). We anticipate this result is a function of the decreased stiffness and thus increased inter-chain mobility as the amount of PNIPAM-

Ald added to the microgels is reduced, resulting in a higher probability for the formation of additional hydrazone bonds as the microgel changes conformation during the swelling-deswelling cycles.

*Microgel Cytotoxicity:* The cytocompatibility of the polymer precursors and base case microgels was assessed using the MTT assay with 3T3 mouse myoblast cells. Figure 4.10 shows the relative cell viabilities measured with respect to a cell-only control (i.e. no microgels present). No significant cytotoxicity was observed when the cells were exposed to the polymer precursors (also the degradation products, based on Fig. 4.8b) or base case microgels at concentrations up to 1 mg/mL. These results are consistent with previous studies for PNIPAM microgels and PNIPAM containing hydrazide and aldehyde functional groups[52]. Microgels prepared with higher PNIPAM-Ald contents exhibit slightly but significantly lower cytocompatibilities than microgels prepared with less PNIPAM-Ald ($p = 0.004$), consistent with linear polymer studies in which increased polymer-bound aldehyde groups increased cytotoxicity[53]. However, the >80% cell viabilities measured for all samples tested suggests that these microgels have potential to be used *in vivo* without inducing significant cytotoxicity.

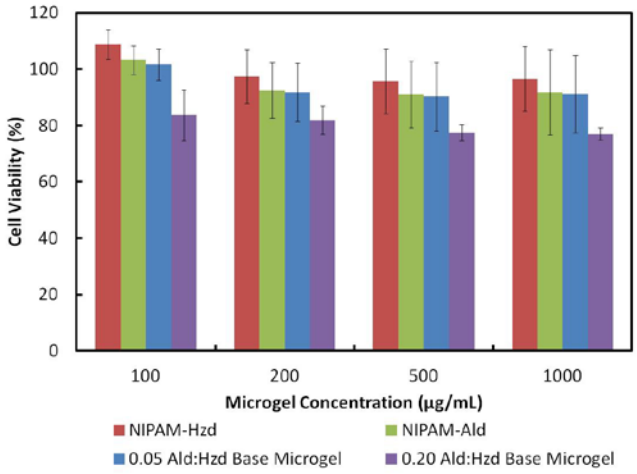


**Figure 4.10:** Cell cytotoxicity to mouse 3T3 fibroblast cells (as measured via the MTT assay) relative to a cell-only (non-treated) control for precursor polymers and the base case self-assembled microgel

Overall, these results suggest that both the size and the thermosensitivity of the microgels can be tuned over an appreciable range by changing the concentrations of both the seed and cross-linking polymers used to fabricate the microgels while still maintaining a clear capacity to produce a monodisperse, thermoresponsive, and cytocompatible material.

## 4.5 Conclusions

Monodisperse degradable PNIPAM-based microgels can be fabricated by simple mixing of PNIPAM-aldehyde and PNIPAM-hydrazide polymer solutions. The facile scalability and high speed of the method (as little as two minutes following PNIPAM-hydrazide solution pre-heating), the tunability of the microgel particle size by changing the process conditions (temperature, mixing time) or the polymer concentrations, the high

monodispersity of the microgels, the physiologically-relevant volume phase transition temperature of the microgels, the well-defined degradation products, and the high cytocompatibility of the resulting microgels and degradation products combine to make this approach of significant interest for addressing the ongoing challenges of translating thermoresponsive microgels to practical *in vivo* applications.

**4.6 Acknowledgements** Funding from the Natural Sciences and Engineering Research Council of Canada (NSERC, Discovery Grant Program) and the Ontario Early Researcher Awards (Ontario Ministry of Research and Innovation) is gratefully acknowledged. Dr. Raquel Epand is acknowledged for her assistance with differential scanning calorimetry measurements.

## 4.7 References

(1) Morris, G. E.; Vincent, B.; Snowden, M. J. *J. Colloid Interface Sci.* **1997**, *190*, 198-205.
(2) Parasuraman, D.; Sarker, A.; Serpe, M. *Colloid. Polym. Sci.* **2013**, *291*, 1795-1802.
(3) Gichinga, M. G.; Striegler, S.; Dunaway, N. A.; Barnett, J. D. *Polymer* **2010**, *51*, 606-615.
(4) Wang, Q.; Libera, M. *Colloids Surf., B* **2014**, *118*, 202-209.
(5) Hoare, T.; Pelton, R. *Langmuir* **2008**, *24*, 1005-1012.
(6) Zhou, T.; Wu, W.; Zhou, S. *Polymer* **2010**, *51*, 3926-3933.
(7) Zhang, X.; Lu, S.; Gao, C.; Chen, C.; Zhang, X.; Liu, M. *Nanoscale* **2013**, *5*, 6498-6506.
(8) Bitar, A.; Fessi, H.; Elaissari, A. *J. Biomed. Nanotechnol.* **2012**, *8*, 709-719.
(9) Wang, Y.; Nie, J.; Chang, B.; Sun, Y.; Yang, W. *Biomacromolecules* **2013**, *14*, 3034-3046.
(10) Balaceanu, A.; Mayorga, V.; Lin, W.; Schürings, M.-P.; Demco, D.; Böker, A.; Winnik, M.; Pich, A. *Colloid. Polym. Sci.* **2013**, *291*, 21-31.
(11) Hoare, T.; Pelton, R. *Biomacromolecules* **2008**, *9*, 733-740.
(12) Hu, X.; Tong, Z.; Lyon, L. A. *J. Am. Chem. Soc.* **2010**, *132*, 11470-11472.
(13) Cai, T.; Marquez, M.; Hu, Z. *Langmuir* **2007**, *23*, 8663-8666.
(14) Ulasan, M.; Yavuz, E.; Bagriacik, E. U.; Cengeloglu, Y.; Yavuz, M. S. *J Biomed Mater Res A* **2014**, DOI: 10.1002/ jbm.a.35146.
(15) Hu, Z.; Cai, T.; Chi, C. *Soft Matter* **2010**, *6*, 2115-2123.
(16) Scott, E. A.; Nichols, M. D.; Cordova, L. H.; George, B. J.; Jun, Y.-S.; Elbert, D. L. *Biomaterials* **2008**, *29*, 4481-4493.
(17) Oh, J. K.; Bencherif, S. A.; Matyjaszewski, K. *Polymer* **2009**, *50*, 4407-4423.
(18) Gaulding, J. C.; Smith, M. H.; Hyatt, J. S.; Fernandez-Nieves, A.; Lyon, L. A. *Macromolecules* **2011**, *45*, 39-45.
(19) Oh, J. K.; Siegwart, D. J.; Lee, H.-i.; Sherwood, G.; Peteanu, L.; Hollinger, J. O.; Kataoka, K.; Matyjaszewski, K. *J. Am. Chem. Soc.* **2007**, *129*, 5939-5945.
(20) Agrawal, G.; Wang, J.; Bruster, B.; Zhu, X.; Moller, M.; Pich, A. *Soft Matter* **2013**, *9*, 5380-5390.
(21) Binauld, S.; Stenzel, M. H. *Chem. Commun.* **2013**, *49*, 2082-2102.
(22) Ghugare, S. V.; Chiessi, E.; Sakai, V. G.; Telling, M. T. F.; Wadgaonkar, P. P.; Paradossi, G. *Macromol. Symp.* **2013**, *329*, 27-34.
(23) Aguirre, G.; Ramos, J.; Forcada, J. *Soft Matter* **2013**, *9*, 261-270.
(24) An, Z.; Qiu, Q.; Liu, G. *Chem. Commun.* **2011**, *47*, 12424-12440.
(25) Zheng, Y.; Turner, W.; Zong, M.; Irvine, D. J.; Howdle, S. M.; Thurecht, K. J. *Macromolecules* **2011**, *44*, 1347-1354.
(26) Liu, G.; Qiu, Q.; An, Z. *Polymer Chemistry* **2012**, *3*, 504-513.

(27) Oliveira, M. A. M.; Boyer, C.; Nele, M.; Pinto, J. C.; Zetterlund, P. B.; Davis, T. P. *Macromolecules* **2011**, *44*, 7167-7175.

(28) Wutzel, H.; Richter, F. H.; Li, Y.; Sheiko, S. S.; Klok, H.-A. *Polymer Chemistry* **2014**, *5*, 1711-1719.

(29) Morimoto, N.; Endo, T.; Ohtomi, M.; Iwasaki, Y.; Akiyoshi, K. *Macromol. Biosci.* **2005**, *5*, 710-716.

(30) Sasaki, Y.; Akiyoshi, K. *The Chemical Record* **2010**, *10*, 366-376.

(31) Chan, N.; An, S. Y.; Yee, N.; Oh, J. K. *Macromol. Rapid Commun.* **2014**, *35*, 752-757.

(32) Zhang, Q.; Re Ko, N.; Kwon Oh, J. *RSC Advances* **2012**, *2*, 8079-8086.

(33) Aleksanian, S.; Khorsand, B.; Schmidt, R.; Oh, J. K. *Polymer Chemistry* **2012**, *3*, 2138-2147.

(34) Morimoto, N.; Qiu, X.-P.; Winnik, F. M.; Akiyoshi, K. *Macromolecules* **2008**, *41*, 5985-5987.

(35) Novoa-Carballal, R.; Pergushov, D. V.; Muller, A. H. E. *Soft Matter* **2013**, *9*, 4297-4303.

(36) Urakami, H.; Hentschel, J.; Seetho, K.; Zeng, H.; Chawla, K.; Guan, Z. *Biomacromolecules* **2013**, *14*, 3682-3688.

(37) Vinogradov, S. V.; Bronich, T. K.; Kabanov, A. V. *Adv. Drug Del. Rev.* **2002**, *54*, 135-147.

(38) Vinogradov, S. V.; Batrakova, E. V.; Kabanov, A. V. *Bioconjugate Chem.* **2003**, *15*, 50-60.

(39) Patenaude, M.; Hoare, T. *ACS Macro Letters* **2012**, *1*, 409-413.

(40) Smeets, N. M. B.; Bakaic, E.; Patenaude, M.; Hoare, T. *Chem. Commun.* **2014**, *50*, 3306-3309.

(41) Campbell, S. B.; Patenaude, M.; Hoare, T. *Biomacromolecules* **2013**, *14*, 644-653.

(42) Pelton, R. *Adv. Colloid Interface Sci.* **2000**, *85*, 1-33.

(43) Tan, S.; Zhao, D.; Yuan, D.; Wang, H.; Tu, K.; Wang, L.-Q. *React. Funct. Polym.* **2011**, *71*, 820-827.

(44) Bysell, H.; Månsson, R.; Hansson, P.; Malmsten, M. *Adv. Drug Del. Rev.* **2011**, *63*, 1172-1185.

(45) Schwarz, C.; Mehnert, W.; Lucks, J. S.; Müller, R. H. *J. Controlled Release* **1994**, *30*, 83-96.

(46) Schwarz, C. *J. Microencapsulation* **1999**, *16*, 205-213.

(47) Lee, H.; Jeong, Y.; Park, T. G. *Biomacromolecules* **2007**, *8*, 3705-3711.

(48) Bai, Y.; Zhang, Z.; Deng, M.; Chen, L.; He, C.; Zhuang, X.; Chen, X. *Polym. Int.* **2012**, *61*, 1151-1157.

(49) Radovic-Moreno, A. F.; Lu, T. K.; Puscasu, V. A.; Yoon, C. J.; Langer, R.; Farokhzad, O. C. *ACS Nano* **2012**, *6*, 4279-4287.

(50) Chiang, W.-H.; Ho, V. T.; Chen, H.-H.; Huang, W.-C.; Huang, Y.-F.; Lin, S.-C.; Chern, C.-S.; Chiu, H.-C. *Langmuir* **2013**, *29*, 6434-6443.

(51) Wu, W.; Shen, J.; Banerjee, P.; Zhou, S. *Biomaterials* **2010**, *31*, 7555-7566.

(52) Sivakumaran, D.; Maitland, D.; Hoare, T. *Biomacromolecules* **2011**, *12*, 4112-4120.

(53) Ito, T.; Yeo, Y.; Highley, C. B.; Bellas, E.; Benitez, C. A.; Kohane, D. S. *Biomaterials* **2007**, *28*, 975-983.

## S4: Chapter 4 – Supplementary Information

## TEMPERATURE-INDUCED ASSEMBLY OF MONODISPERSE, COVALENTLY CROSS-LINKED, and DEGRADABLE POLY(N-ISOPROPYLACRYLAMIDE) MICROGELS BASED ON OLIGOMERIC PRECURSORS

**Authors:** Daryl Sivakumaran, Eva Mueller, and Todd Hoare

**Publication:** Langmuir, 31(21), 5767-5778

**Publication Date:** June 2015

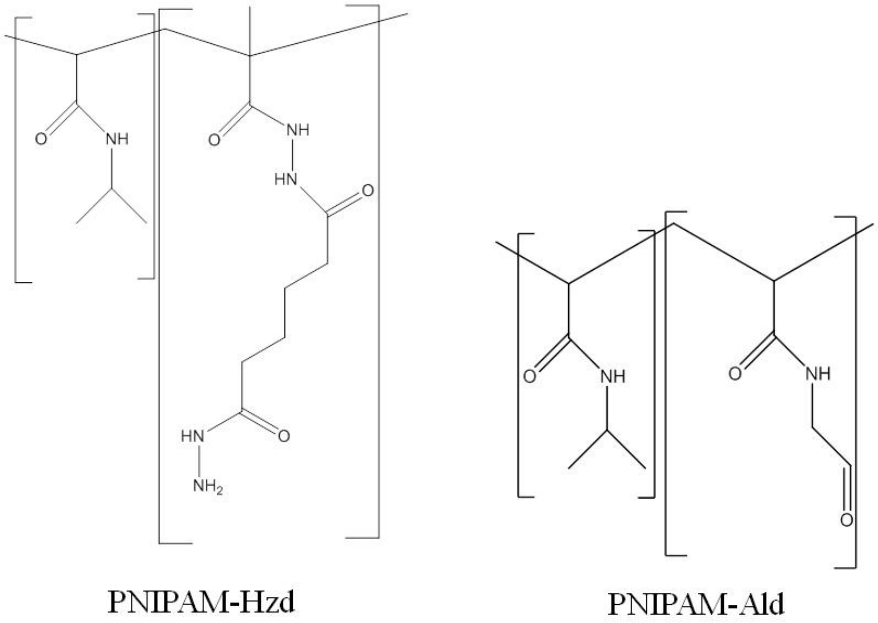


**Figure S4.1**: Chemical structures of PNIPAM-ADH and PNIPAM-Ald

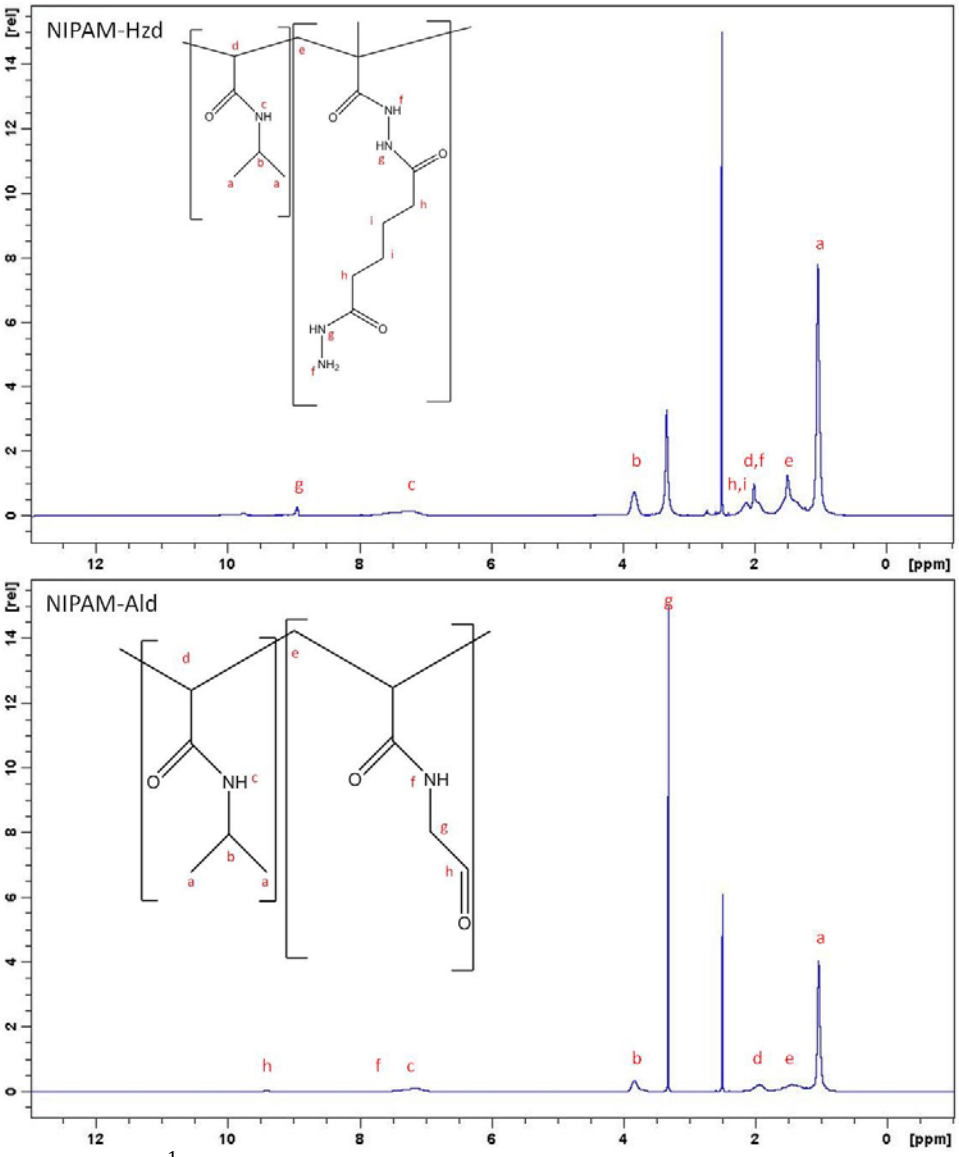


**Figure S4.2:** $^{1}$H-NMR (DMSO, 600 MHz) results for NIPAM-Hzd and NIPAM-Ald
For NIPAM-Hzd: δ = 1.04 (6.1H, -$CH_3$), δ = 1.50 (2.5H, -$CH_2$), δ = 2.01 (1.2H, -$NH_2$, -CH), δ = 2.12 (0.6H, -$CH_2$) , δ = 3.83 (1.0H, -CH) , δ = 7.29 (0.8H, -NH), δ = 8.94 (0.2H, -NH).
For NIPAM-Ald: δ = 1.04 (5.9H, -$CH_3$), δ = 1.50 (1.7H, -$CH_2$), δ = 1.93 (1.0H, -CH), δ = 3.32 (1.72H, -$CH_2$), δ = 3.83 (1.0H, -CH), δ = 7.16 (0.9H, -NH), δ = 7.88 (0.07H, NH), δ = 9.41 (.07H, -CHO).

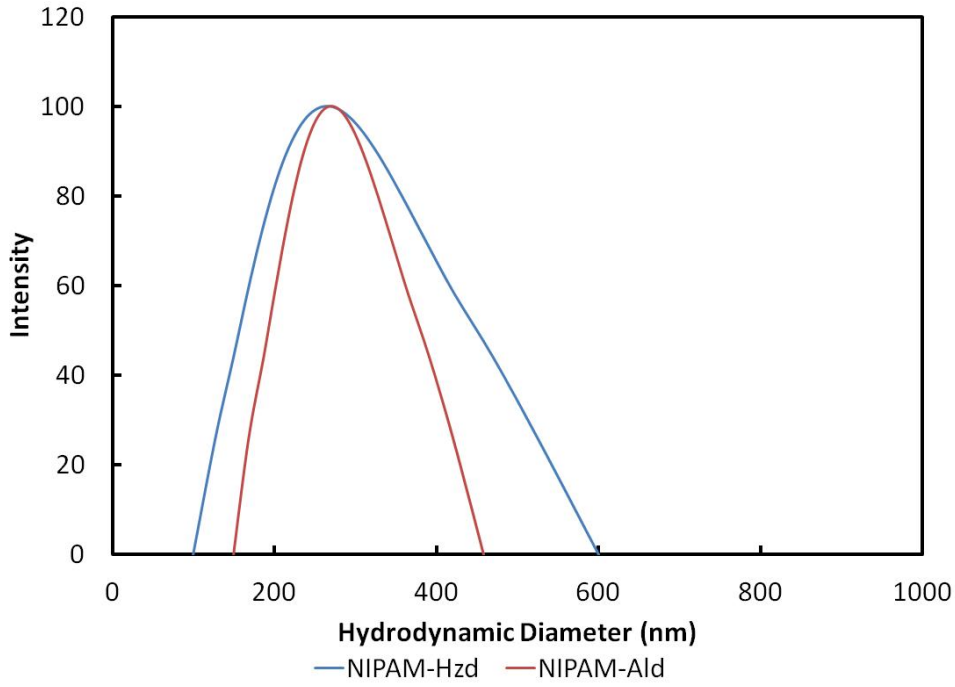


**Figure S4.3:** Size distribution (from dynamic light scattering) of 1 mg/mL solutions of NIPAM-Hzd (blue) and NIPAM-Ald (red) aggregates at 69°C

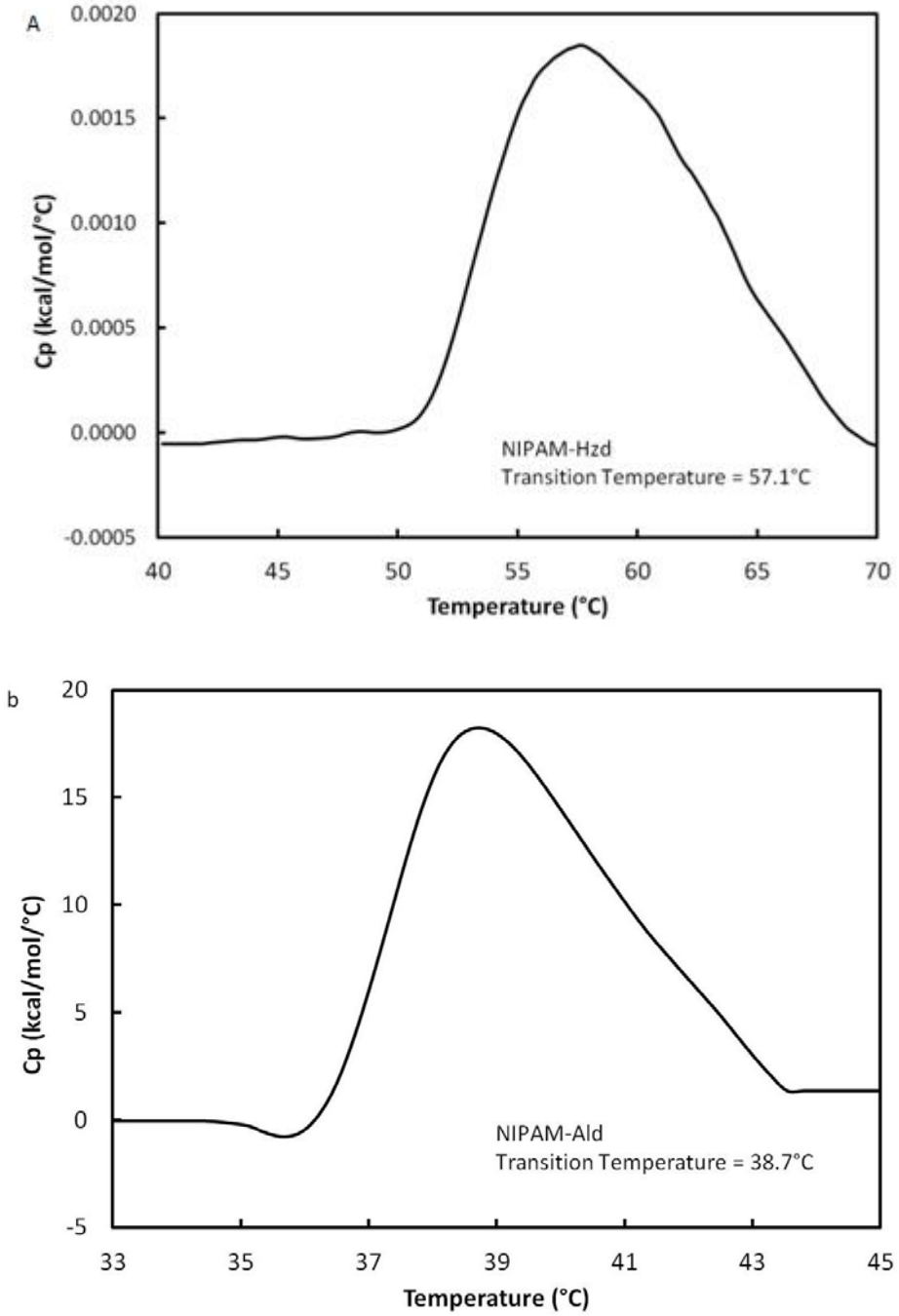


**Figure S4.4:** Differential scanning calorimetry analysis of NIPAM-Hzd (a) and NIPAM-Ald (b) indicating lower critical solution temperatures of the two polymers. These results are similar to those acquired via UV-vis spectrophotometry (Fig. 3a in main manuscript).

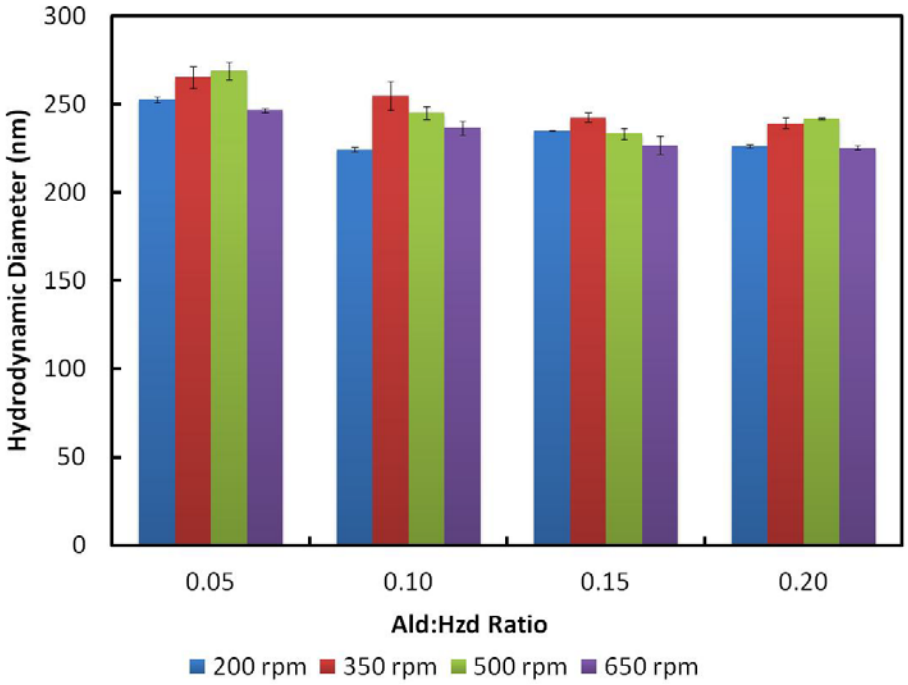


**Figure S4.5:** Hydrodynamic diameter (from dynamic light scattering) of microgels produced using various stir speeds as a function of Ald:Hzd ratio (at 70°C)

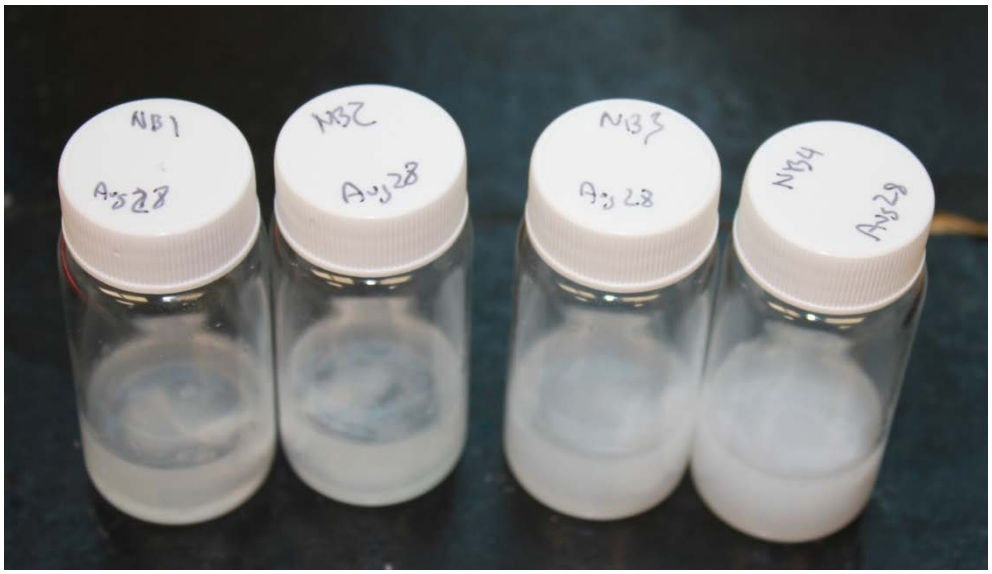

**Figure S4.6:** Aggregation of NIPAM-Ald (1 wt% base polymer concentration) following addition of NIPAM-Hzd as cross-linker (from left to right: 20 Ald:Hzd, 10 Ald:Hzd, 6.7 Ald:Hzd, 5.0 Ald:Hzd)

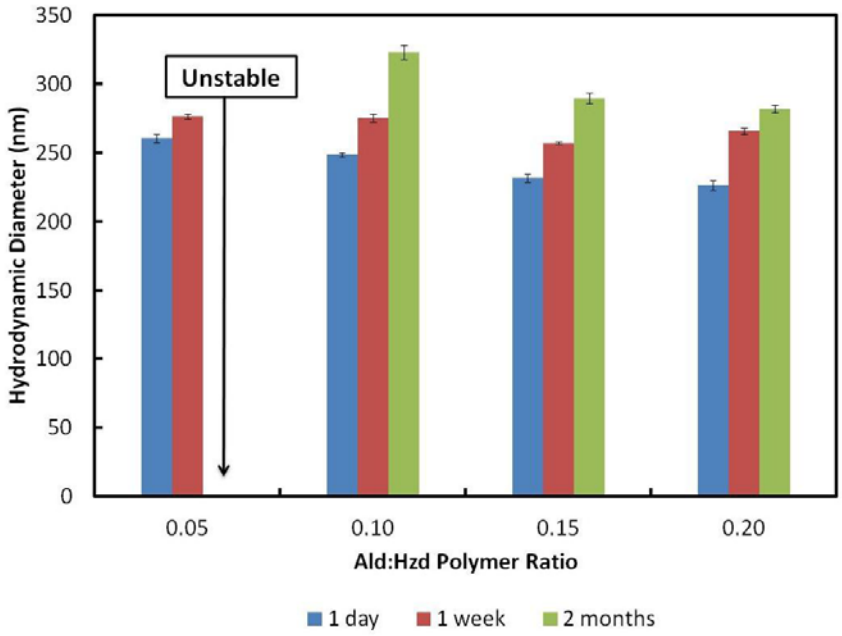


**Figure S4.7:** Microgel size changes at lysosymal pH (4.5) over a period of two months. Note: microgels made at 0.05 Ald:Hzd polymer ratio at a period of 2 months becomes unstable, aggregating and displaying multiple peaks on DLS measurements (indicative of degradation).

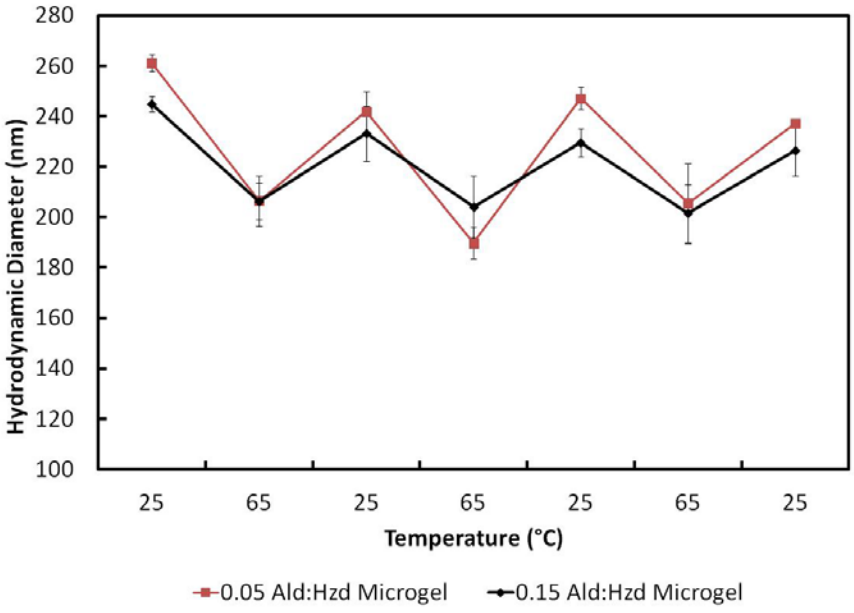


**Figure S4.8:** Thermal cycling of microgels (using dynamic light scattering) over three heating-cooling cycles as a function of Ald:Hzd ratio

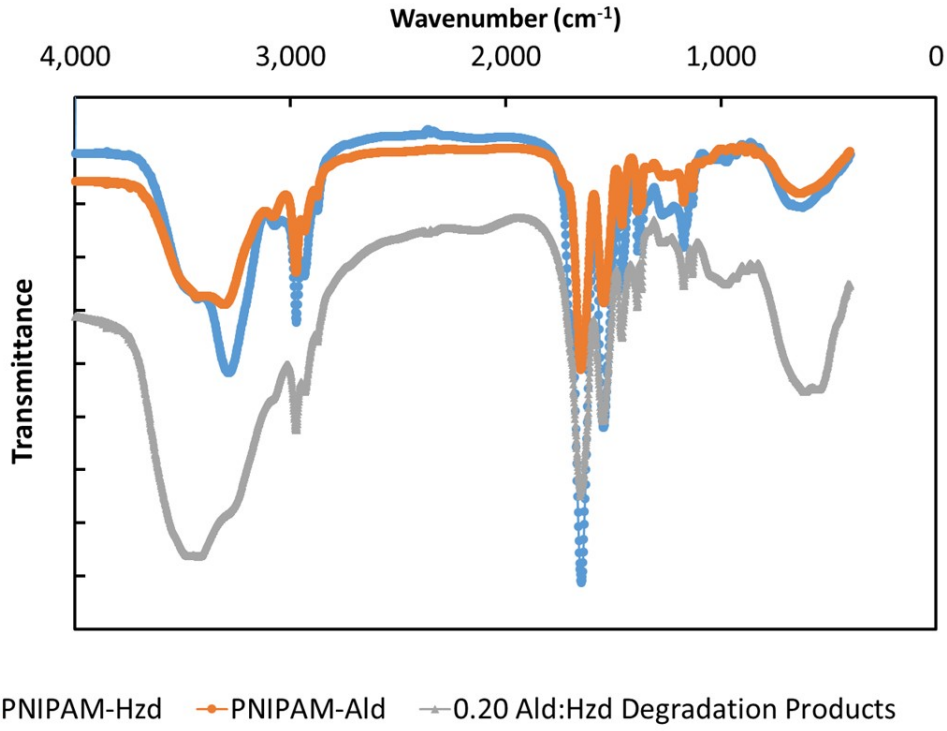


**Figure S4.9:** FTIR spectra of (a) PNIPAM precursors and 0.20 Ald:Hzd degradation products

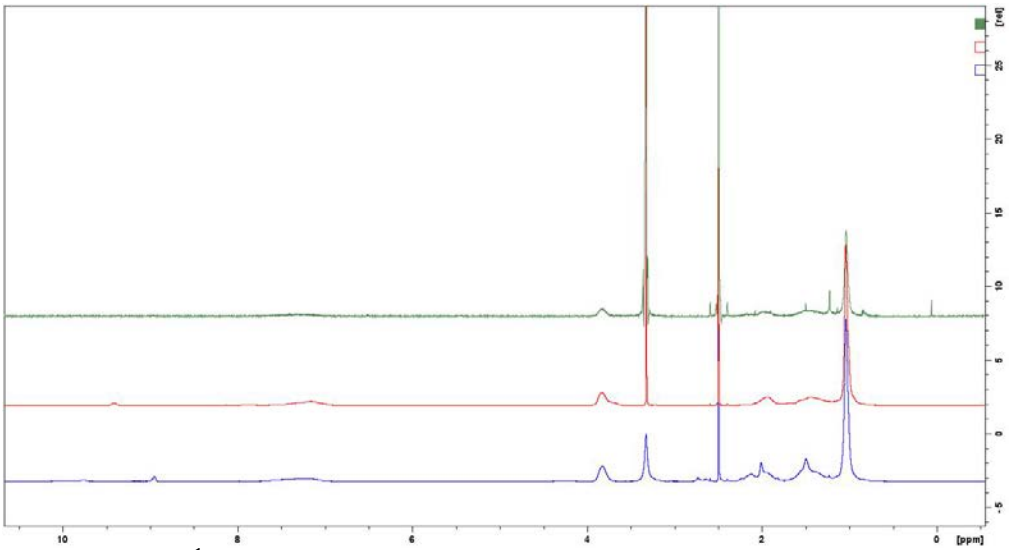


**Figure S4.10:** $^{1}$H NMR of PNIPAM-Hzd precursor (blue), PNIPAM-Ald precursor (red) and degradation products from a 0.20 Ald:Hzd microgel (green)

**Table S4.1:** List of diameters of microgels displayed in main paper

| Table | Microgel | | | | Size (nm) |
|---|---|---|---|---|---|
| | **Ald:Hzd Ratio** | **Production Temperature (°C)** | **Mixing Time (min)** | **Starting PNIPAM-Hzd Concentration (wt %)** | |
| Figure 3 | 0.05 | 50 | 15 | 1 | 277 ± 5 |
| | 0.05 | 60 | 15 | 1 | 245 ± 7 |
| | 0.05 | 70 | 15 | 1 | 265 ± 3 |
| | 0.10 | 50 | 15 | 1 | 281 ± 4 |
| | 0.10 | 60 | 15 | 1 | 236 ± 6 |
| | 0.10 | 70 | 15 | 1 | 255 ± 3 |
| | 0.15 | 50 | 15 | 1 | 262 ± 5 |
| | 0.15 | 60 | 15 | 1 | 225 ± 8 |
| | 0.15 | 70 | 15 | 1 | 243 ± 1 |
| | 0.20 | 50 | 15 | 1 | 266 ± 7 |
| | 0.20 | 60 | 15 | 1 | 207 ± 11 |
| | 0.20 | 70 | 15 | 1 | 239 ± 4 |
| Figure 4 | 0.05 | 70 | 2 | 1 | 286 ± 5 |
| | 0.05 | 70 | 5 | 1 | 265 ± 3 |
| | 0.05 | 70 | 15 | 1 | 265 ± 3 |
| | 0.05 | 70 | 30 | 1 | 258 ± 4 |
| | 0.10 | 70 | 2 | 1 | 282 ± 8 |
| | 0.10 | 70 | 5 | 1 | 251 ± 5 |
| | 0.10 | 70 | 15 | 1 | 255 ± 3 |
| | 0.10 | 70 | 30 | 1 | 243 ± 7 |
| | 0.15 | 70 | 2 | 1 | 253 ± 6 |
| | 0.15 | 70 | 5 | 1 | 246 ± 1 |
| | 0.15 | 70 | 15 | 1 | 243 ± 1 |
| | 0.15 | 70 | 30 | 1 | 234 ± 2 |
| | 0.20 | 70 | 2 | 1 | 238 ± 5 |
| | 0.20 | 70 | 5 | 1 | 236 ± 1 |
| | 0.20 | 70 | 15 | 1 | 239 ± 4 |
| | 0.20 | 70 | 30 | 1 | 227 ± 2 |
| Figure 5 | 0.05 | 70 | 15 | 0.2 | 210 ± 3 |
| | 0.05 | 70 | 15 | 0.5 | 198 ± 2 |
| | 0.05 | 70 | 15 | 1 | 265 ± 3 |
| | 0.05 | 70 | 15 | 2 | 300 ± 4 |
| | 0.10 | 70 | 15 | 0.2 | 195 ± 1 |
| | 0.10 | 70 | 15 | 0.5 | 202 ± 7 |
| | 0.10 | 70 | 15 | 1 | 255 ± 3 |
| | 0.10 | 70 | 15 | 2 | 294 ± 4 |
| | 0.15 | 70 | 15 | 0.2 | 193 ± 3 |
| | 0.15 | 70 | 15 | 0.5 | 217 ± 3 |
| Figure 5 cont. | 0.15 | 70 | 15 | 1 | 243 ± 1 |
| | 0.15 | 70 | 15 | 2 | 259 ± 4 |
| | 0.20 | 70 | 15 | 0.2 | 185 ± 3 |
| | 0.20 | 70 | 15 | 0.5 | 201 ± 3 |
| | 0.20 | 70 | 15 | 1 | 239 ± 4 |
| | 0.20 | 70 | 15 | 2 | 263 ± 5 |

| | **Degradation Time** | |
|---|---|---|
| Figure 7 | 1 Day | 294± 1 |
| | 7 days | 287 ± 6 |
| | 5 months | 318 ± 5 |

**Chapter 5**

# TEMPERATURE-INDUCED ASSEMBLY OF pH AND GLUCOSE RESPONSIVE MONODISPERSE, COVALENTLY CROSS-LINKED, AND DEGRADABLE POLY(N-ISOPROPYLACRYLAMIDE) MICROGELS BASED ON OLIGOMERIC PRECURSORS

**Authors:** Daryl Sivakumaran, Madeline Simpson, Eva Mueller, and Todd Hoare

**Publication:** To be submitted in 2015-2016

## Abstract

A rapid solvent-free thermally driven self-assembly approach is used to make multi-responsive, degradable microgels. Precursor polymers based on hydrazide and aldehyde-functionalized poly(N-isopropylacrylamide) (PNIPAM) were functionalized with pH-responsive functional groups (via copolymerization with 2-dimethylaminoethylmethacrylate, DMAEMA) or glucose-responsive functional groups (via reductive amination of phenylboronic acid, PBA); microgels were then formed by preheating the hydrazide functionalized polymer(s) to form nanoaggregates that are then stabilized via addition of the complementary aldehyde polymer(s). In both cases, changes in microgel swelling can be dictated by microgel environmental changes (pH or glucose concentration) in addition to or instead of changes temperature, with the degree of response tunable based on the cross-link density (i.e. the amount of aldehyde-

functionalized polymer added) and the degree of functionalization of the precursor polymers. Microgels fabricated using this self-assembly approach are degradable, unlike conventional PNIPAM-based microgels, offering promise to use these materials for *in vivo* applications not possible with conventional microgels.

**Keywords:** poly(N-isopropylacrylamide), self-assembly, microgels, degradability, colloidal stability, cationic, pH responsive, glucose responsive

## 5.1 Introduction

Microgels are solvent-swollen cross-linked gel particles on the size scale of 10-1000 nm that have been widely explored as potential technology solutions in fields such as the paint industry[1-4], catalysis[5-7], and a wide array of biomedical imaging[8,9] and drug delivery applications[10-12]. Of particular interest are microgels based on poly(N-isopropylacrylamide) (PNIPAM) that exhibit a reversible volume phase transition temperature (VPTT) as they are heated; this transition occurs at ~ 34°C for non-functionalized polymers but can be altered via incorporation of more or less hydrophilic comonomers[13]. More interestingly, the addition of comonomers that themselves exhibit switchable responses to e.g. pH[14,15], glucose[16,17], ionic strength[18], light[19,20], etc. can render the microgel multi-responsive in terms of enabling tunable changes in pore size, water content, hydrophilicity, and solution stability in response to each individual stimulus and/or only a particular combination of both stimuli[18,21,22]. Alternately, if the thermal responsiveness is not required in a particular application, the use of PNIPAM-based microgel platforms is still useful to provide a mechanism for the synthesis of highly monodisperse microgels (via a convenient solvent-free precipitation-based method)[23,24] and/or enhancing the swelling in response to the target stimulus[21].

From a biomedical applications perspective, microgels responsive to changes in pH and glucose concentration are of particular interest given the naturally-occurring gradients in both variables as a function of location for pH (e.g. stomach pH ~1-1.5[25], lysosomes pH ~4.5[26], mitochondrial matrix pH ~7.5[27], and cancerous tissue pH 6.5-7[28] relative to normal physiological pH 7.4[29]) and time for glucose (before or after meals). pH

variations *in vivo* can facilitate targeted responses of the microgel depending of microgel location within the body, while glucose responsive microgels can be used to monitor glucose levels in the blood stream for applications in triggered insulin delivery[30] or quantification of glucose concentrations within blood-protein mixtures[31].

pH-responsive microgels are typically prepared via copolymerization of monomers with a $pK_a$ in a targeted range for the desired smart response of the microgel vehicle. Ionization of these functional groups leads to swelling of the microgel due to Donnan equilibrium effects[32], facilitating pH-responsive control over microgel size and thus microgel pore size to allow for (as examples) entrapment and target release of molecules or drugs[15,33] or a change in optics for the quantification of metabolites[34-36]. A number of pH microgels have been reported utilizing different polymer backbones and different comonomers. Hoare and Pelton developed a series of anionic PNIPAM-based microgels via copolymerization with different carboxylic acid containing comonomers[21]. Depending on the type of acidic monomer used (methacrylic acid, vinylacetic acid, or acrylic acid) changes in microgel size could be controlled over different pH ranges. Furthermore, the copolymerization kinetics of the comonomers relative to NIPAM were found to dictate the distribution of carboxylic acid groups within the microgel, further enabling tuning of the pH response; for example, vinylacetic acid was primarily incorporated at chain ends at or near the microgel surface via chain transfer processes and thus allowed for a larger and narrower range pH transition of the microgel than was observed for acrylic acid and methacrylic acid copolymer microgels[37,38]. Basic monomers such as 2-(dimethylamino)ethyl methacrylate (DMAEMA), 4-vinylpyridine (VP), or N-3-

dimethylaminopropyl methacrylate have also been copolymerized with NIPAM to provide a platform for pH sensitivity as well as cationic charge[1,39,40]. Copolymerizing multiple pH-ionizable comonomers with differing $pK_a$ ranges and/or copolymerization kinetics can further tune the microgel response achieved; for example, Bradley et al. used free radical precipitation polymerization to create PNIPAM-based microgels with a core-shell configuration containing both DMAEMA and VP that exhibited a cationic charge below pH 6[41,42].

Drug delivery can be significantly aided by the presence of charge in the microgel network by promoting better uptake and subsequent control of release of molecules from microgels. For example, cationic microgels have been shown to effectively bind and then release anionic surfactants[41,42]. Acrylic acid functionalized PNIPAM microgels have been used to encapsulate the protein cytochrome C with higher efficiencies occurring when the charge density of the microgel was highest, promoting electrostatic binding and subsequent deswelling of the microgel[43]. Similar observations were also made using anionically charged PNIPAM microgels for the uptake of cationic bupivacaine[44], with controlled release of bupivacaine achieved depending on the charge density of the microgel[45]. Electrostatic interactions between microgels of opposite charge can also be applied to create highly functional controlled release vehicles. For example, Gao et al.[11] have developed drug trapping microgel aggregates via the formation of electrostatically-assembled hydrogels based on microgels copolymerized with acrylic acid (anionic) or N-[3-dimethylamino)propyl]methacrylamide (cationic). At neutral pH, the resulting hydrogels were able to trap a model drug (methylene blue) within the aggregate; upon

changing the pH of the solution (to titrate the charge from one or the other microgel), the aggregate fell apart, releasing the drug into solution. Thus, utilizing charged microgels allows for many different approaches to binding and releasing therapeutics in the field of drug delivery research.

Chemically-responsive microgels add an additional element of "smart" behaviour to microgels in that they can directly translate the presence or particular concentrations of specific metabolites (such as enzymes[46,47]) in the body into a swelling response within the microgel. Glucose is a particularly interesting target molecule in this regard given that a glucose responsive microgel could possibly be used to quantify glucose concentrations and/or regulate *in vivo* delivery of insulin in response to blood glucose level changes[30]. Such a technology is especially needed in the context of the rise in diabetic conditions among the aging population and would help minimize the possibility of patients experiencing an insulin overdose or hypoglycemia. Significant research effort has been invested into creating glucose sensitive microgels that utilize different glucose responsive functional groups. Wu et al.[48] created emulsion generated microgels which upon glucose oxidase exposure to glucose would result in a drop in localized pH; by using a pH degradable cross-linker, the microgel could then be degraded faster at higher glucose concentrations to enable triggered release of an insulin payload. Similarly, glucose-responsive microgels have been created utilizing the lectin concanavalin A that upon glucose exposure results in the release of encapsulated insulin through a displacement mechanism in which glucose displaces the bound insulin conjugate[49]. However, the major drawback with these approaches is that they are based on proteins and subsequently are

limited by the potential toxicity, antigenicity, instability, and high cost of such ligands[16,30].

Alternatively, microgels based on glucose-responsive phenylboronic acid (PBA) groups can provide a cheaper and more stable option. PBA can form a reversible covalent bond with cis-diol groups in glucose (and other carbohydrates) to create a boronate ester[30,50], resulting in the generation of an anionic charge upon glucose bonding. As more glucose is added to the solution, more PBA-glucose covalent bonding occurs and more boronate acid ionization occurs, leading to a shift in equilibrium of the trigonal boronic acid functional groups[51,52]. This in turn allows more glucose to bind to PBA until equilibrium is reached at a certain glucose concentration. When incorporated into a microgel, this increase in charge associated with the PBA groups results in swelling of the microgel due to Donnan equilibrium effects,[50] driving glucose-responsive microgel swelling. This strategy has been utilized by numerous research groups to create glucose responsive microgels based on NIPAM[50,53,54] and copolymerized with other monomers such as 4-vinylpyridine[55] and acrylamide[56] that enable microgel responses to varying amounts of glucose. The microgels are also able to encapsulate a release payload (insulin most often) to provide a promising platform for glucose sensitive biomedical applications[30,57]. It is recognized that glucose primarily binds with PBA groups at basic pH, as the (ionized) tetrahedral form of PBA ($pK_a$ ~ 8.5) binds significantly more strongly to *cis*-diol groups than the (non-ionized) trigonal form[58,59]. Thus, to effectively use this interaction at physiological pH (~7.4), the $pK_a$ of PBA must be reduced. Three approaches have been reported for this purpose: (1) copolymerization of comonomers

containing lone pairs of electrons that can complex with boron to induce a conformational change into a more trigonal form[60]; (2) functionalization of the aromatic ring of PBA with electron withdrawing groups such as nitro-, sulfonyl- and carboxyl- groups[61,62]; (3) conjugation of the PBA group to the polymer via an electron donating linkage, such as a secondary amine [63,64]. Any of these approaches can create sufficient ionization at normal physiological pH for glucose responses to be induced.

However, despite the promise of the smart responses engineered into the PNIPAM-based microgels described above, the conventional precipitation-induced free radical polymerization method used almost uniformly to prepare these microgels offers challenges in the context of the use of these microgels in biomedical applications. Since these free-radical polymerized microgels contain non-degradable carbon-carbon backbones, they are not clearable *in vivo* and are instead likely to accumulate within the liver or spleen (since renal clearance typically can only clear materials with molecular weight fragments no larger than 60,000 g/mol[65]). The incorporation of degradable cross-linkers based on disulfides (cleavable via redox chemistry or thiol exchange reactions)[66,67] or acetal groups (cleavable via hydrolysis)[68] into microgels could help with clearance of microgels from the body but still cannot effectively control the molecular weight between cross-links, potentially leaving degradation products that remain too large for effective renal clearance.

To address this issue, we have developed a solvent and surfactant free production method to form microgels based on hydrazide (PNIPAM-Hzd) and aldehyde (PNIPAM-Ald)-functionalized PNIPAM oligomers with controlled molecular weights below the

renal cut-off limit that can cross-link to create hydrolysable hydrazone bonds[69]. Microgel formation is driven by the induced precipitation of controlled molecular weight PNIPAM-Hzd oligomers above their lower critical solution temperature (LCST), resulting in the formation of stable nanoaggregates of PNIPAM-Hzd polymer which are then cross-linked by the addition of PNIPAM-Ald polymer to form stable, monodisperse degradable microgels.

Herein, we aim to extend this methodology to produce narrowly dispersed, covalently cross-linked, multi-responsive pH and glucose-sensitive microgels that are fully degradable back into their oligomeric components. Copolymerization of PNIPAM-Hzd with the cationic monomer 2-(dimethylamino)ethyl methacrylate (DMAEMA) is shown to result in pH-sensitive cationic microgels that retain their thermosenstivity but also offer different swelling characteristics depending on the solution pH. Similarly, grafting of phenylboronic acid derivatives to both PNIPAM-Hzd and PNIPAM-Ald precursor polymers via reductive amination (creating a secondary amine linkage to reduce the $pK_a$ of the PBA groups into the physiological range) is demonstrated to result in glucose-responsive microgels. Relative to conventional microgels, these microgels offer significant potential in terms of their use in a real-world biomedical device.

## 5.2 Experimental

*Materials:* N-isopropylacrylamide (NIPAM, 99%), acrylic acid (AA, 99%), thioglycolic acid (98%), aminoacetaldehyde dimethyl acetal (99%), 2,2,6,6-tetramethyl-1-piperidinyloxy (TEMPO, 98%), 4-formylphenylboronic acid (>95%), 3-

aminophenylboronic acid monohydrate (98%), methacryloyl chloride (purum), 2-dimethylaminoethylmethacrylate (98%), sodium cyanoborohydride (98%), and D-(+) glucose (reagent grade) were all purchased from Sigma Aldrich (Oakville, Canada). Adipic acid dihydrazyde (ADH, Alfa Aesar, 98%), *N*'-ethyl-*N*-(3-dimethylaminopropyl)-carbodiimide (EDC, Carbosynth, Compton CA, commercial grade), and 2,2-azobisisobutryic acid dimethyl ester (AIBMe, Wako Chemicals, 98.5%) were all used as received. For all experiments, Milli-Q grade distilled deionized water (DIW) was used. Hydrochloric acid (1M) was received from LabChem Inc. (Pittsburgh, PA), while ethanol was purchased from Commercial Alcohols (Brampton, ON). 3T3 *Mus musculus* mouse cells were acquired from ATCC: Cedarlane Laboratories Ltd. (Burlington, ON). Cell culture supplies included Dulbecco's Modified Eagle Medium-high glucose (DMEM), fetal bovine serum (FBS), penicillin streptomycin (PS), recovery cell culture freezing and trypsin-EDTA, all purchased from Invitrogen Canada (Burlington, ON). Thiazolyl blue tetrazolium bromide (MTT) was purchased from Sigma Aldrich (Oakville, ON).

*Synthesis of N-(2,2-dimethoxyethyl)methacrylamide (DMEMAm) monomer:* The precursor monomer for aldehyde functionalization, *N*-(2,2-dimethoxyethyl) methacrylamide (DMEMAm), was synthesized using recipes produced by Smeets et al[70]. Briefly, 50 mL of aminoacetaldehyde dimethylacetal and 100 mg of TEMPO were dissolved in 100 mL of a 5M sodium hydroxide solution at 10 °C. A total of 47 mL of methacryloyl chloride was then added drop-wise over a period of 2 hours, and the resulting mixture was left to react for 24 hours at room temperature under a nitrogen

purge. This mixture was then extracted with 150 mL of petroleum ether to remove impurities. The aqueous phase was saturated with sodium chloride and extracted three times with 75mL aliquots of tert-butyl methyl ether. The organic phase was dried with magnesium sulfate, filtered, and concentrated under reduced pressure.

*Synthesis of hydrazide-functionalized PNIPAM (PNIPAM-Hzd):* Hydrazide-functionalized PNIPAM was produced through the conjugation of adipic acid dihydrazide to acrylic acid groups via carbodiimide coupling to a PNIPAM-co-AA polymer. The acrylic acid-functionalized PNIPAM backbone polymer was prepared by polymerizing 4.5 g NIPAM with 0.5 g (15 mol% monomer) or 1.0 g (25 mol% monomer) acrylic acid using 0.056 g 2,2-azobisisobutyric acid dimethylester (AIBME) as the initiator. A chain transfer agent (80 μL of thioglycolic acid) was used to control molecular weight of the final polymer. Polymerizations were run overnight in 20 mL of absolute ethanol at 56 °C under nitrogen purge. After polymerization, the solvent was removed by evaporation and the polymer was redissolved in 100 mL of Milli-Q water, dialysed against Milli-Q water over six, six-hour cycles (12-14 kDa MWCO), and then lyophilized. 0.5 g of the resulting PNIPAM-co-AA polymer was dissolved with 10 g or 15 g of adipic acid dihydrazide, and 5.6 g or 8.5 g EDC in 100 or 200 mL of Milli-Q water (for the 15 and 25 mol% AA recipes respectively). The total solution pH was adjusted and maintained at pH 4.75 using 0.1 M HCl to facilitate the conjugation of ADH to the acrylic acid groups. The modified polymer solution was dialysed against Milli-Q water over six, six-hour cycles (12-14 kDa MWCO) and lyophilized. Conductometric titrations (ManTech Inc.) showed that 95

mol% of acrylic acid units were functionalized with hydrazide groups after carbodiimide conjugation.

*Synthesis of cationic hydrazide-functionalized PNIPAM (PNIPAM-Hzd-DMAEMA):* Hydrazide functionalized PNIPAM containing *2*-dimethylaminoethylmethacrylate (DMAEMA) was prepared as described above but using a backbone polymer containing PNIPAM, acrylic acid, and DMAEMA (the latter incorporated to provide a basic pH-ionizable functional group in the final polymer). The PNIPAM-co-AA-co-DMAEMA backbone polymer was synthesized by dissolving 4.5 g NIPAM, 0.5 g (15 mol% monomer) acrylic acid, and 1.95 g (30 mol% monomer) DMAEMA in 20mL of absolute ethanol, using the same chain transfer agent and initiator concentrations, polymerization conditions, and ADH grafting conditions described for the neutral PNIPAM-Hzd copolymer. Conductometric titrations (ManTech Inc.) showed that 95 mol% of acrylic acid units were functionalized with hydrazide groups after carbodiimide conjugation. $^{1}$H-NMR showed a total of ~20 mol% (on a total monomer basis) DMAEMA was incorporated into the polymer.

*Synthesis of aldehyde-functionalized PNIPAM (PNIPAM-Ald):* Aldehyde-functionalized PNIPAM was prepared via copolymerization of NIPAM and DMEMAm followed by subsequent hydrolysis of the acetal groups in DMEMAm. Polymerization occurred at 56 °C under nitrogen in 20 mL of absolute ethanol containing 4 g of NIPAM, 0.95 g of DMEMAm (13.4 mol% total monomer), 0.056 g AIBME initiator, and 80 μL of

thioglycolic acid chain transfer agent. After polymerization, the solvent was evaporated and the polymer was redissolved in 1M HCl for 24 hours to convert the acetal groups into aldehyde groups. After 24 hours of hydrolysis, the polymer was purified via six, six-hour dialysis cycles (12-14 kDa MWCO) and lyophilized. Silver ion titration[71] indicated that 12 mol% of the total monomers in the polymer were functionalized with an aldehyde group, with aldehyde functionalization confirmed by $^{1}$H-NMR (Bruker AV700, 32 scans, deuterated DMSO).

*Synthesis of pheynlboronic acid (PBA) functionalized PNIPAM-Hzd (PNIPAM-Hzd-PBA) and PNIPAM-Ald (PNIPAM-Ald-PBA):* Hydrazide-functionalized PNIPAM (PNIPAM-Hzd) was functionalized with PBA using PNIPAM that contained 25 mol% hydrazide groups instead of the 15 mol% hydrazide groups targeted in the non-functionalized polymers as the base polymer, providing 10 mol% hydrazide groups available for PBA functionalization. 0.5 g of PNIPAM-Hzd (25 mol% hydrazides) was dissolved in 200 mL acetate buffer (pH 5) with 12 mg of 4-formylphenylboronic acid (2.1 mol % in the polymer) and 17.2 mg sodium cyanoborohydride to reductively aminate the excess hydrazide groups with PBA. The resulting mixture was mixed for 24 hours, after which it was dialysed against Milli-Q water over six, six-hour cycles (12-14 kDa MWCO) and lyophilized. $^{1}$H-NMR showed a total of 1.3 mol % of monomer residues were functionalized with a PBA group (62% of available PBA attached). A similar reductive amination technique was used to functionalize PNIPAM-Ald with PBA, in this case using 3-aminophenylboronic acid as the grafting molecule. Briefly, 0.5 g of PNIPAM-Ald was

dissolved in 200mL of acetate buffer (pH 5) along with 10 mg of 3-aminophenylboronic acid (9.8 mol %) and 40 mg of sodium cyanoborohydride. The resulting mixture was mixed for 24 hours, after which it was dialysed against Milli-Q water over six, six-hour cycles (12-14 kDa MWCO) and lyophilized. $^{1}$H-NMR showed a total of 8.2 mol% (in total) of PBA was incorporated into PNIPAM-Ald polymer samples (84% yield).

*Polymer Lower Critical Solution Temperature Measurements:* The lower critical solution temperature (LCST) of the precursor polymers was measured using UV-visible spectrophotometry (Variant Cary Bio 100 UV–vis spectrophotometer). Transmittance measurements were collected over a temperature range of 25 to 80°C (1°C intervals, 0.5°C/minute ramp speed), with the temperature at which the transmittance of the sample was reduced below 95% (onset LCST) recorded and reported.

*Microgel Self-Assembly:* Stock solutions of the precursor polymers (functionalized PNIPAM-Hzd and PNIPAM-Ald) were dissolved at concentrations of 0.5 w/v% or 1 w/v% in deionized water. 5 mL of the PNIPAM-Hzd-DMAEMA or PNIPAM-Hzd-PBA stock solution at the desired starting concentration was heated to 70˚C for 5 minutes under magnetic stirring (350 RPM) at which point the polymer solution became opaque (i.e. above the lower critical solution temperature of functionalized PNIPAM-Hzd). A 1.25 mL aliquot of PNIPAM-Ald (for DMEAMA-functionalized microgels) or PNIPAM-Ald-PBA (for PBA-functionalized microgels) was then added dropwise to the hydrazide functionalized PNIPAM solution over a period of 5-10 seconds and stirred at 70˚C for 15

minutes. The amount of PNIPAM-Ald added to the pre-heated 0.5 w/v% PNIPAM-Hzd solution was varied to change the ratio of PNIPAM-Ald and PNIPAM-Hzd used to prepare the microgels by increasing the concentration of the PNIPAM-Ald stock solution to 1 w/v% (5 wt% of PNIPAM-Hzd), 2 w/v% (10 wt% of PNIPAM-Hzd), 3 w/v% (15 wt% of PNIPAM-Hzd), and 4 w/v% (20 wt% of PNIPAM-Hzd). The Ald:Hzd ratios reported represent the mass ratios of aldehyde:hydrazide polymers used to prepare the microgels using this addition procedure. The subsequent microgel solutions were removed from the high temperature oil bath and allowed to cool overnight at room temperature prior to characterization.

*Microgel Particle Size Measurements:* Microgels particle sizes were measured using dynamic light scattering with a Brookhaven 90Plus Particle Analyser running Particle Solutions Software (Version 2.6, Brookhaven Instruments Corporation, 90° angle, 659 nm laser). Microgel concentrations were adjusted using Milli-Q water until the measured intensity was between 200 to 500 kilocounts per second. Measurements were conducted for a period of 2 minutes with a minimum of 4 replicates per sample, with intensity-weighted particle sizes and particle size distributions reported as averages plus or minus standard deviations of these replicates. Microgel size as a function of temperature was measured using the same apparatus and changing the temperature at 2°C intervals over a temperature range of 25°C to 70°C, with a equilibration period of 5 minutes at each temperature prior to measurement. The pH response of DMAEMA-functionalized microgels was measured by adjusting pH of the samples prepared as above to the desired

value using 1 M HCl or 1M NaOH, while glucose responsiveness of the microgels was assessed by adjusting the glucose concentration of the samples to between 1 mg/mL and 5 mg/mL by adding 1 mL aliquots of concentrated glucose solution to achieve the desired glucose concentration in the microgel solution.

*Electrophoretic Mobility:* Electrophoretic mobility measurements were conducted using a ZetaPlus zeta potential analyzer (Brookhaven Instruments Corporation) operating in PALS (phase analysis light scattering) mode (V.2.5). Samples were prepared at concentrations of ~2.5 mg/mL in 10mM KCl, with 5 replicates consisting of 30 cycles per replicate (150 total runs) used per sample tested; the experimental uncertainties represent the standard error of the replicate measurements. pH and glucose responsive mobilities were assessed via addition of HCl/NaOH or glucose as described for the particle size samples.

**5.3 Results and Discussion**

*Microgel Fabrication*: Microgels were formed from PNIPAM-based polymeric precursors functionalized with hydrazide and aldehyde groups. The thermal phase transition of the polymer from coil to aggregate above the LCST is the main mechanism driving microgel formation, as it is the key step for the formation of the PNIPAM-Hzd nanoaggregates that are ultimately cross-linked with PNIPAM-Ald to form microgels. Copolymerization of 2-dimethylaminoethylmethacrylate into the PNIPAM-Hzd polymer backbone provided monomer units that were cationic at physiological pH (the $pK_a$ of

DMAEMA is ~8.0) but neutral at higher pH values, rendering the microgel pH-responsive. Microgels were produced at pH ~7.0, meaning that microgels were slightly cationic under preparation conditions and swell during production and after being stabilized by the formation of the hydrazone bond following PNIPAM-Ald addition. Analogously, glucose-responsive PBA-containing microgels were produced by grafting 4-formylphenylboronic acid to PNIPAM-Hzd and/or 3-aminophenylboronic acid to PNIPAM-Ald, with microgels produced using the same precipitation/cross-linking method. In addition, the use of reductive amination as the grafting chemistry creates a secondary amine linkage between PBA and the main polymer chain that should effectively lower the $pK_a$ of the PBA groups, making them glucose-responsive at physiological conditions[63]. Note that all functional microgels were created using hydrazide-functionalized PNIPAM solution concentrations of 0.5 w/v% as opposed to the 1 w/v% concentration observed in Chapter 3; at concentrations above 0.5 w/v%, it was found that the functionalized particles exhibited significantly wider polydispersities than those of the base case microgels reported previously (Figure S4.3).

The mechanism of microgel production once again mirrors that of typical precipitation-based formation of PNIPAM microgels from monomer units. In that case, growth of the polymeric chain occurs until a critical oligomer length is achieved at a temperature above the LCST of the polymer, at which point the oligomer collapses as it undergoes phase transition into precipitated precursor particles that result in microgel formation[72]. In our case, the precipitating oligomers are effectively pre-synthesized with controlled molecular weight, ensuring that systemic clearance is ultimately possible.

Creating functionalized PNIPAM precursors takes the place of adding functional comonomers during the polymerization phase of traditional precipitation polymerizations. In addition to enabling degradation of the ultimate microgel, an additional potential advantage of this approach to microgel formation is maintaining a more uniform distribution of functional groups within the final microgel. During precipitation polymerization, monomer distribution is a function of copolymerization kinetics of the monomers in the solution; no such dependence would be observed in our self-assembly system, although it is not yet known if any kind of rearrangement of the functional groups may occur to stabilize the nanoaggregate before addition of the aldehyde polymer.

After addition of the aldehyde polymer, the microgels remain stable at temperatures both above and below the VPTT and do not dissociate back into the starting polymers upon cooling. Figure 5.1 shows the size distributions of the microgels (from DLS measurements) for both PBA-functionalized and DMAEMA-functionalized PNIPAM microgels produced using our self-assembly technique, while Table 5.1 shows the mean particle sizes and polydispersities of the functionalized microgels produced.

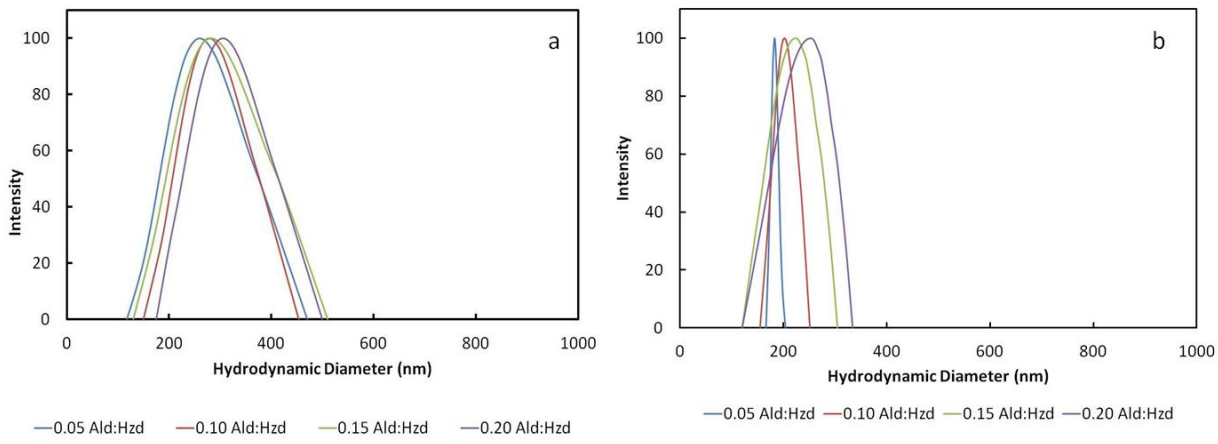


**Figure 5.1.** Particle size distributions measured by dynamic light scattering (intensity distribution, normalized to maximum intensity) of (a) DMAEMA-functionalized and (b) PBA-functionalized microgels

**Table 5.1.** Size and polydispersity of microgels produced at different Ald:Hzd ratios as measured via dynamic light scattering (DLS) at 25°C

| Microgel | DLS Size (nm) | DLS Polydispersity |
|---|---|---|
| 0.05 Ald:Hzd – DMAEMA | 262.1 ± 4.2 | 0.11 ± 0.02 |
| 0.10 Ald:Hzd – DMAEMA | 280.8 ± 4.0 | 0.12 ± 0.03 |
| 0.15 Ald:Hzd – DMAEMA | 287.4 ± 4.8 | 0.13 ± 0.03 |
| 0.20 Ald:Hzd – DMAEMA | 312.9 ± 9.0 | 0.13 ± 0.05 |
| | | |
| 0.05 Ald:Hzd – PBA | 178.4 ± 2.2 | 0.08 ± 0.03 |
| 0.10 Ald:Hzd – PBA | 201.1 ± 3.8 | 0. 10 ± 0.04 |
| 0.15 Ald:Hzd – PBA | 222.9 ± 3.2 | 0.10 ± 0.03 |
| 0.20 Ald:Hzd – PBA | 251.2 ± 4.9 | 0.11 ± 0.03 |

All microgels exhibit a single population DLS peak with relatively narrow polydispersity regardless of concentration of the cross-linker polymer added to the production pot (note that a generated polydispersity value of $\leq 0.1$ is generally interpreted as a monodisperse population in DLS[73]). This polydispersity is especially narrow relative to that typically achieved using inverse emulsion techniques that are commonly used as alternative

strategies to form degradable microgels[74]. Since maintaining monodisperse microgel populations is expected to lead to more predictable behavior *in vivo*[75], the relatively low monodispersity of these functionalized microgels suggests a potential advantage of these microgels in biomedical applications. DMAEMA-functionalized microgels exhibit significantly higher particle sizes relative to non-functionalized and PBA-functionalized microgels, a result that can likely be attributed to the presence of a positive charge provided by the DMAEMA monomer units during the aggregation step, which both limits the degree of chain collapse that occurs under the 70°C preparation conditions (Figure 5.2a) and induces swelling of the microgels under the pH (~7) measurement conditions. Given that the aggregate size distributions between PNIPAM-Hzd and PNIPAM-DMAEMA-Hzd are similar at 70°C (Figure S5.5), this suggests that the chain density inside the aggregates in each case may be different, with PNIPAM-Hzd likely containing a denser aggregate core than PNIPAM-DMAEMA-Hzd. The hypothesis is further supported by the increased transmittance of the PNIPAM-DMAEMA-Hzd polymer (0.91) relative to the PNIPAM-Hzd polymer (0.84) when measured at the 5 mg/mL concentration at the 70˚C condition used to fabricate the nanoparticles. However, both PNIPAM-Hzd and PNIPAM-DMAEMA-Hzd exhibit similar LCSTs (Fig. 5.2a), such that it is not surprising that similar conditions can lead to particle formation in each case.

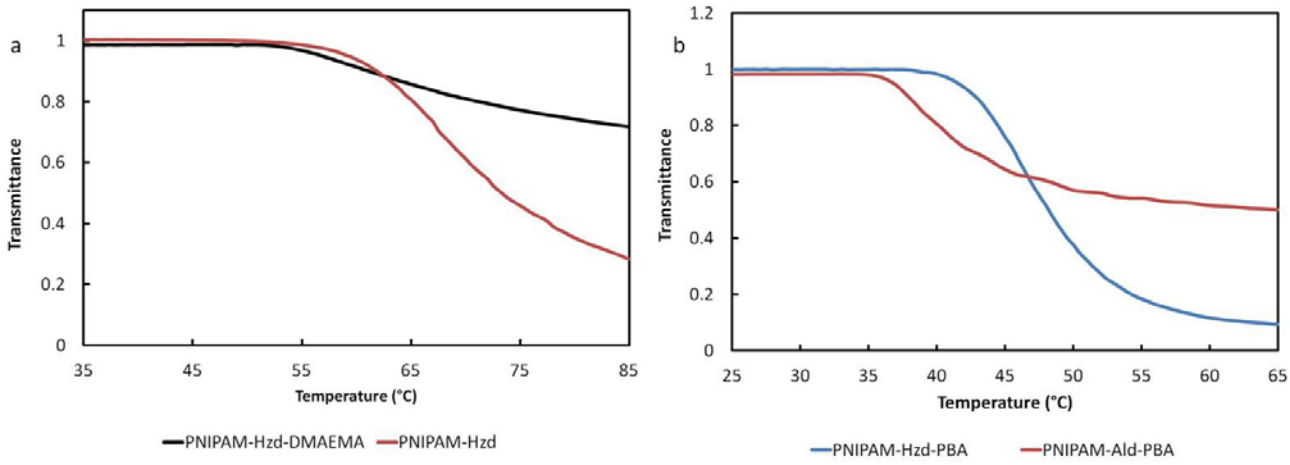


**Figure 5.2:** LCST of DMAEMA (a) and PBA-functionalized (b) precursor polymers

As the amount of PNIPAM-Ald used to produce DMEAMA-functionalized microgels is increased, a significant increase (0.05 to 0.20 Ald:Hzd ratio, $p = 0.025$) in particle size is observed. Interestingly, this result is in direct contrast to the non-functionalized microgels, in which a decrease in size is observed with added PNIPAM-Ald (Table 1). We attribute this effect to the increased hydrophobicity of the nanoparticle as a function of PNIPAM-Ald cross-linking (and thus consumption of the highly hydrophilic hydrazide groups to form significantly less hydrophilic hydrazone bonds), potentially resulting in additional nanoaggregation on the same time scale of the cross-linking reactions to result in larger particles; however, further investigation would be required to fully confirm the reason for this result.

The sizes of PBA-functionalized microgels are significantly smaller than microgels prepared with PNIPAM-Hzd or PNIPAM-Hzd-DMAEMA. The $pK_a$ of PBA groups is ~9, although the secondary amine linkage used to attach the phenylboronic acid

group to the backbone polymer does significantly reduce that $pK_a$ to close to physiological range[76]. However, a significant fraction of PBA groups (at least in the absence of glucose) remain unprotonated and thus relatively hydrophobic at pH 7.4. As a result, functionalization of PBA groups results in lowering of the LCST to ~41°C (significantly lower than PNIPAM-Hzd, Figure 5.2b), with the total transmittance of the solution decreasing significantly (Fig. 5.2b). This result is indicative of increased chain compaction via hydrophobic self-association of PBA groups which reduces the size of the resulting formed microgels.

When the amount of PNIPAM-Ald polymer used to prepare the microgels is increased, the microgel size also increases, similar to that observed for DMEAMA-functionalized microgels but again in contrast to the non-functionalized microgels. We attribute this result to one of two possible effects. First, since the PNIPAM-Hzd-PBA nanoaggregates appear to be highly collapsed based on Fig. 5.2b, the penetration of PNIPAM-Ald into the microgel is likely to be low; as such, adding additional aldehyde polymer may instead create a "hairy" surface layer on the microgel as opposed to effectively increase the cross-link density of the microgel, resulting in a larger microgel hydrodynamic diameter (and potentially a more sterically-stabilized microgel). Second, increased covalent bond formation upon higher PNIPAM-Ald addition would reduce the network mobility and thus potentially reduce the capacity for hydrophobic interactions between PBA groups that can function as physical cross-links; we have previously observed similar effects in bulk hydrogels that contain hydrophobic self-association domains[70]. As a result, while the covalent cross-link density of the microgel would

increase as more PNIPAM-Ald is added, the overall (physical + covalent) cross-link density may effectively be reduced, leading to additional microgel swelling.

*Effects of pH change of DMAEMA functionalized microgel:* The presence of DMAEMA within the microgels allows them to become responsive to changes in pH though the protonation of the amino group at pH values below the $pK_a$ of DMAEMA (~8). Figure 5.3 shows the electrophoretic mobility of the microgels as a function of pH.

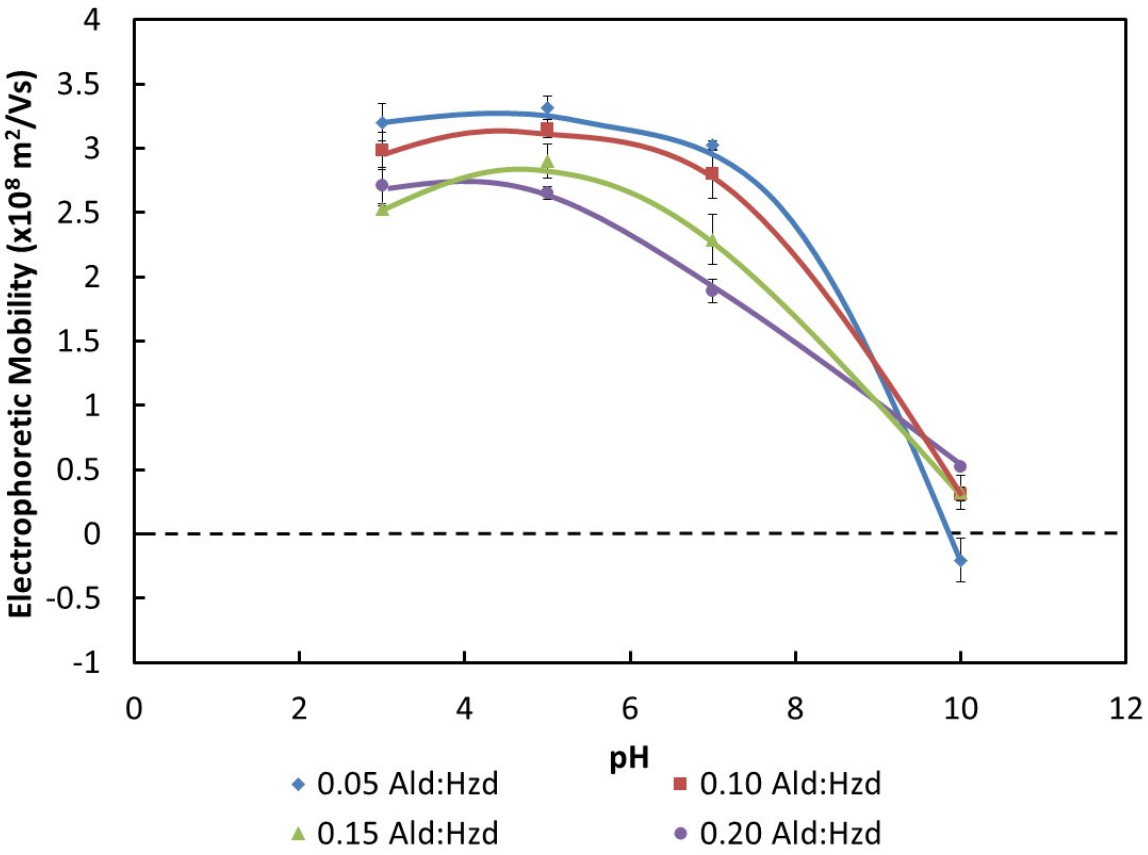


**Figure 5.3:** Changes in electrophoretic mobility of DMAEMA functionalized microgels in response to changes in solution pH (1mM NaCl) at 20°C

All DMAEMA-functionalized microgels exhibit a large cationic charge at lower pH which is reduced to nearly zero for all microgels tested as the pH is increased above the pKa to pH ~10. This change in the charge content of the microgel is directly associated with a significant deswelling of the microgel as the pH is increased, as observed in Figure 5.4.

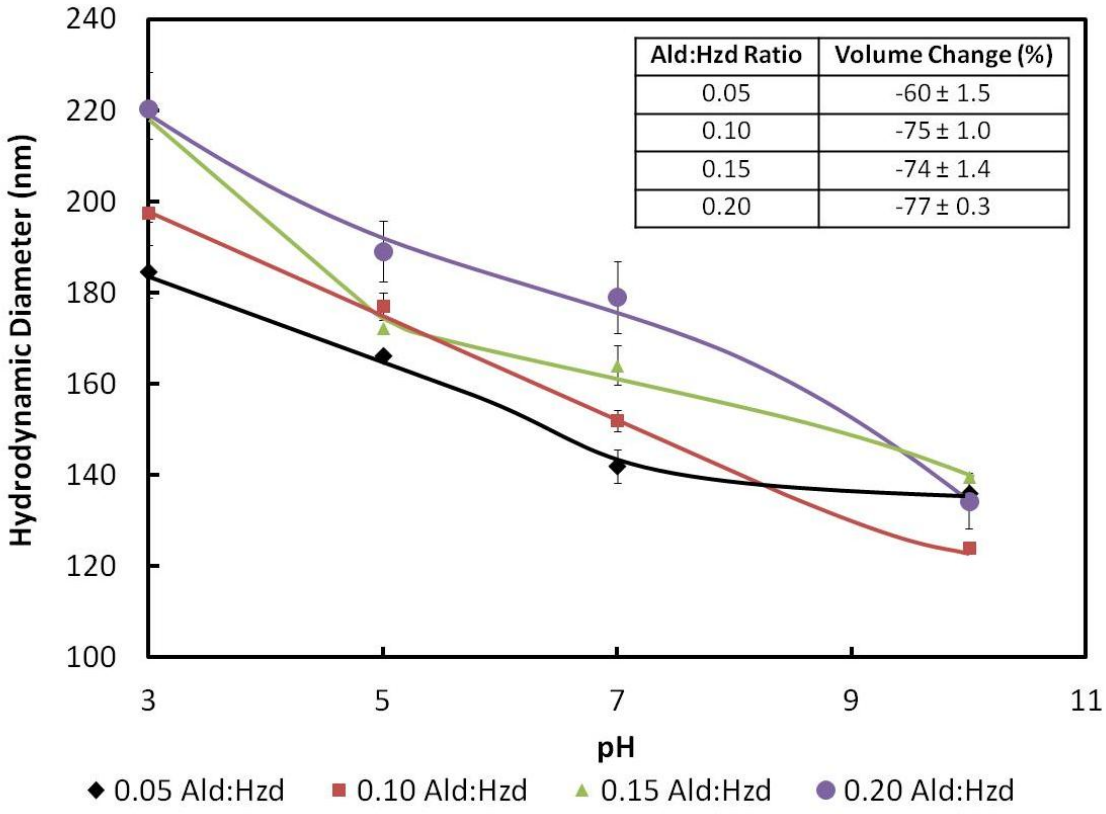


**Figure 5.4:** Microgel hydrodynamic diameter change in response to changes in solution pH (1mM NaCl) at 20°C, including percent change in volume over the pH range (inset)

As the pH of the solution is increased, deprotonation of the charged cationic DMAEMA groups results in a reduction in Donnan equilibrium contributions to microgel swelling and thus a significant decrease in microgel size, resulting in microgels that are ~70%

smaller than when fully swollen. The magnitude of deswelling observed as the pH is increased is similar for all microgel cross-linking densities explored, with deswelling occurring roughly equivalently at each pH value tested for each microgel given that the PNIPAM-Hzd-DMAEMA polymer (which alone governs the pH-responsiveness of the final microgel) is present at the same concentration in each microgel tested.

Note that the colloidal stability of DMAEMA-functionalized microgel is extremely high; microgels remained in suspension over the course of 2 weeks at physiological pH without exhibiting any sign of aggregation and only minimal changes in particle size (associated with slow degradation of the hydrazone cross-links, as observed earlier for the non-functionalized PNIPAM microgels).

*Effects of glucose concentration on PBA-functionalized microgel swelling:* Titration analysis indicated that significant ionization of the secondary amine-linked PBA groups occurs at pH values at and even below physiological pH (Figure S5.7), such that glucose-responsive swelling would be expected at pH 7.4. The glucose responsive swelling of the PBA-functionalized microgels was assessed at room temperature in aqueous solutions at glucose concentrations up to 5 mg/mL. The change in microgel size as a function of solution glucose concentration is shown in Figure 5.5.

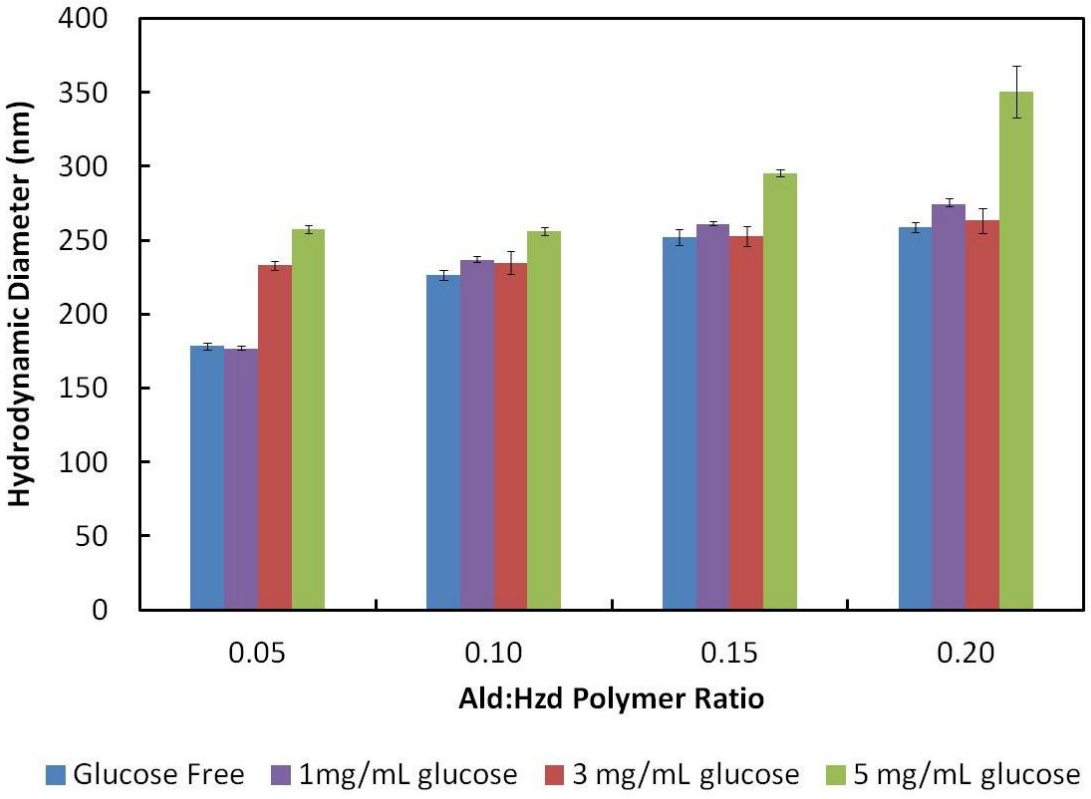


**Figure 5.5:** Microgel hydrodynamic diameter as a function of glucose concentration at 20°C

Note that as more PNIPAM-Ald is added, an increased amount of PBA is incorporated into the microgel since the PNIPAM-Ald used contains 8.2 mol% PBA groups (in contrast, the PNIPAM-Ald used in the DMAEMA study did not contain any additional DMAEMA residues). At all microgel formulations, there is no significant response (0.05, 0.10, 0.15 Ald:Hzd) or only a small (albeit statistically significant) response (0.20 Ald:Hzd) to the addition of glucose at low solution concentrations (1 mg/mL). As the glucose concentration increases to 3 mg/mL, microgels containing less PBA (in

particular, the 0.05 Ald:Hzd microgel) begin to swell. As the concentration of glucose in the microgel environment is increased further (5 mg/mL), all microgel formulations experience a significant increase in swelling. This result can be interpreted in two ways. First, glucose contains two *cis*-diol groups and thus can in theory form a *bis*-bidentate complex with PBA residues[77]. Thus, at lower concentrations at which glucose is less likely to fully saturate all PBA binding sites, the probability of glucose-induced cross-linking is relatively higher, restricting any swelling response that may be observed as a result of the shift in boronate ester ionization observed upon glucose binding. As glucose concentrations are increased, single PBA-glucose interactions become more likely and thus swelling due to boronate ionization is significantly enhanced. Second, a critical concentration of glucose may exist (depending on the PBA content of the microgel) at which an equilibrium shift occurs in the direction of forming more conjugates, leading to a significant increase in localized charge density and microgel hydrophilicity that causes the microgels to swell[54]. This is consistent with other protonation/deprotonation phase transitions, at which a critical charge content is required in order to result in a significant change in microgel swelling[78]. As such, careful manipulation of PBA content can result in different glucose responses and degrees of swelling to meet specific application requirements.

*Microgel Phase Transition:* To ensure that the self-assembled functionalized microgels still maintain a thermal phase transition, particle size was measured as a function of temperature. Figure 5.6a displays the thermal phase transitions of microgels

functionalized with DMAEMA whereas Figure 5.6b shows thermal phase transitions of microgels functionalized with PBA groups.

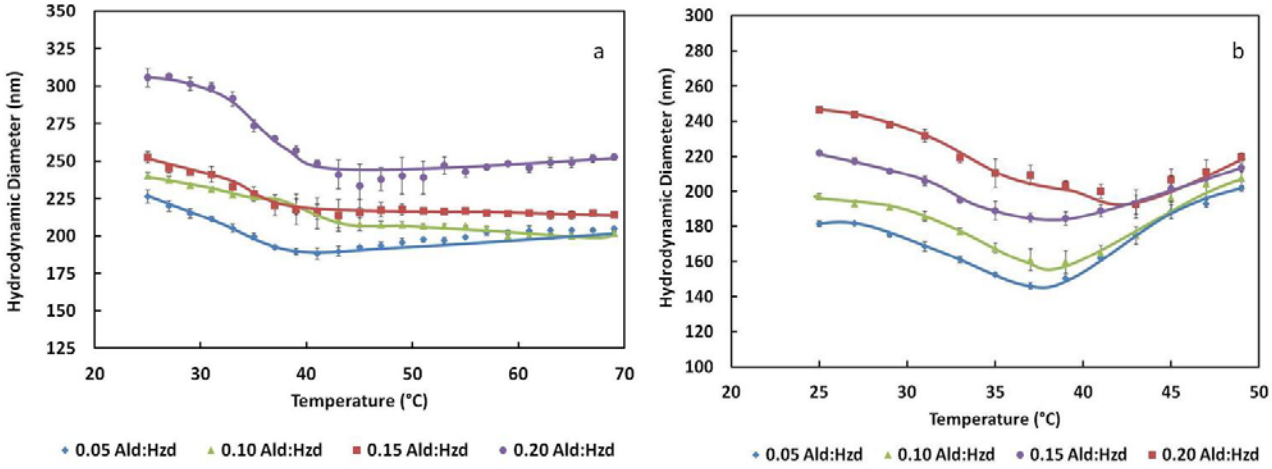


**Figure 5.6.** Hydrodynamic diameter versus temperature profiles (based on DLS) at pH 7 for microgels prepared with (a) DMAEMA functional groups; (b) PBA functional groups

The VPTT of the microgels is similar to that observed for conventional monomer, free radical initiated based NIPAM microgels, with 50% of the overall diameter change observed over the full phase transition occurring at ~37-38°C on average based on the DLS measurements for all microgels tested. The fact that the microgels collapse just above physiological temperature makes these them attractive for biomedical applications, facilitating (for example) triggered release of metabolites or active pharmaceutical ingredients at sites of infection[79] . The breadth of the transition is also relatively narrow, with onset (5% collapse) and offset (95% collapse) VPTT occurring within a ~10°C range for all samples tested. DMAEMA-functionalized microgels remain stable upon heating except for microgels prepared at the lowest Ald:Hzd ratio, which exhibit slight re-

aggregation above the VPTT. In contrast, PBA-functionalized microgels all aggregate to some extent above the VPTT, although the temperature at which this aggregation occurs increases systematically as the Ald:Hzd ratio is increased. We hypothesize this observation is attributable to the higher covalent cross-link density achieved at higher Ald:Hzd ratios, making hydrophobic interactions between uncharged PBA groups less likely to occur and reducing the likelihood of aggregation between collapsed particles via such interactions.

*Colloidal Stability:* PBA-functionalized microgels generated though this self-assembly technique are stable as a function of pH and glucose changes over the course of several days. However, microgel aggregation is observed after approximately 2 weeks in suspension. We anticipate this lower stability is attributable to the high degree of aldehyde groups that get consumed by amination of 3-aminophenylbornic acid during the functionalization process. Approximately 80% of the aldehyde groups are consumed in the current formulation, which does not allow many reactive groups for hydrazone bond formation and stabilization of the microgel. This has two potential impacts on the microgel stability: (1) particle stabilization via the presence of more hydrophilic aldehyde groups at the particle interface is lost and (2) a lower number of hydrazone bonds are formed to stabilize the nanoaggregate such that the degradation of the same total number of cross-links results in significantly reduced stability relative to the other, more highly cross-linked microgel compositions. This degradation is further enhanced by the presence of glucose, which brings additional water into the microgel for hydrolysis of the

bond. It is suggested that less PBA be attached to PNIPAM-Ald and/or higher aldehyde monomer mole fractions be incorporated into PNIPAM-Ald precursor polymers used to fabricate future glucose-responsive microgels; alternately (or concurrently), the PBA content of the PNIPAM-Hzd-PBA precursor could be increased to maintain the same total number of ionizable PBA groups to preserve the glucose sensitivity of the materials.

## 5.5 Conclusions

Using the method of thermal driven self-assembly, functionalized PNIPAM microgels can be made in a facile way by the incorporation of DMAEMA and PBA into the polymeric precursors. DMAEMA functionalized microgels have been shown to elicit a positive charge and pH responsive-swelling changes without compromising the thermosensitivity of the microgel network. PBA-functionalized microgels demonstrated glucose-responsive swelling associated with the ability of PBA to reversibly bond with glucose. Of particular note, glucose-induced swelling was observed primarily once a critical concentration of glucose (tunable by the PBA content and cross-linking density of the microgel) was exceeded, making them prime candidates for potential smart insulin delivery systems. It is however recognized that insulin loading and release needs to be further optimized (degree of functionalization, availability of PBA groups) before such as system materializes, including a thorough assessment of the possible insulin dosings as well as insulin stability/bioavailability following its release. Despite concerns with the presence of aldehyde groups potentially interacting with insulin and other proteins, it has

been demonstrated that hydrogels containing aldehyde groups can still efficiently release proteins payloads, although the bioactivity of released proteins remains to be verified[80].

**5.6 Acknowledgements:** Funding from the Natural Sciences and Engineering Research Council of Canada (NSERC, Discovery Grant Program) and the Ontario Early Researcher Awards (Ontario Ministry of Research and Innovation) is gratefully acknowledged.

## 5.7 References

(1) Nur, H.; Pinkrah, V. T.; Mitchell, J. C.; Benée, L. S.; Snowden, M. J. *Adv. Colloid Interface Sci.* **2010**, *158*, 15.

(2) Ishii, K. *Colloids Surf. Physicochem. Eng. Aspects* **1999**, *153*, 591.

(3) Ishikura, S. *Macromol. Symp.* **1996**, *101*, 115.

(4) Yagi, T. In *Surface Phenomena and Fine Particles in Water-Based Coatings and Printing Technology*; Sharma, M., Micale, F. J., Eds.; Springer US: 1991, p 117.

(5) Terashima, T.; Ouchi, M.; Ando, T.; Sawamoto, M. *Polym J* **2011**, *43*, 770.

(6) Yang, J.; Hu, D.; Song, S.; Sun, L. *Colloid. Polym. Sci.* **2013**, *291*, 2861.

(7) Dubey, N. C.; Tripathi, B. P.; Müller, M.; Stamm, M.; Ionov, L. *ACS Appl. Mater. Interfaces* **2015**, *7*, 1500.

(8) Wang, Q.; Zhang, D.; Yang, X.; Xu, H.; Shen, A. Q.; Yang, Y. *Green Chem.* **2013**, *15*, 2222.

(9) Yallapu, M. M.; Jaggi, M.; Chauhan, S. C. *Drug Discovery Today* **2011**, *16*, 457.

(10) Jiang, Y.; Chen, J.; Deng, C.; Suuronen, E. J.; Zhong, Z. *Biomaterials* **2014**, *35*, 4969.

(11) Gao, Y.; Ahiabu, A.; Serpe, M. J. *ACS Appl. Mater. Interfaces* **2014**, *6*, 13749.

(12) Smeets, N. M. B.; Hoare, T. *J. Polym. Sci., Part A: Polym. Chem.* **2013**, *51*, 3027.

(13) Wang, M.; Gao, Y.; Cao, C.; Chen, K.; Wen, Y.; Fang, D.; Li, L.; Guo, X. *Ind. Eng. Chem. Res.* **2014**, *53*, 18462.

(14) Geisel, K.; Isa, L.; Richtering, W. *Angew. Chem.* **2014**, *126*, 5005.

(15) Dadsetan, M.; Taylor, K. E.; Yong, C.; Bajzer, Ž.; Lu, L.; Yaszemski, M. J. *Acta Biomater.* **2013**, *9*, 5438.

(16) Hoare, T.; Pelton, R. *Macromolecules* **2007**, *40*, 670.

(17) Lapeyre, V.; Ancla, C.; Catargi, B.; Ravaine, V. *J. Colloid Interface Sci.* **2008**, *327*, 316.

(18) Karg, M.; Pastoriza-Santos, I.; Rodriguez-González, B.; von Klitzing, R.; Wellert, S.; Hellweg, T. *Langmuir* **2008**, *24*, 6300.

(19) Zha, L.; Banik, B.; Alexis, F. *Soft Matter* **2011**, *7*, 5908.

(20) Li, M.-H.; Keller, P. *Soft Matter* **2009**, *5*, 927.

(21) Hoare, T.; Pelton, R. *Macromolecules* **2004**, *37*, 2544.

(22) Lou, S.; Gao, S.; Wang, W.; Zhang, M.; Zhang, Q.; Wang, C.; Li, C.; Kong, D. *J. Appl. Polym. Sci.* **2014**, *131*, n/a.

(23) Acciaro, R.; Gilányi, T.; Varga, I. *Langmuir* **2011**, *27*, 7917.

(24) Guan, Y.; Zhang, Y. *Soft Matter* **2011**, *7*, 6375.

(25) Rogers, K. R.; Bradham, K.; Tolaymat, T.; Thomas, D. J.; Hartmann, T.; Ma, L.; Williams, A. *Sci. Total Environ.* **2012**, *420*, 334.

(26) Bach, G.; Chen, C.-S.; Pagano, R. E. *Clin. Chim. Acta* **1999**, *280*, 173.
(27) Akhmedov, D.; Braun, M.; Mataki, C.; Park, K.-S.; Pozzan, T.; Schoonjans, K.; Rorsman, P.; Wollheim, C. B.; Wiederkehr, A. *The FASEB Journal* **2010**, *24*, 4613.
(28) Lee, E. S.; Gao, Z.; Bae, Y. H. *J. Controlled Release* **2008**, *132*, 164.
(29) Schmitt-Willich, H. *The British Journal of Radiology* **2007**, *80*, 581.
(30) Zhang, X.; Lu, S.; Gao, C.; Chen, C.; Zhang, X.; Liu, M. *Nanoscale* **2013**, *5*, 6498.
(31) Li, Y.; Zhou, S. *Sensors Actuators B: Chem.* **2013**, *177*, 792.
(32) Hoare, T.; Pelton, R. *The Journal of Physical Chemistry B* **2007**, *111*, 11895.
(33) Zhao, C.; Chen, Q.; Patel, K.; Li, L.; Li, X.; Wang, Q.; Zhang, G.; Zheng, J. *Soft Matter* **2012**, *8*, 7848.
(34) Sorrell, C. D.; Carter, M. C. D.; Serpe, M. J. *Adv. Funct. Mater.* **2011**, *21*, 425.
(35) Islam, M. R.; Serpe, M. J. *Biosens. Bioelectron.* **2013**, *49*, 133.
(36) Islam, M. R.; Serpe, M. J. *Chem. Commun.* **2013**, *49*, 2646.
(37) Zhou, S.; Chu, B. *The Journal of Physical Chemistry B* **1998**, *102*, 1364.
(38) Dowding, P. J.; Vincent, B.; Williams, E. *J. Colloid Interface Sci.* **2000**, *221*, 268.
(39) Fernandez-Nieves, A.; Wyss, H.; Mattsson, J.; Weitz, D. A. *Microgel Suspensions: Fundamentals and Applications*; John Wiley & Sons, 2011.
(40) Eke, I.; Elmas, B.; Tuncel, M.; Tuncel, A. *Colloids Surf. Physicochem. Eng. Aspects* **2006**, *279*, 247.
(41) Bradley, M.; Vincent, B.; Burnett, G. *Langmuir* **2007**, *23*, 9237.
(42) Bradley, M.; Vincent, B. *Langmuir* **2008**, *24*, 2421.
(43) Smith, M. H.; Lyon, L. A. *Macromolecules* **2011**, *44*, 8154.
(44) Hoare, T.; Sivakumaran, D.; Stefanescu, C. F.; Lawlor, M. W.; Kohane, D. S. *Acta Biomater.* **2012**, *8*, 1450.
(45) Hoare, T.; Young, S.; Lawlor, M. W.; Kohane, D. S. *Acta Biomater.* **2012**, *8*, 3596.
(46) Thornton, P. D.; Mart, R. J.; Ulijn, R. V. *Adv. Mater.* **2007**, *19*, 1252.
(47) Thornton, P. D.; Mart, R. J.; Webb, S. J.; Ulijn, R. V. *Soft Matter* **2008**, *4*, 821.
(48) Wu, Y.; Hu, H.; Hu, J.; Liu, S. *Macromol. Rapid Commun.* **2012**, *33*, 1852.
(49) Yin, R.; Wang, K.; Du, S.; Chen, L.; Nie, J.; Zhang, W. *Carbohydr. Polym.* **2014**, *103*, 369.
(50) Hoare, T.; Pelton, R. *Biomacromolecules* **2008**, *9*, 733.
(51) Matsumoto, A.; Yamamoto, K.; Yoshida, R.; Kataoka, K.; Aoyagi, T.; Miyahara, Y. *Chem. Commun.* **2010**, *46*, 2203.
(52) Matsumoto, A.; Ishii, T.; Nishida, J.; Matsumoto, H.; Kataoka, K.; Miyahara, Y. *Angew. Chem.* **2012**, *124*, 2166.

(53) Tang, Z.; Guan, Y.; Zhang, Y. *Polymer Chemistry* **2014**, *5*, 1782.
(54) Wu, Q.; Wang, L.; Yu, H.; Chen, Z. *Polymer Science Series A* **2012**, *54*, 209.
(55) Farooqi, Z. H.; Wu, W.; Zhou, S.; Siddiq, M. *Macromol. Chem. Phys.* **2011**, *212*, 1510.
(56) Farooqi, Z. H.; Khan, A.; Siddiq, M. *Polym. Int.* **2011**, *60*, 1481.
(57) Zhao, L.; Xiao, C.; Ding, J.; He, P.; Tang, Z.; Pang, X.; Zhuang, X.; Chen, X. *Acta Biomater.* **2013**, *9*, 6535.
(58) Meng, H.; Zheng, J.; Wen, X.; Cai, Z.; Zhang, J.; Chen, T. *Macromol. Rapid Commun.* **2015**, *36*, 533.
(59) Dukler, A.; Freeman, A. *Biotechnol. Bioeng.* **2001**, *75*, 25.
(60) Peng, B.; Qin, Y. *Anal. Chem.* **2008**, *80*, 6137.
(61) Matsumoto, A.; Yoshida, R.; Kataoka, K. *Biomacromolecules* **2004**, *5*, 1038.
(62) Kim, A.; Mujumdar, S.; Siegel, R. *Chemosensors* **2013**, *2*, 1.
(63) Shiino, D.; Kubo, A.; Murata, Y.; Koyama, Y.; Kataoka, K.; Kikuchi, A.; Sakurai, Y.; Okano, T. *J. Biomater. Sci. Polym. Ed.* **1996**, *7*, 697.
(64) Kitano, S.; Hisamitsu, I.; Koyama, Y.; Kataoka, K.; Okano, T.; Sakurai, Y. *Polym. Adv. Technol.* **1991**, *2*, 261.
(65) Scott, E. A.; Nichols, M. D.; Cordova, L. H.; George, B. J.; Jun, Y.-S.; Elbert, D. L. *Biomaterials* **2008**, *29*, 4481.
(66) Wang, Y.; Nie, J.; Chang, B.; Sun, Y.; Yang, W. *Biomacromolecules* **2013**, *14*, 3034.
(67) Ulasan, M.; Yavuz, E.; Bagriacik, E. U.; Cengeloglu, Y.; Yavuz, M. S. *J Biomed Mater Res A* **2014**, DOI: 10.1002/ jbm.a.35146.
(68) Binauld, S.; Stenzel, M. H. *Chem. Commun.* **2013**, *49*, 2082.
(69) Patenaude, M.; Hoare, T. *ACS Macro Letters* **2012**, *1*, 409.
(70) Smeets, N. M. B.; Bakaic, E.; Patenaude, M.; Hoare, T. *Chem. Commun.* **2014**, *50*, 3306.
(71) Campbell, S. B.; Patenaude, M.; Hoare, T. *Biomacromolecules* **2013**, *14*, 644.
(72) Pelton, R. *Adv. Colloid Interface Sci.* **2000**, *85*, 1.
(73) Tan, S.; Zhao, D.; Yuan, D.; Wang, H.; Tu, K.; Wang, L.-Q. *React. Funct. Polym.* **2011**, *71*, 820.
(74) Murthy, N.; Xu, M.; Schuck, S.; Kunisawa, J.; Shastri, N.; Fréchet, J. M. J. *Proceedings of the National Academy of Sciences* **2003**, *100*, 4995.
(75) Bysell, H.; Månsson, R.; Hansson, P.; Malmsten, M. *Adv. Drug Del. Rev.* **2011**, *63*, 1172.
(76) DiCesare, N.; Adhikari, D.; Heynekamp, J.; Heagy, M.; Lakowicz, J. *J. Fluoresc.* **2002**, *12*, 147.
(77) Ben-Moshe, M.; Alexeev, V. L.; Asher, S. A. *Anal. Chem.* **2006**, *78*, 5149.
(78) Thaiboonrod, S.; Berkland, C.; Milani, A. H.; Ulijn, R.; Saunders, B. R. *Soft Matter* **2013**, *9*, 3920.

(79) Radovic-Moreno, A. F.; Lu, T. K.; Puscasu, V. A.; Yoon, C. J.; Langer, R.; Farokhzad, O. C. *ACS Nano* **2012**, *6*, 4279.

(80) Smeets, N. M. B.; Patenaude, M.; Kinio, D.; Yavitt, F. M.; Bakaic, E.; Yang, F.-C.; Rheinstadter, M.; Hoare, T. *Polymer Chemistry* **2014**, *5*, 6811.

**S5: Chapter 5 – Supplementary Information**

**TEMPERATURE-INDUCED ASSEMBLY OF pH AND GLUCOSE RESPONSIVE MONODISPERSE, COVALENTLY CROSS-LINKED, AND DEGRADABLE POLY(N-ISOPROPYLACRYLAMIDE) MICROGELS BASED ON OLIGOMERIC PRECURSORS**

**Authors:** Daryl Sivakumaran, Madeline Simpson, Eva Mueller, and Todd Hoare

**Publication:** To be submitted in 2015-2016

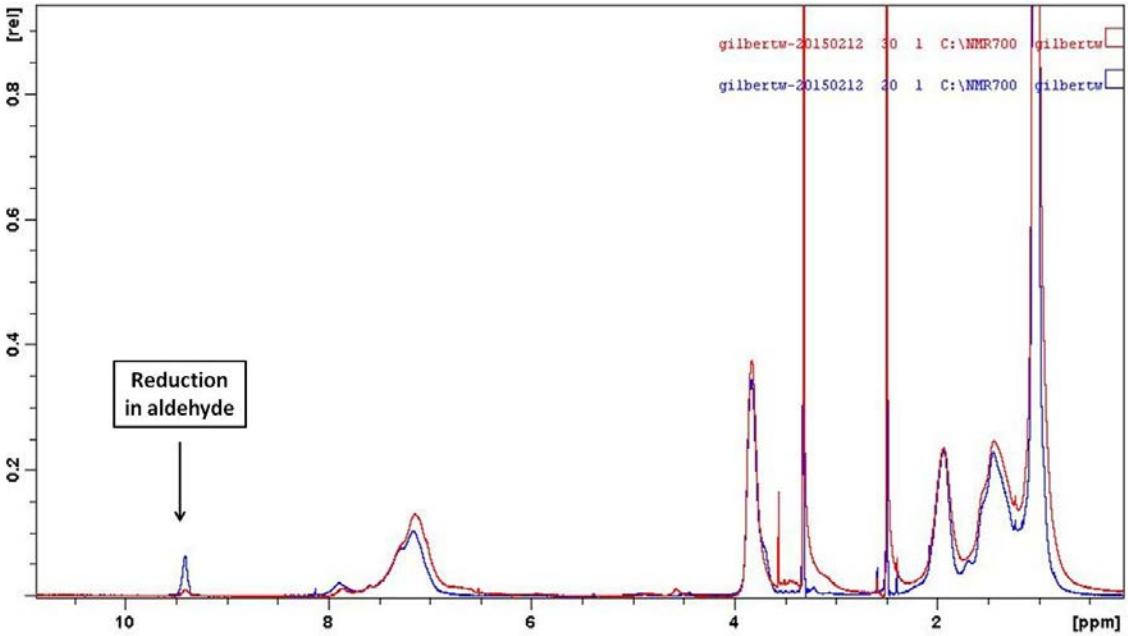


**Figure S5.1:** $^{1}$H NMR of PNIPAM–Ald (blue) and PNIPAM-Ald-PBA (red). Note reduction in aldehyde peak at ~9 ppm, indicating consumption of aldehyde groups upon functionalization with 3-animophenylbornic acid

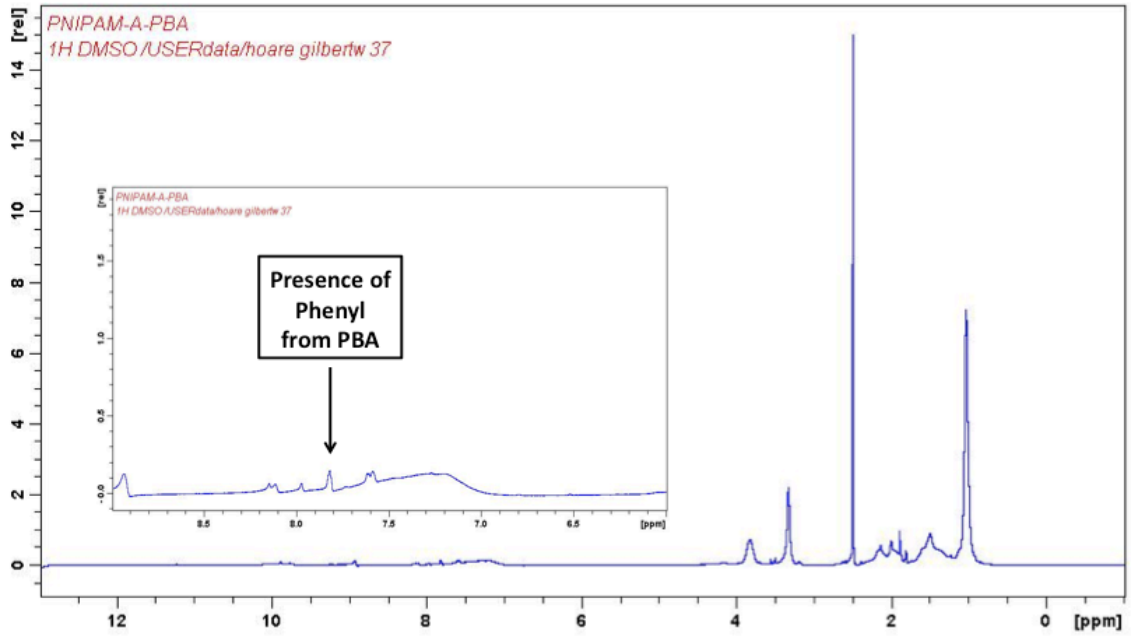


**Figure S5.2:** Confirmation of PBA grafting to PNIPAM-Hzd backbone as indicated by phenyl ring peaks at ~7.4-7.6 ppm

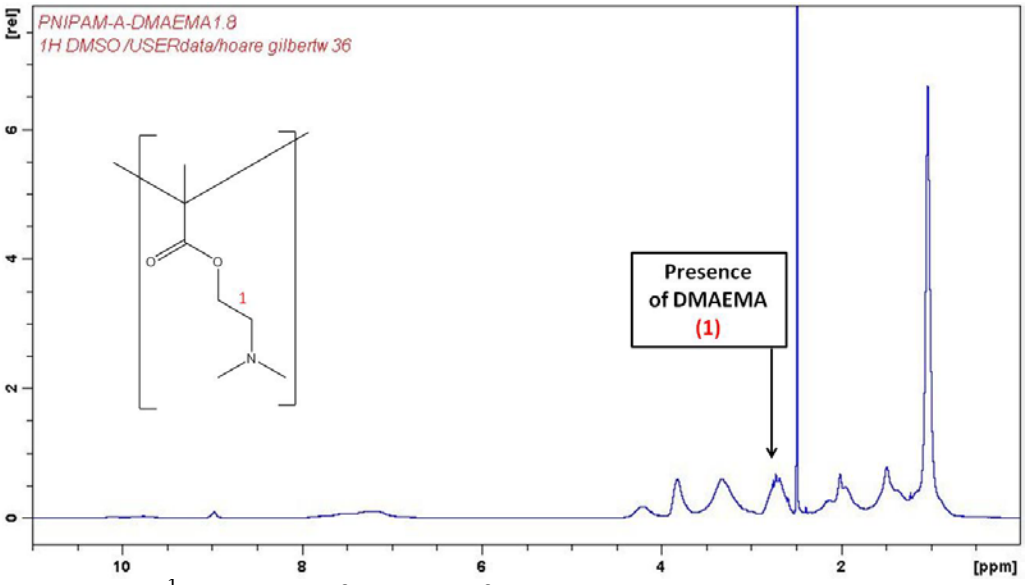


**Figure S5.3:** $^{1}$H NMR confirmation of DMAEMA in NIPAM-Hzd backbone at ~2.5-2.75 ppm (ethyl group)

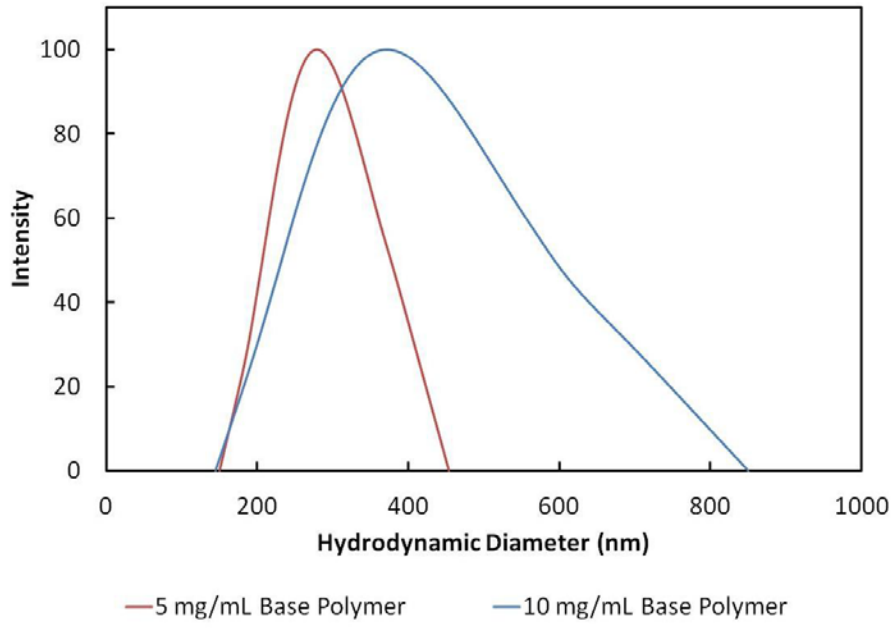


**Figure S5.4.** Particle size distributions measured by dynamic light scattering (intensity distribution, normalized to maximum intensity) of DMAEMA functionalized microgels (0.10 Ald:Hzd) with different starting concentrations of PNIPAM-Hzd-DMAEMA at a solution pH of ~7

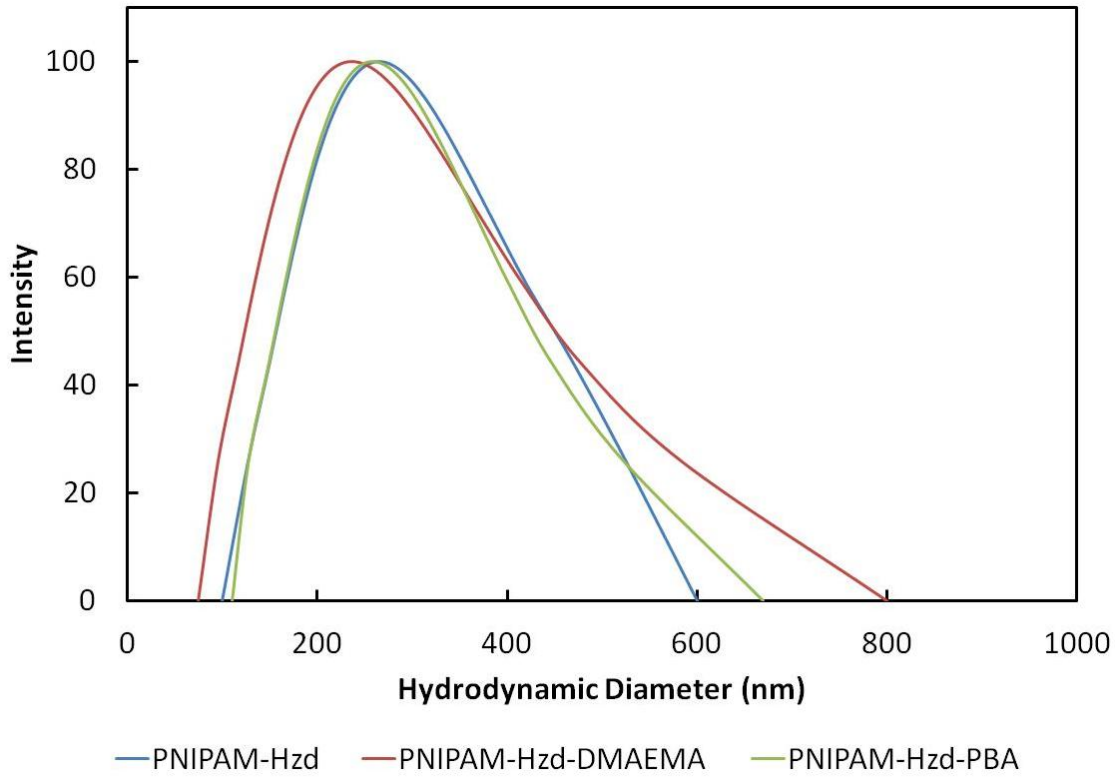


**Figure S5.5:** Aggregate size distributions measured by dynamic light scattering (intensity distribution, normalized to maximum intensity) of PNIPAM-Hzd, PNIPAM-Hzd-DMAEMA and PNIPAM-Hzd- PBA at 70°C and a solution pH of 7.

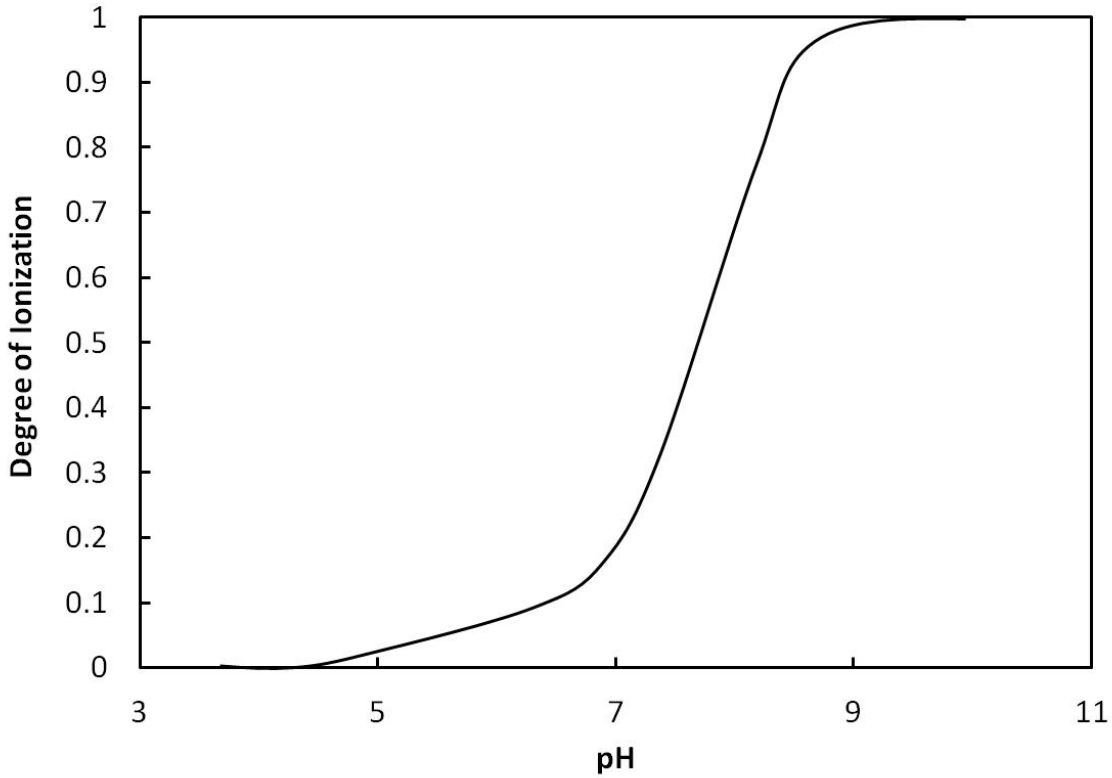


**Figure S5.6:** Degree of ionization versus pH curve for PNIPAM-Hzd-DMAEMA

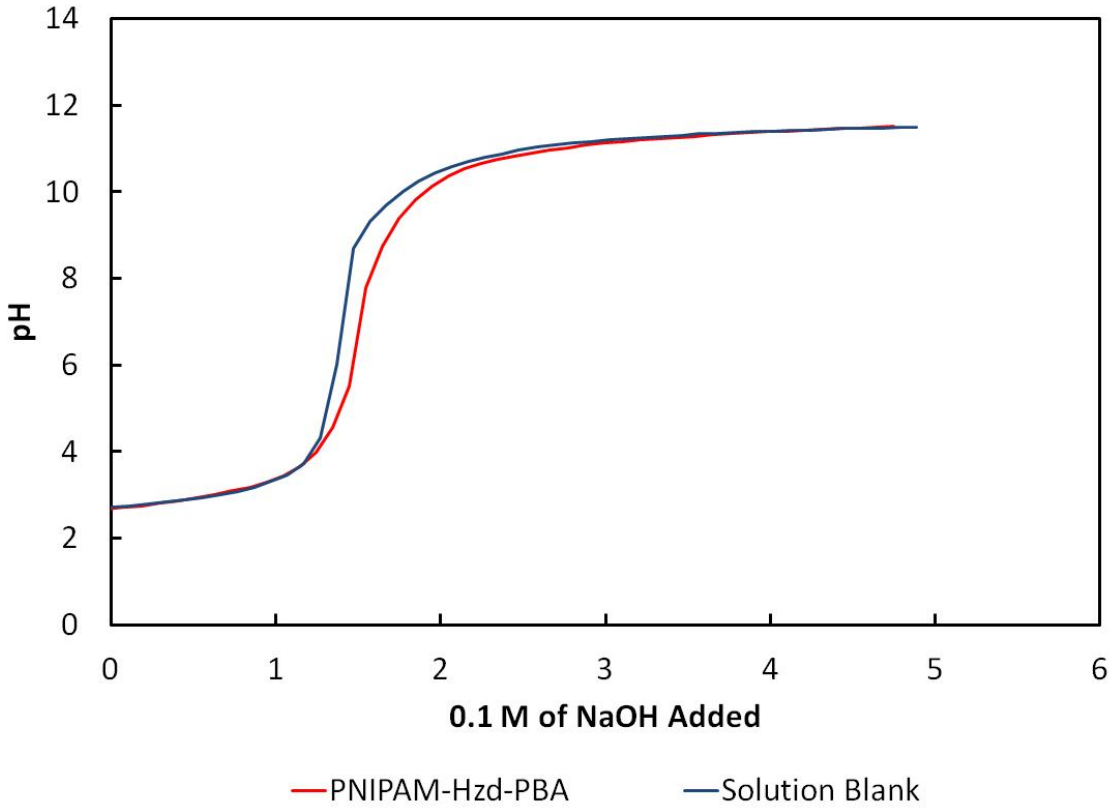


**Figure S5.7:** Potentiometric titration of PNIPAM-Hzd-PBA relative to a saline blank

## C. Summary and Future Work

*Summary of Thesis:*

Chapter 1 describes the effect of manipulating the cross-linking density within the microgel phase of microgel-hydrogel nanocomposites and its impact on drug release from the composite. Release of bupivacaine from nanocomposites consisting of a thermoresponsive microgel phase within a non-thermoresponsive carbohydrate phase can be tuned by altering the magnitude of the thermal phase transition of the microgel. By producing microgels with a higher internal cross-link density or by covalently attaching the microgel to the bulk hydrogel phase, drug release is slowed and burst release from the composite is significantly mitigated. Increased cross-link densities result in less deswelling of the microgel and thus both reduced convective transport of drug from the microgel phase as well as reduced free volume generation within the composite that would occur following microgel deswelling.

Chapter 2 focused on the production of micron-sized microgels utilizing PNIPAM precursors. A microfluidic chip was used to mix and emulsify two reactive precursor polymers based on PNIPAM functionalized with hydrazide and aldehyde respectively. Monodisperse and degradable PNIPAM microgels were made with diameters between 30-90 μm, the size of which can by tuned by altering the flow rate of the continuous oil phase within the chip. The produced microgels have a VPTT of ~34ºC and display reversibility (albeit with some hysteresis) through thermal cycling analogous to conventional PNIPAM particles. The microgels are fully degradable under acidic conditions following the hydrolysis of the cross-linking hydrazone bond.

The microgels produced in Chapter 2 were then utilized in Chapter 3 to explore drug release kinetics as a function of the chemistry and the relative orientation of the two gel phases by making composites with similar cross-link density and distribution in both the bulk and dispersed gel phases. Composites in which the bulk hydrogel phase consisted of carbohydrates exhibited fast drug release regardless of the microgel composition. Composite in which the bulk hydrogel phase was PNIPAM exhibited thermal deswelling when heated from room temperature to test conditions (physiological temperature), resulting in significantly higher drug entrapment that could be further enhanced when a thermosensitive microgel phase was also present in the composite. First-principles modeling of the release kinetics clearly demonstrated the importance of convection on regulating the release kinetics from PNIPAM bulk hydrogel composites.

Chapter 4 focused on the production of microgels from hydrazide and aldehyde-functionalized polymeric precursors to form nano-sized microgels using a novel aggregation/self-assembly technique that mimics traditional microgel synthesis. PNIPAM-hydrazide solutions were heated above their LCST to form a nanoaggregate, which was subsequently cross-linked and thus stabilized in microgel form by addition of PNIPAM-aldehyde polymer. Microgel size can be tuned by changing process conditions (temperature, mixing time) and polymer concentrations, resulting in reproducible monodisperse populations of microgels. The stable microgels exhibit VPTT at ~34-37°C and are degradable to the original starting precursor polymers over time, including at lysosomal pH. The microgels and starting materials have high cytocompatibility which makes them attractive for potential *in vivo* applications.

Chapter 5 is an extension of the research conducted in Chapter 4 in which functionalized microgels are produced in the same thermally driven self-assembly technique. The starting polymers were functionalized with DMAEMA and PBA groups to elicit additional responsiveness (pH and glucose respectively) aside from the thermal response generated by the presence of PNIPAM. Microgels functionalized with DMAEMA have a positive charge at physiological conditions and show pH responsive-swelling changes. PBA-functionalized microgels show glucose-responsive swelling due to the reversible bond formed between glucose and PBA groups, making these microgels interesting candidates for smart insulin delivery systems.

*Limitations of Work:*

Overall, it should be emphasized that the primary goal of this thesis was not to design translatable drug delivery solutions but rather to develop a toolkit of compositions and approaches for better understanding how to control drug release and/or provide solutions to challenges now hindering hydrogel and microgel-based smart materials for drug delivery applications. As such, while the technologies developed in this thesis offer significant promise in addressing challenges in the area of drug delivery, there remain several limitations and key challenges which must be overcome for translation to occur. In Chapter 1 and 3, the actual *in vivo* use of the microgel-hydrogel composites has yet to be determined and, in the context of the exact compositions tested in Chapter 1, is strongly limited by the lack of degradability of the microgels used (although the degradable microgels presented in Chapter 4 may be useful in addressing the latter

limitation). The presence of proteins and enzymes within the body ultimately may make the device ineffective, particularly in the context of (1) changing the volume phase transition behaviour as a result of protein adsorption and (2) changing the degradation rate of the bulk hydrogel or (for Chapter 3) the microgel phases via oxidative or enzymatic mechanisms not easily modeled *in vitro*.

While every effort was made to minimize the number of assumptions made in the modeling of composite drug release in Chapter 3 (for example, using zero fitting parameters), the predictive use of the model for designing new composite drug delivery systems is inherently limited, particularly for gels that have thermoresponsive bulk phases that present changing diffusion coefficients with time coupled with convective mass transport. Microfluidics of gel particles is challenging, particularly when using the *in situ* gelation chemistry used in this thesis in which improper loading of the chip can lead to rapid gelation prior to the nozzle and thus deactivation of the chip entirely). The use of microfluidics within industry is also limited by the low throughput of such systems, with scalability and parallelization particularly challenging given the risk of in-chip gelation with this particular approach. Indeed, it is likely that such a technology would not be commercially suitable except perhaps in very high value-added applications such as cell encapsulation for tissue engineering.

The particles discussed in Chapter 4 and 5 are a new and novel method of creating monodisperse particles from polymeric precursors. Limitations that have to be addressed are the ultimate loading capacity of the microgels, since they were proposed as a drug delivery vehicle. In particular, while we have acquired preliminary data showing highly

effective loading of soluble drug fractions into these gels directly during the assembly process, the loading is inherently limited by drug solubility; drugs that are too hydrophobic will not be loaded in high enough doses while drugs that are too hydrophilic will not partition into the microgel phase. As such, a better understanding of how to effectively load drugs into these microgels to take advantage of the mild self-assembly process is required for effective application moving forward. In addition, further studies need to be conducted to truly understand the mechanisms that govern the controlled swelling seen by PBA and DMAEMA functionalized microgels and optimize those swelling profiles for particular drug delivery challenges. In particular, in the context of the proposed insulin delivery application for PBA-functionalized gels, demonstrating the loading of an adequate amount of insulin, glucose-responsive release of a suitable burst of insulin, and confirming that the released insulin is both bioactive and bioavailable represent significant hurdles to apply such a system in a clinical setting.

*Future Work:*

The bulk of the work conducted in this thesis is focused on the manipulation and design of “smart” microgels, keeping biomedical applications in mind. In particular, the formation of degradable microgels using PNIPAM polymeric precursors was a main theme throughout the studies. In reference to the current studies, some additional experiments are recommended to better understand the fundamental factors at play in regulating drug release kinetics as well as the formation of the microgels.

From Chapter 2, mechanical testing of the particles generated could provide more insight into the cross-linking densities within the particles, confirming our hypothesis in Chapter 3 that the mechanical properties and morphologies of the gels formed on the microscale and the bulk scale are indeed similar. Applications such as cell encapsulation are also well within reach using our current technology and would provide added incentive to further studies in this field; in particular, since often cytotoxic small molecule cross-linkers, UV light, or heat are not needed to facilitate gelation, cell encapsulation using this hydrazone cross-linking approach offers particular promise for creating highly functional encapsulated cells and/or few cell encapsulated beads that are currently challenging to achieve using conventional encapsulation approaches. Mechanical data and a better understanding of swelling/deswelling characteristics of the microgels could also further our understanding of what is occurring during drug release from the nanocomposites in reference to microgel presence. Matching solids contents between micro- and macro-scales in the current nanocomposite work would also be beneficial in terms of enabling better interpretation of the effect of the nanocomposite phase on drug release.

The work in Chapter 4, although fundamentally significant, should be assigned to an application, with drug release and capture being the most interesting possibility. The microgels are degradable and show low cytotoxicity and thus are a prime candidate for such study. Initial target applications recommended include delivery to the brain (exploiting the deformability of microgels that other work in our lab has indicated assists in crossing the blood-brain barrier[1]) and cancer therapy (exploiting the acid-catalyzed

degradation of the hydrazone bond which should degrade faster in the more acidic tumour environment than in normal circulation)[2]. In addition, it would be of significant interest to try to apply this assembly approach to other smart hydrogels (e.g. poly(oligoethylene glycol methacrylate) (POEGMA) or the poly(lactic acid) copolymerized POEGMA materials previously generated in our lab for bulk hydrogel synthesis) to create microgels with targeted thermoresponsive properties as well as self-assembled hydrophobic nanodomains that may be highly relevant for drug delivery[3-5].

From Chapter 5, a better understanding of how the functionalized microgels behave in different conditions as well as drug release studies should be conducted, in particular to assess whether the aforementioned challenges associated with achieving clinically-relevant glucose-responsive insulin delivery can be overcome. In addition, replacement of PNIPAM (whose monomer is a known neurotoxin) with a thermoresponsive polymer more amenable for ultimate regulatory approval (e.g. poly(oligoethylene glycol methacrylate)) would be beneficial in terms of applying the same principles of production to develop applications with real world applicability. The creation of other functional precursor polymers (in particular, anionic pH-ionizable copolymers to create anionic and/or amphoteric smart microgels) also offers significant interest, both in the context of creating degradable analogues for microgels with interesting physical properties as well as creating more effective delivery vehicles for proteins of various isoelectric points.

While this thesis was focused primarily on method development and developing a fundamental understanding of how to engineer hydrogels to facilitate controlled release, there are several potential applications of the research that are worthy of investigation. The microgel-hydrogel composites loaded with bupivacaine are particulary of interest for subcutaneous or on-site delivery of local anestheic for post-surgical applications, with the hydrogel functioning to immobilize the microgels at the desired anesthesia site and promote controlled release over longer time periods than currently possible (i.e. a few hours) for effective pain management. The ability to model the composites based on individual components also allows for the unique design of systems depending on the desired drug load required for effective therepy. The degradable microgels developed can similarly be used for the delivery of thereputics, as these microgels (relative to prior compositions) have the unique ability to clear after degradation. However, given the multiple types of functionality that can be engineered into these microgels, any application in which the degradation of the microgel carrier is useful (e.g. diagnostics, environmental remediation, or agriculture) may also be considered.

**C. 1 References:**

(1) Mishra, R. H., T.; Smeets, N.M.B.; Johnson, R.; Piazza, J.E; Application, U. S. P. P., Ed. 2013.

(2) Lavie, E.; Hirschberg, D.; Schreiber, G.; Thor, K.; Hill, L.; Hellstrom, I.; Hellstrom, K.-E. *Cancer Immunol., Immunother.* **1991**, *33*, 223.

(3) Smeets, N. M. B.; Patenaude, M.; Kinio, D.; Yavitt, F. M.; Bakaic, E.; Yang, F.-C.; Rheinstadter, M.; Hoare, T. *Polymer Chemistry* **2014**, *5*, 6811.

(4) Smeets, N. M. B.; Bakaic, E.; Patenaude, M.; Hoare, T. *Chem. Commun.* **2014**, *50*, 3306.

(5) Bakaic, E.; Smeets, N. M. B.; Dorrington, H.; Hoare, T. *RSC Advances* **2015**, *5*, 33364.